

18 January 2008 | \$10

Science

 AAAS



COVER

Laser-surveyed topography of the elevation in a Pennsylvania landscape, showing evidence of sediment-filled early American millponds along a stream valley. Terraces around the stream channel descend stepwise from upstream to downstream (dark purple, light purple, pink), each associated with a dam. The deeper stream incision into the two downstream terraces is due to more complete dam breaching. See [page 299](#).

Image: U.S. Geological Survey (LIDAR data and preliminary processing); Michael Rahnis (image analysis and generation)

DEPARTMENTS

- 255 [Science Online](#)
- 257 [This Week in Science](#)
- 259 [Editors' Choice](#)
- 260 [Contact Science](#)
- 263 [Random Samples](#)
- 265 [Newsmakers](#)
- 349 [Science Careers](#)

EDITORIAL

- 258 [Engaging Iran](#)
by Glenn Schweitzer and Norman Neureiter

NEWS OF THE WEEK

- Uncle Sam's Biomedical Archive Wants Your Papers 266
- Satellite Company Offers Earth-Observing Researchers a Ride 267
- Mirror Neurons May Help Songbirds Stay in Tune 269
- SCIENCE SCOPE** 269
- New Dark-Matter Map Reveals Where Galaxies Gambol 270
- Polynesians Took the Express Train Through Melanesia to the Pacific 270
- Most-Massive Black Hole Confirms Relativity Rules the Universe 271
- Isolated Tribe Gives Clues to the Origins of Syphilis 272
- Calculating Iraq's Death Toll: WHO Study Backs Lower Estimate 273

NEWS FOCUS

- Gene Tests for Psychiatric Risk Polarize Researchers Hoping for a Glimpse of What's Ahead 274
- Seeking the Roots of Ritual Just Don't Call It the Garden of Eden 278



278

LETTERS

- Conservation with Sense *M. L. M. Lim et al.* 281
- Scientific Meetings: Worth Attending *M. McNutt*
- Scientific Meetings: Call In Instead *R. Roy*
- Putting a Human Face on Energy Usage *R. Burruss*
- Fair Game for Chimpanzees *E. Visalberghi and J. Anderson*
- Response *K. Jensen, J. Call, M. Tomasello*

BOOKS ET AL.

- Cool It** The Skeptical Environmentalist's Guide to Global Warming 285
B. Lomborg, reviewed by W. F. Ruddiman (U.S. and U.K. editions)

POLICY FORUM

- Aging Infrastructure and Ecosystem Restoration *M. W. Doyle et al.* 286

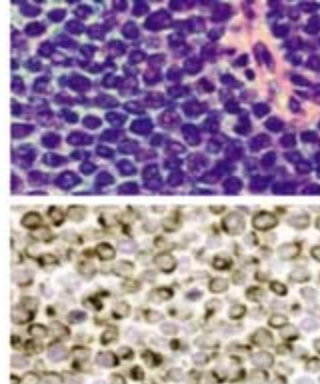
PERSPECTIVES

- Organizing the Source of Memory *E. A. Grove* 288
>> [Research Article p. 304](#)
- Orion Continues to Surprise *C. R. O'Dell and L. K. Townsley* 289
>> [Report p. 309](#)
- Managing Coastal Wetlands *I. Valiela and S. E. Fox* 290
>> [Report p. 321](#)
- [Dreams of Natural Streams](#) *D. R. Montgomery* 291
>> [Research Article p. 299](#)
- [Probing Quantum Magnetism with Cold Atoms](#) *M. Lewenstein and A. Sanpera* 292
>> [Research Article p. 295](#)



288

[CONTENTS continued >>](#)



SCIENCE EXPRESS

www.scienceexpress.org

MOLECULAR BIOLOGY

A Shared Docking Motif in TRF1 and TRF2 Used for Differential Recruitment of Telomeric Proteins

Y. Chen et al.

Two similar members of the protein complex that protects the free ends of chromosomes have distinct binding sites for other complex members and accessory proteins.

[10.1126/science.1151804](https://doi.org/10.1126/science.1151804)

CELL BIOLOGY

Differential Regulation of Dynein and Kinesin Motor Proteins by Tau

R. Dixit, J. L. Ross, Y. E. Goldman, E. L. F. Holzbaur

The motor proteins dynein and kinesin both encounter the protein tau as they move along the microtubules; the former reverses direction, whereas the latter detaches.

[10.1126/science.1152993](https://doi.org/10.1126/science.1152993)

MEDICINE

Clonal Integration of a Polyomavirus in Human Merkel Cell Carcinoma

H. Feng, M. Shuda, Y. Chang, P. S. Moore

A rare, but highly aggressive, form of human skin cancer may be caused by a previously uncharacterized human polyomavirus.

[10.1126/science.1152586](https://doi.org/10.1126/science.1152586)

GEOPHYSICS

Rogue Mantle Helium and Neon

F. Albarède

Anomalously high ratios of ^3He to ^4He in the recycled basalts under ocean islands may result from helium diffusing in from more pristine, primitive mantle.

[10.1126/science.1150060](https://doi.org/10.1126/science.1150060)

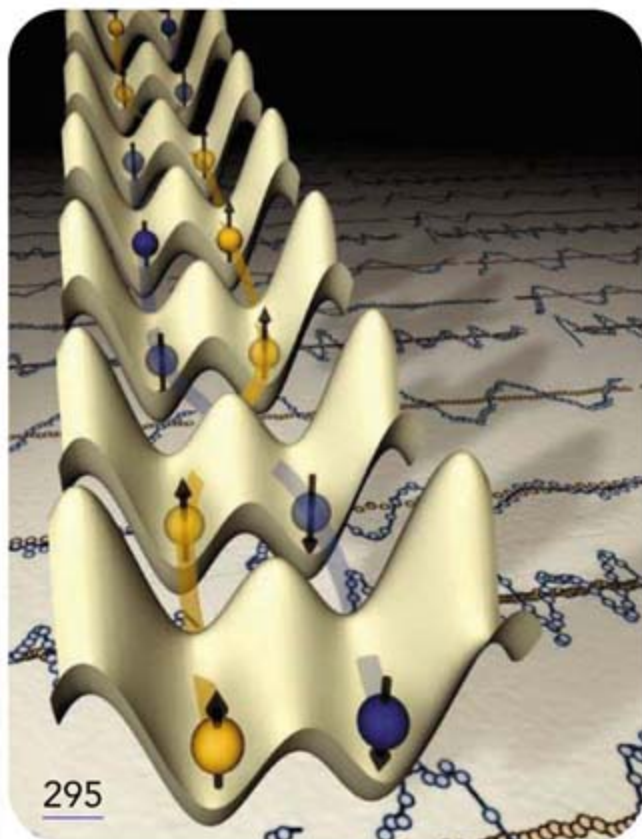
BREVIA

PLANT SCIENCE

***Arabidopsis* CLV3 Peptide Directly Binds CLV1 Ectodomain** 294

M. Ogawa, H. Shinohara, Y. Sakagami, Y. Matsubayashi

Peptides that maintain the stem cells in the shoot apical meristem of *Arabidopsis* act by binding to the extracellular portion of a receptor-like kinase.



CREDIT (BOTTOM): I. BLOCH/UNIVERSITY OF MANIZ

RESEARCH ARTICLES

PHYSICS

Time-Resolved Observation and Control of Superexchange Interactions with Ultracold Atoms in Optical Lattices 295

S. Trotzky et al.

Ultracold atoms trapped at sites of optical lattices are used to investigate the superexchange interaction between neighboring spins. >> *Perspective p. 292*

GEOGRAPHY

Natural Streams and the Legacy of Water-Powered Mills 299

R. C. Walter and D. J. Merritts

Floodplains and streams in the eastern United States were altered extensively by milldams in the 1700s and 1800s, challenging recent hydrologic interpretations and restoration approaches.

>> *Perspective p. 291*

NEUROSCIENCE

Lhx2 Selector Activity Specifies Cortical Identity and Suppresses Hippocampal Organizer Fate 304

V. S. Mangale et al.

The brain's cortex begins as a one-cell-thick sheet of stem cells, whose ultimate identity is specified by a gene that suppresses noncortical cell fates.

>> *Perspective p. 288*

REPORTS

ASTRONOMY

Million-Degree Plasma Pervading the Extended Orion Nebula 309

M. Güdel et al.

Million-degree gas fills the Orion Nebula, implying that shock-heated gas from stellar outflows is common in our Galaxy.

>> *Perspective p. 289*

[CONTENTS continued >>](#)

REPORTS CONTINUED...

CHEMISTRY

Elementary Structural Motifs in a Random Network of Cytosine Adsorbed on a Gold(111) Surface 312

R. Otero et al.

Upon cooling, cytosine molecules on a gold surface form a disordered network based on the assembly of three elementary structural units, which may have analogies with glasses.

GEOPHYSICS

The Subduction Zone Flow Field from Seismic Anisotropy: A Global View 315

M. D. Long and P. G. Silver

Identification of the fastest seismic-wave propagation speed in subduction zones reveals that trench migration induces flow in the mantle above and beneath the subducting slab.

EVOLUTION

A Localized Negative Genetic Correlation Constrains Microevolution of Coat Color in Wild Sheep 318

J. Gratten et al.

Although the fitness of wild sheep increases with size, large, dark sheep are becoming rarer because color is genetically linked to genes that decrease fitness.

ECOLOGY

Coastal Ecosystem-Based Management with Nonlinear Ecological Functions and Values 321

E. B. Barbier et al.

Taking into account the nonlinear relation between preserved habitat area and wave attenuation facilitates integrated management of coastal conservation and development.

>> *Perspective p. 290*

DEVELOPMENTAL BIOLOGY

β -Catenin Defines Head Versus Tail Identity During Planarian Regeneration and Homeostasis 323

K. A. Gurley, J. C. Rink, A. S. Alvarado

***Smed- β catenin-1* Is Required for Anteroposterior Blastema Polarity in Planarian Regeneration** 327

C. P. Petersen and P. W. Reddien

After the head or tail of a planarian is severed, the signal intensity of a prominent developmental signaling pathway controls whether a new head or tail regenerates.

GENETICS

Natural Genetic Variation in *Lycopene Epsilon Cyclase* Tapped for Maize Biofortification 330

C. E. Harjes et al.

Identification of the gene that controls vitamin A levels in maize will allow production of varieties that can improve global health without using transgenic methods.



290 & 321

CELL BIOLOGY

Dual Positive and Negative Regulation of Wingless Signaling by Adenomatous Polyposis Coli 333

C. M. Takacs et al.

An important developmental signaling molecule known to be a tumor suppressor can also activate growth, possibly explaining the responses of some cancers.

MEDICINE

Initiating and Cancer-Propagating Cells in *TEL-AML1*-Associated Childhood Leukemia 336

D. Hong et al.

Identical twins each carry preleukemic cells containing the characteristic chromosomal translocation, but only one undergoes further genetic changes and develops leukemia.

BIOCHEMISTRY

Effects of Molecular Memory and Bursting on Fluctuations in Gene Expression 339

J. M. Pedraza and J. Paulsson

A theory of stochastic gene expression suggests that noise can be modulated without feedback loops, complicating interpretation of single-cell experiments.



A change of heart.

SCIENCE NOW

www.sciencenow.org DAILY NEWS COVERAGE

Building a New Heart From Old Tissue

When newborn cells are transplanted onto a "skeleton" of an adult heart, it becomes a pumping organ in the lab.

How to Make a Submarine Disappear

Researchers think objects can be made acoustically "invisible."

High Prices Just Feel Good

Anticipation of quality activates our brain's pleasure center.



Making a graceful exit.

SCIENCE CAREERS

www.sciencecareers.org CAREER RESOURCES FOR SCIENTISTS

MiSciNet: Following the Image

A. Sasso

Ahna Skop built a career from things others pass over, from cellular detritus to shy high school students.

Mind Matters: Leaving a Lab Gracefully

I. S. Levine

When it's time to leave the lab, the key is to make sure the end isn't bitter.

Tooling Up: Dealing With Men Who Have a Problem With Women

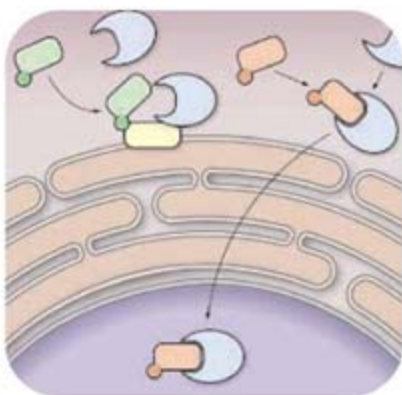
D. Jensen

You're likely to encounter men who have never learned how to relate to strong, competent women.

From the Archives: You've Worked Hard to Get This Far

J. Austin

Don't blow your academic job interview.



Proteins escape from the ER surface.

SCIENCE SIGNALING

www.stke.org THE SIGNAL TRANSDUCTION KNOWLEDGE ENVIRONMENT

PERSPECTIVE: The Endoplasmic Reticulum Takes Center Stage in Cell Cycle Regulation

P. Fearon and O. Cohen-Fix

The ER appears to play a key role in controlling the spatial localization of proteins involved in the cell cycle.

ST NETWATCH: UCSC Genome Bioinformatics

Analyze your gene of interest in a range of organisms using the tools available at the UCSC Genome Browser; in Bioinformatics Resources.

SCIENCE PODCAST



Listen to the 18 January *Science* podcast to hear about genetic testing for psychiatric disorders, a possible viral culprit in a rare skin cancer, the legacy of water-powered mills, and more.

www.sciencemag.org/about/podcast.dtl

Separate individual or institutional subscriptions to these products may be required for full-text access.



<< Shockingly Hot

Four extremely bright and massive stars, called the Trapezium, primarily illuminate the Orion Nebula. **Güdel *et al.*** (p. 309, published online 29 November; see the Perspective by **O'Dell and Townsley**) show that the Orion Nebula glows in x-rays because it is flooded with very hot gas in excess of 1 million kelvin. This heating is likely the result of shocks from powerful outflows from one bright star in the Trapezium. The majority of the stars in our Galaxy are found in regions similar to the Orion Nebula, so this phenomenon should be widespread throughout the galactic plane.

Evolution in Soay Sheep

Quantitative trait loci (QTLs) are genetic loci correlated with a typically additive phenotypic trait such as height or color. In Soay sheep, dark coat color is associated with large body size, which is heritable and positively correlated with fitness. Through mapping of the region associated with the loci determining coat color, **Gratten *et al.*** (p. 318) detail the linkage of several causal mutations within a small genomic region within a free-living sheep population. A strong correlation was found between coat color and weight, but these relations showed antagonistic effects between body size and lifetime fitness. This study provides empirical support for the role of a negative genetic correlation in the evolutionary dynamics of a natural population.

Organizing Brain Development

In early development, the cortex of the mammalian brain is built layer by layer, from the inside out. But before that occurs, the neural epithelium consists of only a single layer of stem cells. **Man-gale *et al.*** (p. 304; see the Perspective by **Grove**) have now determined that in mice the gene *Lhx2* determines cortical identity for cells at these earliest stages. *Lhx2* establishes whether cells give rise to the cortical hem, which is now seen to function as an organizer of hippocampal development.

Describing Disorder

Insights into the structure of amorphous materials usually come from theoretical modeling or from microscopy studies of larger colloidal particles. Although scanning tunneling microscopy (STM) methods can achieve atomic resolution, molecular overlayers on metal substrates tend

either to form bulk-like islands or crystallize into ordered films. **Otero *et al.*** (p. 312, published online 13 December) report STM images of cytosine molecules adsorbed on gold surfaces which show that the molecules are highly mobile at room temperature. Upon cooling to below 150 kelvin, disordered hydrogen-bonded networks form that can be characterized as being built up from three types of subunits—zigzag filaments and five- and six-membered rings.

The Not-So-Old Mill Streams

Our understanding of natural stream development has been greatly influenced by many studies in the eastern United States. **Walter and Merritts** (p. 299, cover; see the Perspective by **Montgomery**) now show that mill dams were pervasive—there were more than 65,000 mills in the 19th century—and that these structures thoroughly changed the natural character of the floodplains and streams. Mapping of about 20 streams in detail showed that these dams, collectively spanning the full length of many streams, along with widespread deforestation could cause up to 5 meters of sediment to accumulate in floodplains. Streams were changed from branching channels across broad wetlands to confined meandering channels.

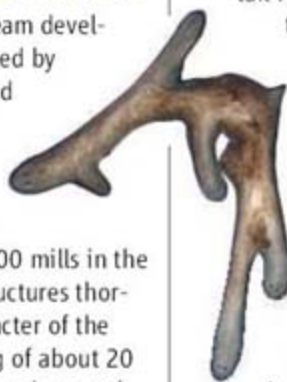
Vitamin A in Corn

Vitamin A deficiency affects the vision of millions of children each year, a problem that could be addressed with dietary adjustments. **Harjes *et al.*** (p. 330) show that natural maize variants offer a wide range of the precursors to vitamin A. The cyclase gene *lcyE* is critical in assigning

carotenoid variants to different metabolic pathways. A selective breeding program, rather than complicated transgenic methods, may be able to deliver more nutritious maize.

Heads or Tails

Planarians—tubular flatworms—can regenerate all of their body parts and entire organ systems after amputation. However, the mechanism by which the animal “knows” how to generate a head after head removal or a tail after tail removal, a property called regeneration polarity, is unknown. **Gurley *et al.*** (p. 323, published online 6 December) and **Petersen and Reddien** (p. 327, published online 6 December) now find that a conserved factor within the Wnt signaling pathway is used to distinguish head from tail. Decreased Wnt signaling through β -catenin causes the regeneration of heads, whereas activation of Wnt signaling induces tails.



Cellular Origin of Leukemia

Little is known about preleukemic cells, in which deleterious mutations first arise and function, because such cells are “clinically silent.” **Hong *et al.*** (p. 336) studied a pair of identical twins, one of whom has childhood acute lymphoblastic leukemia. Both twins possessed a cell population that contained the disease-causing chromosomal translocation but was not yet malignant. Subsequent modeling experiments in mice revealed that these preleukemic cells could go on to generate the self-renewing cells that propagate leukemia.

Engaging Iran

POLITICAL ACRIMONY IN THE WAKE OF 9/11 QUASHED MANY ALREADY-CONSTRAINED scientific interactions between the United States and Iran. Proposed Fulbright and sister-city programs that could have involved universities and medical facilities were also derailed, and obtaining U.S. visas for scientists became a major obstacle. And intensified confrontation over Iran's nuclear ambitions further increased political skepticism as to the value of scientific collaboration.

Though doubted by some, the recent intelligence report that Iran terminated its nuclear weapons program in 2003 may help heighten interest in cooperation in Washington and Tehran. There are good reasons not to let this opportunity slip by. Science-related engagement can not only contribute to solutions of global problems but can also help improve understanding of each country's society and politics, with attendant benefits for bilateral political relations.

The historical attachments of the Iranian scientific community to the United States remain strong. Scientific cooperation has shaped many programs at prestigious universities in Tehran, Shiraz, and other Iranian cities. U.S.-trained Iranian professors have introduced new programs in transportation design, materials research, and molecular genetics. The successful career paths of Iranian students who have studied at U.S. graduate schools in electrical engineering and physics are increasingly recognized in both countries. The number of joint Iranian-American scientific publications in international journals exceeds Iranian publications with any other country. At the same time, U.S. scientists have had access to Iranian research on seismicity, specific cancers, and unique approaches to fish farming in inland ponds.

But bilateral scientific engagement that can build on U.S. and Iranian technical achievements has rapidly atrophied. Many brilliant young Iranian students seeking advanced study abroad are limited to Canada, Europe, or Japan because of difficulties in obtaining U.S. visas. And concerns over the political situation have reduced the interest of U.S. scientists in visiting Iran.

During the past 8 years, the U.S. National Academies have sponsored annual U.S.-Iran scientific workshops in both countries in areas such as limnology, water conservation, science and ethics, and distance education. These workshops and related individual exchanges have shown that cooperation on problems of mutual interest is possible even in very harsh political environments. In some ways, this bridge-building is reminiscent of early U.S. exchanges with the former Soviet Union and China. But more needs to be done to help repair the broken dialogue between the scientific and intellectual communities of the two countries.

The past 3 months have seen a remarkable series of science-related events involving Iran. An October visit by a U.S. scientific delegation concluded with a joint decision to increase the frequency of bilateral workshops and the number of exchange visitors. During that visit, Princeton physicist and Nobel laureate Joseph Taylor delivered a lecture at Sharif University in Tehran that was seen in person and via the Internet by thousands of Iranian faculty members and students. In November, the U.S. Department of State along with the Institute of Medicine and Academy for Educational Development organized a 3-week program for specialists in food-borne diseases from five institutions in Iran, including a joint scientific workshop and visits to U.S. institutions from coast to coast. In December, Thomas Jefferson High School for Science and Technology in Fairfax, Virginia, began planning audio-video teleconferences with an elite high school in Tehran as a first step toward a long-term relationship. A salient new development was the launch of annual U.S.-Iranian seminars on "Science, a Gateway to Understanding." The first was held in Tehran in November and involved scientists, political leaders, philosophers, and theologians to discuss scientific, political, economic, and social topics that affect understanding among nations.

Many political leaders in Iran associate themselves with science, and many technically trained Americans are active within the foreign policy community. Together, they are an influential group that recognizes that science is based on evidence and not on ideology. They are the ones who must become advocates of cooperative programs. Particularly now, at this time of great tension in the U.S.-Iran relationship, creative initiatives from the scientific communities of both countries deserve the broadest possible encouragement and support.

—Glenn Schweitzer and Norman Neureiter

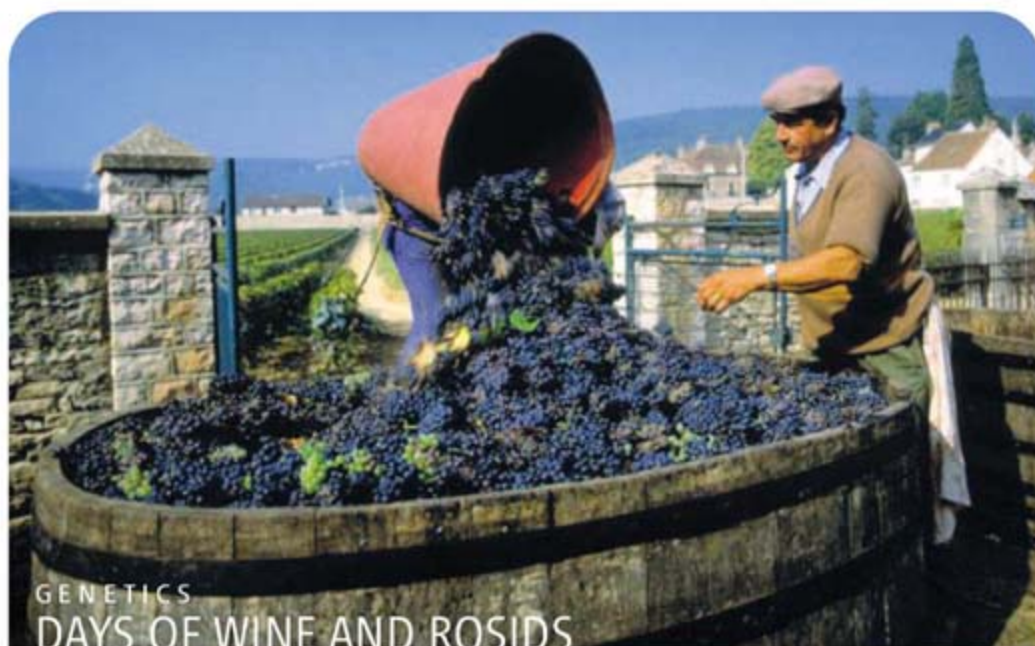


Norman Neureiter is the director of the American Association for the Advancement of Science Center for Science, Technology and Security Policy, Washington, DC. E-mail: nneureit@aaas.org.



Glenn Schweitzer is the director of Eurasian Programs at the U.S. National Academies, Washington, DC. E-mail: gscweit@nas.edu.





GENETICS DAYS OF WINE AND ROSIDS

Understanding variation, particularly in the context of genetic heterozygosity, is an important step in the effort to improve domestic crops, especially in terms of enhancing resistance to pathogens. Having tackled a heterozygous pinot noir cultivar of the grape *Vitis vinifera*, Velasco *et al.* have produced a draft of the genome sequence (estimated to be 82% complete) and uncovered a large-scale partial genome duplication of 10 chromosomes. In addition, they found that homologous chromosomes differed by approximately 11.2% and mapped approximately 2 million single-nucleotide polymorphisms. Analyses of duplication events within the grape genome suggest that the majority of gene duplication is *Vitis*-specific and not due to an earlier rosid duplication, as has been postulated. These genomic resources will support further investigation of grape genetics as applied to secondary metabolites (volatiles) and winemaking, and to the pathogen resistance of long-lived perennials, as well as adding to our understanding of genome evolution in the rosids, which include the already-sequenced poplar and *Arabidopsis*. — LMZ

PLoS ONE 2, e1326 (2007).

IMMUNOLOGY

The First Sign of Defense

Soon after birth, the intestine is exposed to multiple bacterial species, as its colonization by microflora begins. Some of the new immigrants are pathogenic, yet it is not clear how early innate immune protection and the initial maintenance of the normal microbiota are achieved. In particular, the antimicrobial peptide-producing Paneth cells only develop some time after the initial neonatal period, raising the possibility that the neonatal intestine may harbor another means of defense.

In support of this, Ménard *et al.* observed that although established enteric antimicrobial peptides were absent from the neonatal intestinal epithelium, they increased over time. In contrast, expression of the active, processed form of the cathelicidin cathelin-related antimicrobial peptide (CRAMP) was prominent specifically in the early stages of development in the epithelium of the small intestine. This peptide showed significant activity against a bacterial pathogen, as well

as against commensal bacteria, and its importance for neonatal protection was confirmed using infection of mice deficient in CRAMP.

Expression of the peptide diminished postnatally, corresponding with a gradual proliferative replacement of the epithelia, rather than with a down-regulation of transcriptional activity. The results suggest that the newborn intestine uses an ongoing developmental program to help establish control of microbial colonization and infection early on. — SJS

J. Exp. Med. 205,
10.1084/jem.20071022 (2008).

CHEMISTRY

Mild Metal Mixing

Combining a second metal with platinum (Pt) to form an intermetallic can reduce costs, inhibit poisoning, and in certain cases improve the reactivity of this widely used catalyst. However,

the need for particle annealing at high temperature causes sintering that reduces the particle surface area and introduces shape and size distortions. Bauer *et al.* present a milder technique whereby Pt nanoparticles synthesized with specific shape and size dispersity are treated in low-temperature solution with metal salts to form Pt-M intermetallics (M can be tin, lead, or several other metals). When stabilized by growth on a support such as alumina or ceria, the Pt particles did not aggregate. In the case of PtPb particles supported on Vulcan XC-72, a conductive carbon black pigment, the electrocatalytic oxidation of formic acid occurred at a lower onset potential in comparison with commercial PtRu particles on the same support. — MSL

J. Mater. Chem. 18, 275 (2008).

CLIMATE SCIENCE

Whither Antarctic Ice?

Determining how much the Antarctic ice sheet may contribute to sea-level rise through global warming depends on an accurate and precise understanding of the mass balance of two broadly defined regions: the coast and the interior. Essentially, the coasts appear to be losing mass while the interior is closer to being in balance, but considerable uncertainty remains in current estimates of mass change for the ice sheet as a whole. In order to better constrain the coastal element of the problem, Rignot *et al.* have analyzed satellite interferometric synthetic-aperture radar observations of Antarctica's coastline from 1992 to 2006 to estimate ice flux to the oceans. These measurements, which cover 85% of the coast, show that

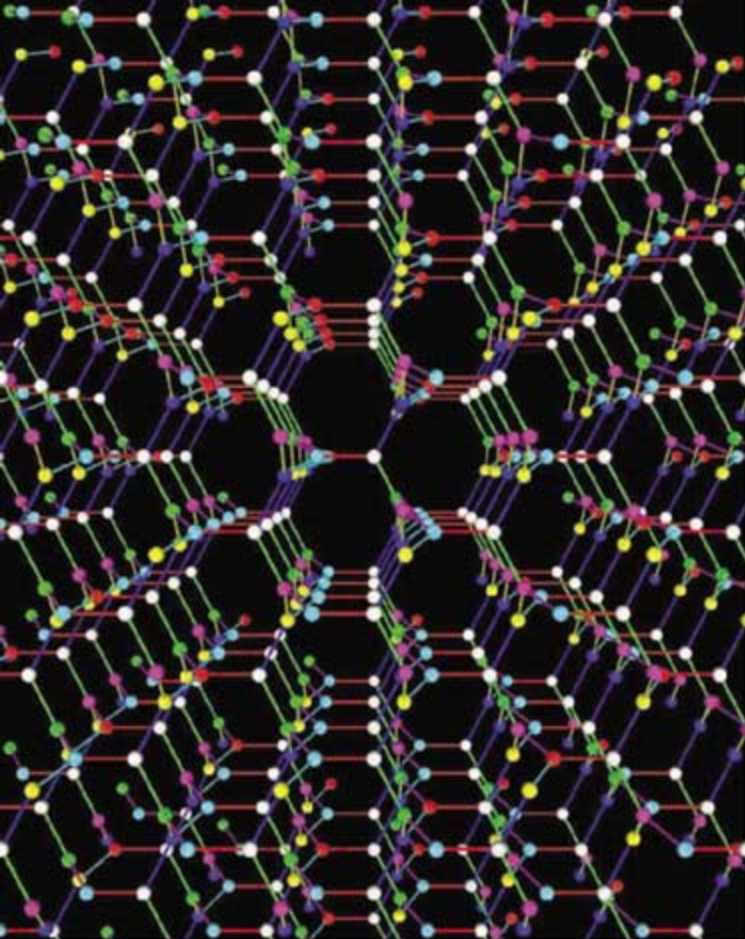
although East Antarctica probably is not losing mass, widespread losses in West Antarctica totaling 132 ± 60 Gt occurred in 2006, and that ice losses that year at the northern tip of the Antarctic Peninsula amounted to 60 ± 46 Gt. Ice mass loss from the coasts increased by 75% over the period of the



Antarctica.

study. These results highlight the importance of changes in glacier dynamics, which are so poorly understood that the Intergovernmental Panel on Climate Change could not include them in projections of sea-level rise in its 2007 report. — HJS

Nat. Geosci. 1, 10.1038/ngeo102 (2008).



A Mathematical Gem

Diamonds may set the standard for beauty in jewelry. But another crystal structure is mathematically as exquisite as diamond's, says mathematician Toshikazu Sunada of Meiji University in Kawasaki, Japan. Diamond and the other structure, which he dubs K_4 , are the only ones that possess both of two key symmetries, Sunada reports in the February issue of the *Notices of the American Mathematical Society*.

A crystal lattice is a repeating spatial pattern of atoms and bonds. But it can also be thought of more abstractly as a list of points, or vertices, and a list of lines, or edges, that connect them. The ordering of the lists can be scrambled, and any scrambling that keeps the same vertices and edges connected is called an automorphism. Diamond and K_4 have "maximal symmetry," which means any automorphism is equivalent to sliding or rotating the structure or reflecting it as in a mirror.

The two also share "strong isotropy." In diamond, each atom has four neighbors, and the crystal lattice is so symmetrical that, by rotating and reflecting it, the neighbors can be made to switch positions in any way. So, too, in K_4 , in which each atom has three neighbors.

Sunada speculates in his paper that K_4 doesn't appear in nature. In fact, it shows up in inorganic compounds, lipid networks, and liquid crystals and has been known for decades by other names, says Stephen Hyde of the Australian National University in Canberra. Still, Sunada has proved that K_4 and diamond share strong isotropy, Hyde says: "It's very elegant mathematically."

Darkest Matter

If you're looking to make yourself a proverbial black box, you may want to talk to Shawn-Yu Lin. The physicist at Rensselaer Polytechnic Institute in Troy, New York, and his colleagues have just turned out the darkest material ever made. It's a thin film made from a forestlike array of carbon nanotubes 10 nanometers thick and up to a millimeter tall. The tubes reflect nearly nothing at all: Not only do they absorb light well, but the random way in which they intertwine with one another scatters nearly all the light they don't absorb.

Whereas the previous low-reflectance record holder, an etched surface of nickel phosphorus, reflected just 0.16% of incoming light, the nanotube array returns merely 0.045%,

Lin's group reported online last week in the journal *Nano Letters*. Ray Baughman, a materials scientist at the University of Texas, Dallas, calls the work very interesting, even though he can't think of a killer application for the new material. Lin says he and his colleagues are staking a claim with *Guinness World Records*.

Mice: Ready for Takeoff

Over the past 100 million years or so, bats have evolved many features that distinguish them from their mammalian cousins. One is long, bony digits to support their wings. Now, by manipulating one small DNA sequence,

Richard Behringer of the University of Texas M. D. Anderson Cancer Center in Houston and colleagues have nudged mice a tiny step along the evolutionary path to bat-hood.

The researchers looked at the expression of a homeobox gene, *prx1*, a key to the development of limbs in all mammals, and found that bats expressed the gene differently from mice in embryonic limbs. So, in mice they removed a chunk of DNA known to control *prx1* expression and replaced it with the same piece from bats. The forelimbs of the resulting mice were 6% longer than those of normal baby mice. Although small, that increase is "important," says developmental biologist Clifford Tabin of Harvard Medical School in Boston.

Similar studies have been done with flies and worms, but this is the first to show how a specific change in control of gene expression—and not an actual gene—can produce a gross morphological change in a mammal, says Behringer, whose study was published this week in *Genes & Development*. "If you play this through with lots and lots of genes, maybe ultimately we could make that mouse fly out of the cage."



NANO-CAR

It looks like a toy and has an engine just a tad more powerful than a lawnmower's. But the new no-frills minicar unveiled by Indian automaker Tata last week is making big waves. At \$2500, the Nano will be the world's cheapest car when it rolls off the assembly lines next year. Tata officials say its price and its 20-kilometers-per-liter fuel economy make it ideal for millions of Indians who can now afford only bicycles and public transportation. But environmentalists worry that it will further clog streets and worsen air quality. And many wonder if the lightweight, no-airbags car will meet safety standards in developed countries.





Three Q's >>>

By day, **Greg Graffin** teaches at the University of California, Los Angeles. By night, the 42-year-old biologist sings for Bad Religion, a punk rock band he co-founded at age 15. Some of his lyrics draw upon the language of science. In one song, for instance, he laments about "Modern man / pathetic example of earth's organic heritage / Just a sample of carbon-based wastage." *Science* spoke with Graffin recently while he was on a tour to promote the group's 14th album, *New Maps of Hell*.

Q: Where does the name "Bad Religion" come from?

I felt that religion was useless as a way to answer the "big" questions about life. I felt that a "bad religion" was an apt name for a belief system that offered incorrect insights into questions of a scientific nature. Today, I recognize that the name implies that there is a "good religion." I guess a good religion is founded on the principle of truth through observation and verification.

Q: How do you use science in your lyrics?

A lot of scientific words are concisely descriptive, and this can be poetic if they are used carefully. I think that questions about evolution particularly are great metaphors that can be incorporated, because traditionally, our songs deal with social hardship, inequality, and general problems with modern man's lifestyle.

Q: Do you keep your two lives separate?

[People sometimes think] that I'm just using my music to promote my science background and vice versa; I'll use my lecture podium to try and enlist new fans. I [try] to never do that. I never talk about music in a lecture hall. If students come by [during] office hours, some of them ask me [about my music], but you'd be surprised how few. ... [And that] keeps things nice and clean.

IN BRIEF

A German neuroethologist and two American surgeons are the winners of this year's King Faisal International Prize, for science and medicine, respectively, given out by Saudi Arabia's King Faisal Foundation. **Rüdiger Wehner**, a researcher at the University of Zurich, Switzerland, wins the \$200,000 science prize for his research on how desert ants navigate. **Donald Trunkey**, a professor of surgery at Oregon Health and Science University in Portland, wins half of the \$200,000 medicine prize for his role in the development of mobile surgical units for better care of trauma victims. The other half of the prize goes to **Basil Pruitt Jr.**, a surgery professor at the University of Texas Health Science Center at San Antonio, whose work has led to improvements in the care of patients with serious burn

injuries. Each winner will also receive a gold medallion.

A California investment banker and his wife have donated \$20 million to Stanford University for stem cell research. **John Scully**, a Stanford business school alumnus, hopes that such donations will help accelerate the discovery of stem cell therapies and persuade the United States government to end restrictions on federal funding for the field.

The latest project to benefit from Microsoft's **Bill Gates's** fortune is the Large Synoptic Survey Telescope, which astronomers plan to build on the mountains of northern Chile. This month, Gates donated \$10 million to the initiative. **Charles Simonyi**, a former Microsoft executive, threw in another \$20 million. The 8.4-m-wide telescope, estimated to cost \$389 million, is scheduled to see first light in 2014.

Got a tip for this page? E-mail people@aaas.org

AWARDS

FROM JAPAN, WITH LOVE.

This year's Japan Prizes honor pioneers in communications and genetics. American computer scientists Vinton Cerf (left) and Robert Kahn (middle) were chosen in "Information Communication Theory and Technology" for creating the basic framework and the communication protocol that undergirds the Internet. Cerf is vice president and chief Internet evangelist for Google in Mountain View, California, and Kahn is chair, CEO, and president of the Corporation for National Research Initiatives in Reston, Virginia.

Victor McKusick (right) was named winner of the "Medical Genomics and Genetics" prize for accomplishments including the creation of the monumental *Mendelian Inheritance in Man*, a catalog of inherited genes associated with diseases. McKusick, a researcher at Johns Hopkins University in Baltimore, Maryland, also served as the first president of the Human Genome Organisation. Each prize carries a cash award of \$455,000 and is sponsored by the Science and Technology Foundation of Japan.





A clue to songbird communication

269



The origin of syphilis

272

SCIENTIFIC PUBLISHING

Uncle Sam's Biomedical Archive Wants Your Papers

If you have a grant from the U.S. National Institutes of Health (NIH), you will soon be required to take some steps to make the results public. Last week, NIH informed its grantees that, to comply with a new law, they must begin sending copies of their accepted, peer-reviewed manuscripts to NIH for posting in a free online archive. Failure to do so could delay a grant or jeopardize current research funding, NIH warns.

The public-access law, touted as a way to enable taxpayers to learn about the research they fund, was part of a spending bill Congress passed in mid-December. It makes mandatory a policy in effect since May 2005 that requests that NIH-funded investigators submit manuscripts accepted by a journal to NIH; the agency posts the full text in the archive, called PubMed Central (PMC), no more than 12 months after the article is published. Only about 12% of authors are complying with the voluntary policy, however, and of 80,000 eligible articles per year, only 20% to 25% are being submitted either by authors or directly by journals, says David Lipman, who oversees PMC.

NIH says it is ready for the glut of manuscripts it will soon receive, but there are signs that some scientists may be confused about what to submit. For example, NIH is already removing old papers that authors mistakenly posted in PMC. Lipman acknowledges that there will be "a learning process" but notes that traffic on the site is already "huge," with 12 million article views each month.

NIH's brief notice simply states that the policy is mandatory for all articles accepted on or after 7 April. Initially, NIH requested that only original research be archived at PMC, but now the agency says the policy has

been expanded to include review articles if they were peer-reviewed. Many journals retain copyright of the manuscripts they publish, so authors must obtain permission to post a copy on the NIH site. It is up to

investigators and their institutions to figure out whether their submissions

SELECTED PUBLIC ACCESS POLICIES

Agency	Grantees must deposit manuscript in	Extra funding for immediate access?
Wellcome Trust	PubMed Central (PMC) or U.K. PMC within 6 months of publication	Yes
U.K. MRC	U.K. PMC within 6 months of publication	Yes
HHMI	PMC upon acceptance for posting within 6 months of publication	Up to \$2000
NIH	PMC upon acceptance for posting within 12 months of publication	No

comply with the journals' policy.

To give scientists a nudge, NIH will require them to include the PMC number when they cite their own papers in grant applications and progress reports. Other possible ways of forcing scofflaws to comply range from having a program director call with a reminder to "the most extreme: suspending funds," says NIH Deputy Director for Extramural Research Norka Ruiz Bravo. "We hope we're not going to get there," she says.

The new law puts NIH in line with some other funding agencies that require grantees to send their papers to PMC or a U.K. version of the archive; these include the U.K.'s Medical Research Council and Wellcome Trust, which adopted such policies in 2006, and the Howard Hughes Medical Institute (HHMI) in Bethesda, Maryland, whose rule goes into effect this month (see table). All three institutions require that papers be posted within 6 months of publication in a journal. NIH differs in one

way: Whereas other funders help pay author fees that some journals charge to make the full text immediately available, NIH is not offering any extra money for "open access," Ruiz Bravo says.

Critics have long warned of potential snags. For example, they note that it will often result in two versions of an article on PMC: the accepted manuscript, which hasn't been copyedited, and the published paper. Publishers also have worried that making articles available for free will cut into the subscription income needed to run journals and other society activities. The Association of American Publishers had no immediate comment on the NIH plan,

but AAP has warned that a mandatory policy "undermines" publishers' copyright and is "inconsistent" with U.S. laws (*Science*, 11 January, p. 145).

Scientists who have been sending their papers to PMC say the process is relatively easy, but keeping track of each journal's copyright policy is not. For example, Karen Allendoerfer, lab manager for HHMI investigator Susan Lindquist of the Whitehead

Institute in Cambridge, Massachusetts, says figuring out whether the author must submit articles directly or can rely on the journal to do it is "a pain in the neck." (NIH has tried to help by posting a list of some 300 journals that automatically upload articles to PMC.)

As for journals, although most major biomedical publications (including *Science*) already allow authors to submit manuscripts to PMC, some publishers say they will need to police the site for articles mistakenly posted, such as those not yet released from the journal's embargo or those published before 2005. Martin Frank, executive director of the American Physiological Society, says APS asked NIH to remove 78 papers last year, and he expects "hundreds" of similar errors when the mandatory policy kicks in. Lipman acknowledges that NIH had to remove some papers. But complying with copyright, he says, is not NIH's responsibility; it's "between the author and the publisher."

—JOCELYN KAISER

SOURCES: WELLCOME TRUST, U.K. MRC, HHMI, AND NIH

REMOTE SENSING

Satellite Company Offers Earth-Observing Researchers a Ride

Looking for a way to get multiple daily observations of Earth from space? A satellite communications company called Iridium may have a deal for you.

Iridium is offering space on its next-generation fleet of 66 satellites for researchers to do earth observation. Built and paid for by government agencies, the instruments would be launched by Iridium, which would manage the data transmissions for a fee. Next week, it will pitch the idea to scientists, funding agencies, and instrument manufacturers at a meeting at the Royal Society in London. But the \$1.6 billion price tag could prove a bit too steep.

"The concept can't be argued with," says Mick Johnson of the European aerospace company EADS Astrium, who also heads the U.K.'s Centre for Earth Observation Instrumentation. "The question is: What's the performance, what's the cost, and what will we then not be doing?"

Motorola set up the Iridium system during the 1990s as a worldwide mobile phone service. But it proved a financial disaster and was bought by a group of private investors in 2000. Iridium, which can handle both voice and data, now has about 225,000 customers, mostly in the military and in the shipping, aviation, and petroleum industries. Remote research outposts such as the Amundsen-Scott South Pole Station rely heavily on it.

The satellites, however, provide limited bandwidth—at 10 kilobits/second, it's slower than a dial-up modem—and are expected to begin failing during the next decade. So

in late 2006, the company began planning a replacement constellation, dubbed Iridium NEXT, and came up with the idea of adding remote-sensing capabilities as a moneymaking venture. It's working with Trident Sensors, a British company that makes Iridium receivers for scientific uses such as ocean-monitoring buoys and autonomous submersibles.

Most earth observation these days is done by single satellites, often huge behemoths bristling with sensors. Although this approach allows researchers to compare different types of data, it is less useful for studying phenomena that evolve rapidly, because a single craft can take days to return to a particular spot. Iridium's idea is entirely different: The satellites' main function will remain communications, but the company will make available on each one enough room for a suitcase-sized instrument, weighing no more than 50 kilograms and using less than 50 watts of power. Government agencies would choose what instruments to install, build them, and control them in orbit; Iridium would charge to download the data.

Because there are 66 satellites with many carrying the same instrument, any location can be viewed many times a day, capturing fast-changing phenomena such as plant growth or how air pollution levels vary with the time of day. "Science needs this. It's unparalleled to have so many plat-

space constraints onboard the satellites mean that not all types of earth observation would work. "Only some instruments would be feasible," says Volker Liebig, head of earth observation at the European Space Agency, adding that similar instruments are two to four times that mass.

The bigger obstacles are timetable and cost. Executive Vice President Don Thoma says Iridium hopes to sign a contract to build the satellites within a year and so needs to know by then whether to make space for instruments. The satellites are scheduled to be launched between 2013 and 2016 and will operate until at least 2030. If government agencies take up the offer and provide instruments, they would have to pay Iridium a "hosting fee" in the form of a pre-

Bird watching. Iridium has suggested adding sensors to its next network of 66 communications satellites.

buy of data services. Bill Simpson of Trident says the \$1.6 billion for instrument construction and hosting is a fraction of what it would cost funders to build and launch their own constellation.

But that doesn't mean funders have budget available for such a project in the next 12 months. The British National Space Centre, which coordinates U.K. spending, calls the Iridium proposal "an interesting opportunity." ESA's Liebig says the total is "an enormously high sum" and says the agency has "no activity in this direction." The U.S. National Oceanic and Atmospheric Administration is having a meeting this month to discuss doing earth observation with commercial satellite systems.

Researchers are hoping that some common ground will be found at next week's London meeting. "It's very easy to say no," says Monks. "But you can't let every opportunity go by just because it's difficult."

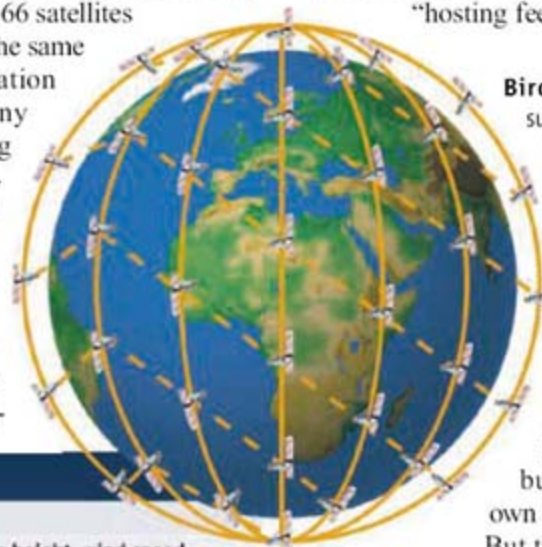
—DANIEL CLERY

NEW TOOLS TO OBSERVE EARTH

Type	Number of sensors	Applications
Altimetry	24	Sea surface, wave height, wind speed, ocean circulation, tsunami early warning
Radiometry	18	Measuring Earth's radiation budget, ice and cloud albedo, weather forecasting
Imaging	12	Deforestation, desertification, ice extent, disaster remediation
Radio occultation	12	Temperature and humidity profiles, electron content of ionosphere, weather forecasting

forms," says atmospheric chemist Paul Monks of the University of Leicester, U.K.

Iridium and Trident have worked out one possible scenario, in which different groups of the 66 satellites would carry out four separate missions (see table): altimetry, radiometry, imaging, and radio occultation, which gives temperature and moisture profiles (*Science*, 7 April 2006, p. 48). But the



NEUROSCIENCE

Mirror Neurons May Help Songbirds Stay in Tune

The discovery of so-called mirror neurons a decade ago has fueled much discussion in neuroscience ever since. The original experiments identified neurons in monkeys that fire when an animal reaches out an arm or sees another animal make a similar movement. Brain-imaging studies have found analogous neural activity in the human brain in a variety of other contexts, prompting speculation that mirror neurons could have roles in perception, learning, and empathy (*Science*, 13 May 2005, p. 945).

In this week's issue of *Nature*, researchers describe mirror neurons in songbirds that fire when a bird sings or hears another bird sing a song similar to its own. The finding may pave the way to insights into how songbirds learn

Duke University mounted an ultralight-weight device on the heads of swamp sparrows that enabled them to record the activity of individual neurons as the birds sang and listened to samples of recorded songs. In a brain region called HVC, part of a forebrain circuit that mediates singing, the researchers identified neurons that fired in a consistent pattern when the bird sang a particular song. (Swamp sparrows typically have several songs in their repertoires.) During singing, for example, a neuron might fire at the onset of a particular sequence of notes. When the researchers played the bird's own song through a speaker, the same neuron would again fire whenever that sequence appeared. Sometimes the same neuron would also fire

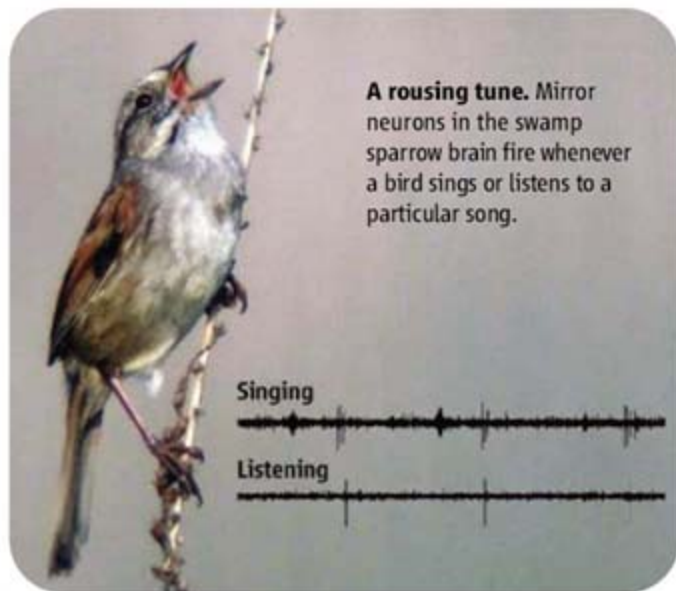
in response to another swamp sparrow's song—but only when the other bird's song contained a similar sequence of notes. Mooney's team also found HVC neurons with similar responses in Bengalese finches, another songbird.

"These were damned difficult experiments," says Daniel Margoliash, a birdsong researcher at the University of Chicago in Illinois. Margoliash says the findings are exciting because the HVC neurons identified by the Duke team may help explain how individual songbirds are able to maintain their complex and distinctive songs

for life. The activity of these neurons during singing may be a neural representation of what the bird intended to sing that it compares against auditory feedback of what it actually sang, Margoliash says. Such a comparison is probably necessary for adult birds to maintain their songs, he says, and it almost certainly plays a role as young birds first learn their songs as well.

The HVC neurons may also help songbirds decode each other's songs, Mooney says. Male swamp sparrows sing back and forth to defend their territories, and hearing the song of a rival would activate some of the HVC neurons that fire when a bird sings a similar song itself, Mooney says. That might enable a bird to compare his rival's song to his own repertoire—and select an appropriate retort.

—GREG MILLER



A rousing tune. Mirror neurons in the swamp sparrow brain fire whenever a bird sings or listens to a particular song.

and maintain their complex songs—one of the few instances of learned communication aside from human language. Some researchers see broader implications as well.

"This is the first description of a mirror system in a species other than primates," says Pier Ferrari, a neuroscientist at the University of Parma in Italy, a current member of the team that made the original mirror neuron discovery in monkeys. Ferrari thinks mirror neurons may turn out to be "a basic feature of the vertebrate brain" that initially evolved to help animals refine their movements and eventually became co-opted, at least in some species, for more complex functions, such as understanding the behavior of others.

In the new study, neuroscientists Jonathan Prather, Richard Mooney, and colleagues at

Cheer Up, Physicists

The Bush Administration plans to ask Congress for another double-digit increase next year for the Department of Energy's (DOE's) Office of Science. Budget documents obtained by *Science* indicate that the president, as part of a 2009 budget to be unveiled next month, will propose boosting the office's current \$4 billion budget to at least \$4.7 billion. (The 2008 request for \$4.4 billion was ultimately trimmed back at the last minute by Congress.) Raymond Orbach, DOE undersecretary for science, would not confirm the final 2009 number but said in an interview last week (www.sciencenow.com/content/full/2008/11/5/1) that it "will be a wonderful budget request." The documents show initial agreement on a \$118 million increase for high-energy physics over the 2008 level as of November.

Orbach also told *Science* that DOE wants to stay involved in the \$6 billion ITER fusion project despite last month's decision by Congress to wipe out its planned \$150 million contribution for 2008. DOE told its partners it would defer its payment this year and keep a small staff working on the project at Oak Ridge National Laboratory. Earlier this month, DOE shuttered the Intense Pulsed Neutron Source, a 26-year-old user facility at Argonne National Laboratory that is considered a predecessor to the new Spallation Neutron Source at Oak Ridge National Laboratory.

—ELI KINTISCH

New Vaccine Strategy

NEW DELHI—In a new approach to vaccine development, a U.S. university will dispatch faculty members to India to help run a new vaccine research center with Indian partners. Until now, U.S. researchers have spent only a few months at a time in India, says Altaf A. Lal, a malaria researcher with the U.S. Embassy in New Delhi. Emory University's School of Medicine in Atlanta, Georgia, will spend \$3 million over 3 years to hire three faculty members for the Emory Vaccine Center, a joint venture with the International Centre for Genetic Engineering and Biotechnology (ICGEB) in New Delhi.

Tops on the center's list is developing a DNA vaccine against clade C of the HIV virus, developed by a team led by Emory University's Rama Rao Amara, a researcher running U.S. phase I clinical trials on a related virus. ICGEB Director Virander Singh Chauhan says the new center does not intend to use Indians as unwitting guinea pigs for new vaccines—an allegation that has dogged some of the more recent Indo-U.S. vaccine trials in India.

—PALLAVA BAGLA

ASTRONOMY

New Dark-Matter Map Reveals Where Galaxies Gambol

AUSTIN, TEXAS—The most detailed map of dark matter ever made confirms that galaxies cluster together where the density of the mysterious dark stuff is highest. The new survey, which spanned a patch of space 16 million light-years across and required 5 days of observing time on the Hubble Space Telescope, also shows that galaxies affect one another most strongly on the outskirts of these high-density regions. “It’s as if people move in from rural areas to city centers, and most interactions occur in the suburbs,” says astronomer Meghan Gray of the University of Nottingham in the United Kingdom, a member of the team that made the map.

Dark matter can’t be seen, and no one knows what it is. But the gravity of a dark-matter clump slightly bends the light from faint galaxies in the background in a process known as weak lensing. Thus, a statistical analysis of the shapes of tens of thousands of remote background galaxies reveals the distribution of dark matter in the foreground. “It’s a very, very weak effect,” says team member Catherine Heymans of the University of British Columbia in Vancouver, Canada.



Space ghosts. In supercluster Abell 901/902, astronomers plotted concentrations of invisible mass (pink regions) from their effects on passing light.

The new survey, presented here last week at the 211th meeting of the American Astronomical Society, was aimed at the relatively nearby supercluster Abell 901/902, 2.6 billion light-years from Earth. As predicted by current theories on cosmic evolution, dark-matter condensations within the supercluster appear to be the gravitational pits that galaxies fall into. Four particularly dense clumps (shown as pink blobs on the map) coincide with strong

concentrations of galaxies. The map also confirms earlier indications that most galaxy interactions (such as tidal deformations and mergers) occur in regions with a moderate dark-matter density, on the outskirts of the densest blobs. Gray says galaxies in the dense cores may be shooting past one another too quickly for much interaction to take place there.

Physicist J. Anthony Tyson of the University of California, Davis, warns that many more clusters need to be studied before researchers can draw firm conclusions about how galaxies evolve and clusters grow. “I think we are witnessing only the beginning of an exciting exploration of the history of assembly of structures in the universe,” says Tyson, who is also

director of the planned Large Synoptic Survey Telescope (LSST) (*Science*, 27 August 2004, p. 1232). “LSST will survey an unprecedented volume of the universe, charting billions of galaxies back to when the universe was a quarter of its current age.” Tyson expects the telescope, to be built in northern Chile, to be ready in 2014.

—GOVERT SCHILLING

Govert Schilling is an astronomy writer in Amersfoort, the Netherlands.

EVOLUTIONARY GENETICS

Polynesians Took the Express Train Through Melanesia to the Pacific

The Polynesians who settled the far-flung islands of Remote Oceania several thousand years ago accomplished one of humanity’s most rapid feats of colonization. But who were these early seafarers? Researchers have long debated various origins for them, from Taiwan to the islands of Melanesia.

Now, modern genetics has offered the most definitive answer yet. A study led by anthropologist Jonathan S. Friedlaender of Temple University in Philadelphia, Pennsylvania, indicates that Polynesians bear a much closer relationship to aboriginal inhabitants of Taiwan than to the Melanesian groups who occupied New Guinea and surrounding islands from 50,000 to 30,000 years ago.

The new study “makes excellent sense,” says archaeologist Peter Bellwood of Australian National University in Canberra. It supports the “express train” theory, which posits

that people from Taiwan moved rapidly through Melanesia, leaving little genetic footprint. Other ideas have included the “slow boat” hypothesis, in which the migrating Polynesians mixed with Melanesians on their way east. Then there is what has been called the “entangled bank” scenario, which holds that patterns of ancient migrations are too enmeshed to be accurately reconstructed (*Science*, 2 March 2001, p. 1735).

Until now, genetic studies have yielded conflicting answers. Data from mitochondrial DNA (solely from women) told of little interbreeding between Polynesians and Melanesians, but a Y chromosome study suggested extensive blending between the two.

The new study, reported online on 17 January in *PLoS Genetics*, is based on 890 genomic markers from the nuclear DNA of 952 people in 41 populations. The conclusion? “There was

remarkably little genetic intermixture,” says Friedlaender. Melanesians speaking Papuan languages—their own ancestral tongues—showed no sign of genetic contributions from Polynesians. Even among Melanesians sharing languages with Polynesians, there was minimal genetic mixing, never more than 20%. “When different peoples interact, ... genes tend to be exchanged far less frequently than ideas and languages,” concludes Friedlaender.

Geneticist and skeptic Martin Richards of the University of Leeds, U.K., says, however, that the researchers could not distinguish whether the Polynesians originated in Indonesia or Taiwan; he argues that the paper “does not really move the debate forward very much.” But archaeologist Patrick Kirch of the University of California, Berkeley, calls the work “truly a major accomplishment.”

—CONSTANCE HOLDEN

ASTRONOMY

Most-Massive Black Hole Confirms Relativity Rules the Universe

AUSTIN, TEXAS—You can run from Einstein, but you can't hide. Astronomers observing a supermassive black hole 3.5 billion light-years from Earth have found that the object brightened dramatically at just the time the equations of general relativity predicted. As a bonus, scientists pegged the black hole's mass at a staggering 18 billion times the mass of the sun, six times as big as the previous record holder.

"This is a pretty spectacular extension of the regime in which the effects of relativity have been measured," says theoretical physicist Robbert Dijkgraaf of the University of Amsterdam, the Netherlands, who was not involved in the study. It's also bad news for proposed alternative theories of gravity that give slightly different predictions, Dijkgraaf says.

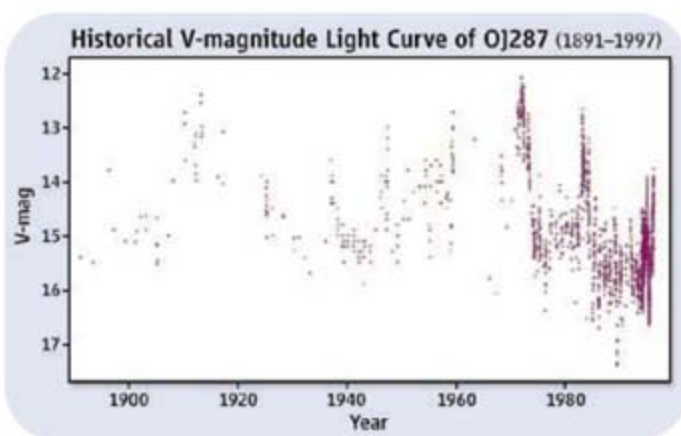
The supermassive black hole, known as OJ287, resides in the core of a distant galaxy, where its gravity sucks in matter from an enormous disk of gas and dust rotating around it. As the matter plunges toward the black hole, the galaxy's core turns into a glowing energy furnace. Twenty years ago, astronomers sifting through photographs dating back to 1891 discovered that every 12 years or so, the radiation from this accretion disk flares up to about 100,000 times normal, in two bursts just over a year apart (see figure).

To astronomers, such periodic behavior smacked of orbital motion. Mauri J. Valtonen of the University of Turku in Finland proposed that a smaller companion goes around the supermassive black hole, following a very elongated orbit strongly tilted with respect to the primary's accretion disk. Every 12 years, at its closest approach, the smaller black hole passes through the accretion disk twice, stirring it up and heating nearby matter enough to produce a brightness peak. After new flares appeared in 1994, 1995, and November 2005, Valtonen and colleagues modeled the binary's orbit and predicted that the next peak would occur on 13 September 2007.

About 30 professional and amateur observatories, including the German 3.5-meter telescope at Calar Alto Observatory in Spain and

the 2.5-meter Nordic Optical Telescope on the Canary Island of La Palma, joined forces to check the forecast. At the 211th meeting of the American Astronomical Society held here last week, Valtonen proudly presented the results: The flare showed up as predicted, beautifully confirming the binary model. From the orbital motion, the researchers calculated the masses of the two black holes to be 18 billion solar masses for the primary and a more modest 100 million suns for the companion.

The observations also marked yet another triumph for Einstein's theory of general relativity, which states that the extremely strong gravitational field near the supermassive black hole should distort spacetime in ways that rapidly change the orientation of the companion's orbit. It also predicts that the loss of energy from the emission of gravitational



Ups and downs. Swings in brightness of a distant energy source mark the orbital waltz of two black holes—one of record size.

waves should cause the orbit to shrink—an effect that won a 1993 Nobel Prize for two physicists who first detected it in a binary neutron star. Without spacetime curvature, the flare would have occurred 10 days earlier than predicted, Valtonen says; without gravitational waves, 20 days later.

"The result is of fundamental importance, since precision measurements that really test general relativity only became available quite recently," Dijkgraaf says. On a cosmic time scale, this particular test case will be gone soon as well: The two black holes are expected to collide and merge within some 10,000 years. When that happens, astronomers will *really* have something to stare at.

—GOVERT SCHILLING

Govert Schilling is an astronomy writer in Amersfoort, the Netherlands.

JPL Workers Win in Court

Scientists and engineers at NASA's Jet Propulsion Laboratory (JPL) have won a temporary reprieve from a new rule mandating extensive background checks of all government employees and contractors. Last week, a federal judge in Los Angeles abided by an order from an appellate court and allowed the 28 employees to continue working at the Pasadena, California, facility without giving the government permission to investigate their personal histories. NASA officials said the new checks, which went into effect this fall, are needed to improve lab security. But the appellate court said that the employees, who sued NASA and JPL in August, were facing "a stark choice: either violation of their constitutional rights or loss of their jobs." The case will now go to trial. "We were subjected to a lot of pressure from JPL, and we are glad to have survived," says planetary scientist Robert Nelson, one of the plaintiffs.

—YUDHIJIT BHATTACHARJEE

Korean Science Shakeup Looms

SEOUL—South Korea's research community is worried that former construction magnate Lee Myung-bak could bulldoze the Ministry of Science and Technology (MOST) when he takes over as president on 25 February. As part of his pro-business, small-government agenda, Lee has pledged to eliminate four of 18 ministries, with final details to come. Speculation is rampant that the science ministry's education components—including management of the Korea Advanced Institute of Science and Technology (KAIST)—will be handed to the Education Ministry, while the rest of MOST is folded into other ministries. Merging MOST with the Ministry of Education may only weaken it, KAIST president Suh Nam-pyo wrote in a statement last week.

—MARK RUSSELL

Soiled: Nanotech's Reputation

Nanotech experts agree that the health risks of nanotechnology need more study, but the British Soil Association, which sets standards for organic farming, isn't waiting for the data. This week the group launched a preemptive "ban" announcing that it would not allow engineered nanoparticles smaller than 200 nanometers in the products that it certifies as organic. "Companies are going to face greater pressure to clarify risks and benefits," says David Rejeski, who directs the Project on Emerging Nanotechnologies of the Woodrow Wilson International Center for Scholars.

—ERIK STOKSTAD

INFECTIOUS DISEASES

Isolated Tribe Gives Clues to the Origins of Syphilis

In 1494, King Charles VIII of France invaded Italy. Within months, his army collapsed and fled. It was routed not by the Italian army but by a microbe. A mysterious new disease spread through sex killed many of Charles's soldiers and left survivors weak and disfigured. French soldiers spread the disease across much of Europe, and then it moved into Africa and Asia. Many called it the French disease. The French called it the Italian disease. Arabs called it the Christian disease. Today, it is called syphilis.

The sensational debut of syphilis inspired centuries of debate. Some have argued that Columbus's crew brought the disease from the New World to Europe; others say the disease existed unrecognized for centuries in the Old World before turning virulent. This week in the journal *PLoS Neglected Tropical Diseases*, a team of researchers argues that neither hypothesis is correct. Syphilis originated as a milder, nonsexual disease in the New World, they say, and it evolved into its current form after Europeans arrived. Among the evidence they offer is a mysterious disease restricted to an isolated tribe in a South American jungle. Its DNA, they argue, reveals that it is a kind of protosyphilis.

The disease was discovered in 1999 by a team of Canadian doctors who travel each summer into remote jungles in Guyana to provide medical care to the Akwio tribe. Michael Silverman, a clinician at the University of Toronto, noticed that some of the Akwio children had open sores on their arms and legs.

To Silverman, it seemed like a combination of two diseases, syphilis and yaws. The former, caused by bacteria known as *Treponema pallidum pallidum*, produces open sores. But it is spread through sexual contact and forms sores around the genitals. Another strain, *T. p. pertenue*, causes yaws, which is spread by skin contact rather than sex and produces sores on the limbs. But the Guyana disease was not quite like yaws either. That disease causes raspberry-like eruptions, not the open sores the doctors saw. "I thought, 'This is bizarre,'" says Silverman.

The following year, Silverman and his colleagues proved that the disease was caused by a

form of *Treponema*, which infected about 5% of the children in the tribe. They began treating them with penicillin. Just before boarding a flight for his 2005 mission, Silverman got a call from Kristin Harper, a graduate student at Emory University in Atlanta, Georgia. She was sequencing DNA from every known strain of *Treponema* and asked him to get her some from Guyana.

Harper thought genetic analysis could shed new light on the origins of syphilis. Until recently, the debate revolved around bones, which can be scarred by syphilis. Some researchers claimed to have found lesioned bones of Europeans who lived centuries before Columbus's voyages; others dismissed those findings as inconclusive.

Harper and her colleagues hoped to reconstruct the evolution of different strains

of a strange *Treponema* strain in Guyana sat on a relatively young branch, suggesting that yaws had been carried into the New World by the first immigrants some 12,000 years ago, and that the Guyana strain evolved there. It shares a close ancestry with all strains of syphilis. The relationship also suggests that the Guyana strain is a transitional form that had already acquired some of syphilis's traits, such as the open sores.

In this form, the bacteria could move easily through skin contact, because its hosts wore little clothing. But once the bacteria infected the more heavily clad European explorers, the researchers speculate, it may have had to find a new route of transmission. "You bring in the Europeans who only touch skin when they have sex, and it takes off as a venereal disease," Silverman says. For reasons scientists don't yet understand, the pathogen also evolved into a far more dangerous form that could trigger an epidemic in Europe.

John Logsdon, an evolutionary biologist at the University of Iowa in Iowa City, praises the research but doesn't think it offers definitive proof of where syphilis came from. "There's very little data to distinguish between the hypotheses," he says. The new evolutionary tree is based on variations at only four sites in the *Treponema* DNA, which Harper agrees is a small number. One reason the data are so sparse is the challenging work conditions in the jungles of

Guyana, where Silverman preserved samples in unrefrigerated alcohol—far from the ideal way to keep DNA from degrading.

Logsdon and Harper agree that the best way to test the new hypothesis would be to draw another evolutionary tree based on the entire genomes of the strains. But that may not be possible, as Silverman and his colleagues have not been able to get any more DNA from the Guyanese strain. On subsequent missions, they failed to find anyone infected with it. It appears that they have eradicated the disease. "We're still looking for one more case," says Silverman.

—CARL ZIMMER

Carl Zimmer is the author of *Microcosm: E. coli and the New Science of Life*, to be published in May.



Taking the cure. Whatever its origins, syphilis hit the Old World hard. This illustration shows a man being treated with a concoction made from the *Guaiaecum* tree.

of *Treponema* by comparing their DNA. But gathering the DNA was difficult. Although syphilis is common, the other strains are rare, and none can be cultured easily outside its human host. To get the DNA samples, Silverman dipped swabs into sores, preserved them in alcohol, and sent them to Harper, who extracted fragments of *Treponema* DNA. Months later, Silverman got a call from Harper. "She said, 'You found the origin of syphilis!'" he recalls.

When Harper and colleagues used the variations in the *Treponema* DNA to draw an evolutionary tree, the deepest branches belonged to samples of yaws from the Old World. Newer forms of yawslike diseases emerged from the ancestral bacteria. The

EPIDEMIOLOGY

Calculating Iraq's Death Toll: WHO Study Backs Lower Estimate

A team led by the World Health Organization (WHO) has produced a new estimate of the number of Iraqis who died violently in the first 40 months following the U.S.-led invasion: between 104,000 and 223,000. This figure, published online last week by the *New England Journal of Medicine*, hews close to some other attempts to quantify the toll but comes in far below a controversial 2006 study led by researchers at Johns Hopkins University in Baltimore, Maryland. That group estimated approximately 600,000 violent deaths during the same period. The discrepancy has prompted critics to renew their charge that the Johns Hopkins results are not credible.

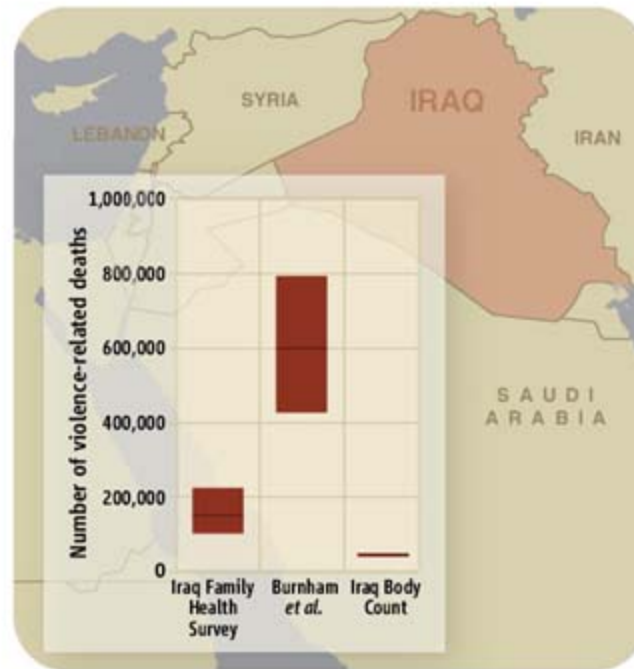
Data from a war zone are never fully reliable; the best researchers can hope for is "getting the numbers roughly right," says Fritz Scheuren, a statistician at the University of Chicago in Illinois and past president of the American Statistical Association. Escalating violence in Iraq after 2003 put a limit on quality control, but researchers do have a quantitative starting point: the casualty tally made by Iraq Body Count, a non-profit advocacy group based in London. By controlling for multiple accounts of the same car bombs and shootings, the group estimates from media reports that between 81,000 and 88,000 violent deaths have occurred in Iraq since the invasion. The figure is useful as "a lower bound on the true number," says Jon Pedersen, a statistician at the Fafo Institute for Applied International Studies in Oslo, Norway.

To get the upper bound, says Pedersen, you have to knock on doors in what is known as a two-stage cluster survey. That's the method used by the WHO and Johns Hopkins teams, among others. Researchers divide the country into regions and then sample clusters of households within each. Finally, they extrapolate mortality rates from those clusters to the total population.

Epidemiologists Les Roberts and Gilbert Burnham of Johns Hopkins published the first Iraq cluster study in November 2004 in *The Lancet*. They used data collected by Roberts and an Iraqi team, which, in September 2004, surveyed 988 households in 33 clusters across the country. They arrived at a figure of 98,000 "extra" deaths since the invasion, about half due to violence. Soon after this, a team led by Pedersen and the

United Nations Development Programme, which had used a much larger sample of 21,668 households in 2200 clusters, produced an estimate for roughly the same period of about 25,000 violent deaths.

As the invasion gave way to occupation and insurgency, Roberts and Burnham



Human cost. The WHO-led Iraq Family Health Survey estimated as many as 223,000 deaths since the Iraq invasion, far fewer than a survey by Burnham and Roberts estimated.

mounted another study. This time they left the surveying entirely to the Iraqi team, communicating from abroad. Published in October 2006 in *The Lancet*, the second survey—based on 1849 households in 47 clusters—estimated that 601,000 Iraqis died violent deaths between the 2003 invasion and July 2006. To many, the number seemed unrealistically high. Some also faulted the authors for not fully answering questions about the survey's methods (*Science*, 20 October 2006, p. 396).

Now comes the WHO survey. Conducted with the help of the Iraqi government, it is by far the most comprehensive mortality assessment to date. Interviewers visited 9345 homes in more than 1000 clusters. But its estimate of 151,000 violent deaths has come in for some criticism, too. Unlike other Iraq casualty surveys, this one includes an upward adjustment of 35% to account for "underreporting" of deaths due to migration, memory lapse, and dishonesty. "That is

really an arbitrary fudge factor," says Debarati Guha-Sapir, an epidemiologist at the WHO Collaborating Centre for Research on the Epidemiology of Disasters in Brussels, Belgium. But the number falls squarely within the range produced by a meta-analysis of all available mortality studies by Guha-Sapir and fellow centre epidemiologist Olivier Degomme. The Johns Hopkins figure is an outlier, she says.

Why the Hopkins study came up with such a high figure is not clear. Criticism of the study has in fact intensified since Burnham and Roberts released a data set to selected peers last year. "It did not include the standard kinds of data," says Seppo Laaksonen, a statistician at the University of Helsinki in Finland and a specialist in survey methodology. For example, he says, it was impossible "to check the objectivity and randomness of cluster selection." Scheuren, who also received the data, wanted to compare results obtained by different interviewers to "get a handle on noise" and check for fabrication by surveyors. Roberts declined to provide all the details, according to Scheuren, saying that he was concerned that this would risk the safety of the interviewers.

Burnham told *Science*, however, that the Johns Hopkins team does not have such detailed information. "Our goal was to reduce any type of risk to the community and the participants," says Burnham. "While we have much of the raw data, we requested that anything designating the interviewers or the location of the neighborhoods visited not be sent to us." Laaksonen responds that he would not have published "any figures for the country" if he didn't have direct access to such raw information from surveyors.

Burnham is not retreating. Because the WHO survey was conducted by Iraqi government personnel, "people may have been hesitant to answer honestly," he says. He claims that unlike those in the WHO study, nearly all of the deaths tallied by the 2006 *Lancet* study were verified with death certificates. Even if the debate may be drawing to a close about whether the number of violent deaths in postinvasion Iraq could be as high as 600,000, the argument about methods is clearly far from settled.

—JOHN BOHANNON

Gene Tests for Psychiatric Risk Polarize Researchers

A small California company is the first to venture into psychiatric gene testing. But is the science ready?

SAN DIEGO, CALIFORNIA—Starting a biotechnology company was not part of John Kelsoe's life plan. A respected psychiatric geneticist here at the University of California, San Diego (UCSD), he has spent 20 years patiently searching for the genes behind bipolar disorder, tracing patterns of inheritance in families from Amish Pennsylvania to Iceland. Kelsoe has now laid this solid reputation on the line: He has founded a company that last year quietly began selling the first gene test to help diagnose people with bipolar disorder, which affects about 1% of the population.

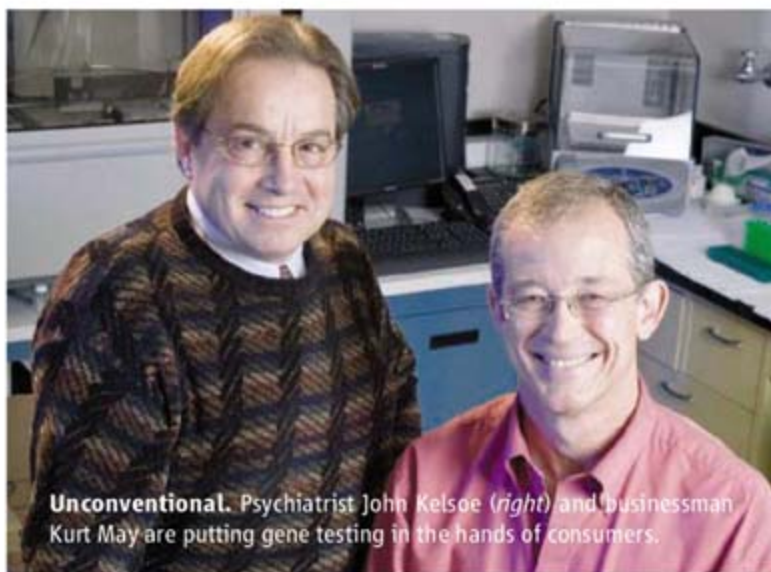
Kelsoe knows well that he is opening himself up to harsh criticism. And it has begun: Francis Collins, director of the National Human Genome Research Institute (NHGRI) in Bethesda, Maryland, was taken aback to learn that a gene test for bipolar disorder was on the market. Being diagnosed with a mental disorder carries "great significance," says Collins, who, like many in the field, thinks a test based on current knowledge is likely to be misleading. In Collins's list of accepted genes for common diseases, "there are no entries" yet for bipolar disorder, he says.

Kelsoe, tall and trim, with the slight stoop of an academic who has spent years in the laboratory, agrees that the genetics of bipolar are still cloudy. But he has grown frustrated with the slow diagnosis and spotty treatment of the disease. On average, 7 years elapse from the onset of symptoms to diagnosis, and patients are misdiagnosed three times. "There is a huge need" for information, Kelsoe says. "As opposed to playing it safe and conservative scientifically, I think we also have to think about our obligation to provide something" for physicians and for patients.

His company, Psynomics, is the first to market a test in psychiatric genetics, but it won't be unique for long. Another company, in Louisville, Kentucky, plans next year to start offering a similar test for schizophrenia. A third, in Boulder, Colorado, will launch a genetic screen to help identify those at risk of suicidal thinking from antidepressants.

Psychiatric genetic testing is only a slice of the fast-expanding genetic testing market, but it arouses fierce emotions. The new gene tests are very different from traditional ones for rare and often fatal diseases like cystic fibrosis, Tay-Sachs, and sickle cell anemia. With these, the cause is not in question: An individual cursed with faulty genes from both parents has a 100% chance of contracting the disease.

Bipolar disorder is another animal entirely. Dozens, perhaps even hundreds of genes may contribute to its onset, along with largely unknown environmental triggers. This makes it similar to heart disease, adult cancer, and type 2 diabetes. Each gene variant may raise risk only slightly—say, from 1% to 2%—meaning that the vast majority of people with these variants never fall ill



Unconventional. Psychiatrist John Kelsoe (right) and businessman Kurt May are putting gene testing in the hands of consumers.

CREDITS (TOP TO BOTTOM): ROBERT ESSEL; NYC/CORBIS; GARY PAYNE/GETTY

Moving target. Many researchers say that early studies linking genes and mental illness need to be replicated.

from that disease. Furthermore, in bipolar disorder, suspect genes are still being uncovered. There's much debate about which findings will endure and which will be picked up once or twice and never seen again.

Because of this uncertainty, not to mention concern about how test results will be interpreted, researchers and ethicists are asking difficult questions. Why test for genes whose science is shaky or that boost risk only slightly? Who will buy these tests? And how will consumers understand and cope with the genetic information they're given?

The genes

The men running Psynomics, including Kelsoe, its chief scientific officer, see themselves guiding this nascent field and carving out an early niche. They also believe, in the words of UCSD business school assistant dean and Psynomics CEO Kurt May, that "we ... don't have to win the Nobel Prize on this one, and we don't have to solve the problem for all time. All we have to do is present a business model that is one better than psychiatry today."

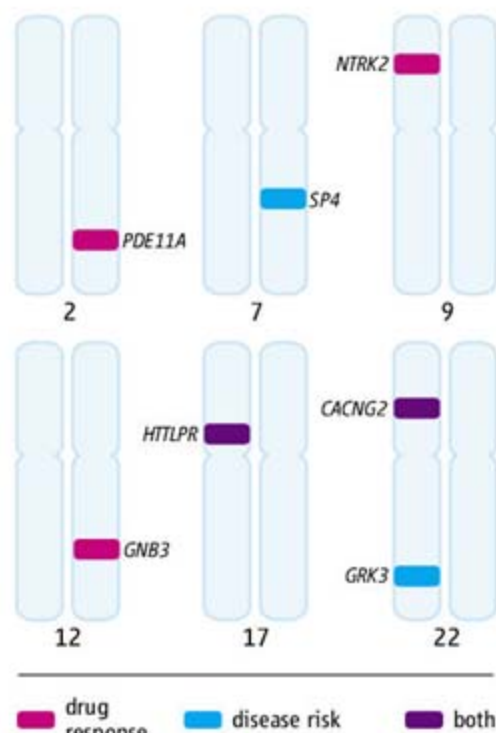
At the heart of that business model is *GRK3*, a gene on chromosome 22 that Kelsoe identified in the late 1990s. In 2003, he reported in *Molecular Psychiatry* that a change in an individual DNA base in *GRK3*, called a single-nucleotide polymorphism (SNP), was associated with about a three times increase in the risk of bipolar disorder in 428 families studied. But the variant was rare, found in only 3% of those with bipolar and 1% of the unaffected.

Since then, Kelsoe has hit on a combination of four SNPs in *GRK3* that together seem to be associated with a doubling of disease risk and are more common. They were found in 15% of bipolar patients (and 5% of those without the disorder) in 181 Caucasian families. That work was published last month. UCSD has filed for global patent protection on both sets of variants and licensed them to Psynomics; Kelsoe will share in licensing fees and any profit. The Psynomics test looks for both *GRK3* variants. It also checks for a publicly available mutation in the serotonin transporter gene, which is believed to influence a person's response to certain antidepressants, often a component of treatment for bipolar disorder.

Does *GRK3* play a compelling role in bipolar disorder? It may or it may not. "It's always possible" that it's involved, but "to

me it seems unlikely," says David Collier, a neuropsychiatric geneticist at the Institute of Psychiatry in London. In December 2006, he published a paper arguing that bipolar I disorder, the more severe of two known forms of bipolar disorder, was not associated with *GRK3* in a sample of 410 patients and controls from Scotland. But Collier adds that because of its relatively small size, his own study "can't be regarded as definitive."

Collier is keeping an eye on genome-wide association studies, which are revolutionizing the genetics of complex disorders such as type 2 diabetes. One of the first whole-genome studies that included bipolar disorder, published last year by the U.K.'s Wellcome Trust Case Control Consortium, did not find *GRK3*; it also failed to find many other genes previously linked to



Expanding. Psynomics expects its test to grow from two genes to seven. Critics say few, if any, genes for bipolar disorder have been validated.

the disease, says consortium member Collier. Although such scans are not designed to pick up every disease gene, some proponents of the whole-genome approach say their confidence in genes identified the old-fashioned way, in large sets of affected families, is declining. Psynomics "is using data from the other side of the bridge, the bad side," says NHGRI's Collins, referring to family linkage studies that have been hard to replicate.

Pablo Gejman, a psychiatric geneticist with Evanston Northwestern Healthcare and Northwestern University in Evanston, Illi-

nois, is leading a project that he hopes can confirm or reject initial schizophrenia gene discoveries: a genome-wide association study of 4500 people with this disease and 4500 without. Results are due out later this year. (Kelsoe is leading a parallel study in bipolar disorder.) Gejman wonders if even larger trials—of 15,000 people, perhaps—will be necessary. This week, he published a paper in the *American Journal of Psychiatry*, reporting that none of 14 previously described schizophrenia genes played a big role in disease risk in nearly 3900 people. "My message," says the native Argentinean, "would be that we need to be patient, [conduct] systematic studies, collaborate, ... and try not to jam too rapidly the gun" by selling genetic tests before the data are solid.

The doctors

Kelsoe acknowledges that *GRK3* may turn out to play a minor role in bipolar disorder, or even no role at all, although he considers that unlikely. No independent group has published a second *GRK3*-bipolar disorder association, but Kelsoe says he knows of two groups, in Israel and in Canada, that have found a link. Meanwhile, in the next 3 months Psynomics hopes to add five more genes to its test, including four that Kelsoe discovered, and then ramp up marketing to physicians and patients. Of the five, three are thought to modulate response to lithium, a mood-stabilizing drug used to treat bipolar disorder; one, *CACNG2*, is considered indicative of bipolar risk and lithium response; and another, *SP4*, has been linked to both bipolar disorder and schizophrenia.

In determining which genes are ready for commercialization, "we've cut kind of a low threshold, and that is replication in at least one independent study," says Kelsoe—either by a different group or his own group examining new samples. "Does make decisions every day on a lot less information" than this.

Gejman and Collins may shake their heads, but psychiatric gene tests are coming. Mark Brennan, founder of SureGene, a schizophrenia-based test company in Louisville, says such tests are "going to happen with or without" his own efforts. Brennan is SureGene's chief scientific officer and a human geneticist at the University of Louisville in Kentucky. His company is designing a risk predictor and diagnostic test around six schizophrenia genes that Brennan discovered. It's good for scientists to get into marketing, he argues, because "we have to step up and make sure it's done in a way that really helps people."

Brennan has so far published informa-

Hoping for a Glimpse of What's Ahead

It's one of the first questions people ask about testing for a gene associated with mental illness: Who would want to know the result? One ready volunteer for testing is Holly Finn, 13, who lives in Grand Rapids, Michigan, with her parents and her 16-year-old sister, Katherine. Holly's mother, Kristin Finn, was diagnosed with bipolar disorder 3 months before her 17th birthday. She says that Katherine began showing signs of depression and difficulty concentrating in the fourth grade. Initially pegged as having attention deficit hyperactivity disorder (ADHD), Katherine received a bipolar diagnosis in July of 2004, when she was 12. It's been a rocky road: Katherine has switched schools three times and suffered taunting from her peers, says her mother, an active member of the Depression and Bipolar Support Alliance in Chicago, Illinois.

Now the younger Finn daughter, Holly, is being treated for ADHD and anxiety. Her symptoms are different from her sister's, and she is not thought to have bipolar disorder. But, Holly says, having witnessed her sister struggle for years, she would welcome testing for a bipolar gene. "I think I might have a chance of having bipolar disorder," says Holly, who writes songs she plays on her guitar to cope with her sister's ups and downs. A test could help her "get to the bottom of" her symptoms, Holly says, or at least prod her and her psychiatrist to keep an eye out for bipolar disorder down the road. "It certainly wouldn't hurt."

But hurt is exactly what many are afraid of. "Some people would say individuals have a right to this information and shouldn't be barred by the medical community from receiving it," says psychiatrist Jinger Hoop of the

Medical College of Wisconsin in Milwaukee, who is studying how people with schizophrenia or at risk for it respond to genetic data. Her work has confirmed what others have seen: Consumers often react favorably to hypothetical genetic knowledge. "But we don't know a lot about what the actual risks and benefits are" of receiving genetic results, Hoop notes. "We really need empirical data to let us know how people would interpret very subtle changes in risk."

One of the few projects tackling this question is the Risk Evaluation and Education for Alzheimer's Disease (REVEAL) study headquartered at Boston University School of Medicine. Neurologist and epidemiologist Robert Green and his colleagues here and at other centers are examining how nearly 700 volunteers with a family history of Alzheimer's disease respond to learning whether they carry a deleterious version of the *APOE* gene. A single copy raises Alzheimer's risk roughly three times, and two copies raise risk 12 to 15 times. "The bottom line is that people do want this information, and they seem to self-select for people who can handle it," says Green. Those "who felt that they couldn't handle such information generally didn't follow through and obtain" their test results.

REVEAL has examined the role of genetic counseling; whether individuals with the hazardous form, called *APOE e4*, are more likely to buy long-term care insurance—they are—and more broadly, what they take away from knowing their *APOE e4* status, especially given that there is no way to stall the onset of Alzheimer's.

One concern, notes Hoop, is that the REVEAL study has found that consumers tend to recall not their numerical risk of disease but whether they

tion on two of the genes, which are on chromosome 22; SureGene is working with outside scientists to replicate the results. The company declines to name them all. But one who agreed to be identified is Herbert Meltzer, a longtime schizophrenia specialist at Vanderbilt University in Nashville, Tennessee. Meltzer, who is on SureGene's advisory board and says he has received company stock, is enthusiastic. "If we proceed and it doesn't look as promising to me as it looks right now, then I'll do my best to keep it off" the market, he promises.

Before launching the SureGene test—slated to happen about 18 months from now—Brennan wants the genes repli-

cated "in at least several hundred samples from different centers." That's far fewer than the thousands Gejman argues are necessary.

Even if the genetic associations he and Brennan have found are small clues, Kelsoe believes that they can still help. One reason for pushing forward, he says, is that patients need information now. Among the veterans he sees at the local VA hospital, a short walk from his UCSD office down paths lined by eucalyptus

trees, are many bipolar patients who have been misdiagnosed and erroneously put on antidepressants alone, which can exacerbate their disease.

"Doctors are operating in constant uncertainty," he says, struggling to find the right diagnosis, the proper recipe of medications. "Not to get snooty about it—it's fine to sit in your ivory tower and say, 'We don't want to offer this until it's perfect.' Meanwhile, that

paying up to \$750 and providing a physician's name. Soon after, a small blue and white plastic container arrives in the mail. The capsule preserves a saliva sample, which the consumer ships to a certified UCSD lab for genetic testing, with DNA results going back to the company. Results also go to the designated physician but not to the consumer.

The process is meant to control who takes the test: Kelsoe has rejected risk test-

ing for individuals who have no symptoms but are curious. For a healthy person, he says, receiving a positive test result could do more harm than good, especially because data from asymptomatic people are lacking. Even so, Kelsoe admits that there are ways to

get around Psynomics's procedures. A bipolar patient, for example, could send in her child's saliva sample and claim it's her own. In the end, predicts May, the market will demand risk testing, and "the market is going to win."

Business has already won out in another facet of the Psynomics test: how the consumer will be advised of the results. Kelsoe says he initially wanted the company to provide individual counseling for clients. After about

Players in the Psychiatric Gene-Testing Business

Company	Test available	Disease	Type of test	Number of genes
NeuroMark	mid-2008	Major depression	Risk of suicidality from antidepressants	4
Psynomics	now	Bipolar disorder	Diagnosis and response to antidepressants	2*
SureGene	mid-2009	Schizophrenia	Risk of psychosis and response to antipsychotics	6

* Psynomics plans to add five more genes early this year.

doctor's down there trying to work with whatever he's got."

The market

Psynomics is not relying much on doctors, however, to help it reach its goal of selling 1800 tests in 2008 and 30,000 in the next 5 years. "This is going to initially be driven by the patients," says Kelsoe, who believes that doctors are wary of a psychiatric gene test. Psynomics allows anyone to order its test by

harbor the “bad” gene. This is a concern in testing for bipolar disorder or any psychiatric illness: People may think that carrying the gene means that they have or will develop the disease. Making this mistake could, among other things, induce stress, which can exacerbate psychiatric disorders.

How much of a boost in risk is meaningful to consumers? The bipolar test from the company Psynomics in San Diego, California, currently includes the gene *GRK3*, which the company says increases risk two to three times.

In someone of average risk, that’s a shift from 1% to 2% or 3%. For an individual with a bipolar parent or sibling, whose baseline risk is about 10%, the increase may be more meaningful—but only if the gene compounds family predisposition.

Another concern is how having such information will alter a person’s life. “To me, the question is not really the risk relationship” between genes and disease, says Wylie Burke, a geneticist and bioethicist at the University of Washington, Seattle. “It’s what are you going to do differently with that information?”



In the family. Kristin Finn (right) and her daughter Katherine (left) have bipolar disorder. Younger daughter Holly wants to know if she carries bipolar genes.

Holly is already contemplating this question. As she grows up and considers having a child of her own, she says, she could imagine testing her son or daughter at about age 2 for genes associated with the disorder so as to be ready to spot it if it surfaces.

Currently, testing of children without symptoms is not available, nor is prenatal testing. Physicians focus instead on stabilizing a woman’s bipolar disorder while pregnant—something that Kristin Finn discussed in her 2007 book, *Bipolar and Pregnant*. But even the skeptics agree

that validated genes for schizophrenia, bipolar disorder, and other psychiatric diseases are likely to emerge soon. “Biotech companies are going to do what they’re going to do within the limits of the law,” says Kay Jamison, a psychologist at Johns Hopkins University School of Medicine in Baltimore, Maryland, who has written extensively about her personal battle with bipolar disorder and who generally supports making gene tests available. It may take years before it’s clear what that means for people with psychiatric illnesses and their families. —J.C.

2 years, he came to see that this was “no longer necessary or practical.” Interpreting and counseling on test results will be up to doctors, who receive a six-page summary noting that “a positive *GRK3* test ... makes a diagnosis of Bipolar Disorder 2–3 times more likely” for individuals with symptoms and a family history.

This is not much help, some say. “I’m in the bipolar disorder genetics field, and I wouldn’t know how to interpret the results of a bipolar genetic test,” says James Potash, director of mood disorders research at Johns Hopkins University in Baltimore, Maryland. Potash, who knows Kelsoe and calls him a “very capable, very solid guy,” says that offering a test now is premature and that doctors cannot be counted on to decode it.

Paradoxically, interpreting the results of Psynomics’s test is likely to grow knottier as the test is refined and more genes are included. Interactions among genes are poorly understood, and many psychiatric disease genes may predispose a person to more than one psychiatric disease. Indeed, even though SureGene has positioned itself in schizophrenia, Brennan notes that its test may be more instructive about psychosis risk generally. Psynomics’s CEO May frames this as an opportunity: “We would like to establish that as a brand, this is the destination for information, for diagnostics, for therapeutics” in psychiatric illness.

Another company, NeuroMark in Boulder, Colorado, has similar ideas. NeuroMark

is designing a pharmacogenetic test for suicidality risk from antidepressants, a side effect for 2% to 6% of those taking the drugs. The company hopes to launch its test, focused on one antidepressant, Celexa, later this year, before extending it to related drugs and developing bipolar and schizophrenia risk tests as well. Then there are broader gene testing companies such as 23andMe in Mountain View, California, which offer information on SNPs behind a host of diseases. Although 23andMe could test for SNPs in depression and other psychiatric illnesses, it would need permission from companies like Psynomics and SureGene to sell information on the SNPs those companies have licensed.

Despite being first in the psychiatric space, Psynomics is very much a work in progress. Only about a dozen people have taken the test so far. The company hasn’t determined how it will follow its clients, although May says it is sending them a satisfaction questionnaire. Meanwhile, Psynomics is hunting for venture capital to tide it over until test sales ramp up.

One critical but unsettled factor is whether Congress will pass the Genetic Information Nondiscrimination Act, which would protect individuals against discrimination by insurance companies and employers based on genetic information. Biotech companies and researchers have lobbied for it for years, but it hasn’t been approved. Another uncertainty is how gene tests will be regulated. For many genetic tests, includ-

ing that offered by Psynomics, regulation consists of lab certification but no assessment of the science behind the test.

“This is a different kind of information” than has been provided in the past, says Boston University neurologist and epidemiologist Robert Green, who studies Alzheimer’s genetics and early detection. “It’s not always clear what it’s telling us.”

Gene testing could be done prenatally, for example, to check for bipolar risk in the fetus. Kelsoe shudders at the thought, especially because bipolar genes are unlikely to guarantee disease: “I think this is very dangerous, scary, eugenics-type stuff, and I don’t want to get anywhere near it,” he says. Kelsoe says his company would refuse to honor such a request. But if the question comes up in the future, the decision may not be his to make.

In Kelsoe’s UCSD office, decorated with his children’s art, a small scrap of paper is taped to his computer. In black ink is scrawled a quote from Virgil: “Fortune Favors the BOLD!” Despite that encouragement, “it’s a little scary,” he says over lunch. “I’ve spent my whole career trying ... to gain people’s respect that I’m responsible and cautious. So the concern is, are they going to think this is irresponsible, am I going to lose credibility because of it?” But then Kelsoe leans in, a wicked grin on his face. “Sometimes,” he says in a low voice, “it’s fun to stir things up.” —JENNIFER COUZIN



◀ **Sacred circle.** Carved central slabs are surrounded by massive monoliths nearly 5 meters tall.

riticated wheats are from this region. “You can make a good case this area is the real origin of complex Neolithic societies.”

If Göbekli Tepe is truly 11,000 years old, it also challenges the idea that symbolism and agriculture were first developed in the Levant—the area that includes modern Jordan, Israel, and Syria—and spread north. “The idea that the origins of monumental architecture were in the south has been turned on its head,” says archaeologist Gary Rollefson of Whitman College in Walla Walla, Washington, and an editor of the journal *Neolithics*. “What Klaus is picking out there now is far earlier than anyone expected. That’s all back on the drawing board now.”

A hunter-gatherer’s paradise

Göbekli Tepe means “navel hill” in Turkish, and at 780 meters high, it seems a natural gathering spot, the highest point for kilometers. The site was first examined—and dismissed—in the 1960s by University of Chicago anthropologist Peter Benedict, who assumed that the flints and broken slabs of limestone littering the area were the remnants of an abandoned medieval or Byzantine cemetery.

Schmidt first visited the hilltop in 1994, after a local farmer had run his plow into a rectangular piece of limestone. Schmidt found not a gravestone but the top of a large, buried pillar, and he quickly recognized that the scattered flint tools on the surface resembled those from nearby sites that pre-date pottery. As he began digging, the mystery grew. He uncovered one huge, elaborately carved ritual structure after another, but no houses or signs of settlement. The people who built the monuments apparently backfilled them thousands of years ago, and the bones that turned up in the loose fill were all from either humans or wild animals, not from domesticated animals.

So just how old are the monuments? Because most of the bones found are from backfill, dating them yields muddled results, and Schmidt has fewer than two dozen direct radiocarbon dates. Instead, he chiefly relies on comparing the stone tools and other artifacts with those from sites with more radiocarbon dates. This relative

ARCHAEOLOGY

Seeking the Roots of Ritual

In the hills of Turkey, researchers are slowly uncovering the world’s oldest monumental structures, strange monoliths built by hunter-gatherers perhaps 11,000 years ago

GÖBEKLI TEPE, TURKEY—Dawn was still half an hour away when Klaus Schmidt arrived at his hilltop dig site here, but a half-dozen workers from a nearby village were already waiting for him. It was the end of the dig season, and the enthusiastic, white-haired German was there for one last look. He picked his way down steep excavation layers toward a massive, T-shaped slab of rock rising 3 meters out of the ground.

The gentle light of dawn illuminated more T-shaped limestone megaliths and then still more, arranged in circles and ovals down the hillside. Some were carved with stylized arms; on others, a carved menagerie of snakes, spiders, boars, foxes, birds, and other beasts crawled and soared.

Schmidt, of the German Archaeological Institute (DAI) in Berlin, claims that these are the world’s oldest monumental structures, which he has painstakingly uncovered since 1995 (see sidebar, p. 280). Radiocarbon dating and stone tool comparisons indicate that they are 11,000 years old. So these great stone circles were erected before metalworking, before pottery, before the domestication of animals, even before most signs of agriculture.

Although people began painting in caves thousands of years earlier, Göbekli

Tepe, in southeastern Turkey, “is the first manmade holy place,” says Schmidt. He and others say that the site upends traditional notions about the development of symbolism. Archaeologists once hypothesized that agriculture gave early people the time and food surpluses that they needed to build monuments and develop a rich sym-



bolitic vocabulary. But Göbekli Tepe raises the alternative possibility that the need to feed large groups who gathered to build or worship at the huge structures spurred the first steps toward agriculture. “This shows sociocultural changes come first; agriculture comes later,” says archaeologist Ian Hodder of Stanford University in Palo Alto, California, who notes that the first domes-

dating puts the early layers at Göbekli Tepe in the beginning of a distinctive period called the Pre-Pottery Neolithic B, dated elsewhere to about 11,000 years ago. Although the dates aren't precise, the artifact comparisons are convincing, and a few hundred years of fudge time "don't really matter," says Harvard University archaeologist Ofer Bar-Yosef.

Although the site may predate systematic agriculture, the people who carved these pillars faced no shortage of resources. Animal and plant remains suggest that 11,000 years ago this place teemed with gazelle, aurochs, and deer. Groves of fruit and nut trees lined the rivers, and flocks of migrating birds paused here regularly. "It must have looked like a paradise, ideal for hunter-gatherers," says Angela von den Driesch, an emeritus archaeozoology professor at Ludwig Maximilian University in Munich, Germany, who has classified animal remains at the site. The region was so rich that people could have settled down while still supporting themselves with hunting and gathering; archaeologists have found such villages within 160 kilometers of the site.

Von den Driesch is one of a number of archaeologists, plus a revolving cast of eager German students and about 60 local workers, who excavate the site for 4 months each year. They drive to the site before dawn to dig, returning in the afternoon to a traditional, high-walled compound Schmidt owns in the middle of Urfa's old city. One day last fall, a dozen students quietly sorted and weighed bone fragments and artifacts in the compound's courtyard as the afternoon cooled into evening. It's a surprisingly unpretentious operation, given the imposing nature of the site and the roughly \$300,000 in funding Schmidt receives each year from DAI and the German Research Foundation.

Clearing a space at a long table, Schmidt pulled out a mottled, purple schematic of the site—a sort of bird's-eye x-ray put together after a ground-penetrating radar scan in 2003. The excavated portion—3500 square meters, just 5% of the 9-hectare site's total—was represented by a white square. All around it, the scan revealed oval groups of buried monoliths dotting the hillside like dark-purple bomb craters.

Schmidt says there are at least 20 ceremonial structures still underneath the soil, and perhaps more. "It's much more complex and advanced than we thought," he says. "Clearly, they could communicate with each

other and organize something really complicated. I didn't expect hunter-gatherers could or would build something like this."

The most spectacular ritual space, which encompasses features seen at the others, is nestled in the dig's western corner. Two 5-meter-tall, T-shaped pillars stand in the center of a circle of slightly smaller slabs, each weighing an estimated 5 to 7 tons. Parallel lines carved into the slabs' sides slant back in a V and meet at the narrow front edge like clasped hands, suggesting a stylized person. The two central stones face the valley, and the surrounding pillars face

inward toward the center of the circle. In sharp contrast to the stylized human shapes, the sides of the slabs are carved with images of animals: complex arrangements of spiders and snakes, foxes and wild boars, vultures and cranes.

There's no way to know for sure what these figures meant, but there are some clues. Schmidt says the lack of female symbolism largely rules out fertility rituals. And the contrast between the designs carved on the pillars and bones that litter the backfill seems meaningful. The backfill yields gazelle, aurochs, red deer, boar, goats, sheep,

oxen—all wild—plus a dozen different bird species, including vultures, ducks, and geese. Yet the pillar carvings are dominated not by prey but by more dangerous creatures: leopards, lions, foxes, and vultures, plus spiders, snakes, and scorpions. "The symbology is dominated by nasty animals," says Stanford's Hodder. "It's a scary, fantastic world of nasty-looking beasts."

The cathedral on the hill

So what was this place? Schmidt is adamant about what it's not, although not everyone agrees with him. Despite the site's size, and the contemporary villages not far away, Schmidt insists this was no settlement. He's convinced that the circles were designed to be open to the sky, like Stonehenge. Telltale signs of settlement—such as hearths, trash pits, and small fertility figurines—are conspicuously absent. And the hilltop is a long hike from any water sources. "We know what settlements from these times look like," Schmidt says. "This isn't one of them." Instead, Schmidt argues that hunter-gatherers from across the region gathered here periodically, pooled their resources temporarily to build the monuments for some ritual purpose, and then left.

Rollefson and others see that as unlikely, arguing that the scale of the site would have required at least a small group of year-round residents. "To have this kind of magnet out in the middle of nowhere would be unprece-



Peering into the past. Klaus Schmidt (*top*) uncovered pillars carved with frightening beasts like this lion.

Just Don't Call It the Garden of Eden

URFA, TURKEY—From his one-man booth at the Urfa bus station, tourist official Serdar Avcı spends his days handing out maps to the sights around this Turkish city. To his dismay, one destination is conspicuously missing from the tourist guides: Göbekli Tepe. "People want to come here to see these temples, but Klaus Schmidt is digging so slow!" Avcı says. "How many years do we have to wait to go inside? This is a big problem, I think."

Everyone in this city of almost a million people seems to know Schmidt's name and have an opinion about his work excavating the world's first monumental architecture (see main text). Schmidt's progress is charted by regular reports in the local papers, and a 2006 cover story in the German weekly *Der Spiegel* speculated that the site might be linked to the biblical Garden of Eden. Much to Schmidt's dismay, Turkish papers picked up the story, and the ensuing debate about whether the site was the birthplace of Adam—considered a Muslim prophet—briefly threatened to derail further excavation on religious grounds.

Schmidt has been assigned a full-time monitor from the Turkish Ministry of Culture and Tourism in Ankara to make sure he sticks to a preapproved dig plan

submitted months in advance. Colleagues say the notoriety has made it difficult for him to run the small, controlled dig he'd like. "He's always under pressure from the Turkish government," says colleague Gary Rollefson of Whitman College in Walla Walla, Washington. "He's whipsawed back and forth. If he digs too fast, he's accused of not paying attention to detail. Too slow, and there's pressure for him to get something for tourists to see."

As the site's fame spreads beyond Urfa, tourism may become Schmidt's biggest concern. Together with Turkish authorities, he's developing plans for a tourist center that would house replicas of the site's striking T-shaped pillars and spectacular carvings, to take pressure off the excavators and bring money to the impoverished village nearby. Construction may begin next year.

But with funding hard to come by, a finished facility is years away. In the meantime, tourists find their way to the dig even without Avcı's helpful directions—about a busload of them every other day. One day this fall, 11 buses full of German retirees rolled up in a cloud of dust. Schmidt assigns a student to show visitors around or sometimes does guide duty himself. "As archaeologists, we're not used to attention like that," says Julia Wagner, an excavator and student at the Free University of Berlin. "Working at the site every day, you forget a little how important it is." **—A.C.**

ded. There would have to be so much work to carve these pillars," he says. Indeed, Schmidt says molding and carving a single pillar would have taken months.

Some say it's just a matter of time before evidence of settlement shows up. "They haven't found much human habitation, but they will," predicts Bar-Yosef. "It's impossible to have such a large site without people there to take care of it." Schmidt acknowledges there must have been a few people—"personnel," he says—but insists the site was exclusively a ritual destination rather than a settlement, which would make it unique for this period.

And researchers agree that Göbekli Tepe was a convergence point. "Certainly it was a major focus for regional celebrations or ritual activity," says Rollefson. There are hints of a regional culture: The symbols found at Göbekli Tepe are echoed at similarly aged villages hundreds of kilometers to the south in Syria, such as one called Jerf el-Ahmar, and at slightly younger sites closer to hand in Anatolia, such as Nevalı Çori. But Göbekli Tepe is clearly the grandest site and the oldest of such magnitude. "Göbekli Tepe's really the only one with that megatemple approach," says Rollefson. "After it was built, quite a few sites with the same architecture and iconography and style appeared." Schmidt agrees: "Here we have the religious center for settlements at least 50 kilometers away," he says.

"Those were village churches; this is the cathedral on a hill."

Schmidt argues that the site's antiquity and the lack of domesticated animal and plant remains is strong circumstantial evidence that symbolism and religion led to agriculture and domestication, not the other way around. "Developing from hunter-gatherers to farmers happened here and spread south," Schmidt says. "Not just architecture and monumental architecture, but turning wild animals into domestic livestock happened here. This is the starting point for a whole front of innovation." Indeed, the region is home to a number of domestication "firsts," including the first domesticated wheat, which emerged only 30 kilometers away at Nevalı Çori about 500 years after the Göbekli monuments were built. "Its real

importance is that it's early and large and symbolic a long time before agriculture," says Hodder of the site.

But there are claims of domesticated rye in Syria as far back as 13,000 years ago. And many researchers think people planted wild crops for a long period before actual domesticated varieties appear (*Science*, 29 June 2007, p. 1830). Bar-Yosef notes that there's no evidence to rule out farming in this area at this time, complicating the vision of a hunter-gatherer paradise. "There's no reason to assume the builders were simple hunter-gatherers," he says. "People can be planting wild foods."

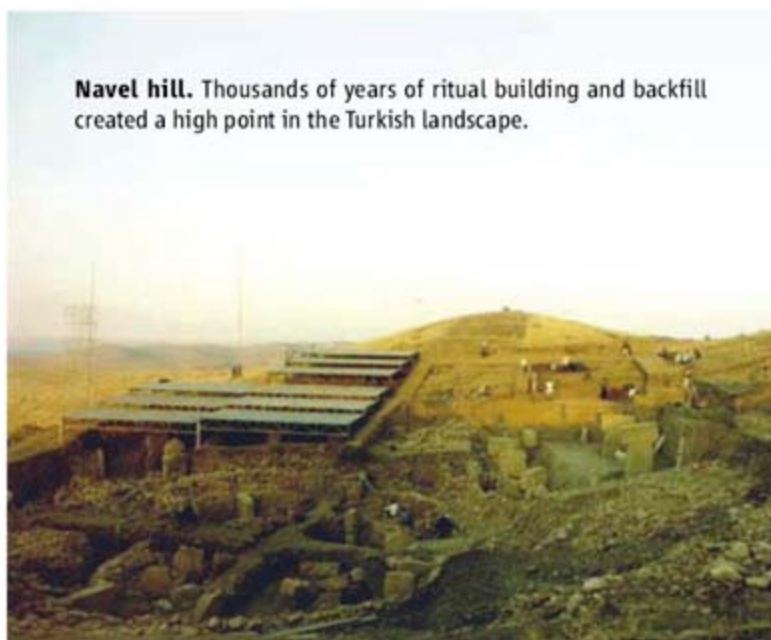
Bar-Yosef is also eager to have more context about the larger society that produced the site. How big did the tribe need to be to support such an intense process? "And in a simple American way," he asks, "who paid for it all?"

Schmidt, mindful that future archaeologists may develop better techniques, refuses to be rushed. At 53, he's got 12 more years of digging until he retires, and he envisions the site's excavations lasting another half-century. Mindful of archaeology's destructive nature, he's carefully leaving something for future excavators. "The idea is not to excavate the entire settlement. The idea is to excavate as little as possible," he says. "We just have to have enough to be sure we understand what was really going on at the site."

—ANDREW CURRY

Andrew Curry is a writer based in Berlin.

Neval hill. Thousands of years of ritual building and backfill created a high point in the Turkish landscape.



Developmental organizers

288



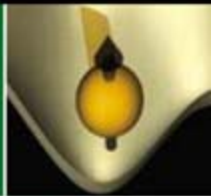
Costs of mangrove conversion

290



Magnetism at the atomic scale

292



LETTERS | BOOKS | POLICY FORUM | EDUCATION FORUM | PERSPECTIVES

LETTERS

edited by Jennifer Sills

Conservation with Sense

WITH HABITAT LOSS AND DEGRADATION OCCURRING AT AN UNPRECEDENTED rate, the protection of imperiled ecosystems has become a priority in conservation efforts (1). Amidst the urgency to conserve wildlife, we propose a word of caution: Relying on the human perceptual world, instead of the sometimes very different perceptual worlds of animals, may compromise conservation endeavors.

Humans have traditionally relied on anthropogenic senses to understand the animals' "world." In fact, our perceptual fields differ profoundly from most animals. Many animals possess unique sensory systems [such as echolocation (2), electroreception (3), magnetoreception (4), and thermoreception (5)] or familiar senses with unfamiliar properties [such as polarization (6) and ultraviolet (7) vision, and infra- and ultrasound (2)].



A different view. Less familiar sensory systems, such as polarization vision in the dragonfly (*Rhodothemis* sp.), should be taken into account in conservation efforts.

Little is known about the way that human-driven habitat degradation affects animals. For instance, changes in ambient light and microhabitat from deforestation or other habitat disturbance can affect the behavior of animals

that rely on vision (8–10), sound (2), or olfaction (11). Sensory systems that influence habitat choice and behavior of nocturnal and crepuscular animals require further exploration. For example, our previous assumptions that nocturnal animals lacked color vision (12) and camouflage colorations (13) have been proven wrong.

The adoption of conservation informed by sensory ecology is clearly needed to decipher optimal habitats and to mitigate the effects of habitat alterations. This approach is vital not only to conservation, but also to behavioral ecology, animal husbandry, and forestry.

MATTHEW L. M. LIM,¹ NAVJOT S. SODHI,¹ JOHN A. ENDLER²

¹Department of Biological Sciences, National University of Singapore, 117543, Singapore.

²Animal Behaviour Research Group, School of Psychology, Washington Singer Labs, University of Exeter, Exeter EX4 4WG, UK.

References

1. Millennium Ecosystem Assessment, *Ecosystems and Human Well-Being: Synthesis* (Island Press, Washington, DC, 2005).
2. L. F. Baptista, S. L. L. Gaunt, in *Behavioral Approaches to Conservation in the Wild*, J. R. Clemmons, R. Buchholz, Eds. (Cambridge Univ. Press, Cambridge, 1997), pp. 212–242.
3. H. Scheich, G. Langner, C. Tidemann, R. B. Coles, A. Guppy, *Nature* **319**, 401 (1986).
4. F. J. Diego-Rasilla, R. M. Luengo, J. B. Phillips, *Behav. Ecol. Sociobiol.* **58**, 361 (2005).
5. A. L. Campbell, R. R. Naik, L. Sowards, M. O. Stone, *Micron* **33**, 211 (2002).
6. T. W. Cronin *et al.*, *Integ. Comp. Biol.* **43**, 549 (2003).
7. M. J. Tóvée, *Trends Ecol. Evol.* **10**, 455 (1995).
8. J. A. Endler, in *Behavioral Approaches to Conservation in the Wild*, J. R. Clemmons, R. Buchholz, Eds. (Cambridge Univ. Press, Cambridge, 1997), pp. 330–356.
9. U. Candolin, T. Salesto, M. Evers, *J. Evol. Biol.* **20**, 233 (2007).
10. O. Seehausen, J. J. M. van Alphen, F. Witte, *Science* **277**, 1808 (1997).
11. H. S. Fisher, B. B. M. Wong, G. G. Rosenthal, *Proc. R. Soc. London Ser. B* **273**, 1187 (2006).
12. E. Warrant, *J. Comp. Physiol. A* **190**, 765 (2004).
13. E. J. Warrant, *Curr. Biol.* **17**, R209 (2007).

Scientific Meetings: Worth Attending

AS AN OCEAN SCIENTIST CONCERNED ABOUT ocean acidification and other environmental impacts from carbon emissions, I was interested to read B. Lester's News Focus story "Greening the meeting" (5 October 2007, p. 36) for ideas on how scientists can reduce the carbon footprint of our professional activities. I thought his aim was off-target, however, when he set his sights on the Fall Meeting of the American Geophysical Union (AGU). This is the one time of the year that an international group of scientists from all fields relevant to climate science share their

as-yet-unpublished results. Furthermore, the Fall AGU Meeting saves carbon dioxide, time, and money by eliminating the need for over 100 other separate gatherings (agency town halls, committee meetings, and workshops). In addition, more than 70 AGU committee meetings take place at the Fall Meeting, and it is an important venue for communicating with the press, including reporters from *Science*! Indeed, we all need to look for ways to reduce our carbon emissions, but there are other ways to do it that don't sacrifice the unique contribution we can make to solving the problem as professional scientists.

MARCIA MCNUIT

Monterey Bay Aquarium Research Institute, Moss Landing, CA 95039-0628, USA.

Scientific Meetings: Call In Instead

B. LESTER'S NEWS FOCUS STORY (5 OCTOBER 2007, p. 36) highlights one major plague affecting modern science: There are far too many meetings in faraway, upscale places. It is especially ironic that we in the science community, who are so familiar with modern communication tools, have failed to take full advantage of this technology.

For nearly a decade, when invited to give a lecture, I have excused myself from international travel (even with all expenses and honorarium paid!). Instead, I provide my lecture in PowerPoint with voice and take live

AAAS Travels

Come explore the world with AAAS this year. You will discover excellent itineraries and leaders, and congenial groups of like-minded travelers who share a love of learning and discovery.



Agean Odyssey

May 14-28, 2008

With optional Istanbul Extension to May 31

Experience a classic adventure with **Dr. Ken Sheedy**. Explore Athens, Delphi, Delos, Santorini & Knossos. \$3,895 + 2-for-1 air from JFK + ext.

Wild & Prehistoric France

May 23-June 5, 2008

Explore prehistoric sites in Haute Provence, the Massif Central, and the Dordogne. See spectacular gorge country, remote villages, and images of great cave paintings at Lascaux II. \$3,695 + air.



Tibet Eclipse

July 17-August 3, 2008

Discover Lhasa, historic center of the Tibetan world, including Jhorkang Temple, the winter palace, and Ganden Monastery. Explore the high plateau and Namco Lake, and the cradle of Tibetan civilization. Take the train to Lanzhou. Fly to see the Total Solar Eclipse. \$4,495 + air.

Xinjiang & Hunza

September 7-24, 2008

This fall explore the northern Silk Road, including the oasis cities of Urumqi and Kashgar in northwest China. Visit the Hunza Valley of far northern Pakistan which is encircled by peaks of the Karakoram range. \$3,895 + air.



Backroads China

October 3-19, 2008

With **FREE Angkor Wat Ext.** (+ air) Join our guide **David Huang** and discover the delights of Southwestern China, edging 18,000-foot Himalayan peaks, the most scenic and culturally rich area in China. \$3,695 + air + ext.



Call for trip brochures & the Expedition Calendar

(800) 252-4910

AAAS Travels

17050 Montebello Road
Cupertino, California 95014

Email: AAASinfo@betchartexpeditions.com
On the Web: www.betchartexpeditions.com

LETTERS

questions on a telephone (from Singapore or India or Europe). It works extremely well, and the hosts love it. They save a lot of money and get to keep the CD, copy it, and pass it around all the local universities. I keep the carbon credits and the time.

I await a position paper from AAAS on this subject!

RUSTUM ROY

The Pennsylvania State University, University Park, PA 16802, USA.

Putting a Human Face on Energy Usage

IN THE NEWS FOCUS STORY, "GREENING THE meeting" (5 October 2007, p. 36), B. Lester compares the fossil fuel energy required to transport scientists to and from a conference by airplane to the energy used by "2250 Honda Civics during a year's worth of normal driving." Another way to put a human face on fossil energy usage is to think in terms of "Virtual Persons" (VPs).

One VP represents 100 watts of average annual fossil energy usage, which corresponds to the nominal dietary energy of one healthy person: 2000 calories per day (96.9 watts). Dividing the world average energy use rate of ~13-trillion watts by 6.5-billion humans gives 2000 watts per person, or 20 VPs. This means that, on average, each living person is, from an energy point of view, equivalent to 20 people.

Of course, energy usage is not distributed evenly. For the United States, the ratio of energy use to population works out to ~115 VPs per person. It is as if each American has the physical power of 115 people. Each European has about half the VPs of each American. If you subtract Americans and Europeans and their energy usage from the world total, each of the remaining human beings has only ~13 VPs, on average.

The 115 VPs of each American are used for heating and cooling, cooking, personal transport, food production and delivery, lighting, and computers. Averaged over a year, one round-trip flight from Washington, DC, to

London works out to ~4 VPs [assuming 70 passenger-miles per gallon]. Domestic utility usage in a 2000-square-foot house (without air conditioning) in Chevy Chase, Maryland, comes to 60 VPs, shared among those who live there. A 100-watt computer that operates year round is about 3.5 VPs (the "energy rate" of the fuel burned to generate and deliver 100 watts of electric power is about 350 watts). A 20-mpg SUV that goes 10,000 miles in a year is ~20 VPs.

ROBERT BURRUSS

6726 Fairfax Road, Chevy Chase, MD 20815, USA.

Fair Game for Chimpanzees

RECENTLY, JENSEN *ET AL.* ("CHIMPANZEES ARE rational maximizers in an ultimatum game," Reports, 5 October 2007, p. 107) contributed to the debate on the origins of cooperation and fairness by reporting that in a modified version of the ultimatum game, chimpanzees fail to act fairly. In the ultimatum game, the human responder refuses to play if the proposer offers too small a share. Generally, the proposer takes this into account by making fair offers. Given that the responder chimpanzees willingly accept all types of offers (even those that a typical human player would deem unfair), we suggest that the chimpanzee proposers have no motivation to play fairly instead of acting as rational maximizers.

Picture yourself in the position of a captive chimpanzee with a history of little control over the availability of food in terms of timing, quality, and quantity. Why, when paired with a group member in the ultimatum game, should you expect that refusing an inequitable offer influences the outcome of later trials? Only by repeated experience could you learn this. But the chimpanzees tested by Jensen *et al.* apparently suffer from a sense of powerlessness, as they accepted all offers, including zero food over 33% of the time. Now, picture yourself in the position of a proposer chimpanzee facing a responder that accepts your offer regardless of how uneven it is. Why should you not be greedy, or learn to be so? We argue that being greedy is a likely consequence of interacting with a compliant partner: The two attitudes feed off each other. In short, do the results really inform us about chimpanzees' sense of fairness, given such compliant partners?

Regarding the recent rise of articles concerning fairness and inequity aversion in non-human primates (1-4), we note that there is another explanation for why chimpanzees should not consider themselves as equals that deserve fairness. Valuing fairness to others is a rather recent human moral principle, at least in Western cultures, grounded in the theoretical

Letters to the Editor

Letters (~300 words) discuss material published in *Science* in the previous 3 months or issues of general interest. They can be submitted through the Web (www.submit2science.org) or by regular mail (1200 New York Ave., NW, Washington, DC 20005, USA). Letters are not acknowledged upon receipt, nor are authors generally consulted before publication. Whether published in full or in part, letters are subject to editing for clarity and space.

stance—expressed by French Enlightenment philosophers—that people are equal.

ELISABETTA VISALBERGHI¹ AND
JAMES ANDERSON²

¹Istituto di Scienze e Tecnologie della Cognizione, Consiglio Nazionale delle Ricerche, 00197 Rome, Italy. ²Department of Psychology, University of Stirling, Stirling FK9 4LA, Scotland.

References

1. S. F. Brosnan, F. B. M. de Waal, *Nature* **425**, 297 (2003).
2. S. F. Brosnan, H. C. Schiff, F. B. M. de Waal, *Proc. R. Soc. London Ser. B* **272**, 253 (2005).
3. P. G. Roma, A. Silberberg, A. M. Ruggiero, *J. Comp. Psychol.* **120**, 67 (2006).
4. S. F. Brosnan, *J. Soc. Just.* **19**, 153 (2006).

Response

E. VISALBERGHI AND J. ANDERSON THINK THAT it is unreasonable to expect chimpanzee proposers to be fair given their captive environment, as in our Report (5 October 2007, p. 107). We feel that this argument is backward. Proposers, including human proposers, are expected to try to maximize personal gains. In the dictator game, in which the responder is powerless (1, 2), humans make selfish offers, but in the ultimatum game, the threat of rejection by the responder drives the proposer to make offers approaching parity

(1, 3). The interesting subject, therefore, is the responder. According to standard economic models of utility maximization, responder rejection of any nonzero offer is not rational because he must forfeit gains to lower those of the proposer. The interesting question then is not to “picture yourself in the position of a proposer chimpanzee,” but to ask why the responder chimpanzee should be insensitive to receiving less than the proposer—a question that is not easily answered through an appeal to captive conditions.

Our captive chimpanzees do not exhibit “learned helplessness” in feeding contexts. For instance, they show a respect for possession (4) when feeding in the group, and they retaliate against others who steal their food (5). Learned helplessness is therefore unlikely to account for acceptance of any food offers. If responders do learn to reject low unfair offers through repeated testing, as Visalberghi and Anderson suggest, this finding would not provide a measure of social preferences. Such a result would suggest instrumental learning—i.e., learning to play a long-term maximizing strategy over repeated interactions—in a testing situation, rather than sensitivity to fairness. In fact, we

found no change in proposer offers or responder rejections across the course of our study. Still, the point of repeated games and reciprocity bears testing, particularly with other chimpanzee populations and more species.

Concerning the second point on fairness and inequity aversion, Visalberghi and Anderson conflate equality with fairness. Norms of fairness do not always dictate equality. Cross-cultural studies [e.g., (6)] suggest that although fairness norms are culturally universal, the absolute values for what constitutes fairness differ widely. Chimpanzees in our study could thus have shown fairness without relying on any sense of equality.

KEITH JENSEN, JOSEF CALL, MICHAEL TOMASELLO

Max Planck Institute for Evolutionary Anthropology, D-04103 Leipzig, Germany.

References

1. C. F. Camerer, *Behavioral Game Theory—Experiments in Strategic Interaction* (Princeton Univ. Press, Princeton, NJ, 2003).
2. A. Falk, E. Fehr, U. Fischbacher, *Econ. Inq.* **41**, 20 (2003).
3. W. Güth, R. Schmittberger, B. Schwarze, *J. Econ. Behav. Organ.* **3**, 367 (1982).
4. H. Kummer, M. Cards, *Anim. Behav.* **42**, 529 (1991).
5. K. Jensen et al., *Proc. Natl. Acad. Sci. U.S.A.*, **104**, 13046 (2007).
6. J. Henrich et al., *Science* **312**, 1767 (2006).

National Institutes of Health Rapid Access to Interventional Development

FREE Drug Development Resources for the Academic/Not-for-Profit Investigator

On a competitive basis, the NIH offers certain critical resources needed for the development of new small molecule therapeutic agents. The NIH-RAID Pilot is not a grant program. Successful projects will gain access to the government's contract resources. Services include: Synthesis in bulk of small molecules; Synthesis of oligonucleotides; Chemical synthesis of peptides; Scale-up production; Development of analytical methods; Isolation and purification of natural products; Pharmacokinetic/ADME studies including bioanalytical method development; Development of suitable formulations; Manufacture of clinical trial drug supplies; Range-finding initial toxicology; IND-directed toxicology; Product development planning and advice in IND preparation. The program also is open to non-U.S. applicants.

Applications are received electronically through Grants.gov. Ideas arising solely from a corporate source without academic collaborators are not eligible.

NIH-RAID Pilot Program Office
301-594-4660; [nih-raid@mail.nih.gov](mailto:.nih-raid@mail.nih.gov)
URL: <http://nihroadmap.nih.gov/raid>



Missing an issue of *Science*? Looking for articles on a specific topic?

You can order *Science* back issues and articles from our website <http://www.sciencemag.org/about/order.dtl> or call the Member Services toll free number 1-866-434-AAAS (2227).



ECONOMICS AND CLIMATE CHANGE

Act Now (But How?)

William F. Ruddiman

A science adviser to the U.K. government foresees the Antarctic as the only habitable continent by century's end. Taking a north-polar view, a prominent environmental scientist suggests that all of humanity will be reduced to a few Arctic breeding pairs. A well-known environmental spokesperson warns that future sea-level rise will drown much of creation. In *Cool It (1)*, Bjorn Lomborg takes aim at this kind of overheated rhetoric on global warming.

Lomborg (an adjunct professor at the Copenhagen Business School) also cites published studies that rebut the one-sided treatment of future climatic impacts on humans by some environmentalists and media sources. He argues that increased economic damage by hurricanes and floods will primarily result from unwise placement of valuable structures along coastlines and in floodplains, rather than from changes in hurricane or flood intensity. He sees the potential effects of spreading tropical diseases negated by improved disease control in increasingly wealthy nations. He predicts that more lives will be saved from reduced cardiovascular deaths during milder winters than will be lost to increased respiratory deaths during hotter summers.

Despite leveling such criticisms, Lomborg accepts the conclusions of the 2007 report from the Intergovernmental Panel on Climate Change (IPCC) that anticipates a sizable (~2°C) warming, a moderate (~30 cm) sea-level rise, and many large but not apocalyptic changes during this century. He notes: "Global warming is happening; the consequences are important and mostly negative." Following his own advice, he has "cooled" (moderated) some of the views he expressed in *The Skeptical Environmentalist (2)*.

Lomborg asks whether it makes more sense committing a relatively large amount of money to try to reduce future global warming by suppressing carbon emissions or spending a smaller amount to deal with many of the problems that currently afflict humans and the environment. He assumes that people and nations will find it difficult to overcome their self-interest and commit to deep carbon-emission sacrifices for a common good that lies mainly in the future.

The book's central message is accompanied by surprisingly good news, which Lomborg documented in (2): most global indices of the human condition (disease, malnutrition, dirty air and water, poverty, infant mortality, and inadequate education) have greatly improved in recent decades as wealth has risen. Because he draws on data from institutions like the United Nations, his compilations are difficult to refute—organizations dedicated to improving human well-being would hardly present an overly optimistic view. Lomborg argues that spending moderate amounts of money to accelerate these positive trends will also, by increasing global wealth, reduce human vulnerability to future warming.

Lomborg's recommendations dovetail with most economic models, which indicate that the most cost-effective way of dealing with global warming is to spend modest amounts reducing carbon emissions now and then ramp up expenditures later, when global wealth is greater. Critics of this cost-benefit approach note that it does not call for a full-scale assault on carbon emissions levels and would allow a major increase in atmospheric CO₂. Lomborg, however, also proposes a sustained tenfold increase in global expenditures on carbon emission-free energy technologies. In effect, he takes up Al Gore's idea of a "generational mission" but proposes a more cost-effective approach.

Some critics have ignored Lomborg's central message and attacked aspects of his treatment of science. At times, he does undercut his credibility by recycling disingenuous arguments from global warming skeptics. For example, he cites evidence of warm Arctic summers several thousand years ago in such a way as to imply that current summer temperatures in the Arctic are nothing unusual. He fails to point out that those earlier warm summers were caused by summer solar radiation levels several percent higher than at present and that the subsequent reduction in radiation had been driving a slow Arctic cooling until humans abruptly reversed the trend during the industrial era. He also implies that a part of the warming in the 150 years since the Little Ice Age ended was natural in origin, but the 2007 IPCC report

concluded that anthropogenic warming dominated (3).

Ecological issues receive relatively little attention in this book. *The Skeptical Environmentalist* upset some ecologists because they felt Lomborg downplayed the threat of biodiversity loss. Yet some of their criticisms conflate the extinctions that will be caused by future large-scale shifts in ecosystems with those underway now because of habitat fragmentation, poaching, overhunting, and overfishing.

Some critics accuse Lomborg of posing a false choice through his implicit assumption that expenditures on human and environmental well-being will remain constant, and several recent developments support that objection. Well-targeted new expenditures from private foundations (e.g., Bill and Melinda Gates and Warren Buffett) and international foundations that integrate small-scale local resources (e.g., the Clinton Global Initiative) have now joined the effort.

Ice sheets are a wild card in projections of future climates. In contrast to the modest sea-level rise that the IPCC predicts for the next century, climate scientist Jim Hansen foresees an oncoming "tipping point" that will cause the irreversible destruction of Greenland ice and a sea-level rise of several meters within a few centuries or less (4). At present, Hansen's fear of total ice-sheet collapse remains a minority view; glaciologists simply do not know how much of the ice cap will melt or when.

Scientists have waited for years for upper-level U.S. politicians to encourage an open debate about the place of global warming in national environmental priorities. Now that such a discussion has begun, it makes no sense to dismiss the thought-provoking arguments Lomborg poses in *Cool It*.

References and Notes

1. Despite having identical full titles, the U.S. and U.K. editions are rather different books. In the U.S. acknowledgments (at the back), Lomborg describes that edition as "a short book on a complex issue" and the London version as "longer ... with plenty of graphs and more explanation." In the U.K. acknowledgments (up front), the Cyan edition is "a long and dedicated book" whereas the Knopf version contains "a text-based summary."
2. B. Lomborg, *The Skeptical Environmentalist* (Cambridge Univ. Press, Cambridge, 2001); reviewed by M. Grubb, *Science* **294**, 1285 (2001).
3. IPCC, "Summary for policymakers," in *Climate Change 2007: The Physical Science Basis: Contribution of Working Group I to the Fourth Assessment Report of the Intergovernmental Panel on Climate Change*, S. Solomon et al., Eds. (Cambridge Univ. Press, Cambridge, 2007).
4. J. Hansen et al., *Phil. Trans. R. Soc. A* **365**, 1925 (2007).

The reviewer is at the Department of Environmental Sciences, Clark Hall, University of Virginia, Charlottesville, VA 22903, USA. E-mail: wfr5c@virginia.edu

ENVIRONMENTAL SCIENCE

Aging Infrastructure and Ecosystem Restoration

Martin W. Doyle,^{1*} Emily H. Stanley,² David G. Havlick,³ Mark J. Kaiser,⁴ George Steinbach,⁵ William L. Graf,⁶ Gerald E. Galloway,⁷ J. Adam Riggsbee⁸

As a result of recent infrastructure failures, particularly the tragic failure of the Interstate-35 bridge in Minnesota, the U.S. Senate passed the National Infrastructure Improvement Act (NIIA), which would create the National Commission on the Infrastructure of the U.S.A. The commission's broad mandate would be to assess the nation's infrastructure and its ability to meet current and future demands. Such policy development coincides with ongoing efforts to manage and restore degraded ecosystems. This provocative intersection of aging infrastructure and environmental degradation provides unprecedented and largely unappreciated opportunities for ecosystem restoration.

Convergence of Phenomena

The United States is at an unusual juncture of three growing phenomena. First is the widespread decay of infrastructure. The 20th century saw rapid growth in population, the economy, and infrastructure (see chart, right). Many structures have been in place for 50 years or more, and an increasing portion of national infrastructure is now approaching or exceeding its originally intended design life and will require over \$1.6 trillion to reach acceptable levels of safety and function (1).

The second phenomenon is the degradation of the environment and the loss of associated ecosystem services (2). Substantial ecological degradation can be attributed, at least in part, to infrastructure expansion. Roads increase sediment erosion, fragment habitat, and facilitate the spread of invasive species (3). Dams and levees restrict fish migration and have drastically altered river flow regimes (4). Offshore platforms discharge waste, release atmospheric pollution, and compete with commercial fishing (5).

¹University of North Carolina at Chapel Hill, NC 27599, USA. ²University of Wisconsin, Madison, WI, USA. ³University of Colorado at Colorado Springs, CO, USA. ⁴Center for Energy Studies, Louisiana State University, Baton Rouge, LA, USA. ⁵California Artificial Reef Enhancement Program, Santa Barbara, CA, USA. ⁶University of South Carolina, Columbia, SC, USA. ⁷University of Maryland, College Park, MD, USA. ⁸Restoration Systems, LLC, Raleigh, NC, USA.

*Author for correspondence. E-mail: mwdoyle@email.unc.edu

Third is the burgeoning of ecosystem restoration as both a science and an industry (6). To date, restoration has often been limited in scale, and its effectiveness is frequently unclear (7). Nevertheless, there is growing demand, political will, and funding for restoring degraded ecosystems (7, 8).

Restoration via Decommissioning

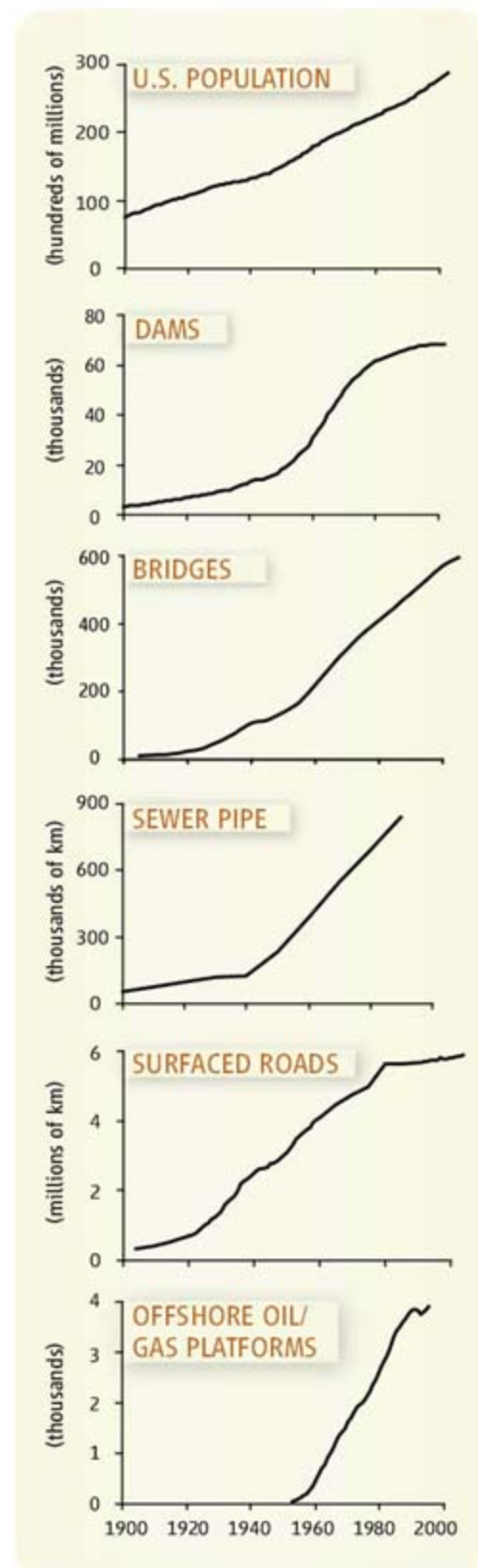
Decommissioning can take several forms, including full removal, partial removal of key components, or abandonment. Publicly versus privately owned infrastructure may differ in decommissioning procedures and ability, but all are subject to the National Environmental Policy Act and equivalent state laws, although these laws generally do not facilitate ecological restoration.

On rivers, dam decommissioning is increasingly common, whereas levee decommissioning is rare. Of the >79,000 dams in the United States, 3500 have been rated as unsafe, collectively in need of \$30 billion for rehabilitation, repair, or removal (1). Levee inventories are less clear, but estimates exceed 25,000 km (9), many with unknown structural integrity (10). To date, >600 dams have been removed, primarily for safety and economic reasons. Dam removal is followed by rapid recovery of invertebrate, fish, and riparian vegetation communities (11). Levee decommissioning, often abandoning breached levees, reduces economic demands of levee reconstruction while improving floodplain habitat and water quality (12).

Of the >6 million km of roads in the United States, 885,000 km are on public lands maintained by federal land agencies, a portion of which are rarely used (13). The U.S. Forest Service (USFS), with >250,000 km of roads over 50 years old, estimated its maintenance backlog at ~\$10 billion for 26% of system roads (13). The USFS decommissioned 7900 km of roads between 2002 and 2005 and has identified almost 300,000 km for possible decommissioning over the next 40 years (14). Decommissioning decreases economic liabilities but is also an important tool for restoring forest ecosystems (13).

In U.S. federal waters, there are >3900 offshore oil and gas platforms, primarily in the Gulf of Mexico (GOM), about one-third of

Targeted decommissioning of deteriorated and obsolete infrastructure can provide opportunities for restoring degraded ecosystems.



U.S. infrastructure inventory. For sources, see (21).

which are idle (15). Federal policies require that platforms be removed within 1 year of lease expiration, and >2700 platforms have been removed. Removed platforms have been primarily shallow-water platforms and mostly disposed of onshore (15). Costs and environment impacts of removing deep water platforms are substantial.

Full platform removal has drawbacks, including environmental impacts and loss of the potential ecological value of the structure as an artificial reef (16). Research shows that platforms facilitate the expansion of coral populations in the GOM (17) and act as refuges for juvenile fish, increasing fish production off the coast of California (18). Rigs-to-Reefs Programs allow reuse of decommissioned structures as artificial reefs. Through 2004, >190 retired platforms were dedicated for fisheries enhancement, which reduced decommissioning costs and led to >\$20 million in industry donations to state environmental management trust funds (15).

Department of Defense (DOD) facilities pose an unusual challenge and opportunity. Of the 257 million ha of federal lands in the United States, >10 million ha belong to the DOD (19). Access restrictions have made military bases some of the richest ecological reserves of any of the nation's public lands (19). Through the Base Realignment and Closure (BRAC) program, 400 military sites were closed or reclassified between 1988 and 2002. To date, management of 21 bases on >445,000 ha has been transferred from the DOD to the U.S. Fish and Wildlife Service to become National Wildlife Refuges (e.g., Jefferson Proving Ground became Big Oaks National Wildlife Refuge).

Perhaps the largest combination of infrastructure management and ecosystem restoration is the Comprehensive Everglades Restoration Project (CERP), an effort to restore the 2.3 million-ha watershed and its ecosystem (8). Hydrology in the Everglades is manipulated through hundreds of control gates, thousands of kilometers of levees, 2900 km of canals, and dozens of pump stations, which largely continue to function well. The CERP is based on infrastructure modification and partial removal to move the ecosystem to a more natural and sustainable configuration through a 40-year, \$20 billion project.



Infrastructure decommissioning and removal. Removal of Caribton Dam resulted in rapid recovery of the federally listed endangered Cape Fear shiner (*Notropis mekistocholas*), found in the former impoundment after <2 years of removal. The dam was removed to generate environmental restoration credits, which were then sold to offset stream impacts elsewhere.

Policy Directions and Exit Strategies

Infrastructure policy should do more than fund projects; it should set national priorities and initiatives. The National Commission on Infrastructure would set such strategic priorities and consider infrastructure financing, rehabilitation, and maintenance. Rehabilitation under the NIIA includes considering removal of infrastructure that is deteriorated or no longer useful. When infrastructure has been decommissioned, ecological restoration has been a side benefit. Prioritizing decommissioning sites based on a combination of ecological, economic, and safety concerns can benefit multiple stakeholders, possibly reducing overall decommissioning costs (15).

Infrastructure decommissioning is likely to occur during discrete windows of opportunity. These may be policy-related (e.g., expiration of a dam license), natural (e.g., flooding), or through deliberate legislation (e.g., CERP). However, political will for such expenditures is difficult to maintain, particularly during political transitions (20). A less broadly applied funding mechanism is the use of market-like principles in which infrastructure decommissioning is used to generate credits to offset environmental impacts elsewhere (see figure above).

The greatest lesson from current aging infrastructure is the need for exit strategies, which vary greatly among infrastructure types. Policies for decommissioning dams are surprisingly rare and vague (11), whereas policies for decommissioning offshore platforms are unambiguous (15). Because the costs of decommissioning and cleanup for infrastructure can be substantial, more explicit policies should require provisions for decommissioning

as part of infrastructure license or lease terms, perhaps similar to that for offshore facilities, where bonding requirements are specified and based on the estimated cost of full removal.

Any infrastructure policy approach must confront the national conundrum of pressing infrastructure problems and continuing environmental degradation. Specifically, a National Commission on Infrastructure should squarely face decommissioning as a viable option, and the environmental benefits gained through such decommissioning should be assessed as definable benefits and leveraged when possible and practicable.

References and Notes

1. American Society of Civil Engineers (ASCE), *Report Card for America's Infrastructure* (ASCE, New York, 2005).
2. Heinz Center, *State of the Nation's Ecosystems* (Cambridge Univ. Press, Cambridge, 2002).
3. National Research Council (NRC), *Assessing and Managing the Ecological Impacts of Paved Roads* (National Academies Press, Washington, DC, 2005).
4. C. Nilsson et al., *Science* **308**, 405 (2005).
5. S. Patin, *Environmental Impact of the Offshore Oil and Gas Industry* (EcoMonitor Publishing, East Northport, NY, 1999).
6. NRC, *Compensating for Wetland Losses Under the Clean Water Act* (National Academy Press, Washington, DC, 2001).
7. E. S. Bernhardt et al., *Science* **308**, 636 (2005).
8. NRC, *Progress Toward Restoring the Everglades* (National Academies Press, Washington, DC, 2006).
9. G. Tobin, *Water Resour. Bull.* **31**, 359 (1995).
10. Interagency Levee Policy Review Committee, *The National Levee Challenge* (Federal Emergency Management Association, Washington, DC, 2006).
11. M. W. Doyle et al., *Geomorphology* **71**, 227 (2005).
12. D. Galat et al., *BioScience* **48**, 721 (1998).
13. D. Havlick, *No Place Distant* (Island Press, Washington, DC, 2002).
14. D. Ihara et al., *Reinvesting in Jobs, Communities, and Forests* (Center for Environmental Economic Development, Arcata, CA, 2003).
15. M. Kaiser, A. Pulsipher, *Ocean Dev. Int. Law* **36**, 125 (2005).
16. D. M. Schroeder, M. S. Love, *Ocean Coast. Manag.* **47**, 21 (2004).
17. P. W. Sammarco et al., *Mar. Ecol. Prog. Ser.* **280**, 129 (2004).
18. M. S. Love et al., *Fish. Bull.* **104**, 383 (2006).
19. M. Leslie et al., *Conserving Biodiversity on Military Lands* (U.S. Department of Defense, Washington, DC, 1996).
20. National Council on Public Works Improvement (NCPWI), *Fragile Foundation: Final Report to the President and Congress* (NCPWI, Washington, DC, 1988).
21. Sources: Population (U.S. Census Bureau, 2007); bridges (U.S. Federal Highway Administration (FHWA), 2007); surfaced roads (FHWA *Annual Highway Statistics*; surfaced roads include soil-surfaced; slag, gravel or stone; asphalt; or concrete); dams (ASCE, *National Inventory of Dams*, New York, 2007); sanitary sewer pipe (U.S. Environmental Protection Agency, *The Clean Water and Drinking Water Infrastructure Gap Analysis*, 2002); and offshore platforms (Minerals Management Service, U.S. Department of the Interior, 2007) (installation numbers are only for the U.S. outer continental shelf).
22. Funding: U.S. Department of Agriculture (2004-35102-14793) and NSF (DDIG 0521728). Views expressed here do not represent the views of any supporting organization. We thank E. S. Bernhardt, L. Band, M. J. Small, and D. Carr for comments.

10.1126/science.1149852

Organizing the Source of Memory

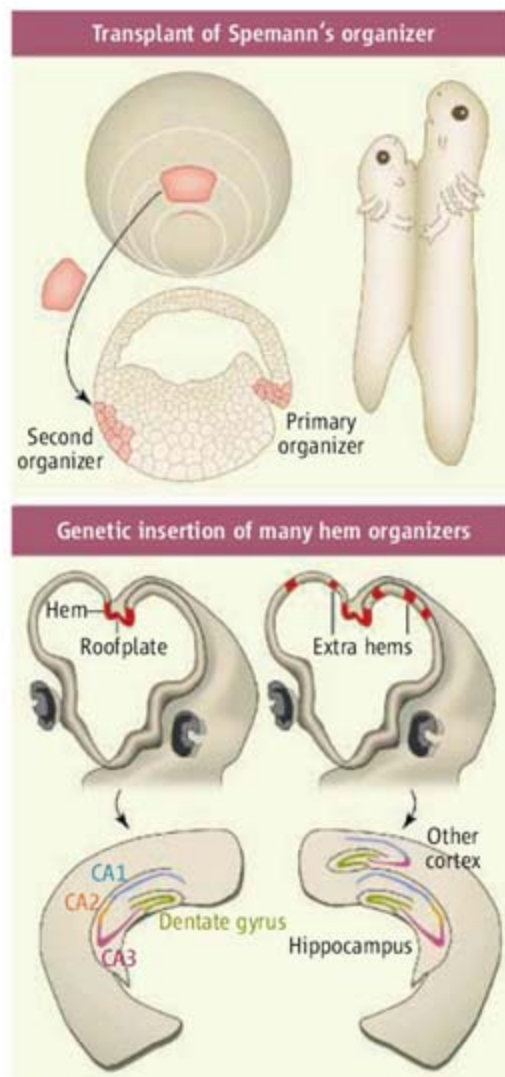
Elizabeth A. Grove

The hippocampus is essential for a meaningful human life. Without it, we cannot form new memories. Engaging in a normal social life would not be possible because new experiences would fade from memory within minutes (1). In keeping with its complex function, the hippocampus, part of the brain's cerebral cortex, has a distinctive, intricate anatomy. A rolled layer of pyramidal-shaped neurons, divided into subregions called CA1, CA2, and CA3, is capped by the dentate gyrus, a packed sheet of granule neurons, curved around the pyramidal cell layer. Dissected free of the brain, the entire rolled structure bears an uncanny resemblance to a seahorse, or, in Greek, "hippocampus" (2). On page 304 of this issue, Mangale *et al.* (3) reveal how this intricate structure develops in the mammalian embryo.

One hippocampus develops on each side of the brain, close to the brain's midline. Within this midline lies the "cortical hem," a source of secreted proteins that regulate a variety of developmental processes (4). Among these signaling molecules are bone morphogenetic proteins (BMPs) and Wingless-Int (Wnt) proteins, whose functions include directing fields of cells to develop as a specific cell type or part of the body.

Although the cortical hem has been a likely candidate to specify the hippocampus, evidence has been surprisingly hard to find. Investigators have focused on manipulating Wnt or BMP signaling in mice, the favored species for studies of mammalian development. When Wnt signaling is disrupted, hippocampal fields are reduced or lost, but this can be explained by decreased cell division or increased cell death (5–7). When Wnt signaling is activated throughout the embryonic cortex, small patches of cells resembling hippocampal neurons develop out of place; however, no particular source of specifying signals can be distinguished (8). Loss of BMP receptor activity causes loss of the hem itself (9).

Mangale *et al.* identified an elegant solution to the technical problems of transplanting a hem into a mammalian brain, to test its effect on hippocampus development. They used genetic methods to implant several hems into



Organizers. (Top) Transplant of a second Spemann's organizer in the early frog embryo generates a second body axis, resulting in joined, twin tadpoles. (Bottom) Insertion of extra cortical hem organizers into the mouse forebrain induces extra hippocampi to form (right; normal brain, left).

the embryonic forebrain, next to tissue competent to become the hippocampus. In the chimeric mice that they generated, normal cortical cells intermixed with cells that were labeled with green fluorescent protein and genetically engineered to lack the transcription factor *Lhx2*. In the absence of functional *Lhx2*, cells are predicted to express a complement of other genes typical of the hem, including *Wnt* and *Bmp* (10, 11).

This method of introducing new hems into a chimeric forebrain would not have worked without an interesting cell property demonstrated by Mangale *et al.* *Lhx2*-deficient cells prefer to stick to each other, as do cells

Signals from the midline of the embryonic brain direct formation of the hippocampus.

expressing *Lhx2*. Thus, in chimeric mice, cell adhesion created patches of each cell type. In normal development, Mangale *et al.* suggest that such cell affinities help to form a sharp boundary between the *Lhx2*-negative hem and *Lhx2*-expressing cortex.

Next to patches of hem tissue, new hippocampal fields emerged in regions with *Lhx2* function. The dentate gyrus, CA3, and CA1 were oriented in the appropriate order beside hem tissue. The most straightforward interpretation of these results is that *Lhx2* makes a region of the forebrain competent to generate cerebral cortex, and the hem organizes a hippocampus in the competent tissue.

Identification of any embryonic tissue with "organizer function" recalls the historic discovery of a primary embryonic organizer by Spemann and Mangold (12). At a stage of development when the salamander embryo looks like a hollow, collapsing ball of dividing cells, transplanting a portion of the ball, "Spemann's organizer," to another embryo duplicates the body axis, resulting in conjoined twin animals (see the figure). The hem is not a primary, but a "secondary" organizer: It regulates a particular component of the body, the hippocampus. Nonetheless, the position of this secondary organizer determines a major developmental axis that runs from the dentate gyrus through the CA fields. Integrity of the hippocampal axis is important to its function, because information travels largely one way, from the dentate gyrus through the CA fields. Disruption of the axis after birth causes profound memory loss (1).

Remaining questions concern the mechanisms of axis formation and the molecular identity of hippocampal organizing signals including, but probably not limited to, BMPs and Wnts. Answers may shape investigation into the genetic basis of human disorders that implicate the hippocampus, such as epilepsy and schizophrenia. As for experimental mice engineered to develop more than one hippocampus per hemisphere, are more hippocampi better or worse for their memory after birth?

Other putative organizers have been identified in and around the embryonic cortex, based on their expression of genes encoding secreted signaling proteins (4). A model has been proposed in which organizers regulate the cell types, subdivisions, and functionally

The author is in the Department of Neurobiology, University of Chicago, Chicago, IL 60637, USA. E-mail: egrove@bsd.uchicago.edu

specialized areas of the cerebral cortex. Organizer function has now been demonstrated for two such signaling sources: the cortical hem, and a region of the forebrain that secretes fibroblast growth factors to direct neocortical organization (13, 14). A broad implication of the work by Mangale *et al.* is that it tips the balance in favor of this model, transforming it from a provisional to a working model and a platform for future studies of how the cortex is first organized (4, 15).

References

1. L. R. Squire, *Memory and Brain* (Oxford Univ. Press, New York, 1987).
2. W. J. H. Nauta, M. Feirtag, *Fundamental Neuroanatomy* (Freeman, New York, 1986).
3. V. S. Mangale *et al.*, *Science* **319**, 304 (2008).
4. C. W. Ragsdale, E. A. Grove, *Curr. Opin. Neurobiol.* **11**, 50 (2001).
5. S. M. Lee, S. Tole *et al.*, *Development* **127**, 457 (2000).
6. J. Galceran *et al.*, *Development* **127**, 469 (2000).
7. A. Miquelajauregui *et al.*, *Proc. Natl. Acad. Sci. U.S.A.* **104**, 12919 (2007).
8. O. Machon *et al.*, *Dev. Biol.* **311**, 223 (2007).
9. M. Fernandes *et al.*, *Development* **134**, 3789 (2007).
10. S. Bulchand *et al.*, *Mech. Dev.* **100**, 165 (2001).
11. E. S. Monuki, F. D. Porter, C. A. Walsh, *Neuron* **32**, 591 (2001).
12. H. Spemann, H. Mangold, *Roux's Arch. Entw. Mech.* **100**, 599 (1924).
13. T. Fukuchi-Shimogori, E. A. Grove, *Science* **294**, 1071 (2001).
14. S. Garel *et al.*, *Development* **130**, 1903 (2003).
15. D. D. O'Leary *et al.*, *Neuron* **56**, 252 (2007).

10.1126/science.1153743

ASTRONOMY

Orion Continues to Surprise

C. R. O'Dell and Leisa K. Townsley

The closest example of a region of massive-star formation is the famous Orion Nebula, which is easily visible even with small binoculars. The accompanying figure is a mosaic of Hubble Space Telescope optical images and shows the rich detail in this beautiful object. The brightest stars in the middle are the most massive of the several thousand stars that form the eponymous cluster. Star formation within Orion's Giant Molecular Cloud began about 2.5 million years ago and has continued through recent times. The Orion Nebula has frequently been one of the first targets viewed with new astronomical techniques (1), beginning with the optical telescope, the introduction of astronomical spectroscopy, and most recently, radio-wavelength observations. Now on page 309 in this issue, Güdel *et al.* (2) present x-ray measurements with the X-Ray Multi-Mirror (XMM)-Newton satellite that reveal something new: hot gas that can only be powered by hypersonic winds from the massive stars.

Understanding these new observations requires understanding the three-dimensional structure of the Orion Nebula (3). The location of the center of star formation is somewhat like Goldilocks's porridge, neither too deep within the cloud (or we wouldn't see the stars) or too close to its surface (or there would not have been enough material to form the cluster stars). This selection effect means that the Orion Nebula is an irregular concave thin layer of gas being ionized by ultraviolet photons coming from the hottest star. The ionized

thin layer is near the surface of the molecular cloud. The massive stars lie at the center of the cluster and are on the observer's side of the ionized layer. Finally, there is a thin layer of neutral gas and dust that lies in the foreground and forms a semitransparent veil through which we see the nebula. The thickest portion of the veil extends across part of the brightest region of the nebula, superimposing a dark thumb outline in the figure. The cavity between the ionized layer and the veil opens to the lower right in the figure, and there is a slow flow of low-density gas in that direction.

The ionized gas of the visible nebula has a temperature of about 9000 K. This is the equilibrium established between the heating that occurs from the excess energy of the photons that ionize the nebula's hydrogen and the cooling that occurs by collisional excitation of heavy elements such as carbon, nitrogen, and oxygen. The hot gas observed by Güdel *et al.* is at a temperature of 2 million K and so must be formed in a very different manner. Higher-temperature gas has been seen in earlier studies of other similar objects, but the diffuse light caused by scattering in the Chandra Observatory's camera precluded detecting any diffuse source of x-rays in Orion

Observations of a nearby nebula reveal an unusual region of extremely hot gas whose high temperature is the result of wind from massive stars.

(4) near the brightest star. It may also be that the thickest veil material obscures emission from hot gas in the central region.

The new study shows two extended regions of gas at 2 million K, one in the 3:30 o'clock direction from the compact group of four bright stars in the center of the nebula and the other in the 5:00 o'clock direction, both lying within the outer rim of the extended nebula.



Cradle of star formation. This mosaic image depicts a 12.8 square light-year portion of the Orion Nebula, the nearest region of massive-star formation. The bright area in the upper left center is the well-studied Trapezium region of 9000 K gas, and the much larger nearly circular region to the lower right is the Extended Orion Nebula within which diffuse x-ray emission from 2 million K gas was observed by Güdel *et al.*

C. R. O'Dell is in the Department of Physics and Astronomy, Vanderbilt University, Nashville, TN 37235, USA. L. K. Townsley is in the Department of Astronomy and Astrophysics, Pennsylvania State University, University Park, PA 16802, USA. E-mail: crodell@vanderbilt.edu, townsley@astro.psu.edu

Starlight cannot heat gas to this high temperature, and the power must come from the hypersonic wind emitted by massive stars (5).

This wind carries about 10,000 times as much power as the observed x-rays, which means that it is the prime candidate to be the engine driving the x-ray emission. The wind will overtake the escaping low-density gas in the outer nebula, producing shock fronts that immediately reach temperatures of millions of kelvin. This is the same mechanism invoked to explain the hotter x-ray emission in the similar but more populous Omega and Rosette nebulae (4), but many questions remain in Orion. Why is the x-ray emission confined to these two areas? Is there a channeling effect of the stellar wind, a rapid cooling of any other shocked gas closer to the star, or does extinction in the veil simply preclude observation of hot gas in the optically brightest part of the nebula?

Researchers can answer these questions by reanalyzing the earlier Chandra Observatory

observations and by employing careful subtraction of the instrumental scattered light and mapping the extinction of optical light from the Extended Orion Nebula. Once these observational questions have been resolved, the ball will be in the theoreticians' court; it is they who must then confront the problems of why the Orion gas is at 2 million K and why it is located where it is.

References and Notes

1. C. R. O'Dell, *The Orion Nebula* (Harvard Univ. Press, Cambridge, MA, 2003).
2. M. Güdel *et al.*, *Science* **319**, 309 (2008); published online 29 November 2007 (10.1126/science.1149926).
3. C. R. O'Dell, *Annu. Rev. Astron. Astrophys.* **39**, 99 (2001).
4. L. K. Townsley *et al.*, *Astrophys. J.* **593**, 874 (2003).
5. C. Leitherer *et al.*, *Astrophys. J.* **326**, 356 (1988).
6. The preparation of this article was supported in part by the Space Telescope Science Institute (grant GO 10967 to Vanderbilt University) and Chandra X-ray Observatory (grant GO6-7006X to Pennsylvania State University).

10.1126/science.1153476

ECOLOGY

Managing Coastal Wetlands

Ivan Valiela and Sophia E. Fox

Wetland management may be improved by evaluating nonlinear relationships of economic value and ecological services.

About 30 to 50% of the area of Earth's major coastal environments has been degraded during past decades (1). The rates of these losses exceed those of the much better publicized losses of tropical forest. Loss of coastal habitat areas reduces key ecological services; for example, fish and shellfish stocks may decline and shorelines may be destabilized (2). On page 321 of this issue, Barbier *et al.* (3) find that habitat area might not relate linearly to economic value of certain ecological services furnished by coastal wetlands and argue that ecosystem management strategies might benefit from consideration of such nonlinear functions as a basis for coastal preservation.

Previous work has suggested that the more salt marsh area present, the greater the likely harvest of shrimp in adjacent coastal waters (4). Such linear results suggest that the best course is to protect as much of these environ-

ments as possible; this has largely been the basis for management strategies. Barbier *et al.* show that for at least one ecological service provided by wetlands such as marshes and mangroves—the wave attenuation service



Costs and benefits of conversion. Ponds are constructed to raise shrimp in areas previously covered by mangrove forests in north-west Java, Indonesia.

that protects coastal areas from storms and tsunamis—the relation between service and wetland area is not linear, but is decidedly curved.

Such nonlinear links have consequences for management. Barbier *et al.* focus on the key management problem in mangroves: conversion of forests to shrimp ponds. Is there some best solution to the dilemma of weighing the value of ecosystem services against the economic value of the shrimp crop? The authors calculated the “economic value” of intact mangrove forests in Thailand, incorporating the nonlinear behavior of wave attenuation as well as the value of shrimp production after mangrove conversion. Economic value peaked at an intermediate level of conversion from mangrove forest to shrimp ponds. Thus, it may be possible to define an economic optimum for conversion of mangrove forest area to shrimp ponds.

The work is based on the premise that an ecological function can be converted into a currency directly equivalent to money (5, 6). We have at least two qualms with regard to this interesting idea. First, given the paucity of available information, practitioners of ecosystem valuation are often forced to make daring (and not always compelling) leaps of faith to convert ecological service to monetary value.

Second, by putting a price on a natural environment, we put it up for sale—and the monetary value of natural services will seldom reach the value accrued by conversion to industrial or commercial use. For instance, some years ago there was a proposal to build an industrial plant on a wetland parcel in the Hackensack Meadowlands of New Jersey. As a counterpoint to the proposal for construction, decision-makers asked for a valuation of the wetland, which came to about \$9000 per acre, per year, in perpetuity. The builders offered \$200,000 per acre and showed that the added jobs, taxes, etc., would by far exceed wetland “proceeds” in the short and long term. Today a refinery stands on the site.

That said, there are several valuable features of the results reported by Barbier *et al.* They show that consideration of nonlinear aspects of coastal variables improved the ability to incorporate conflicting demands in management strategies. Use of nonlinear relationships could elucidate diminishing ecological returns associated with different amounts of area preserved. This may pro-

The authors are at the Ecosystems Center and Boston University Marine Program, Marine Biological Laboratory, Woods Hole, MA 02543, USA. E-mail: ivaliela@mbi.edu; sefox@mbi.edu

vide an objective way to decide on the degree of preservation of different environments of the world's coasts.

The results also suggest several fertile areas for further research. First, it is important to determine how general nonlinearities may be; in the Thai mangrove example, the value of coastal protection by wave attenuation was nonlinearly related to the area of mangrove loss, but yields of fishery and wood products were linearly related to habitat area. Second, scientists must establish whether the deviations from linearity are significant in both ecological and management terms to make sure that implementation of policies resulting from use of curved functions leads to detectable differences. Third, more solid evidence is needed that a service is actually being provided; for instance, there has been considerable debate about how much wave protection is provided by mangroves (7–11). Fourth, future studies should more comprehensively cover the suite of locally relevant factors influencing economic value. Barbier (12) made a good start toward addressing local issues by quantifying the net effects of economic costs and benefits resulting from conversion of mangrove forests to shrimp farming, but the valuation might benefit by addition of a few

key terms. In Ecuador, for example, the shrimp industry came to a standstill not because of deficit income, but because the supply of juvenile shrimp in nearby waters (used as the “seed” for shrimp ponds) was depleted by overfishing. In Ecuador and elsewhere, the mangrove conversion rate may be accelerated by the need to abandon ponds that, as a result of high-yield culture methods, have become too chemically altered to be suitable for shrimp growth.

Finally, Barbier *et al.* point to the need to determine ecosystem-based management for coastal areas by weighing and incorporating the interests of several players: shrimp farmers, who will think about the price of shrimp, but are unlikely to consider long-term, regional benefits of coastal protection when deciding whether to dig another pond; outside investors, who might not know or care about mangrove services; and officials, who might be responsible for implementing regional environmental strategies that foster ecological services.

The report by Barbier *et al.* highlights the complexities involved in making the compromises needed for future coastal management. Research from the study areas pointed

out above will show whether “bent” relationships make for compromises that are not only ecologically desirable, but also enable compromises for planned management of coastal wetlands that are acceptable to the diverse stakeholders.

References and Notes

1. C. Duarte, Ed., *Global Loss of Coastal Habitats* (Fundación BBVA, Madrid, 10 October 2007). A video of the conference is available at www.bbva.es/coastalhabitats.
2. I. Valiela, *Global Coastal Change* (Blackwell, Oxford, 2006).
3. E. B. Barbier *et al.*, *Science* **319**, 321 (2008).
4. R. E. Turner, in *Stemming the Tide of Coastal Habitat Loss*, R. H. Shroud, Ed. (National Coalition for Marine Conservation, Savannah, GA, 1992), pp. 97–104.
5. R. Costanza *et al.*, *Nature* **387**, 253 (1997).
6. E. B. Barbier, *Econ. Policy* **22**, 177 (2007).
7. K. Kathiresan, N. Rajendran, *Estuarine Coastal Shelf Sci.* **65**, 601 (2005).
8. A. M. Kerr *et al.*, *Estuarine Coastal Shelf Sci.* **67**, 539 (2005).
9. J. E. Vermaat, U. Thampanya, *Estuarine Coastal Shelf Sci.* **69**, 1 (2006).
10. J. E. Vermaat, U. Thampanya, *Estuarine Coastal Shelf Sci.* **75**, 564 (2007).
11. T. Smith III, 19th Biennial Conference of the Estuarine Research Federation (Providence, RI, 4 to 8 November 2007), abstr.
12. E. B. Barbier, *Contemp. Econ. Policy* **21**, 59 (2003).
13. Supported by NSF grant DEB-0516430.

10.1126/science.1153477

GEOLOGY

Dreams of Natural Streams

David R. Montgomery

What does a natural river look like? Centuries of human influence can mask historically distinctive river forms in and among regions around the world (see the figure). Results reported by Walter and Merritts on page 299 of this issue (1) suggest that human modification of riverscapes has been so extensive that even some fundamental ideas about how rivers work bear the stamp of human influence. The authors show how colonial mill dams and land use changed New England's streams from a marshy multi-channel morphology to today's meandering single-channel form.

This transformation is obviously fascinating to students of regional environmental history, but it is not only of academic interest. Understanding how natural streams work is

crucial for river restoration, an academically young discipline that is rapidly maturing into a billion-dollar-a-year industry. The classic sinuous form of meandering channels (2) has come to represent a natural ideal in channel-restoration design—even for rivers for which such an ideal is historical fiction.

Modern fluvial geomorphology—the study of rivers—evolved out of the studies of Luna Leopold, M. Gordon Wolman, and their colleagues in the 1950s. As the field developed, pioneering studies of streams in the eastern United States contributed to a standard model for how fluvial processes shape rivers and floodplain environments. This model has been elaborated upon and exported around the world. Indeed, these now classic studies provided the basis for the so-called natural channel design central to many river-restoration efforts across the United States (3).

Walter and Merritts now show that some of the rivers studied by Leopold, Wolman, and colleagues were not so natural after all. The

Human influences have fundamentally changed river morphologies in temperate regions around the world.

new study does not challenge their fundamental insights into how the interplay of hydraulics and sediment transport shapes river and stream channels, but in light of the new findings, what constitutes a natural channel form requires reexamination.

The results parallel findings in Europe and the Pacific Northwest of how historical clearing of large wood and logjams altered river morphology. Before European rivers were cleared to promote waterborne commerce, large trees and logjams obstructed many rivers; local blockages split flow into multichannel networks of branching streams (4). Similarly, downed wood split channels into branching networks of small channels flowing across slough-rich valley bottoms in the forested floodplains of the Pacific Northwest (5, 6).

Walter and Merritts now present compelling evidence for a similar change that radically altered rivers in the eastern United States. Thus, a comparable transition from

The author is in the Department of Earth and Space Sciences, Quaternary Research Center, University of Washington, Seattle, WA 98195, USA. E-mail: dave@ess.washington.edu



Natural or not? A single-channel meandering form provides the template for many river engineering and restoration projects, but as Walter and Merritts show in this issue, it may not reflect forms that predated anthropogenic modifications.

long-standing geographical conundrum. Recent studies have confirmed the long-articulated idea that modern agriculture greatly accelerated rates of soil erosion (7–9), but at the same time, sediment delivery to oceans declined by half (10). Where is all the dirt thought to have been stripped from upland farms? Walter and Merritts show that tremendous amounts of floodplain sediment previously thought to date back thousands of years actually represents material impounded behind mill dams. Here may lie much of New England's precolonial topsoil.

The study by Walter and Merritts also has substantial implications for river restoration. The implicit mantra of such restoration programs—enough studying, let's just fix it—has been based on the idea of reengineering an archetypal meandering channel form. Given the compelling demonstrations of extensive human alteration of the fundamental morphology of river systems in New England (1),

multithread channels to meandering single-thread channels occurred in all three regions. This observation suggests that a common transformation accompanied human development of temperate forest rivers.

Walter and Merritts also help to resolve a

Europe (4), and the Pacific Northwest (5, 6), the first step in a river-restoration program should instead be to develop a solid understanding of what the targeted rivers were actually like before the changes that restorationists seek to undo or mitigate.

Over recent decades, substantial progress has been made in deepening the understanding of how rivers work and addressing how different environmental contexts in different regions left their own mark on rivers. The report by Walter and Merritts shows that it pays to do the painstaking work of historical sleuthing—even in areas thought to define benchmarks in understanding.

References

1. R. C. Walter, D. J. Merritts, *Science* **319**, 299 (2008).
2. L. B. Leopold, M. G. Wolman, J. P. Miller, *Fluvial Processes in Geomorphology* (Freeman, San Francisco, 1964).
3. D. Rosgen, *Applied River Morphology* (Wildland Hydrology, Pagosa Springs, CO, 1996).
4. K. Harwood, A. G. Brown, *Earth Surf. Process. Landforms* **18**, 741 (1993).
5. B. D. Collins, D. R. Montgomery, *Restor. Ecol.* **10**, 237 (2002).
6. D. R. Montgomery, *King of Fish: The Thousand-Year Run of Salmon* (Westview, Boulder, CO, 2003).
7. D. R. Montgomery, *Dirt: The Erosion of Civilizations* (Univ. of California Press, Berkeley, 2007).
8. D. R. Montgomery, *Proc. Natl. Acad. Sci. U.S.A.* **104**, 13268 (2007).
9. B. H. Wilkinson, B. J. McElroy, *Geol. Soc. Am. Bull.* **119**, 140 (2007).
10. J. P. M. Syvitski, C. J. Vörösmarty, A. J. Kettner, P. Green, *Science* **308**, 376 (2005).

10.1126/science.1153480

PHYSICS

Probing Quantum Magnetism with Cold Atoms

Maciej Lewenstein and Anna Sanpera

In 1995, ultracold atoms were experimentally locked together in a single quantum state known as a Bose-Einstein condensate (1). Since then, researchers keep broadening the scope of research with ultracold atoms. On page 295 of this issue, Trotzky *et al.* (2) report measurement of interactions between atoms trapped in an optical lattice that are analogous to the interactions between atomic

spins in magnetic materials, a phenomenon called “superexchange.” This is an essential step toward experimental realization of models for studying arrangements of quantum spins. These relatively simple models will help us study and understand the most fundamental physics associated with quantum magnetic ordering, quantum phase transitions, and a large zoo of exotic quantum phases.

Although spin models have been traditionally constructed as ideal approximations of real magnetic materials, many theorists have pointed out that ultracold atoms in optical lattices allow for an almost perfect realization of these systems [see review (3) and

The interactions of atoms held in an optical trap reveal fundamental mechanisms of magnetism.

references therein]. An optical lattice is a spatially ordered array of potential wells or traps produced by the interference pattern of counterpropagating laser beams. In simpler terms, the optical lattice looks effectively like an egg carton, where the atoms, like eggs, can be arranged one per well to form crystals of quantum matter.

These quantum crystals can be controlled and manipulated by modifying the frequency, intensity, or polarization of the lasers forming the lattice. One can also superimpose a secondary optical lattice (or “superlattice”) on top of the primary one to further modify the potential in which the atoms are trapped.

The authors are at the Institut de Recerca i Estudis Avançats, E-08010, Barcelona, Spain. M. Lewenstein is also at the Institut de Ciències Fotòniques, E-08860, Castelldefels, Spain. A. Sanpera is also in the Grup de Física Teòrica, Universitat Autònoma de Barcelona, E-08193, Bellaterra, Spain. E-mail: maciej.lewenstein@icfo.es

Moreover, one can use internal atomic properties, such as the magnetic moment of atoms (the spins), to design strongly correlated quantum spin models with a variety of exotic properties. In condensed matter, interactions between spins arise from the overlapping of different electronic orbitals. In optical lattices, however, where there is only one atom in each potential well, the overlap between the electronic orbitals is very small. Nevertheless, interactions between spins can be induced through virtual hopping of atoms between adjacent lattice wells. In other words, quantum mechanics allows the atoms to tunnel through the barrier so the spins can interact. These are called superexchange interactions and were discovered by Kramers (4) and Anderson (5).

The experiment of Trotzky *et al.* uses a superlattice to examine the dynamical evolution of the simplest matter crystal consisting of a pair of wells, where each well is loaded with an individual rubidium atom (see the figure). The two atoms are initially prepared in different spin states. Although the average number of atoms in each potential well does not change in time, the atoms are allowed to interact by virtual tunneling. Passing through a virtual state of double occupancy, the energy of the system can increase as a result of collisions inside a single potential well, giving in this way a clear signature of superexchange interactions.

By imposing an additional magnetic field to mismatch the potential energies of the two wells, it is possible to tune the hopping (that is, the hopping increases from a shallower well) while keeping the collision energy unchanged. This allows the researchers to test the accuracy of the underlying theoretical spin model (in this case, the so-called Bose-Hubbard model) and even to control the sign of the interactions. Depending on the value of the applied field, the superexchange interactions can either be antiferromagnetic or ferromagnetic, where at

zero temperature the spins orient in antiparallel or aligned fashion, respectively.

The experiment of Trotzky *et al.*, although dealing with an ensemble of nearly noninteracting pairs of atoms, opens a direct path toward realization of low-temperature quantum magnets and a variety of many-body spin models with ultracold atoms. Studies of this kind focus on both the equilibrium state and the dynamics of such systems. Trotzky *et al.* discuss some particular spin models in lattices of various geometries and anisotropic interactions. Even more fascinating is the possibility of studying polymerized lattices that consist of regular arrays of plaquettes (i.e., complexes of a few close sites, forming dimers, trimers, etc.). Such systems could be used to mimic some theoretical models of particle physics, such as lattice gauge theories that occur in quark physics.

The three-dimensional lattice of double

wells, used in the present experiment, is an example of a dimerized cubic lattice. A trimerized kagome lattice (i.e., a triangular lattice of smaller triangles) was originally introduced by Mila (6) to study resonating valence-bond (RVB) states that are superpositions of states in which random pairs of neighboring atoms attain zero total spin, and are examples of a so-called quantum spin liquid. The RVB state is important for, among other reasons, the possibility that it may be the basis for high-temperature superconductivity. The possibility of realizing trimerized kagome and other polymerized lattices, such as a quadruply polymerized square lattice of square plaquettes, using cold atoms and superlattices was suggested by one of us (7). A very simple proposal for a quadruply polymerized square lattice was recently formulated by Paredes and Bloch (8) and is expected to be investigated by several experimental groups for novel quantum information processing applications.

One of the most challenging questions concerns not only how to experimentally create "exotic" quantum magnetic phases but also how to detect them. Recent prominent examples of detection schemes include interferometry that seeks correlations in noisy signals (9), methods involving cavity quantum electrodynamics (10), or quantum spin polarization spectroscopy, formulated by us (11) as a quantum nondemolition method (i.e., where the quantum state is examined but not destroyed) particularly suited for studying unusual quantum magnetic phases.

Since the first Bose-Einstein condensates were created, researchers have started to unify atomic, molecular, and quantum optics with condensed matter physics and quantum information. Now recent developments (2, 3, 8, 10) show that experiments with ultracold gases can address quantum magnetism and might even allow us to make progress on some unsolved problems of high-energy physics in benchtop experiments.

References

1. M. H. Anderson *et al.*, *Science* **269**, 198 (1995).
2. S. Trotzky *et al.*, *Science* **319**, 295 (2008); published online 20 December 2007 (10.1126/science.1150841).
3. M. Lewenstein *et al.*, *Adv. Phys.* **56**, 243 (2007).
4. H. A. Kramers, *Physica* **1**, 182 (1934).
5. P. W. Anderson, *Phys. Rev.* **79**, 350 (1950).
6. F. W. Mila, *Phys. Rev. Lett.* **81**, 2356 (1998).
7. B. Damski *et al.*, *Phys. Rev. A* **72**, 052612 (2005).
8. B. Paredes, I. Bloch, <http://arxiv.org/abs/0711.3796>.
9. E. Altman, E. Demler, M. D. Lukin, *Phys. Rev. A* **70**, 013603 (2004).
10. L. Jiang *et al.*, <http://arxiv.org/abs/0711.1365>.
11. K. Eckert *et al.*, *Nature Phys.*, 10.1038/nphys776 (2007).



Atomic hopping. An array of double well potentials, where each well contains a single atom. Adjacent atoms interact through superexchange spin-spin coupling in which atoms quantum-mechanically tunnel from one well to the adjacent well and back, as studied by Trotzky *et al.*

Arabidopsis CLV3 Peptide Directly Binds CLV1 Ectodomain

Mari Ogawa, Hidefumi Shinohara, Youji Sakagami, Yoshikatsu Matsubayashi*

Plants continuously produce organs from self-renewing shoot apical meristem (SAM). A feedback signaling loop between stem cells and the underlying organizing center balances stem cell renewal and differentiation (1). *CLAVATA1* (*CLV1*) and *CLAVATA3* (*CLV3*), which are expressed in adjacent regions in SAM and function in the same genetic pathway, are key components of the regulatory network controlling this balance in *Arabidopsis*. Mutations in the *CLV* genes cause accumulation of stem cells and enlargement of the SAM. In contrast, overexpression of *CLV3* causes loss of stem cells and, in turn, developmental arrest. *CLV1* encodes a leucine-rich repeat receptor kinase (LRR-RK) (2), and *CLV3* encodes a secreted polypeptide that is converted into a 12-amino acid peptide by proteolytic processing (3, 4). Although these molecules are thought to act as a ligand-receptor pair, biochemical evidence remains lacking.

The ligand-binding characteristics of *CLV1* are difficult to assess because it acts as a negative regulator of cell growth and therefore cannot be overexpressed in plant cells in sufficient quantities for ligand-binding assays. Deletion of the cytoplasmic kinase domain improves expression of LRR-RK proteins without affecting ligand-binding affinity of the extracellular domain (5). We therefore overexpressed a *CLV1* in which the kinase domain was replaced with HaloTag (Promega, Madison, WI) (*CLV1-ΔKD-HT*) in tobacco BY-2 cells (Fig. 1, A and B).

To test whether *CLV1-ΔKD-HT* specifically interacts with *CLV3*, we incubated membrane fractions derived from wild-type and transgenic BY-2 cells with [³H]*CLV3*. Membrane fractions derived from transgenic BY-2 cells overexpressing *CLV1-ΔKD-HT* had significantly higher specific [³H]*CLV3* binding activity than fractions derived from wild-type BY-2 cells (Fig. 1C). The specific [³H]*CLV3* binding to membranes was rapid, saturable, and reversible (fig. S1A). Incubation of the mem-

brane fractions derived from transgenic BY-2 cells with a photoactivable [¹²⁵I]ASA-*CLV3* (fig. S1, B and C) followed by cross-linking by ultraviolet (UV) irradiation resulted in specific labeling of the 130-kD band that corresponds to *CLV1-ΔKD-HT* (Fig. 1D). These results indicate that *CLV3* directly binds the *CLV1* ectodomain. A broad 90-kD labeled band probably represents C-terminal-truncated *CLV1-ΔKD-HT* in which the HT domain was lost. Truncated receptor kinases are often detected at considerable amounts in membrane fractions (5). Scatchard analysis revealed that *CLV1-ΔKD-HT* interacts with [³H]*CLV3* with a dissociation constant (*K_d*) of 17.5 nM (Fig. 1E). The interaction was only partially inhibited by excess [³H]*CLV3*, a less-active *CLV3* analog corresponding to *clv3-1* and *clv3-5* alleles (3), indicating that the observed binding is specific (Fig. 1F).

Several *CLE* peptides, structurally related to *CLV3*, play pleiotropic roles in plant growth and development (6). Of the total of 31 *CLE* genes in *Arabidopsis*, 16 can be grouped into three phy-

logenetic clades: *CLE1* to *CLE7*, *CLE9* to *CLE13*, and *CLE41* to *CLE44* (7). Overexpression of the first group of *CLE* genes caused phenotypes similar to, but milder than, those caused by *CLV3* overexpression (7). Overexpression of the second *CLE* group induced termination of SAM with high mortality, similar to the SAM of *CLV3*-overexpressing plants. Overexpression of the third group of *CLE* genes did not affect the SAM. [³H]*CLV3* binding to *CLV1-ΔKD-HT* was inhibited similarly by either *CLE9* or *CLV3* (Fig. 1F). *CLE2* also inhibited [³H]*CLV3* binding to a considerable degree, whereas *CLE44* only partially inhibited binding (Fig. 1F). Thus, *CLV1* interacts both with *CLV3* and also *CLE* peptides, each with unique affinities. The relative binding affinities of the *CLV* and *CLE* peptides for the ectodomain of *CLV3* and related receptors may, together with the location and timing of expression of these components, form the basis for the physiological importance of these signals in the SAM and other tissues.

Our results provide direct evidence that *CLV3* and *CLV1* function as a ligand-receptor pair involved in stem cell maintenance. Our results also indicate that the *CLV1* ectodomain alone is sufficient for *CLV3* binding. This suggests that arrays of ectodomains derived from LRR-RKs phylogenetically related to *CLV1* may be able to bind *CLE* peptides in a sequence-specific manner in vitro. Such a biochemical approach could help clarify highly redundant and pleiotropic *CLE* signaling by identifying the individual ligand-receptor interactions.

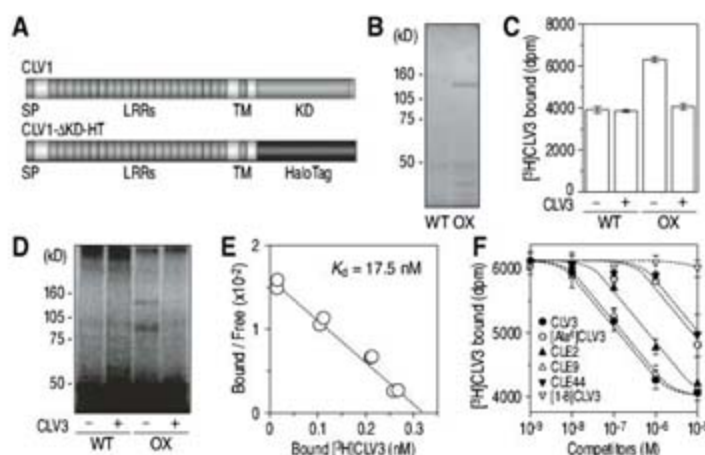


Fig. 1. (A) Schematic structures of *CLV1* and its HaloTag fusion protein (*CLV1-ΔKD-HT*). *CLV1* is a 980-amino acid LRR-RK containing a signal peptide (SP), 22 tandem LRRs, a transmembrane domain (TM), and a cytoplasmic kinase domain (KD). (B) Visualization of *CLV1-ΔKD-HT* in wild-type (WT) BY-2 cells and in transgenic BY-2 cells overexpressing *CLV1-ΔKD-HT* (OX) by specific incorporation of the fluorescent dye HaloTag TMR (Promega, Madison, WI). (C) [³H]*CLV3* binding assay of microsomal fractions derived from WT cells and transgenic cells overexpressing *CLV1-ΔKD-HT* (OX) in the absence or presence of excess unlabeled *CLV3* as a competitor (mean ± SD, *n* = 3). (D) Photoaffinity labeling of *CLV1-ΔKD-HT* by [¹²⁵I]ASA-*CLV3* in the absence or presence of excess unlabeled *CLV3*. (E) Scatchard plot of the [³H]*CLV3* binding to *CLV1-ΔKD-HT*. (F) Competitive replacement of [³H]*CLV3* (32 nM) binding to *CLV1-ΔKD-HT* by *CLV3*, [Ala⁶]*CLV3*, *CLE2*, *CLE9*, *CLE44*, and [1-8]*CLV3* peptides (mean ± SD, *n* = 3). Amino acid sequence of each peptide is given in fig. S1D.

References and Notes

- J. C. Fletcher, E. M. Meyerowitz, *Curr. Opin. Plant Biol.* **3**, 23 (2000).
- S. E. Clark, R. W. Williams, E. M. Meyerowitz, *Cell* **89**, 575 (1997).
- J. C. Fletcher, U. Brand, M. P. Running, R. Simon, E. M. Meyerowitz, *Science* **283**, 1911 (1999).
- T. Kondo *et al.*, *Science* **313**, 845 (2006).
- H. Shinohara, Y. Matsubayashi, *Plant J.* **52**, 175 (2007).
- Y. Ito *et al.*, *Science* **313**, 842 (2006).
- T. J. Strabala *et al.*, *Plant Physiol.* **140**, 1331 (2006).
- This research was supported by Grant-in-Aid for Scientific Research for Priority Areas from the Ministry of Education, Culture, Sports, Science, and Technology (MEXT) (no. 19060010 to Y.M.), Grant-in-Aid for Young Scientists (A) from MEXT (no. 18687003 to Y.M.), Grant-in-Aid for Creative Scientific Research from Japan Society for the Promotion of Science (no. 19GS0315 to Y.M.), and Program of Basic Research Activities for Innovative Biosciences from Bio-oriented Technology Research Advancement Institution (BRAIN) (Y.S.).

Supporting Online Material

www.sciencemag.org/cgi/content/full/319/5861/294/DC1

Materials and Methods

Fig. S1

4 September 2007; accepted 8 November 2007

10.1126/science.1150083

Graduate School of Bio-Agricultural Sciences, Nagoya University, Chikusa, Nagoya 464-8601, Japan.

*To whom correspondence should be addressed. E-mail: matsu@agr.nagoya-u.ac.jp

Time-Resolved Observation and Control of Superexchange Interactions with Ultracold Atoms in Optical Lattices

S. Trotzky,^{1*} P. Cheinet,^{1*} S. Fölling,¹ M. Feld,^{1,2} U. Schnorrberger,¹ A. M. Rey,³ A. Polkovnikov,⁴ E. A. Demler,^{3,5} M. D. Lukin,^{3,5} I. Bloch^{1†}

Quantum mechanical superexchange interactions form the basis of quantum magnetism in strongly correlated electronic media. We report on the direct measurement of superexchange interactions with ultracold atoms in optical lattices. After preparing a spin-mixture of ultracold atoms in an antiferromagnetically ordered state, we measured coherent superexchange-mediated spin dynamics with coupling energies from 5 hertz up to 1 kilohertz. By dynamically modifying the potential bias between neighboring lattice sites, the magnitude and sign of the superexchange interaction can be controlled, thus allowing the system to be switched between antiferromagnetic and ferromagnetic spin interactions. We compare our findings to predictions of a two-site Bose-Hubbard model and find very good agreement, but are also able to identify corrections that can be explained by the inclusion of direct nearest-neighbor interactions.

Quantum spin systems on a lattice have served for decades as paradigms for condensed matter and statistical physics, elucidating fundamental properties of phase transitions and acting as models for the emergence of quantum magnetism in strongly correlated electronic media. In all these cases, the underlying systems rely on a spin-spin interaction between particles on neighboring lattice sites, such as in the Ising or Heisenberg model (1–3). As initially proposed for electrons by Dirac (4, 5) and Heisenberg (2, 6), effective spin-spin interactions can arise due to the interplay between the spin-independent Coulomb repulsion and exchange symmetry and do not require any direct coupling between the spins of the particles. The nature of such spin-exchange interactions is typically short-ranged, as it is governed by the wave function overlap of the underlying electronic orbitals. However, in several topical insulators, such as ionic solids like CuO and MnO, antiferromagnetic order arises even though the wave function overlap between the magnetic ions is practically zero. In this case, a “superexchange” interaction mediated by higher-order virtual hopping processes can be effective over a large distance (7, 8), which leads to an (anti-)ferromagnetic coupling between bosons (fermions) on neighboring lattice sites (3). Such superexchange inter-

actions are believed to play an important role in the context of high-temperature superconductivity (9). Furthermore, they can form the basis for the generation of robust quantum gates similar to that recently described in electronic double quantum dot systems (10, 11) and can be used for the efficient generation of multiparticle entangled states (12, 13), as well as for the production of many-body quantum phases with topological order (14–16).

We report on the direct observation of superexchange interactions with ultracold atoms in optical lattices (17, 18). Previous experiments have shown that spin-spin interactions between neighboring atoms can be implemented in discrete time steps (19, 20) by bringing the atoms together on a single site and carrying out controlled collisions (20–22) or on-site exchange interactions (23). The superexchange interactions demonstrated here, however, directly implement nearest-neighbor spin interactions in the many-body system and allow for a continuous “analog” simulation of spin lattice Hamiltonians.

We probe the superexchange interactions by first preparing two atomic spin states of ⁸⁷Rb in an antiferromagnetic order (24) and then recording the time evolution of the spins of neighboring atoms in isolated double-well potentials (25–27) for weak to strong tunnel couplings. For dominating on-site interactions over the tunnel coupling between lattice sites, we find pronounced sinusoidal spin oscillations due to an effective Heisenberg-type superexchange Hamiltonian, whereas for stronger tunnel coupling, a more complex dynamics emerges. In addition, we show how the strength and sign of the superexchange interaction can be directly controlled by introducing a potential bias between neighboring wells. Furthermore, we find that corrections to the two-site Bose-Hubbard model (BHM) that take into account the direct interaction between particles on neighboring lattice sites are needed to fully explain our data.

Theoretical model. An isolated system of two coupled potential wells constitutes the simplest concept for the investigation of superexchange-mediated spin dynamics between neighboring atoms. We consider a single double-well potential occupied by a pair of bosonic atoms with two different spin states denoted by $|\uparrow\rangle$ and $|\downarrow\rangle$. If the vibrational level splitting in each well is much larger than all other relevant energy scales and intersite interactions are neglected, the system can be described in a two-mode approximation by a two-site version of the Bose-Hubbard Hamiltonian

$$\hat{H} = \sum_{\sigma=\uparrow,\downarrow} \left[-J(\hat{a}_{\sigma L}^\dagger \hat{a}_{\sigma R} + \hat{a}_{\sigma R}^\dagger \hat{a}_{\sigma L}) - \frac{1}{2} \Delta (\hat{n}_{\sigma L} - \hat{n}_{\sigma R}) \right] + U(\hat{n}_{\uparrow L} \hat{n}_{\downarrow L} + \hat{n}_{\uparrow R} \hat{n}_{\downarrow R}) \quad (1)$$

where the operators $\hat{a}_{\sigma L,R}^\dagger$ and $\hat{a}_{\sigma L,R}$ create and annihilate an atom with spin σ in the left and right well respectively, $\hat{n}_{\sigma L,R}$ count the number of atoms per spin state and well, J is the tunnel matrix element, Δ is the potential bias or tilt along the double-well axis, and $U = U_{\uparrow\downarrow} = g \times \int_{\text{well}} \psi_{\uparrow,R}^\dagger(\mathbf{x}) \psi_{\downarrow,R}(\mathbf{x}) d^3x$ is the on-site interaction energy between two

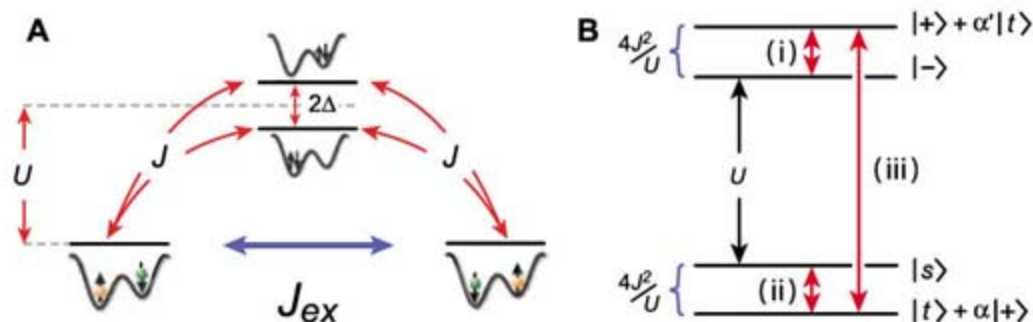


Fig. 1. Schematics of superexchange interactions. (A) Second-order hopping via $|\uparrow\downarrow, 0\rangle$ and $|0, \uparrow\downarrow\rangle$ mediates the spin-spin interactions between atoms on different sides of the double well. (B) Energy levels for $\Delta = 0$ and $U \gg J$. The evolution in the upper doublet of states (i) corresponds to the correlated tunneling of atom pairs (27), whereas the superexchange takes place in the lower one (ii). Both doublets are coupled by first-order tunneling processes (iii).

¹Institut für Physik, Johannes Gutenberg-Universität, 55099 Mainz, Germany. ²Fachbereich Physik, Technische Universität Kaiserslautern, 67663 Kaiserslautern, Germany. ³Institute for Theoretical Atomic, Molecular and Optical Physics, Harvard-Smithsonian Center of Astrophysics, Cambridge, MA 02138, USA. ⁴Department of Physics, Boston University, Boston, MA 02215, USA. ⁵Physics Department, Harvard University, Cambridge, MA 02138, USA.

*These authors contributed equally to this work.

†To whom correspondence should be addressed. E-mail: bloch@uni-mainz.de

atoms in $|\uparrow\rangle$ and $|\downarrow\rangle$. Here, $g = (4\pi\hbar^2 a_s^{\uparrow\downarrow})/M$ is the effective interaction strength with $a_s^{\uparrow\downarrow}$ being the positive scattering length for the spin states used in the experiment, M is the mass of a single atom, and $w_{L,R}(\mathbf{x})$ denote the wave functions for a particle localized on the left or right side of the double well. The state of the system can be described as a superposition of the Fock states $\{|\uparrow,\downarrow\rangle, |\downarrow,\uparrow\rangle, |\uparrow,\uparrow\rangle, |\downarrow,\downarrow\rangle\}$, where the left and right side in the notation represent the occupation of the left and right well, respectively, and the states $|\uparrow,\downarrow\rangle$ and $|\downarrow,\uparrow\rangle$ are spin triplet states. In the following, we will focus on the dynamical evolution of the population imbalance $x = n_L - n_R$ and the Néel order parameter or “spin imbalance” $N_z = (n_{\uparrow L} + n_{\downarrow R} - n_{\uparrow R} - n_{\downarrow L})/2$ starting with double wells initially prepared in $|\uparrow,\downarrow\rangle$. Here, $n_{\uparrow,\downarrow,L,R} = \langle \hat{n}_{\uparrow,\downarrow,L,R} \rangle$ denote the corresponding quantum mechanical expectation values and $n_{L,R} = n_{\uparrow L,R} + n_{\downarrow L,R}$.

In the limit of dominating interactions ($U \gg J$), when starting in the subspace of singly occupied wells spanned by $|\uparrow,\downarrow\rangle$ and $|\downarrow,\uparrow\rangle$, the energetically high-lying states $|\uparrow,\uparrow\rangle$ and $|\downarrow,\downarrow\rangle$ can only be reached as “virtual” intermediate states in second-order tunneling processes. Such processes lead to a nonlocal (super) spin-exchange interaction, which couples the states $|\uparrow,\downarrow\rangle$ and $|\downarrow,\uparrow\rangle$ (Fig. 1A). More generally, for an arbitrary spin configuration with equal interaction energies $U_{\uparrow\uparrow} = U_{\downarrow\downarrow} = U_{\uparrow\downarrow}$ (28), the second-order hopping events are described by an isotropic Heisenberg-type effective spin Hamiltonian in the limit $U \gg J$ (3, 15, 29, 30):

$$\begin{aligned} \hat{H}_{\text{eff}} &= -2J_{\text{ex}} \hat{S}_L \cdot \hat{S}_R \\ &= -J_{\text{ex}} (\hat{S}_L^+ \hat{S}_R^- + \hat{S}_L^- \hat{S}_R^+) - 2J_{\text{ex}} \hat{S}_L^z \hat{S}_R^z \end{aligned} \quad (2)$$

where $\hat{S}_{L,R}^+ = |\uparrow\rangle\langle\downarrow|_{L,R}$, $\hat{S}_{L,R}^- = |\downarrow\rangle\langle\uparrow|_{L,R}$ and $\hat{S}_{L,R}^z = (\hat{n}_{\uparrow L,R} - \hat{n}_{\downarrow L,R})/2$ denote the corresponding spin operators of the system, with $\hat{S}_{L,R}^x \pm i\hat{S}_{L,R}^y$. The effective coupling strength J_{ex} represents the superexchange and can readily be evaluated by perturbation theory up to quadratic order in the tunneling operator, which yields $J_{\text{ex}} = 2J^2/U$.

When a potential bias $\Delta > 0$ is applied, the degeneracy of the two intermediate states in the superexchange process is lifted (Fig. 1A). For $J, \Delta \ll U$ this leads to a modification of the effective superexchange coupling with now $J_{\text{ex}} = J^2/(U + \Delta) + J^2/(U - \Delta) = 2J^2U/(U^2 - \Delta^2)$ (15). By tuning the bias to $\Delta > U$, it is possible to change the sign of J_{ex} and therefore to switch between ferromagnetic and antiferromagnetic superexchange interactions. For $J \ll |U - \Delta|$, the picture of an effective coupling via two virtual intermediate states is again valid, and the full reversal to $J_{\text{ex}} = -2J^2/U$ is found to be reached for $\Delta = \sqrt{2}U$.

For symmetric double wells ($\Delta = 0$), the Hamiltonian Eq. 1 can be diagonalized analytically to give a valid picture for all values of J and U within the single-band BHM. A convenient basis is given by the spin triplet and singlet state $|t/s\rangle = (|\uparrow,\downarrow\rangle \pm |\downarrow,\uparrow\rangle)/\sqrt{2}$ and the states $|\pm\rangle \equiv$

$(|\uparrow,\downarrow\rangle \pm |0,\uparrow\rangle)/\sqrt{2}$. Two of the eigenstates are linear combinations of $|t\rangle$ and $|\pm\rangle$, where the one having the larger overlap with $|t\rangle$ is the ground state. The spin singlet $|s\rangle$ and the state $|\pm\rangle$ are already eigenstates themselves with energy 0 and U , respectively (Fig. 1B). As a direct consequence, $|\pm\rangle$ cannot be reached from the initial state $|\uparrow,\downarrow\rangle = (|s\rangle + |t\rangle)/\sqrt{2}$. Therefore, the dynamical evolution of the spin imbalance contains only two frequencies

$$h\omega_{1,2} = \frac{U}{2} \left(\sqrt{\left(\frac{4J}{U}\right)^2 + 1} \pm 1 \right) \quad (3)$$

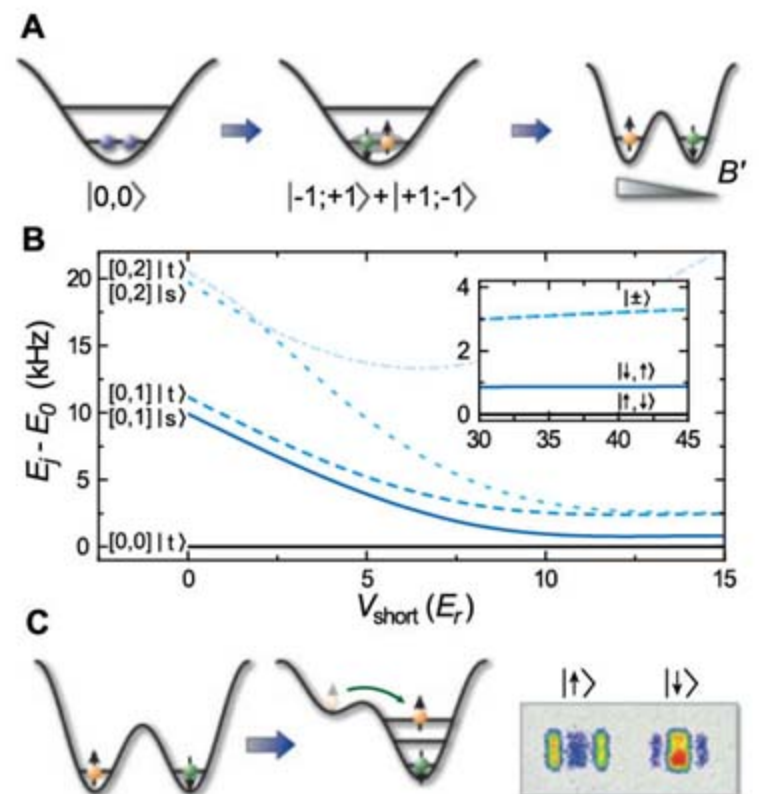
The extraction of these frequencies from time-resolved measurements allows for the determination of $2J = \hbar\sqrt{\omega_1\omega_2}$ and $U = \hbar(\omega_1 - \omega_2)$ within the BHM.

Because these frequencies can be measured with high accuracy, we are able to observe deviations from the simple BHM. We obtain a first correction by the inclusion of nearest-neighbor interactions (3) in an extended two-site Bose-Hubbard model [EBHM; see Eq. S1 in (31)]. This modification introduces the interwell interaction energy $U_{LR} = g \times \int w_L^2(\mathbf{x})w_R^2(\mathbf{x})d^3x$ and a correction to the tunneling matrix element, which becomes $J = J + \Delta J$, where $\Delta J = -g \times \int w_L^2(\mathbf{x})w_R(\mathbf{x})d^3x$. The interwell interaction leads to a direct spin-exchange term, which in the limit $U \gg J$ reduces the corrected superexchange coupling to $J_{\text{ex}} = 2J^2/U - U_{LR}$. Although we find that the corrections to the pure two-site BHM are not negligible in the experimentally relevant parameter region, numerical

calculations based on the multiband Schrödinger equation show that the direct exchange can never overcome the superexchange coupling term (fig. S1) and therefore change the nature of the ground state to be antiferromagnetic. This is in agreement with the Lieb-Mattis theorem (32), which states that the ground state for two bosons has to be a spin-triplet state.

Initial state preparation. To investigate the spin dynamics between neighboring atoms, we initially prepare a sample of ultracold neutral atoms with two relevant internal states $|\uparrow\rangle$ and $|\downarrow\rangle$ in a three-dimensional (3D) array of double wells with Néel-type antiferromagnetic order $|\uparrow\downarrow\uparrow\downarrow\dots\rangle$ along one spatial direction (Fig. 2A). State preparation was started by loading a ^{87}Rb Bose-Einstein condensate of typically $\sim 8 \times 10^4$ atoms in the $|F = 1, m_F = -1\rangle$ Zeeman sublevel with no discernible thermal fraction from a magnetic trap with high offset field into a 3D optical lattice of double-well potentials (25). This “superlattice” potential is obtained by superimposing on one axis two standing light fields with periodicity 382.5 nm (short lattice) and 765 nm (long lattice) and additional standing waves with periodicity 420 nm on the two perpendicular axes (27). Controlling all depths and the relative phase of the short and long lattice allows one to tune the double-well configuration in terms of the Hamiltonian parameters J , U , and Δ . The depths of the lattices are given in units of the short-lattice recoil energy $E_r = \hbar^2/(2M\lambda^2)$ with $\lambda = 765$ nm throughout the article. The loading ramps were optimized to favor an occupation of two atoms per double well and to avoid heating to higher vibrational levels (31). After merging the double wells by

Fig. 2. State preparation and detection. (A) Spin triplet pairs are created on doubly occupied lattice sites and subsequently split under the influence of a magnetic field gradient B' to obtain antiferromagnetic Néel order. (B) Evolution of the eigenenergies with respect to the ground-state energy during the splitting with $V_{\text{long}} = 10 E_r$, $V_{\text{trans}} = 25 E_r$, and a gradient of $B' = 17$ G/cm. The notation $[v_1, v_2]$ denotes the number of vibrational excitations for the first and second particle. The inset shows the eigenenergies and (eigen)-states for the final barrier height of $V_{\text{short}} = 44 E_r$. (C) Detection of the population and spin imbalance. The population of the left well is transferred to a higher vibrational level of the underlying long-lattice well (25, 27). Subsequent band mapping and a Stern-Gerlach filter allow one to determine $x(t)$ and $N_z(t)$ from the time-of-flight images.



ramping down the short lattice, a microwave rapid adiabatic passage was used to transfer all atoms into the $|F = 1, m_F = 0\rangle$ state. Subsequently, the magnetic trap is switched off and while maintaining a homogeneous offset field of ~ 1.2 G, atom pairs were coherently transferred from $|m_F = 0; m_F = 0\rangle$ into spin triplet pairs $(|+1; -1\rangle + |-1; +1\rangle)/\sqrt{2}$ by means of spin-changing collisions (33, 34). The two magnetic sublevels $|m_F = \pm 1\rangle$ correspond to the two spin states $|\uparrow\rangle$ and $|\downarrow\rangle$. The remaining atoms in the $|m_F = 0\rangle$ state, e.g., on singly occupied sites, are transferred into $|F = 2, m_F = 0\rangle$ and removed in a filtering sequence before the detection (31).

Finally, the short lattice was ramped up slowly in 20 ms, thereby inhibiting a coherent splitting of the atom pairs and leaving the double wells in a state with one atom on each side (26). For the time of the ramping up, a magnetic field gradient of $B' \approx 17$ G/cm in the direction of the superlattice is switched on. Therefore, the degeneracy of the states $|\uparrow, \downarrow\rangle$ and $|\downarrow, \uparrow\rangle$ in the double well is lifted by ~ 900 Hz, which enables an adiabatic loading of the state $|\uparrow, \downarrow\rangle$ during the splitting process (Fig. 2B). Numerical integration of a multiband ansatz for this procedure yields an expected fidelity of $>99\%$ for creating an antiferromagnetic order along the axis of the superlattice. The mean population imbalance $x(t)$ and spin imbalance $N_z(t)$ of the ensemble of double wells was detected by applying a mapping technique (26, 27) combined with a Stern-Gerlach filter (Fig. 2C). A maximum spin imbalance of 60 to 70% was observed for our initial state corresponding to a probability of 80 to 85% for having prepared the desired state $|\uparrow, \downarrow\rangle$. We believe that this measured value is mainly reduced as a result of our detection method. Direct spin-exchange processes emerge during the mapping sequence (23) and can lead to a mixing of the spin configuration and thus a reduction of the measured Néel order parameter (31).

Time-resolved observation of superexchange interactions. The spin dynamics are initiated by rapidly ramping down the short lattice and thereby the double-well barrier in 200 μ s, thus substantially increasing the tunneling and superexchange couplings. After letting the system evolve for a hold time t , the spin configuration was frozen out by ramping up the barrier in 200 μ s, quenching both J and J_{ex} again. The measurement of the ensemble averages $x(t)$ and $N_z(t)$ is carried out as described above.

Three typical time traces obtained by this procedure are shown in Fig. 3. For low barrier depths ($J/U > 1$), we observe a pronounced time evolution of the spin imbalance $N_z(t)$ consisting of two frequency components with comparable amplitudes and frequencies (Fig. 3A). With increasing interaction energy U relative to J , the frequency ratio increases, leaving a slow component with almost full amplitude and an additional high-frequency modulation with small amplitude (Fig. 3B). The fast component corresponds to first-order tunneling due to the coupling of $|t\rangle$ and $|+\rangle$, which becomes more and more off-resonant as the barrier height is increased and therefore J/U is decreased. For $J/U \ll 1$, it is completely suppressed, and the only process visible is the superexchange oscillation (Fig. 3C). For all barrier heights, the population imbalance $x(t)$ stays flat, emphasizing that even though strong spin currents are present in the system, no net mass flow can be observed for our initial state. We fit the traces for $N_z(t)$ with a sum of two damped sine waves with variable frequencies $\omega_{1,2}/2\pi$ and amplitudes $A_{1,2}$. For the damping we assume Gaussian characteristics with $1/e$ -damping constants $\gamma_{1,2}$. The results of the fit are displayed in Fig. 4. For $V_{\text{short}} \geq 15 E_r$ (Fig. 4A, inset), we can identify only a single frequency component corresponding to the superexchange oscillation with $4J^2/hU$ and full relative amplitude (Fig. 4B). We are able to observe this frequency down to $4.8(4)$ Hz at

$J/U = 0.023$ for $V_{\text{short}} = 20 E_r$. The damping of the signal can be explained by the inhomogeneous distribution of coupling parameters due to the Gaussian shape of the lattice beams, which leads to a dephasing of the evolution within the ensemble. For $V_{\text{short}} \geq 17 E_r$, additional damping mechanisms like tunneling to empty adjacent lattice sites (defects) or small residual inhomogeneous magnetic field gradients become relevant and limit the measurements (Fig. 4C).

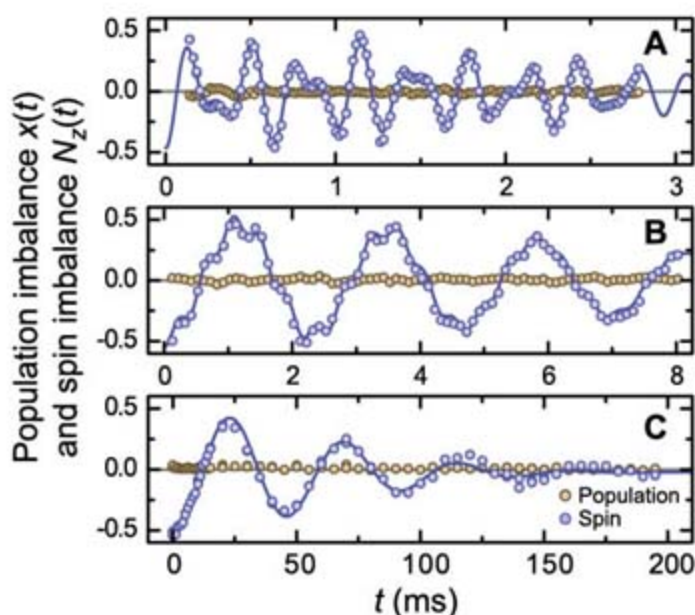
The comparison of the results with the theoretical predictions by the simple BHM shows statistically significant deviations at low barrier heights, which cannot be explained by our uncertainties in the lattice depths. In this region, the EBHM can model the experimental data much more accurately. This can be understood by the fact that the interwell interaction energy increases with decreasing barrier and begins to noticeably influence the dynamics (31). In fact, the EBHM description yields $\hbar(\omega_1 - \omega_2) = U + 3U_{\text{LR}}$ and therefore directly explains the upward trend of this frequency difference for small short-lattice depths (fig. S2). For large barrier heights, our experimental data are compatible with both models within the uncertainties of the lattice depths. However, here the predictions of the EBHM are always closer to the measured values.

Sign reversal of the effective coupling parameter. To demonstrate the controllability of superexchange interactions, we investigated the spin dynamics with an applied bias on the double wells for a short lattice depth of $15 E_r$ and the same depths for the long and transverse lattice as before. Starting with an initial antiferromagnetically ordered state, as above, we first let the system evolve in symmetric double wells ($\Delta = 0$) for $t_0 = 4.5$ ms until the first node $N_z(t) = 0$ of the spin imbalance is reached for the state $(|t\rangle + |s\rangle)/\sqrt{2}$ (Fig. 5). After freezing out the relative phase between $|s\rangle$ and $|t\rangle$ by ramping up the potential barrier, a defined potential bias Δ is applied and a second evolution sequence with hold time $t' = t - t_0$ is initialized by ramping down the short lattice again to $15 E_r$. The subsequent detection follows the scheme described above.

Figure 5A shows the evolution of the spin imbalance $N_z(t)$ in symmetric double wells together with the time traces for two different bias energies $\Delta > U$, yielding an effective coupling of $J_{\text{ex}}(\Delta) \approx -J_{\text{ex}}(\Delta = 0)$ and $-J_{\text{ex}}(\Delta = 0)/2$, respectively. The sign reversal of J_{ex} due to the introduction of the bias is directly visible by the change in slope of the spin imbalance $t = t_0$. It should be noted that the now negative sign of J_{ex} for bosons does not imply a violation of the Lieb-Mattis theorem, because the new ground state in this regime is the spin triplet state $|\uparrow\downarrow, 0\rangle$ and the superexchange couples the first and second excited states $|s\rangle$ and $|t\rangle$, which have reversed order for $\Delta > U$ (Fig. 5B, left inset).

The introduction of a nonzero tilt leads to an increased sensitivity of the exchange frequency to fluctuations due to the inhomogeneities in the

Fig. 3. Spin and population dynamics in symmetric double wells. The time evolution of the mean spin $N_z(t)$ (blue circles) and population imbalance $x(t)$ (brown circles) are shown for three barrier depths within the double-well potential: (A) $V_{\text{short}} = 6 E_r$, $J/U = 1.25$; (B) $V_{\text{short}} = 11 E_r$, $J/U = 0.26$; and (C) $V_{\text{short}} = 17 E_r$, $J/U = 0.048$. The measured traces for the spin imbalance are fitted with the sum of two damped sine waves (blue lines). The population imbalance $x(t)$ stays flat for all traces.



array of double wells, which are most effective around $\Delta \approx U$. Therefore, the damping of the signal due to dephasing is stronger as Δ approaches U . A fit of a single damped sine

wave to the time traces obtained for various tilts yields the frequency curve shown in Fig. 5B together with the amplitude of the oscillation. Starting around 50 Hz, the oscillation frequency

reaches a resonance for $\Delta/U \approx 1$, where the amplitude reverses sign, leading to the observed time reversal in the dynamics.

Summary and outlook. We have demonstrated time-resolved measurements of superexchange spin interactions between ultracold atoms on neighboring lattice sites and have shown how to control such interactions with optical superlattices. Comparing the measurements to theoretical predictions of these spin interactions from first principles, we find excellent agreement of our data to an extended two-site version of the BHM. Although superexchange interactions become exponentially suppressed for deep optical lattices, the coupling strength $2J_{\text{ex}}/\hbar$ can be several hundred hertz for lattice depths of around 12 to 15 E_r and thus almost a factor of 1000 larger than the direct magnetic dipole-dipole interaction of Rb atoms on neighboring lattice sites. Coupling strengths one order of magnitude larger than the ones shown here, however, could still be achieved with the use of electric dipole-dipole-mediated spin interactions between ground-state polar molecules (35).

The demonstrated scheme to change the superexchange coupling strength and reverse the sign of the spin interaction can also be applied to the full 1D chain, offering new possibilities for engineering spin-spin interactions in optical lattices. It is now, e.g., conceivable to engineer a setup with ferromagnetic interactions along one and antiferromagnetic interactions along another lattice direction. Furthermore, one can dynamically switch between ferro- and antiferromagnetic interactions along a given lattice direction and follow the subsequent dynamical evolution of the quantum spin system.

When the presented loading scheme is carried out without any magnetic gradient field during the splitting process, a valence-bond solid (VBS) type spin state (3, 36) can be efficiently engineered. Such VBS states can be viewed as a large array of robust Bell pairs (37, 38). In principle, the superexchange interaction can be changed to be of Ising type, e.g., by tuning the interspecies scattering length (15). Thereby, it can be used to create large entangled states out of the initially disconnected pairs, which have been shown to be powerful resources for measurement-based quantum computation (13, 39). Moreover, controlling the superexchange interactions along different lattice directions also offers novel possibilities for the generation of topological many-body states for quantum information processing (14, 15).

References and Notes

1. E. Ising, *Z. Phys. A* **31**, 253 (1925).
2. W. Heisenberg, *Z. Phys. A* **38**, 411 (1926).
3. A. Auerbach, *Interacting Electrons and Quantum Magnetism* (Springer, Berlin, 2006).
4. P. A. M. Dirac, *Proc. R. Soc. London Ser. A* **112**, 661 (1926).
5. P. A. M. Dirac, *Proc. R. Soc. London Ser. A* **123**, 714 (1929).
6. W. Heisenberg, *Z. Phys.* **49**, 619 (1928).
7. H. A. Kramers, *Physica* **1**, 182 (1934).
8. P. Anderson, *Phys. Rev.* **79**, 350 (1950).

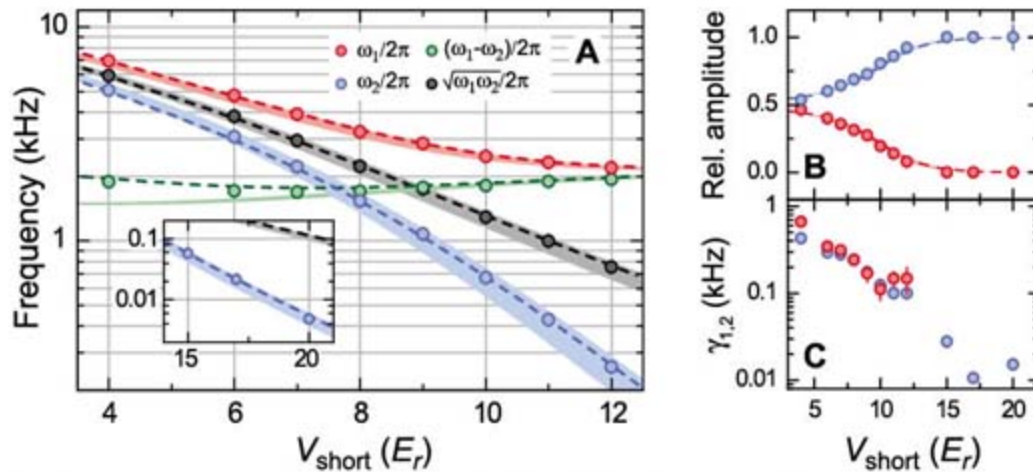
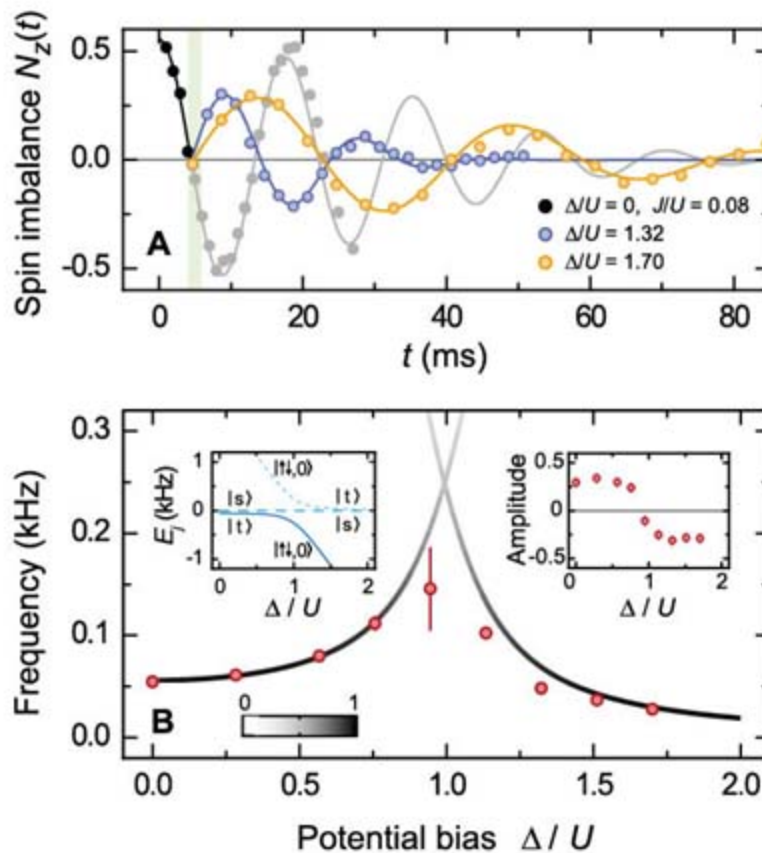


Fig. 4. Frequency components of the spin oscillations. (A) The frequencies obtained by fitting the spin imbalance data for various values of V_{short} (red and blue circles), as well as the frequency difference and the geometrical mean (green and black circles), are compared to the theoretical predictions of the simple BHM (colored regions). The width of the regions represents a 2% uncertainty in all lattice depths. The 2σ error bars on the fit results and extracted values are in all cases smaller than the data points. The dashed lines are the predictions of the EBHM. The inset shows the data for high barriers, where only a single frequency component can be identified. (B) The plot of relative amplitudes versus short lattice depth shows the suppression of the first-order tunneling process toward small values of J/U . The damping coefficients for the two oscillatory components versus lattice depth are displayed in (C). The error bars denote the 2σ uncertainties as obtained from the fit results.

Fig. 5. Sign reversal of the superexchange coupling. (A) After a quarter of a superexchange oscillation in symmetric double wells (black and gray dots, $J/U = 0.08$), a defined bias is applied, leading to a reversal in the slope of the spin imbalance and ongoing oscillations. For $\Delta/U = 1.32$ (blue circles), the magnitude of the coupling is almost the same as for $\Delta = 0$, whereas it is decreased to $\sim 50\%$ for $\Delta/U = 1.70$ (orange circles). (B) The fit of the data for various tilts to a damped sine yields a resonance in frequency at $\Delta \approx U$, where the amplitude reverses sign (right inset). The solid lines show the theoretically expected frequencies for the given parameters where the shading reflects the amplitude of the corresponding Fourier component. The left inset shows the three lowest eigenenergies of the Bose-Hubbard Hamiltonian versus the potential bias. The error bars denote the 2σ uncertainties as obtained from the fit results.



9. P. Lee, N. Nagaosa, X.-G. Wen, *Rev. Mod. Phys.* **78**, 17 (2006).
10. G. Burkard, D. Loss, D. P. DiVincenzo, *Phys. Rev. B* **59**, 2070 (1999).
11. J. R. Petta *et al.*, *Science* **309**, 2180 (2005).
12. A. M. Rey, V. Gritsev, I. Bloch, E. Demler, M. D. Lukin, *Phys. Rev. Lett.* **99**, 140601 (2007).
13. H. J. Briegel, R. Raussendorf, *Phys. Rev. Lett.* **86**, 910 (2001).
14. A. Kitaev, *Ann. Phys.* **321**, 2 (2006).
15. L.-M. Duan, E. Demler, M. D. Lukin, *Phys. Rev. Lett.* **91**, 090402 (2003).
16. L. Santos *et al.*, *Phys. Rev. Lett.* **93**, 030601 (2004).
17. M. Lewenstein *et al.*, *Adv. Phys.* **56**, 243 (2007).
18. K. Eckert, L. Zawitkowski, M. J. Leskinen, A. Sanpera, M. Lewenstein, *N. J. Phys.* **9**, 1 (2007).
19. E. Jané, G. Vidal, W. Dür, P. Zoller, J. Cirac, *Quantum Inf. Comput.* **3**, 15 (2003).
20. A. Sørensen, K. Mølmer, *Phys. Rev. Lett.* **83**, 2274 (1999).
21. D. Jaksch, H. J. Briegel, J. I. Cirac, C. W. Gardiner, P. Zoller, *Phys. Rev. Lett.* **82**, 1975 (1999).
22. O. Mandel *et al.*, *Nature* **425**, 937 (2003).
23. M. Anderlini *et al.*, *Nature* **448**, 452 (2007).
24. L. Néel, *Ann. Phys. IIe Ser.* **5**, 232 (1936).
25. J. Sebby-Strabley, M. Anderlini, P. Jessen, J. Porto, *Phys. Rev. A* **73**, 033605 (2006).
26. J. Sebby-Strabley *et al.*, *Phys. Rev. Lett.* **98**, 200405 (2007).
27. S. Fölling *et al.*, *Nature* **448**, 1029 (2007).
28. For the spin states used in our experiment, the interaction energies for the different intercombinations of spins vary by only a few percent.
29. A. B. Kuklov, B. V. Svistunov, *Phys. Rev. Lett.* **90**, 100401 (2003).
30. E. Altman, W. Hofstetter, E. Demler, M. D. Lukin, *N. J. Phys.* **5**, 113 (2003).
31. Materials and methods are available as supporting material on Science Online.
32. E. Lieb, D. Mattis, *Phys. Rev.* **125**, 164 (1962).
33. A. Widera *et al.*, *Phys. Rev. Lett.* **95**, 190405 (2005).
34. F. Gerbier, A. Widera, S. Fölling, O. Mandel, I. Bloch, *Phys. Rev. A* **73**, 041602(R) (2006).
35. A. Micheli, G. K. Brennen, P. Zoller, *Nat. Phys.* **2**, 341 (2006).
36. F. Alet, A. M. Walczak, M. P. A. Fisher, *Physica A* **369**, 122 (2006).
37. C. F. Roos *et al.*, *Phys. Rev. Lett.* **92**, 220402 (2004).
38. C. Langer *et al.*, *Phys. Rev. Lett.* **95**, 060502 (2005).
39. F. Verstraete, J. I. Cirac, *Phys. Rev. A* **70**, 060302(R) (2004).
40. We acknowledge helpful discussions with B. Paredes and funding by the Deutsche Forschungsgemeinschaft, the European Union (OLAQUI, SCALA), NSF, Air Force Office of Scientific Research (MURI, FA8655-07-1-3090), and the Packard Foundation. S.T. acknowledges financial support from the graduate class of excellence on materials with strong correlations (MATCOR).

Supporting Online Material

www.sciencemag.org/cgi/content/full/1150841/DC1

SOM Text

Figs. S1 and S2

References and Notes

21 September 2007; accepted 6 December 2007

Published online 20 December 2007;

10.1126/science.1150841

Include this information when citing this paper.

Natural Streams and the Legacy of Water-Powered Mills

Robert C. Walter*† and Dorothy J. Merritts*†

Gravel-bedded streams are thought to have a characteristic meandering form bordered by a self-formed, fine-grained floodplain. This ideal guides a multibillion-dollar stream restoration industry. We have mapped and dated many of the deposits along mid-Atlantic streams that formed the basis for this widely accepted model. These data, as well as historical maps and records, show instead that before European settlement, the streams were small anabranching channels within extensive vegetated wetlands that accumulated little sediment but stored substantial organic carbon. Subsequently, 1 to 5 meters of slackwater sedimentation, behind tens of thousands of 17th- to 19th-century milldams, buried the presettlement wetlands with fine sediment. These findings show that most floodplains along mid-Atlantic streams are actually fill terraces, and historically incised channels are not natural archetypes for meandering streams.

The meandering gravel-bedded stream bordered by a self-formed, fine-grained floodplain emerged as the characteristic river form based on pioneering studies in mid-Atlantic and western streams of the United States (1–4). Today, this ideal—of alternating pools and riffles along sinuous channels with gravel point bars and fine-grained overbank floodplain deposits—guides a multibillion-dollar stream restoration industry (5, 6). Many streams in the low-relief, tectonically inactive mid-Atlantic Piedmont of the United States are deeply incised, with steep eroding banks, and carry anomalously high amounts of suspended sediment (7). Fine-grained deposits bordering many eastern streams are thicker than would be expected from just their recent flood deposits (1, 3). These Holocene deposits typically form broad surfaces, referred to as the “valley

flat,” that were interpreted as floodplains formed by a combination of migrating, meandering stream channels and overbank deposition of silts and clays (1, 3, 8). The geometry of single-channel meandering streams has been viewed as the result of self-adjusting hydraulic variables in response to changing discharge and sediment load, and agriculture and urbanization have been cited widely as the causes of recent aggradation and degradation (1, 3, 4, 8–10). This pattern of stream development and morphology has been considered as typical of streams and rivers in stable landscapes.

We observe that crests of breached, historic milldams merge with valley-flat surfaces and that most modern streams are incised deeply below this surface. This observation led us to hypothesize that a rapid, regional transformation of stream valleys had occurred in eastern North America, from widespread aggradation as a result of damming (base-level rise) to subsequent incision and bank erosion due to dam breaching (base-level fall). We propose that valley sedimentation not only resulted from accelerated hillslope erosion caused by deforestation and agricultural

development (8, 11) but also was coupled with widespread valley-bottom damming for water power, after European settlement, from the late 17th century through the early 20th century. Damming was essential to the extensive trapping of sediment in broad valley flats that correspond to reservoir surfaces.

We test this hypothesis by examining the following lines of evidence: (i) historical accounts of widespread, intensive water-powered milling that impacted most first- to third-order streams in the mid-Atlantic region; (ii) historical maps showing multiple dams and ponds, and our observations in the field and from light detection and ranging (LIDAR) data of aggradation in these ponds that caused sedimentation upstream into tributaries and swales; (iii) historical, geological, and geochemical data showing rapid sedimentation in valley bottoms during the period of early land clearing; (iv) field observations and remote-sensing data, including LIDAR, showing that downstream-thickening wedges of sediment grade to milldam heights and, hence, that dams produced temporary, higher base levels; and (v) field observations and laboratory data showing that the morphologies and functions of presettlement streams were substantially different from those of modern streams. We revisited the same streams and specific reaches used in early studies that pioneered modern fluvial geomorphology, including fundamental ideas regarding meander migration, floodplain formation, hydraulic geometry, and fluvial response to land clearing. These streams include the Brandywine River (in Pennsylvania and Delaware) and Seneca Creek, Watts Branch, and Western Run (in Maryland) (1–4, 8, 9, 11), all of which lie within the Piedmont physiographic province of the mid-Atlantic region. In all, we studied Piedmont streams in 20 watersheds throughout Pennsylvania and Maryland (drainage areas from 11 to 1230 km²; fig. S1).

Milldam history. Dam building for water power in the eastern United States began in the

Department of Earth and Environment, Franklin and Marshall College, Post Office Box 3003, Lancaster, PA 17604–3003, USA.

*These authors contributed equally to this work.

†To whom correspondence should be addressed. E-mail: robert.walter@fandm.edu (R.C.W.); dorothy.merritts@fandm.edu (D.J.M.)

late 1600s and persisted until the early 1900s. Dams and races that delivered water from the pond upstream of a dam were built to run iron forges, furnaces, mining operations, and—most commonly—mills; we refer to all of these water-powered activities as milling. Before the adoption of steam engines during the late 19th century, every mill required a milldam reservoir to supply a relatively constant head and reliable supply of water. Early American settlers brought milling

technologies from Europe, where thousands of water-powered mills lined streams as early as 1100 CE (12) [see supporting online material (SOM) text, table S4, and fig. S5]. Milling intensified with economic growth in early America, and dozens of mill acts dating to the 1700s encouraged mill and dam building. Our analysis of historic records in Lancaster County, Pennsylvania, for example, indicates that peak mill development was from 1780 to 1860, but water-

powered milling extended from 1710 to 1940. Our county-by-county compilation of U.S. manufacturing census data reveals >65,000 water-powered mills in 872 counties in the eastern United States by 1840 (13) (Fig. 1). Water-powered milling was especially intensive in the mid-Atlantic Piedmont region along and west of the fall line, where stream gradients are conducive to milldam construction and shipping ports of the Coastal Plain are in close proximity (e.g., Wilmington, Delaware; Philadelphia, Pennsylvania; and Baltimore, Maryland). The Piedmont provided the bulk of manufacturing and agricultural goods to port cities and a large portion of the wheat and flour for mid-Atlantic shipping (14, 15).

Historic maps show locations of mill buildings, millponds, and races dating to early American history, and historic photos of dams date to the late 19th century. Lancaster, York, and Chester counties, Pennsylvania, have large-scale mid- to late 19th-century historic maps from which we located 1025 milldams (Fig. 2), which is similar to the number of mills recorded in the 1840 U.S. manufacturing census. From county historical societies and the Pennsylvania commonwealth's inventory of dams, we acquired photographs and records of hundreds of historic milldams. The Pennsylvania Department of Environmental Protection (PA DEP) has an inventory of about 8400 dams in the commonwealth, of which 4100 are breached, and estimates that 8000 to 10,000 more might exist (16). These estimates result in an average density of 0.14 to 0.15 dams per km² for the commonwealth of Pennsylvania. The possibility of 16,000 to 18,000 dams in Pennsylvania is consistent with the ~10,000 mills listed for Pennsylvania in the 1840 U.S. manufacturing census, considering that mill and dam building continued throughout the 19th century. In Chester County, Pennsylvania, for example, which includes much of the drainage area of the Brandywine River, the 1840 U.S. manufacturing census lists 379 water-powered operations, and our examination of historic maps from the 1840s to the 1860s revealed at least 377 dams. The Brandywine Valley contained "the most notable concentration of mill industries in the colonies," with 60 paper mills alone in 1797 (17). Using 1840-era county boundaries, we calculate a density of 0.19 milldams per km² in Chester County, which is only slightly greater than the density of water-powered mills in other Piedmont counties of Pennsylvania, Maryland, and Virginia calculated from the 1840 U.S. manufacturing census data.

Our field observations and LIDAR analysis ($n > 200$ millpond reaches) for the Conestoga, Brandywine, and Codorus Rivers (among others) in Pennsylvania, and for Western Run, Seneca Creek, Watts Branch, and the Monocacy River in Maryland (figs. S1 to S4), demonstrate a series of aggradational wedges of fine-grained sediment that thins and extends upstream of dams on all

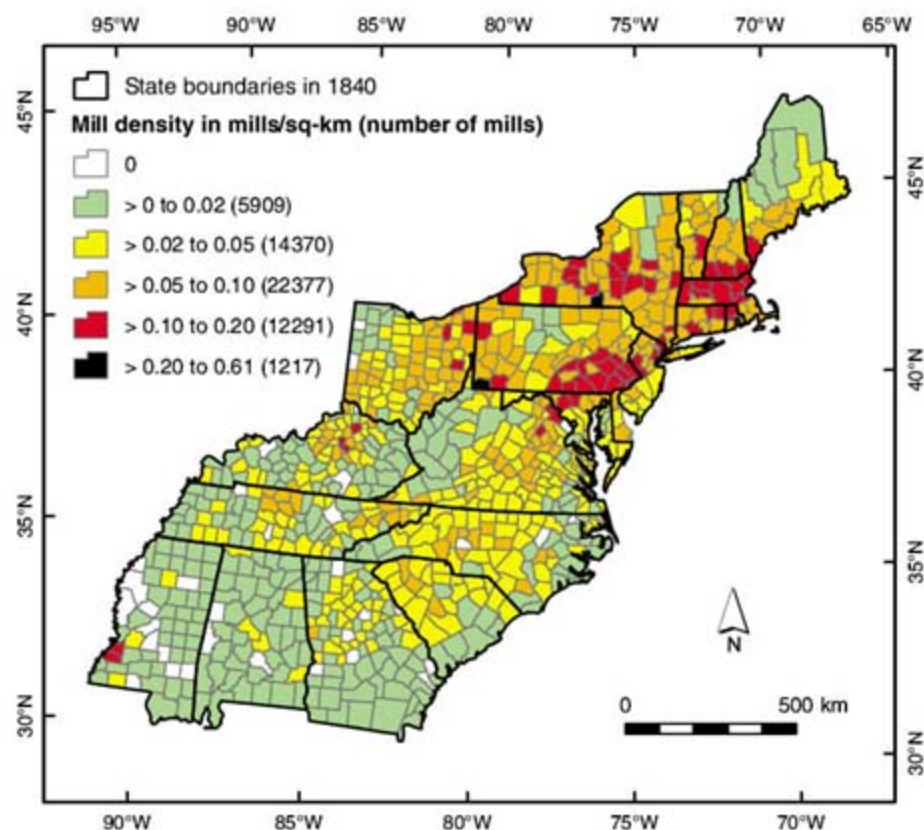


Fig. 1. Density of water-powered mills along eastern U.S. streams by 1840 by county (872 county boundaries are shown for 1840). The highest densities are in the Piedmont and the Ridge-and-Valley physiographic provinces of Maryland, Pennsylvania, New York, and central New England.

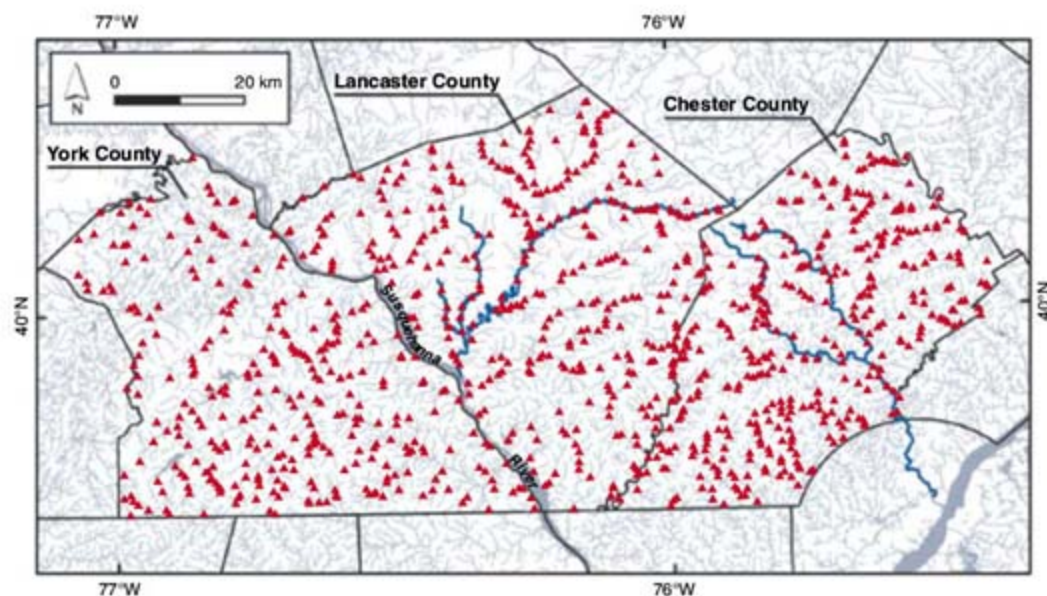


Fig. 2. Historic 19th-century milldams (triangles) on Piedmont streams in York, Lancaster, and Chester counties, southeastern Pennsylvania, located from >100 large-scale township maps dating to 1876 (York), 1875 (Lancaster), and 1847 (Chester). The total number of dams shown is 1025. Main stems of Conestoga (Lancaster) and Brandywine (Chester) rivers are highlighted in dark blue.

of these streams for several kilometers. Aggradational impacts extended upstream to many undammed tributaries as well, as a result of backwater effects.

Low stream gradients (0.001 to 0.004 in the Piedmont) and low to moderate dam heights controlled milldam spacing; typically, one dam was placed every 2.4 to 5 km along the Brandywine, Conestoga, and Codorus rivers, Seneca Creek, and Western Run. Historic photos and our field observations indicate that early milldams spanned entire valley bottoms of what are now first-, second-, and third-order streams (fig. S3). Such streams comprise greater than 70% of stream length in the region, and damming them would have a substantial impact on a large portion of watersheds, including upstream tributaries. Milldam heights were generally 2.5 to 3.7 m. Direct step calculations (18) imply that flow velocity would have been reduced by as much as 60% at least 1 to 3 km upstream of milldams (flow reduction is impacted to a greater extent by higher dams and/or lower stream gradients). Our estimates of trap efficiencies (19) of >60% for Piedmont reservoirs suggest that sedimentation rates would have been high during periods of accelerated soil erosion. Various early American mill acts that regulated the raising of dams and compensation for flooded lands, both of

which were common occurrences, also indicate that milldams had well-known backwater effects on valley bottoms (see SOM text). Because of these backwater effects, later mill acts were passed to control mill crowding (17, 20) (see SOM text). Historical accounts also show that milldams altered the original stream ecology: (i) In 1731, settlers tore down a milldam on the Conestoga River because it was ruining the local fishing industry, and (ii) in 1763, a petition cited complaints regarding the abundance of milldams on the Conestoga River “as destroying the former fishery of shad, salmon, and rock fish, which were before in abundance, and the tributary streams had plenty of trout—all now gone” (21).

Stream sediments. Based on geochemical and stratigraphic analysis of sediments exposed in stream banks (~100 sites) and samples from 45 backhoe trenches and >110 hydraulic cores in adjacent fill terraces, we constructed a composite stratigraphic profile for a representative Piedmont stream (first to third order) (Fig. 3). Similar profiles have been described throughout the Piedmont, from South Carolina to Pennsylvania (8, 22–24). The bedrock (weathered) valley floor typically is overlain by: (i) a thin (<0.5-m) bed of angular to subangular quartz-rich gravel; (ii) a thin (<0.5- to 1-m), dark

(black, 10YR 2/1), organic-rich silt loam; and (iii) a thick (1- to 5-m) pale to yellowish brown sequence of fine sand, silt, and clay [commonly referred to as silt loam and clay loam; U.S. Department of Agriculture (USDA)/Natural Resources Conservation Service classification]. Exceptions to this typical sequence occur where stream channels were diverted along valley walls (e.g., to drain valley bottoms for agriculture) or where stream beds were mined for metal ores and gravel.

We interpret the dark, organic-rich silt loam (2 to 9% by weight total carbon in the <2.0-mm fraction) above the basal gravel as a buried hydric (wetland) soil (tables S1 and S2). Throughout the region, this hydric soil contains abundant, well-preserved woody debris, seeds, nuts, roots, algal mats, and pollen, and sometimes is a peat with mosses. At multiple sites, we observe deciduous tree stumps (which often show evidence of having been logged) rooted in this stratum and corduroy (wooden log or plank) roads upon its surface. The overlying fine-grained, pale brown sediments are lower in organic matter (~1 to 2% by weight total carbon in the <2.0-mm fraction), generally horizontally bedded, typically finely laminated, and contain rare lenses of subrounded gravels and historic artifacts that include brick fragments, cut logs and planks, and pieces of coal. Seventy radiocarbon dates from this buried wetland soil (samples of wood, leaves, or seeds) throughout Pennsylvania and Maryland yield ages ranging from 11,240 to 300 years before the present (table S3), indicating that these soils accumulated and stored organic matter throughout the Holocene epoch. We estimate that these valley-bottom wetlands were efficient carbon sinks, storing from 2.5×10^5 to 1.35×10^6 kg of carbon per hectare that now is buried beneath historic sediment (25).

We interpret the underlying gravels as derived from long-term (10^6 to 10^7 years) hillslope erosion and denudation of the landscape. Many may have formed from downslope movement associated with episodic periglacial processes and tundra conditions during the late Pleistocene or earlier. The predominance of quartz, a highly resistant mineral, and the position of these colluvial gravels beneath pervasive Holocene interglacial hydric soils support this deduction.

We constrained the timing of millpond sedimentation using ^{210}Pb geochronology (26) and historic documents. Analysis at two sites where historic sediment is 1 and 5 m thick indicates that secular equilibrium for ^{210}Pb is reached at a depth of 15 to 20 cm below the surface. This finding indicates that sediments near the surface were deposited by 1850 or earlier and that these slackwater reservoirs reached sediment storage capacity by at least that year (fig. S3). At multiple sites in Maryland and Pennsylvania, we observe groves of large trees estimated to be up to 150 years old on valley fill deposits. This is consistent with fossil seed and pollen evidence showing that a riparian forest became

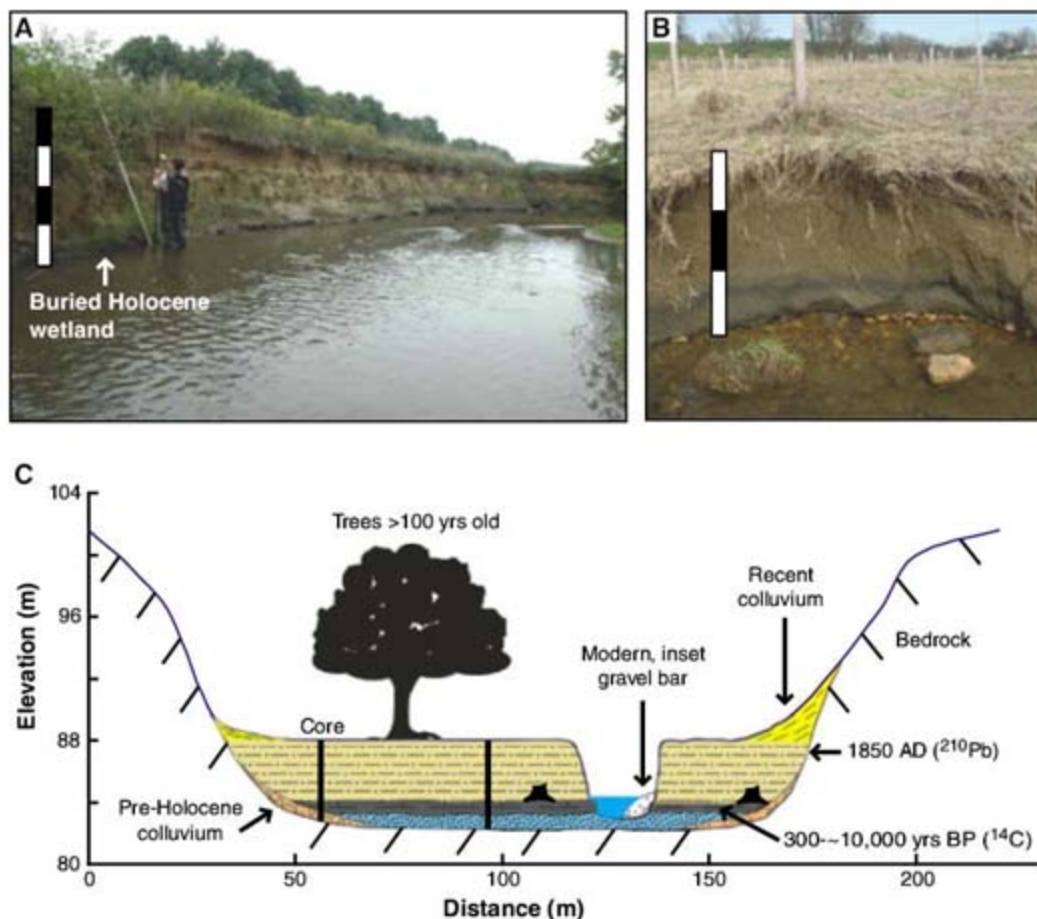


Fig. 3. Streams throughout the mid-Atlantic region (see also figs. S1 and S2) have similar characteristics: vertical to near-vertical banks consisting of 1 to 5 m of laminated to massive fine-grained sediment overlying a Holocene hydric soil and a basal gravel overlying bedrock. (A) Western Run, Maryland. (B) Big Spring Run, Pennsylvania. Scale bars in (A) and (B) are marked in 0.5-m increments; the banks in (A) and (B) are ~2.2 and ~1.4 m high, respectively. (C) Conceptual model based on composite stratigraphy from multiple sites, including stream-bank exposures, trenches, and cores.

established circa 1850 in an estuary fill deposit in the upper Chesapeake Bay, after peak sedimentation from the watershed occurred between 1840 and 1880 (27). Historic air photos dating to the 1930s and maps dating to the early 1800s indicate that ponds diminished in size until the mid- to late 1800s and became stable swamps

and meadows thereafter, until dam breaching and incision.

The characteristics of the presettlement sediments and organic material suggest that valley bottoms were broad, forested wetlands (alder shrub-scrub) with small, shallow (<1-m) anabranching and chain-of-pool streams that experienced

frequent overbank flow, which is consistent with accounts by early explorers of ubiquitous swampy meadows and marshes fed by springs at the base of valley side-slopes (28). The upper surface of the dark hydric soil has low relief and typically extends across valley bottoms [see Fig. 3 and valley cross sections in (8, 24)]. Along a rural section of Western Run northwest of Baltimore, Maryland, for example, we followed the modern deeply incised channel from one side of the valley to the other and mapped a Holocene hydric soil (buried beneath 2 m of historic sediment) for the entire distance; no buried channel deposit was encountered, and at times the hydric soil became more peaty and rested directly upon bedrock. This regional network of small streams and low, vegetated islands within the flood zone was probably impacted heavily by beaver dams and small ponds, which could explain the lack of buried stream channels at all sites observed to date (29). Plant fragments and seeds extracted from these buried hydric soils indicate obligate and facultative wetland species, including various hydrophytic trees, shrubs, sedges, rushes, and cresses. Groundwater flow throughout valley-bottom gravels would have supplied a near-continuous base flow to these wetlands.

Recent responses. In the past 100 years, many historic dams have been breached as mills were abandoned. Breaching has led to incision of streams into the milldam reservoir sediments and to locally heavy erosion of steep stream banks. High-resolution (15-cm-vertical) LIDAR data for the Conestoga River and Western Run indicate that dam height controls stream-bank height (via depth of incision) above the water surface (Fig. 4). These remote-sensing observations are consistent with our field studies, which encompass a much greater area. Fill terraces increase in height downstream toward the tops of breached dams and then drop to the level of backwater effects from the next slackwater reach downstream. By mapping channel banks on high-resolution digital orthophotos from the early 1990s to 2005 for Lancaster and York counties, Pennsylvania, we estimate that bank erosion rates are >0.2 m/year locally and at least 0.05 m/year along many stream reaches upstream of 20th-century dam breaches. In Maryland, stream cross sections monitored for 41 years in a study of meander migration and floodplain formation near the headwaters of Watts Branch, Maryland (2, 9), are located <1 km upstream of a breached 19th-century dam, which was not recognized by previous workers. This dam supplied water from a millpond to Wootton's Mill, which operated until 1905 (fig. S4). Our historic research indicates that the dam breached sometime between 1905 and 1952. The higher valley-flat surfaces upstream of the dam are interpreted here as fill terraces rather than floodplains, even though they might receive occasional overbank flow. Although previous workers interpreted late 20th-century enlargement of the channel to upstream urbanization, we propose that enlargement was a natural response to dam breaching and incision.

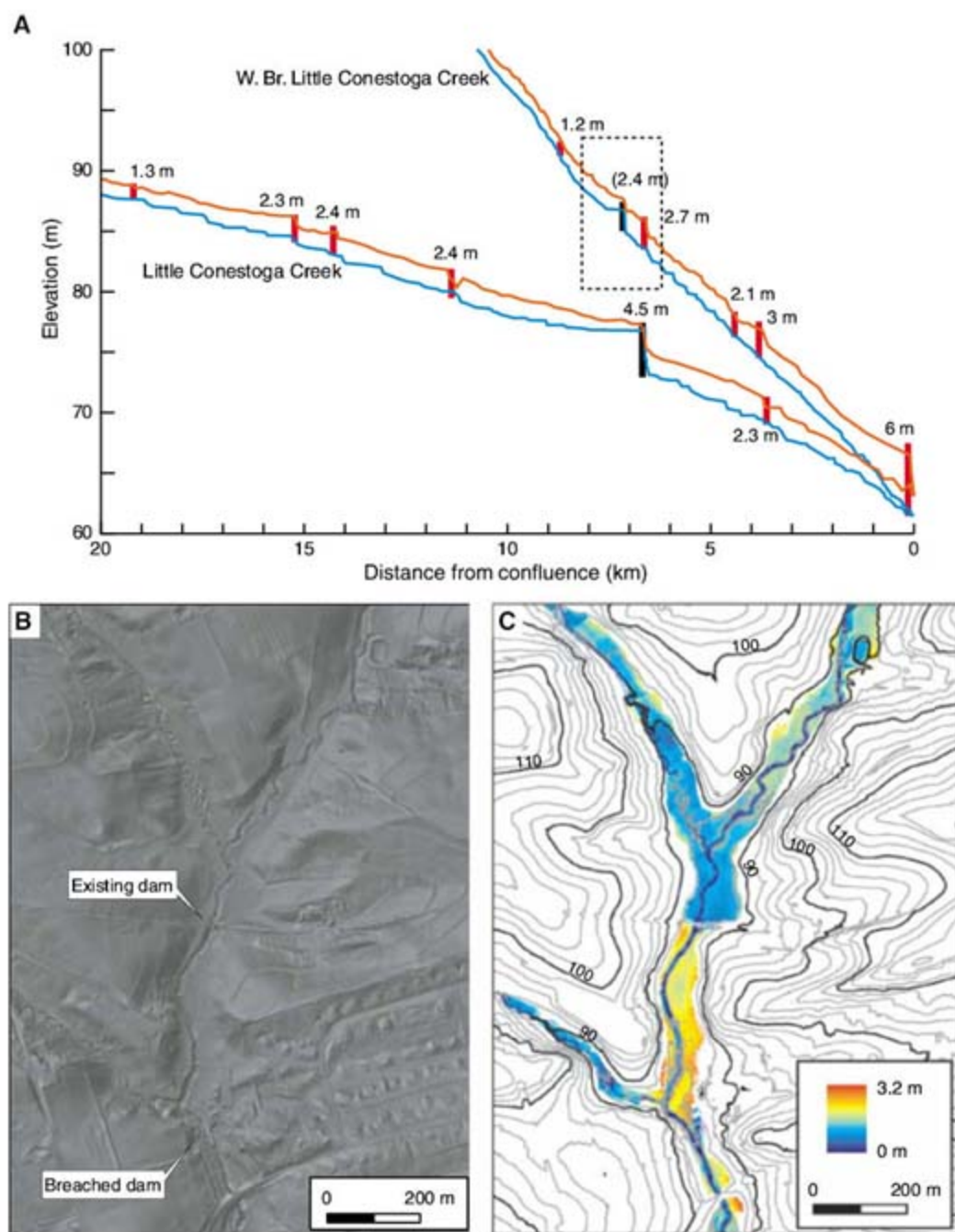


Fig. 4. Methods for locating dams and assessing their impact on reservoir sedimentation, subsequent channel incision, and bank erosion with high-resolution LIDAR. (A) Long profile of Little Conestoga Creek and West Branch Little Conestoga Creek extracted from LIDAR-derived DTM (digital terrain model), depicting locations of milldams (black and red vertical bars). The lower (blue) line for stream profiles approximates the water surface, whereas the upper (red) line approximates banks above streams (i.e., reservoir fill surface). Dams shown in black are still in place; those in red are breached, some only partially. The influence of dams on relative terrace height is apparent, such as at kilometer 7, where the Lake Mill dam is still in place on the Little Conestoga. The area in the dashed box is illustrated in (B) and (C). (B) Hillshade rendering of LIDAR-derived DTM clearly depicts the low-gradient relict millpond surface along the valley corridor. Note that channel incision occurs upstream of the breached dam (denoted at bottom) but not upstream of the partially breached dam ("existing dam," denoted in middle). This difference is documented in (C), which maps the height of the terrace surface above the stream water surface. Upstream of the breached dam, the terrace is up to 3.2 m above the water surface, rising upward toward the dam in the downstream direction. Upstream of the unbreached dam, the terrace height is less than 1 m. Light and dark gray contour lines in (C) are 2- and 10-m intervals, respectively.

Where dams are unbreached or partially breached, deep incision has not yet occurred, and streams are shallow and wide as they spill over the historic dams. In some cases, more recent dams have been constructed within incised channels near the site of older breaches; many of these second-generation dams are also breached. In Pennsylvania, these inset dams typically were constructed in the late 1800s to early 1900s.

Increasing channel width at a breached dam site on the Brandywine River during the past ~100 years is consistent with 671 repeat measurements of fair to excellent quality for less than bankfull discharge at the Chadds Ford U.S. Geological Survey (USGS) gage station, which is located between two closely spaced breached milldams (see SOM text). Our analysis of these data indicates that the ratio of width to discharge for a given discharge range increased from 0.4 to 0.5 between 1908 and 2007. This increase yields an estimate of at least a 10-m increase in channel width, likely resulting from bank erosion, since 1908 and is consistent with (i) our mapping of bank erosion along this reach, (ii) air photos from 1937 to the present that show channel widening, and (iii) the marked rise in suspended sediment loads recorded at this gage station from 1964 to 1978 (USGS data; see SOM text). Similarly, we calculate a power function exponent of 0.26 for the relation between width and discharge at the Chadds Ford gage station, whereas an analysis of hydraulic geometry relations in 1955 yielded an exponent of 0.17 (3). A 50% increase in this exponent during the past ~50 years is consistent with channel evolution by lateral erosion and long-term widening after incision in response to dam breaching (30).

Similar to earlier studies (2, 3, 8), our measurements of sediment size indicate that modern channel-bed sediments are much coarser grained (coarse sands and gravels) than the fine sediments (mostly silt and clay and some sand) that are exposed along stream banks. We attribute this difference not to a meandering stream that deposits gravel in bars and silt and clay on floodplains during overbank flow but rather to increased flow velocities and shear stresses that accompany deep incision of streams into fine-grained millpond sediment. After dam breaching, incised channels have shear stresses >5 to 10 times as high as those of presettlement streams (shear stress is proportional to water depth and slope) and, consequently, are capable of transporting Pleistocene gravels that eroded from the buried toes of hillslopes (Fig. 4). Further, bank erosion removes not only vast amounts of postsettlement alluvium but also wide areas of Holocene wetland soils and Pleistocene basal gravels that covered stream valleys in this region since the end of the last ice age.

To assess the impact of bank erosion on sediment load of the modern streams, we collected ¹³⁷Cs data on sediments from several southeastern Pennsylvania streams and stream banks.

Cesium-137, produced by atmospheric nuclear bomb testing, reached its peak production in 1963 and ceased in the mid-1970s with the banning of atmospheric bomb tests. This non-natural isotope readily infiltrated surface sediments and is strongly adsorbed onto the surfaces of fine-grained soil particles (31, 32). It thus provides a metric for sediment loads and surface erosion (33). Comparison with suspended load data from gage stations indicates that 30 to 80% of suspended sediment is derived from bank erosion (25). Historic stream-bank sediments, which we measured at 15 sites, also have high levels of total carbon, nitrogen, and phosphorus, ranging from 0.5 to 3.1% (C), 400 to 2100 parts per million (N), and 340 to 958 ppm (P); thus, bank erosion is contributing to the high nutrient loads of many of these streams (25). These results are consistent with bank erosion rates and with sediment and nutrient loads measured in other watersheds in the United States and around the world (34–36).

Conclusions. We conclude that fluvial aggradation and degradation in the eastern United States were caused by human-induced base-level changes from the following processes: (i) widespread milldam construction that inundated presettlement valleys and converted them into a series of linked slackwater ponds, coupled with deforestation and agricultural practices that increased sediment supply; (ii) sedimentation in ubiquitous millponds that gradually converted these ponds to sediment-filled reservoirs; (iii) subsequent dam breaching that resulted in channel incision through postsettlement alluvium and accelerated bank erosion by meandering streams; and (iv) the formation of an abandoned valley-flat terrace and a lower inset floodplain. This evolution explains why so many eastern streams have bankfull (discharge) heights that are much lower than actual bank heights. Assessments of bankfull discharge are crucial to estimates of flood potential and to design criteria for stream restoration.

Early workers considered western and eastern streams in the United States to have similar origins and forms [compare with plate 2 in (1)]. However, western streams are in a more tectonically active region, generally have high stream gradients, and carry substantial bed-load fractions, whereas eastern Piedmont streams are in a tectonically quiescent region, have low stream gradients, and largely did not carry gravel (or even much fine sediment) during the Holocene before formation of modern incised channels. Formation of gravel bars in the wake of eroding, meandering channels, followed by overbank deposition of fine sediment, was not the natural process of floodplain formation in the eastern United States before mill damming and subsequent channel incision after dam breaching. Valley bottoms along eastern streams were characterized by laterally extensive, wetland-dominated systems of forested meadows with stable vegetated islands and multiple small channels during the

Holocene. These findings are consistent with research on streams in the Pacific Northwest, which revealed that large woody debris from forested riverine areas was critical to geomorphic processes and habitat before logging, channel clearing, and ditching during the late 1800s to early 1900s (37–39). In particular, logjams blocked channels and led to the formation of side channels and floodplain sloughs, producing multiple anabranching channels and riverine wetlands that are in stark contrast to the large, single channels that exist in these streams today.

Our results explain the unusually thick deposits of fine sediment in stream banks relative to the limited amount of modern overbank deposition (1, 3). They also explain the lack of levees on mid-Atlantic streams (1); the great contrast between fine stream-bank and coarse stream-bed material; the observation that eastern (incised) streams, in comparison with western streams, change little in width as discharge increases at a station (3, 10); and the anomalously high suspended sediment and nutrient loads measured in Piedmont streams (7).

Postsettlement milldam construction and millpond sedimentation were rapid and pervasive. This process inundated, buried, and sequestered presettlement wetlands and altered regional stream functions probably within two generations of settlement. Our field and historical research shows that stream valleys were once lined with millponds, which then silted in to form broad, flat bottom lands. The modern, incised, meandering stream is an artifact of the rise and fall of mid-Atlantic streams in response to human manipulation of stream valleys for water power. Our results indicate that a substantial portion of modern suspended sediment and nutrient loads could be due to dam breaching and erosion of reservoir sediment, which is consistent with studies of recent dam removals elsewhere in the United States (40, 41).

These conclusions change the interpretation of hydraulic geometry in eastern U.S. streams that is based on the archetype of an “ideal meandering river form” and imply the need to reconsider current procedures for stream restoration that rely on reference reach conditions and the assumption that eroding channel banks are natural and replenishable. The current condition of single gravel-bedded channels with high, fine-grained banks and relatively dry valley-flat surfaces disconnected from groundwater is in stark contrast to the presettlement condition of swampy meadows (shrub-scrub) and shallow anabranching streams described here.

This work has implications for interpretation of alluvial sedimentation and stream channel form and evolution in Europe as well as in the United States. Tens of thousands of mills existed throughout Europe by the 18th century, and it is possible that European streams have been responding to anthropogenic base-level rise and fall for up to a millennium (SOM text and fig. S5). We propose that widespread mid- to late

medieval alluviation and burial of pre-Roman organic-rich soils observed in "all lowland and piedmont river valleys in Britain and much of Northern Europe" (42) might have been the result of mill damming.

References and Notes

- M. G. Wolman, L. B. Leopold, *River Flood Plains: Some Observations on Their Formation* (USGS Professional Paper 282-C, Government Printing Office, Washington, DC, 1957), pp. 87–107.
- L. B. Leopold, *Geol. Soc. Am. Bull.* **84**, 1845 (1973).
- M. G. Wolman, *The Natural Channel of Brandywine Creek, Pennsylvania* (USGS Professional Paper 271, Government Printing Office, Washington, DC, 1955).
- M. G. Wolman, *Geogr. Ann. Ser. A Phys. Geogr.* **49**, 385 (1967).
- D. Malakoff, *Science* **305**, 937 (2004).
- E. S. Bernhardt *et al.*, *Science* **308**, 636 (2005).
- A. C. Gellis, W. S. L. Banks, M. J. Langland, S. K. Martucci, *Summary of Suspended-Sediment Data for Streams Draining the Chesapeake Bay Watershed, Water Years 1952–2002* (USGS Scientific Investigations Report 2004-5056, USGS, Reston, VA, 2005).
- R. B. Jacobson, D. J. Coleman, *Am. J. Sci.* **286**, 617 (1986).
- L. B. Leopold, R. Huppman, A. Miller, *Proc. Am. Philos. Soc.* **149**, 349 (2005).
- L. B. Leopold, T. J. Maddock Jr., *The Hydraulic Geometry of Stream Channels and Some Physiographic Implications* (USGS Professional Paper 252, Government Printing Office, Washington, DC, 1953).
- J. E. Costa, *Geol. Soc. Am. Bull.* **86**, 1281 (1975).
- T. S. Reynolds, *Stronger Than a Hundred Men: A History of the Vertical Water Wheel* (Johns Hopkins Univ. Press, Baltimore, 1983).
- U.S. Department of State, *Compendium of the Enumeration of the Inhabitants and Statistics of the United States as Obtained at the Department of State, from the Returns of the Sixth Census* (Thomas Allen, Washington, DC, 1841).
- B. Hunter, *William Mary Q.* **62**, 505 (2005).
- J. T. Lemon, *William Mary Q.* **24**, 501 (1967).
- J. Hartranft, personal communication.
- J. F. Hart, *J. Legal Stud.* **27**, 455 (1998).
- V. T. Chow, *Open-Channel Hydraulics* (McGraw-Hill, New York, 1959).
- G. Verstraeten, J. Poesen, *Prog. Phys. Geogr.* **24**, 219 (2000).
- J. F. Hart, *Am. J. Legal Hist.* **39**, 1 (1995).
- J. F. Watson, *Annals of Philadelphia, and Pennsylvania, in the Olden Time: Being a Collection of Memoirs, Anecdotes, and Incidents of the City and its Inhabitants, and of the Earliest Settlements of the Inland Part of Pennsylvania: Intended to Preserve the Recollections of Olden Time, and to Exhibit Society in its Changes of Manners and Customs, and the City and Country in Their Local Changes and Improvements* (J. M. Stoddart, Philadelphia, 1830).
- S. C. Happ, G. Rittenhouse, G. C. Dobson, *Some Principles of Accelerated Stream and Valley Sedimentation* (USDA, Washington, DC, 1940).
- S. W. Trimble, *Man-Induced Soil Erosion on the Southern Piedmont, 1700–1970* (Soil Conservation Society of America, Ankeny, IA, 1974).
- J. E. Pizzuto, *Sedimentology* **34**, 301 (1987).
- Materials and methods are available as supporting material on Science Online.
- M. E. Ketterer, B. R. Watson, D. Matisoff, C. G. Wilson, *Environ. Sci. Technol.* **36**, 1307 (2002).
- W. B. Hilgartner, G. S. Brush, *Holocene* **16**, 479 (2006).
- P. Kalm, *Peter Kalm's Travels in North America: The English Version of 1770*, A. B. Benson, Ed. (Dover, New York, 1987).
- D. R. Butler, G. P. Malanson, *Geomorphology* **71**, 48 (2005).
- A. Cantelli, C. Paola, G. Parker, *Water Resour. Res.* **40**, W03304 (2004).
- J. C. Ritchie, J. A. Spraberry, J. R. McHenry, *Soil Sci. Soc. Am. Proc.* **38**, 137 (1974).
- D. E. Walling, T. A. Quine, *Land Degrad. Dev.* **2**, 161 (1990).
- J. C. Ritchie, J. R. McHenry, *J. Environ. Qual.* **19**, 215 (1990).
- A. Laubel, B. Kronvang, A. B. Hald, C. Jensen, *Hydrol. Process.* **17**, 3443 (2003).
- A. C. Sekely, D. J. Mulla, D. W. Bauer, *J. Soil Water Conserv.* **57**, 243 (2002).
- A. J. Odgaard, *Water Resour. Res.* **23**, 1225 (1987).
- B. D. Collins, D. R. Montgomery, in *Geomorphic Processes and Riverine Habitat*, J. M. Dorava, D. R. Montgomery, B. B. Paksak, F. A. Fitzpatrick, Eds. (American Geophysical Union, Washington, DC, 2001), pp. 227–243.
- B. D. Collins, D. R. Montgomery, *Restor. Ecol.* **10**, 237 (2002).
- D. R. Montgomery, B. D. Collins, T. B. Abbe, J. M. Buffington, in *The Ecology and Management of Wood in World Rivers*, S. V. Gregory, K. L. Boyer, A. M. Gurnell, Eds. (American Fisheries Society, Bethesda, MD, 2003), pp. 21–47.
- E. H. Stanley, M. W. Doyle, *Bioscience* **52**, 693 (2002).
- M. W. Doyle *et al.*, *Geomorphology* **71**, 227 (2005).
- A. G. Brown, *Alluvial Geomorphology: Floodplain Archaeology and Environmental Change* (Cambridge Univ. Press, Cambridge, 1997).
- We thank M. Rahnis, W. Oberholtzer, J. Hartranft, K. Mertzman, C. Scheid, M. Voli (particularly for the Brandywine Holocene seed analysis), L. Manion, C. Lippincott, S. Siddiqui, Y. Voynova, A. Sullivan, J. Weitzman, Z. Stein, G. Boardman, A. Ross, A. Voynov, Z. Rehman, C. Buchanan, E. Ohlsen, M. Pavich, A. Gellis, M. Langland, F. Kinsey, D. Hood, B. Hackett, B. Hilgartner, N. Potter, R. Sternberg, A. DeWet, C. Williams, J. Strick, S. Sylvester, S. Mertzman, K. Wright, R. Pepino, J. Piotrowski, D. Esher, J. Lape, G. Zern, M. Helmke, M. Trumble, I. Weaver, M. Gutshall, D. Altland, S. Chunks, J. Shuman, D. Hess, R. Thomas, R. Fluck, A. Steiner, B. Pipes, L. Bonchek, R. Bonchek, E. Reilly, J. Morris, L. Irwin, J. Boyle, C. Art, K. Steck, L. McCawley, K. Pattison, A. Stubblefield, G. Matisoff, L. Linker, R. Clark, R. Barlow, C. Myers, G. Wolff, N. Wenger, M. Waugh, M. Raub, A. Swanson, L. Herr, M. Brubaker, and the PA DEP Legacy Sediment Workgroup for providing analyses, data, insights, information, and resources. For discussions, we thank W. Oberholtzer, M. Gutshall, D. Altland, M. G. Wolman, W. Dietrich, C. Braudrick, F. Pazzaglia, P. Wilcock, A. Miller, S. Smith, J. Pizzuto, E. Wohl, R. Slingerland, and the NSF/National Center for Laser Airborne Swath Mapping committee. Research was supported by grants from Franklin and Marshall College, PA DEP, the Pennsylvania Delegation of the Chesapeake Bay Commission, the Franklin and Marshall Geoscience Founders Society, and a Presidential fellowship (R.C.W.) and a sabbatical fellowship [(D.J.M.), Flora Stone Mather Foundation] from Case Western Reserve University. We also acknowledge the landowners who granted us permission to work on their property, particularly J. Sweeney, R. Wimer, G. Wimer, P. Heisey, G. Heisey, J. McFall, A. McFall, R. Mann, D. Mann, G. Mann, J. Dawes, and K. Dawes.

Supporting Online Material

www.sciencemag.org/cgi/content/full/319/5861/299/DC1

Materials and Methods

SOM Text

Figs. S1 to S5

Tables S1 to S4

References

15 October 2007; accepted 14 December 2007

10.1126/science.1151716

Lhx2 Selector Activity Specifies Cortical Identity and Suppresses Hippocampal Organizer Fate

Vishakha S. Mangale,^{1*} Karla E. Hirokawa,^{2*} Prasad R. V. Satyaki,^{1*} Nandini Gokulchandran,^{1*} Satyadeep Chikbire,¹ Lakshmi Subramanian,¹ Ashwin S. Shetty,¹ Ben Martynoga,¹ Jolly Paul,¹ Mark V. Mai,³ Yuqing Li,⁴ Lisa A. Flanagan,⁵ Shubha Tole,^{1†} Edwin S. Monuki^{2,5†}

The earliest step in creating the cerebral cortex is the specification of neuroepithelium to a cortical fate. Using mouse genetic mosaics and timed inactivations, we demonstrated that *Lhx2* acts as a classic selector gene and essential intrinsic determinant of cortical identity. *Lhx2* selector activity is restricted to an early critical period when stem cells comprise the cortical neuroepithelium, where it acts cell-autonomously to specify cortical identity and suppress alternative fates in a spatially dependent manner. Laterally, *Lhx2* null cells adopt antihem identity, whereas medially they become cortical hem cells, which can induce and organize ectopic hippocampal fields. In addition to providing functional evidence for *Lhx2* selector activity, these findings show that the cortical hem is a hippocampal organizer.

Classic genetic analyses in *Drosophila* have described the roles of "selector" genes (1–3), which drive developmental patterning events by cell-autonomously specifying cell identity, suppressing alternative fates, regulating cell affinity, and positioning developmental borders that often serve as secondary signaling centers. The LIM homeobox gene *Lhx2*—a vertebrate ortholog of the well-described *Drosophila* selector gene *Apterous* (*Ap*) (1)—has been postulated to act as a selector gene in the developing mouse cerebral cortex (4). *Lhx2* is expressed in cortical precursor cells but not in the adjacent telencephalic dorsal

midline, which consists of choroid plexus epithelium (CPE) and the intervening cortical hem, a secondary source of bone morphogenetic protein (Bmp) and wingless-int (Wnt) signals (figs. S1 and S4) (4, 5). Previous studies indicate that the hem is required for hippocampal induction and/or expansion (6, 7), but evidence that the hem is sufficient to induce and organize hippocampal tissue has been lacking. Conventional *Lhx2* null embryos ("standard" knockout, or sKO) (8) possess excessive hem and CPE at the expense of hippocampus and neocortex (4, 5). Although this is consistent with a selector gene phenotype, the basic issue of cell autonomy

could not be resolved, because a cell-autonomous fate transformation (cortex-to-hem/CPe) could not be distinguished from a nonautonomous hem/CPe expansion as a result of defects in cortical precursor proliferation (8).

The preneurogenic critical period. Lhx2 expression arises in the forebrain before neurulation and is strong in the cortical neuroepithelium, but absent from the dorsal midline, after neural tube closure (fig. S1, A and B). At embryonic day 10.5 (E10.5), Lhx2 and Lmx1a (hem marker) displayed substantial spatial overlap, which became markedly reduced by E12.5 (Fig. 1A) (4, 5). These patterns suggest a cross-suppression mechanism (2) regulating cortex-hem cell fate and contributing to cortex-hem border (CHB) formation and refinement. Consistent with this, Lhx2 sKO embryos displayed expanded hem (Fig. 1B and fig. S1C) and Lhx2-hem overlap domains (fig. S1D) by E10.5.

To better define the critical period for hem fate suppression by Lhx2, we performed timed inactivations with an Lhx2 conditional knockout (cKO) mouse (fig. S2) (9). Lhx2 inactivation at E0.5 (ACTBCre driver) (10) or E8.5 (tamoxifen-inducible R26CreER driver) (11) resulted in E12.5 hem expansion or diminished dorsal telencephalic phenotypes that were qualitatively and quantitatively indistinguishable (Fig. 1, C and D, and fig. S3A) (12). This indicated a critical period starting on or after E8.5 and no essential Lhx2 functions in the forebrain before this stage.

Tamoxifen (TM)-mediated recombination typically occurs within 48 hours of administration (11, 13). To test E10.5 as the critical period endpoint, we used E10.5 TM injections or Emx1Cre, which drives dorsal telencephalon-specific Cre recombination by E10.5 (14). Both strategies resulted in subtle to inapparent E12.5 phenotypes (Fig. 1, C and D, and fig. S3A). This defines E8.5 to E10.5 as the critical period for hem suppression by Lhx2, a period when the cortical neuroepithelium is composed almost exclusively of stem cells (15) and is not yet producing definitive cortical plate neurons (16).

Lhx2 selector activity at the molecular level. To examine cell-autonomy unambiguously, we generated Lhx2 null mosaics using two complementary methods: (i) mouse embryonic stem cell (ESC) aggregation chimeras (17, 18) using green fluorescent protein (GFP)-expressing Lhx2 null ESCs derived from Lhx2^{-/-} matings

¹Department of Biological Sciences, Tata Institute of Fundamental Research, Mumbai 400005, India. ²Department of Developmental and Cell Biology, School of Biological Sciences, University of California Irvine, Irvine, CA 92697, USA. ³Department of Biology, Swarthmore College, Swarthmore, PA 19081, USA. ⁴Center for Neurodegeneration and Experimental Therapeutics, Department of Neurology, School of Medicine, University of Alabama at Birmingham, Birmingham, AL 35294, USA. ⁵Department of Pathology and Laboratory Medicine, School of Medicine, University of California Irvine, Irvine, CA 92697, USA.

*These authors contributed equally to this work.

†To whom correspondence should be addressed. E-mail: emonuki@uci.edu (E.S.M., cKO component); stole@tifr.res.in (S.T., ESC chimeras)

Fig. 1. Hem fate suppression by Lhx2 during an E8.5 to E10.5 critical period. (A) Double fluorescent in situ hybridization (ISH), boxed regions enlarged (right). At E10.5, cortical (Lhx2, green) and hem (Lmx1, red) markers overlap. By E12.5, this overlap is reduced (arrowheads). Scale bars, 100 μ m (Hoechst panels, 300 μ m). (B) Lmx1a ISH. By E10.5, the excessive hem phenotype (dotted lines) is present in Lhx2 sKO mutants. Scale bar, 300 μ m. (C) Temporal inactivation studies; Wnt3a ISH. E12.5 cKO hem expansion (dotted lines) is similar after E0.5 (ACTBCre) or E8.5 (R26CreER) inactivations but inapparent after E10.5 inactivations (R26CreER or Emx1Cre). Scale bar, 300 μ m. (D) Quantification of hem:dorsal telencephalon area ratios (Wnt3a: Ngn2 areas). White bars, littermate controls; black bars, Lhx2 cKO mutants; error bars, SEM; *t* test, **P* < 0.05; ***P* < 0.005. Unless otherwise noted, all images henceforth are coronal sections, medial left.

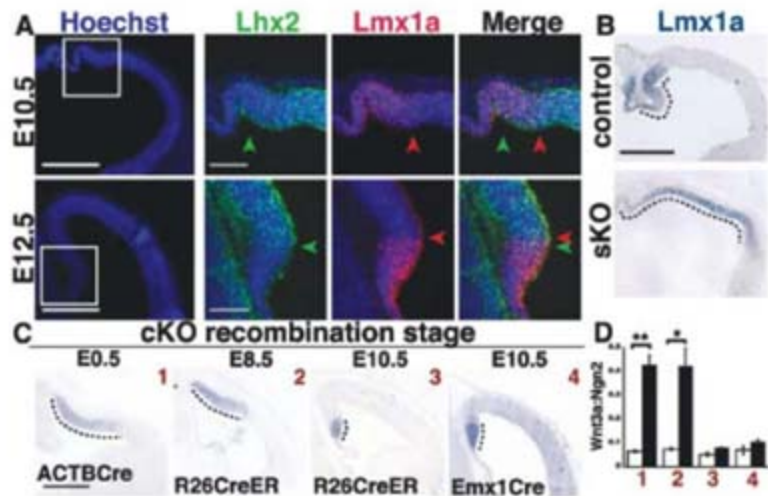
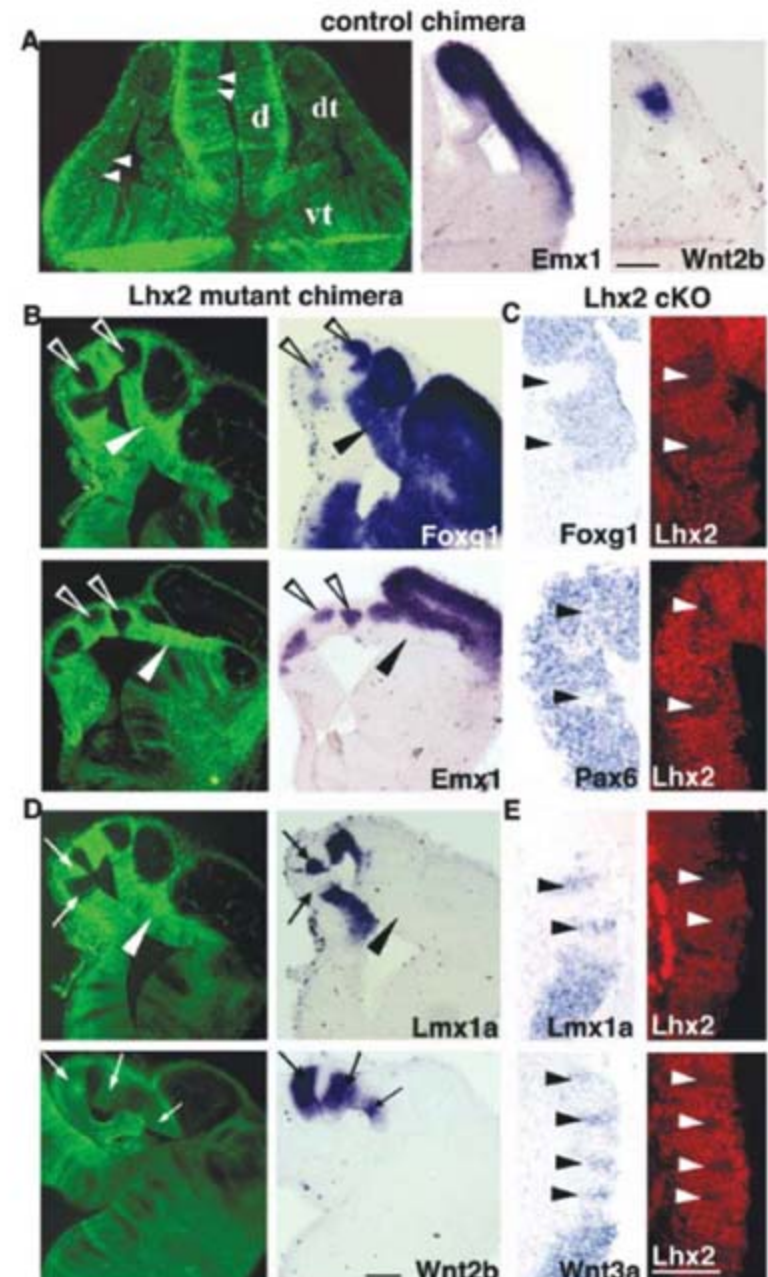


Fig. 2. Cell-autonomous cortex-to-hem fate transformation in Lhx2 null mosaics. (A) In control ESC chimeras, GFP-expressing cells intermix randomly with host cells, and dorsal telencephalic patterning is normal. (B and C) Lhx2-null cells in mutant ESC chimeras [GFP-positive cells in (B)] or in tamoxifen-generated cKO mosaics [Lhx2-negative patches in (C)] do not express Foxg1, Emx1, or Pax6 in medial cortical regions [arrowheads in (C)]. Surrounding wild-type cells express these markers [open arrowheads in (B)]. Laterally, Lhx2-null cells express Foxg1 but not Emx1 [black arrowheads in (B)]. (D and E) Lhx2-null cells express cortical hem markers Lmx1a, Wnt2b, and Wnt3a medially [arrows in (D), arrowheads in (E)] but not laterally in the dorsal telencephalon [arrowheads in (D)]. Scale bars, 100 μ m. d, diencephalon; dt, dorsal telencephalon; vt, ventral telencephalon.



(fig. S4) and (ii) low-dose TM injections at E5.5 in *Lhx2* cKO mice (12). To identify null cells in *Lhx2* cKO mosaics, we developed and validated an affinity-purified *Lhx2*-specific polyclonal antiserum (12).

Whereas control ESC chimeras had random distributions of GFP-expressing cells and normal dorsal telencephalic patterning (Fig. 2A), *Lhx2* null cells in mutant ESC chimeras and cKO mosaics clustered into patches. Null patches within medial cortex displayed down-regulation or absence of cortically expressed *Emx1*, *Foxg1* or *Pax6* (Fig. 2, B and C, and fig. S5C) and ectopic induction of hem markers *Lmx1a*, *Wnt2b*, or *Wnt3a* (Fig. 2, D and E). These results establish a cell-autonomous role for *Lhx2* in the molecular specification of cor-

tical identity and suppression of hem fate. Interestingly, although *Lhx2* null embryos have excessive CPe in addition to hem (-), no molecular (Tr) or morphologic (epithelial simplification) evidence of ectopic CPe was detected in mosaic embryos (Fig. 2). Thus, *Lhx2* activity in cortical stem cells specifically regulates a cortex-hem rather than cortex-CPe fate decision.

The cortex-to-hem transformation in *Lhx2* null cells was spatially dependent (Fig. 2, B and D, and fig. S5). Similar to *Lhx2* sKO mutants (4, 5), the "hem competent zone" in mutant ESC chimeras and cKO mosaics comprised the medial telencephalic wall and extended some distance laterally but did not include the entire pallium. Lateral *Lhx2* null patches did not express hem markers or the

definitive cortical marker *Emx1* but had reduced *Pax6* and unaffected *Foxg1* levels (Fig. 2 and fig. S5). This marker profile characterizes the subpallium; however, like *Lhx2* sKO mutants (4, 5), subpallial genes *Dlx1*, *Dlx2*, and *Mash1* were not ectopically induced in lateral *Lhx2* null patches (fig. S4).

Emx1 absence, with *Pax6* and *Foxg1* presence, also characterizes the antihem, a putative secondary signaling center at the lateral extreme of the pallium (19, 20). Strikingly, the antihem-specific marker *Dbx1* was induced in lateral *Lhx2* null patches in mutant ESC chimeras (Fig. 3D) and in lateral regions of the *Lhx2* sKO dorsal telencephalon (Fig. 3, A and B, and fig. S6). Adjacent sections demonstrated an *Lhx2* sKO pallium composed almost exclusively of antihem and hem fates (Fig. 3B). *Lhx2* activity in cortical precursors therefore suppresses two alternative fates (hem and antihem) at the edges of cortex and results in an *Lhx2* null pallium devoid of hippocampal and neocortical identity at the molecular level (5), a distinct phenotype among cortical transcription factor mutants (Fig. 3C).

Lhx2 selector activity at the cellular level.

In mosaic embryos, a high degree of *Lhx2* null cell clustering was apparent in dorsal telencephalon, lesser degrees in ventral telencephalon, and no obvious clustering elsewhere in the forebrain (Figs. 2 and 4). Conversely, wild-type (*Lhx2*-positive) dorsal telencephalic cells also aggregated in mutant ESC chimeras and often formed true neural rosettes (Fig. 2, B and D, and fig. S7), a morphology not displayed by any *Lhx2* null cell aggregate. To examine clustering further, we compared E12.5 distributions of cells recombined for *Lhx2* or an unlinked locus (*rosa26*) using the low-dose TM strategy. Both qualitatively and quantitatively, *Lhx2* null cells displayed significant clustering throughout the dorsal telencephalon, whereas *rosa26* recombined cells did not (Fig. 4, A and B, and fig. S3, B and C). Taken together, these findings indi-

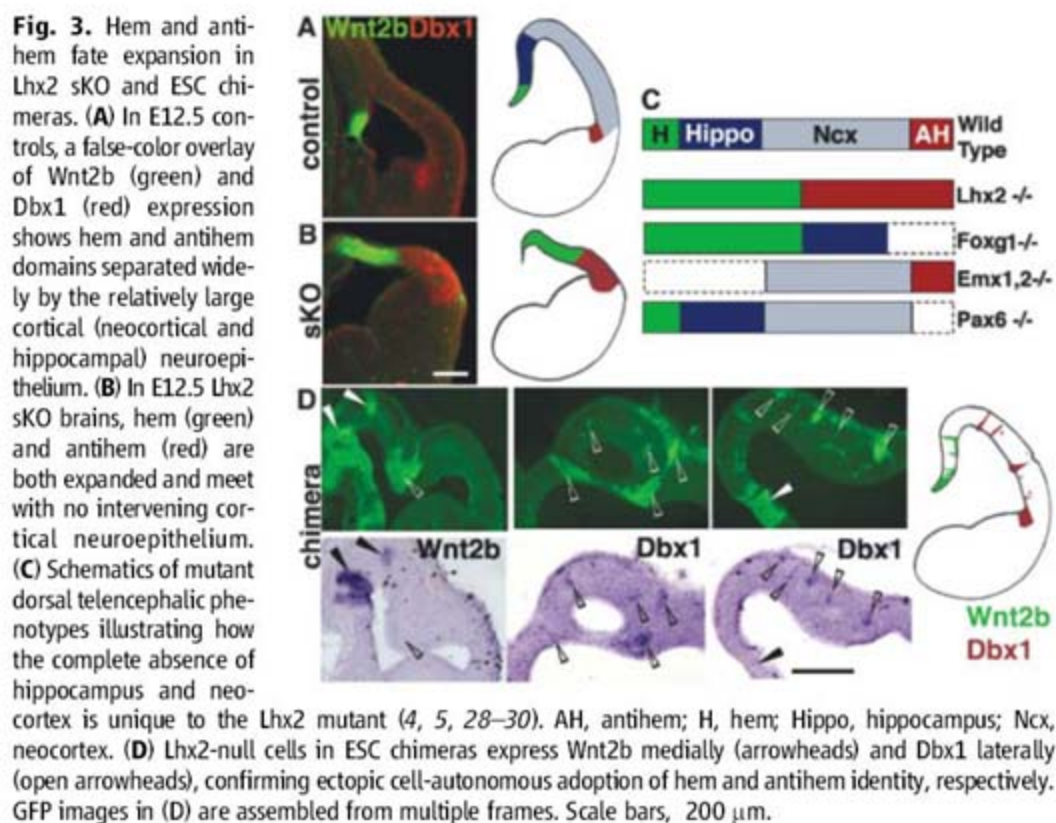
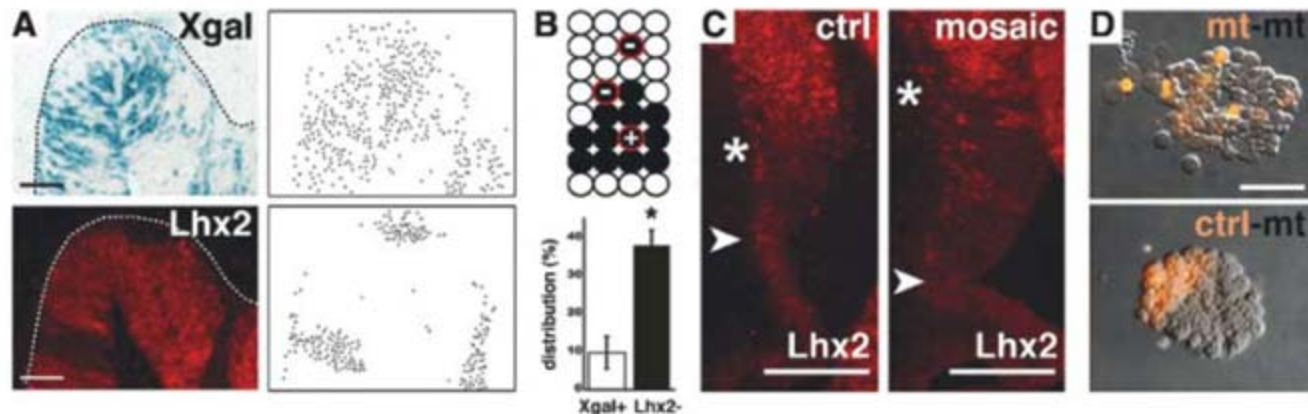
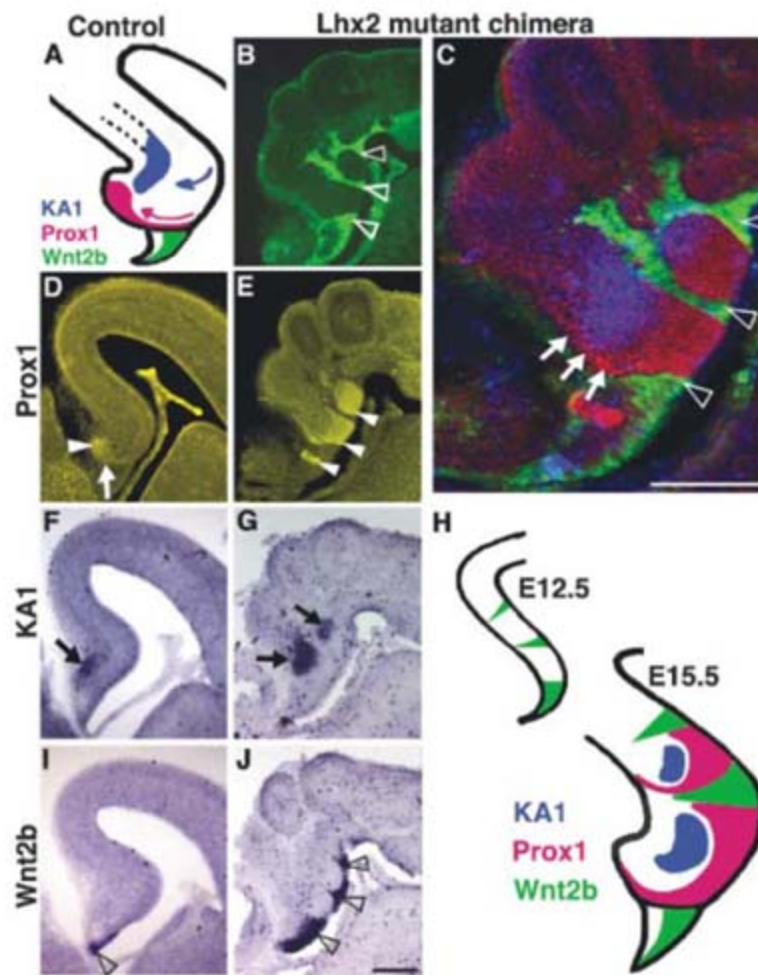


Fig. 4. *Lhx2* on-off state confers differential cell affinity. E12.5 mosaic (*Lhx2*^{cKO/sKO}; *R26*^{CreER/fl}) and control (*Lhx2*^{cKO/+}; *R26*^{CreER/fl}) littermates after 5 μ g per gram of weight TM injection on E5.5. (A) X-gal histochemistry (blue) and *Lhx2* immunohistochemistry (IHC) (red), with corresponding dot panels. X-gal-positive cells in mosaic animals are scattered, whereas *Lhx2*-negative cells in mosaics form contiguous patches. Dotted lines designate pial surfaces. Scale bar, 50 μ m. (B) Quantification of recombined cells (black circles) completely isolated from nonrecombined cells. The percentage of completely isolated X-gal-positive cells in *Lhx2* cKO mosaic embryos (9.8%) was similar to that calculated in *R26*R embryos lacking the



Lhx2 cKO allele (8.5%). (C) *Lhx2* IHC. Compared with controls, the medial *Lhx2*-negative domain (between arrowhead and asterisk) in mosaic embryos is enlarged. Scale bar, 100 μ m. (D) Three-hour in vitro aggregation (21) of E14.5 *Emx1Cre*;*Lhx2* cKO mutant and control littermate cells. Cells in mutant-mutant mixes distribute randomly, whereas cells in mutant-control mixes segregate into discrete clusters. Scale bar, 25 μ m.

Fig. 5. Multiple hippocampal fields induced by ectopic hem cells in *Lhx2* null ESC chimeras. (A, D, F, and I) At E15.5, control *Prox1*-positive dentate granule cells [arrowhead in (D)] have accumulated after migrating along a curved trajectory [pink arrow in (A), arrow in (D)]. *KA1* expression [arrow in (F)] identifies the adjacent hippocampal field CA3. *Wnt2b*-expressing cortical hem is reduced to the fimbrial ventricular surface [open arrowhead in (I)]. (B, E, G, and J) In mutant chimeras, GFP expression and *Prox1* staining (same section) show dentate cells [arrowheads in (E)] juxtaposed to *Lhx2* mutant patches [open arrowheads in (B) and (C)] and an adjacent region of *KA1* expression [arrows in (G)]. *Lhx2* mutant patches express *Wnt2b* in the ventricular zone [open arrowheads in (J)]. (C and H) Overlay of (B), (E), and (G) shows *Prox1*-expressing cells arranged around the *KA1* patch, suggestive of a migrating stream [arrows in (C)]. Images in (B) and (C) assembled from multiple frames. Scale bars, 300 μ m.



(C and H) Overlay of (B), (E), and (G) shows *Prox1*-expressing cells arranged around the *KA1* patch, suggestive of a migrating stream [arrows in (C)]. Images in (B) and (C) assembled from multiple frames. Scale bars, 300 μ m.

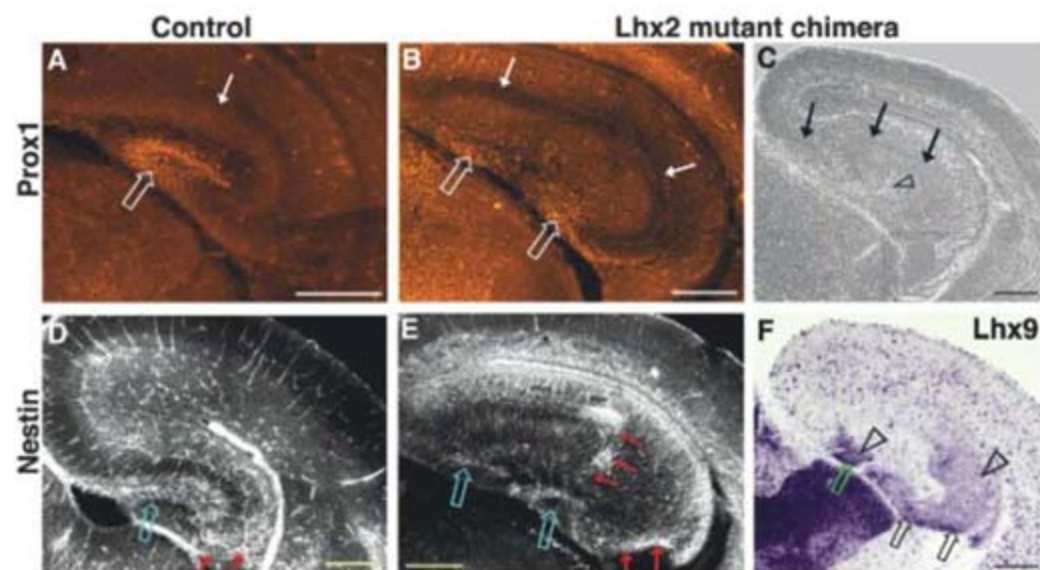


Fig. 6. Structural organization of ectopic hippocampi in *Lhx2*-null ESC chimeras. (A and B) At E17.5, *Prox1* immunostaining labels the control dentate gyrus and two morphologically distinct dentate gyri in the mutant chimeric brain (open arrows). (C) A phase-contrast image of an adjacent section reveals that the normally continuous cell-dense layer of the CA fields has split in the chimeric brain (arrows). (F) This split layer corresponds to two distinct Ammon's horns, labeled by CA3+DG marker *Lhx9*. (D and E) Nestin immunostaining labels the control radial glial palisade and marks two such palisades in the mutant chimera, which take a curved trajectory (red arrows) from the ventricular zone, terminating adjacent to the two dentate gyri (open arrows). (G) Schematic of migration paths in chimeric brain (pink arrows, dentate; blue arrows, CA1/CA3). Images in (A), (B), (D), and (E) were assembled from multiple frames.

cate that both *Lhx2*-null and *Lhx2*-positive cells have homophilic affinity preferences.

In mutant ESC chimeras, including those containing a very low percentage of dorsal telencephalic ESC incorporation, the endogenous cortical hem invariably contained *Lhx2* null cells (fig. S4), consistent with loss of *Lhx2* conferring hem identity. *Lhx2* null cells in these chimeras also preferentially colonized the dorsomedial cortex. To examine this further, we inspected *Lhx2* and *rosa26* recombined cells in low-dose TM embryos. Whereas *rosa26* recombination or accumulation did not display a dorsomedial bias (fig. S3C) (20 sections from three embryos), the dorsomedial telencephalon in the cKO almost invariably displayed an enlarged *Lhx2*-negative domain (Fig. 4C) (50 of 54 sections from four embryos). *Lhx2* null cells therefore preferentially colonize, sort, and/or migrate to the endogenous hem and dorsomedial cortex.

To determine whether cell surface properties account for differential clustering in vivo, we performed short-term in vitro aggregation studies (21). Mixes of *Lhx2* mutant and control littermate cells displayed significant segregation compared with mutant-mutant mixes within 3 hours (Fig. 4D) (82% versus 37% segregation ratios, $\chi^2 P < 0.01$). The *Lhx2* mutant-mutant segregation ratio (37%) was similar to control ratios described previously for embryonic cortical cells (~36%) (21, 22), whereas the *Lhx2* control-mutant ratio (82%) appeared greater than control-*Pax^{sey/sey}* mixes (~50%) (22). Thus, in addition to molecular markers, *Lhx2* specifies cortex versus hem fates at the level of cell surface properties that drive differential cell clustering in vivo.

***Lhx2* selector activity at the functional level.**

Because definitive evidence for hem activity as an organizer has been lacking (23), we examined whether ectopic hem cells exerted cell-nonautonomous effects on neighboring wild-type (*Lhx2*-positive) cortical tissue. In E15.5 mutant ESC chimeras, *Wnt2b* expression in *Lhx2* null patches became restricted to the ventricular surface (Fig. 5, B and J), as occurs in the normal hem (Fig. 5I). Juxtaposed to the ectopic *Wnt2b* domains were *Prox1*-expressing regions (dentate granule cell marker) (Fig. 5, C and E) (24), which in turn were adjacent to *KA1*-expressing clusters (hippocampal CA3 field marker) (Fig. 5, C and G) (25), thus recapitulating the normal hem-dentate-CA3 spatial relationships. Multiple *Prox1*/*KA1* patches were created at considerable distances from their normal locations (Fig. 5, D and F) and at several rostrocaudal levels. Within each patch, *Prox1* staining was typically strongest adjacent to the ectopic hem tissue (arrowheads in Fig. 5E), which suggests recapitulation of normal dentate cell migration patterns (Fig. 5A). Notably, all *Prox1* and *KA1* patches were limited to wild-type tissue, consistent with a cell-nonautonomous effect by ectopic hem cells and an inability of *Lhx2* null cells to take on hippocampal identities.

By E17.5, hem size and Wnt expression are normally diminished; correspondingly, ectopic hem patches were often undetectable. Nonetheless, one chimeric hemisphere displayed two distinct Prox1-expressing dentate gyri oriented in the same direction (Fig. 6B). Notably, each gyrus was associated with its own presumptive Ammon's horn (Figs. 6C), as well as an independent radial glial palisade (Fig. 6E), a scaffolding that guides the migration of dentate cells (26). The two radial glial palisades originated from widely separated positions in the ventricular zone, with intervening regions corresponding to CA field origins (Lhx9) (Fig. 6, F and G), consistent with hippocampal duplication. Wnt signaling is also known to organize the radial glial palisade (27), providing a basis for both the specification and organization of ectopic hippocampi that form adjacent to ectopic hem patches.

Ectopic induction of multiple hippocampal fields was also apparent in another E17.5 hemisphere that contained detectable GFP-positive cells distant from the endogenous hem (fig. S8). These patches were associated with ectopic expression of dentate/CA3 marker Lhx9 adjacent to CA1/neocortex marker SCIP, which appeared between Lhx9-positive domains (fig. S8), indicating the presence of distinct hippocampal fields at a considerable distance from the normal hippocampus.

Discussion. The molecular, cellular (affinity), and functional (organizer and responder activities) evidence for classic selector functions (1) define *Lhx2* as a cortical selector gene. *Lhx2* selector activity is specifically required by cortical stem cells, without which these cells eventually adopt hem or antihem fates rather than hippocampal or neocortical identities. *Lhx2*-negative hem cells, in turn, act nonautonomously on *Lhx2*-positive cortical cells to induce and pattern hippocampal tissue. The absence of neocortex and hippocampus in *Lhx2*-null embryos contrasts with the preservation of one or both of these cortical structures in *Pax6*-, *Foxg1*-, and *Emx1/2*-null mutants (Fig. 3C) (28–30). These transcription factors are therefore likely to act after *Lhx2*, with *Foxg1* being a mediator (28) of *Lhx2*-dependent hem fate suppression (fig. S9). *Lhx2* is itself downstream of *Six3* in zebrafish (31), which is required to form the entire rostral prosencephalon (32), suggesting that *Six3* creates a rostral forebrain field within which *Lhx2* specifies cortical identity. The similarities between *Lhx2* in the cortex and *Ap* in the *Drosophila* dorsal wing compartment—which specifies cell identity (dorsal), suppresses alternative fate (ventral), and confers differential affinity properties that position a signaling center (dorsoventral wing boundary) (33, 34)—are striking. Thus, conserved *Ap/Lhx2* selector functions, as demonstrated in human/fly rescue experiments (35), apparently extend to the mammalian cerebral cortex.

Cross-suppression and differential affinity are typical mechanisms used by selector genes to make tissue borders (2), and our studies

implicate *Lhx2* selector activity in CHB formation and refinement. CHB refinement may also involve cell sorting and/or migration (Fig. 4C). Differential affinity is typically central to cell lineage restrictions at tissue borders (2), and previous studies provide evidence for lineage restrictions at the CHB. *Wnt3a-Cre* (7) and *Gdf7-Cre* lineage analyses (4, 36), as well as *Frizzled10-lacZ* studies based on evidence for *lacZ* perdurance (37), indicate strong confinement of hem precursors from E10.5 to E12.5, and *D6-Cre* lineage tracing provides similar evidence from the cortical side of the CHB (38). Together, these data imply that the CHB is an *Lhx2*-dependent lineage boundary. As both a developmental compartment and secondary signaling center, the hem may share similarities to the zona limitans intrathalamica (ZLI), a secondary Sonic hedgehog (*Shh*) production site that also displays lineage restriction (39).

Although *Lhx2* also regulates the cortex-antihem border (CAB), *Lhx2* roles at the CAB and CHB probably differ, because *Lhx2* is expressed in a continuous fashion across the lateral pallium-ventral pallium (antihem) border. However, *Lhx2* does not regulate the pallial-subpallial boundary (PSB), which instead relies on *Pax6* selector gene activities (2, 5, 40). Moreover, *Pax6* is required to generate antihem (19). Thus, reduced but maintained *Pax6* expression in lateral *Lhx2* null cells suffices to maintain antihem and suppress subpallial fates (40), allowing distinct CAB (*Lhx2*-dependent) and PSB (*Pax6*-dependent) formation mechanisms to be distinguished (fig. S9).

That ectopic hem cells can induce and organize ectopic hippocampal tissue in a cell-nonautonomous fashion provides definitive functional evidence that the hem is a hippocampal organizer. These hem functions may occur before E12.5, because previous explant studies did not uncover hem organizer activity at this stage (41). Hem organizer activity is likely mediated by Wnt signals (6, 27, 42, 43), whereas *Bmps* may specify hem fate rather than hippocampal identity (4, 44, 45). *Fgf8*, a rostromedially localized signaling molecule, may serve as an intermediary, because it is inhibited by *Bmps* and in turn suppresses Wnt expression (46). Our findings extend the known early interactions of the *Bmp-Fgf8-Wnt* signaling mechanisms at the telencephalic midline. Within this signaling framework, *Lhx2* plays a dual role in suppressing hem fate while specifying the fate of hem-responsive tissue to allow for hippocampal specification within the *Lhx2*-positive cortical field.

References and Notes

1. A. García-Bellido, *Ciba Found. Symp.* **0**, 161 (1975).
2. K. D. Irvine, C. Rauskolb, *Annu. Rev. Cell Dev. Biol.* **17**, 189 (2001).
3. P. A. Lawrence, G. Struhl, *Cell* **85**, 951 (1996).
4. E. S. Monuki, F. D. Porter, C. A. Walsh, *Neuron* **32**, 591 (2001).
5. S. Bulchand, E. A. Grove, F. D. Porter, S. Tole, *Mech. Dev.* **100**, 165 (2001).
6. S. M. Lee, S. Tole, E. Grove, A. P. McMahon, *Development* **127**, 457 (2000).

7. M. Yoshida, S. Assimakopoulos, K. R. Jones, E. A. Grove, *Development* **133**, 537 (2006).
8. F. D. Porter et al., *Development* **124**, 2935 (1997).
9. Materials and methods are available as supporting material on Science Online.
10. M. Lewandowski, E. N. Meyers, G. R. Martin, *Cold Spring Harb. Symp. Quant. Biol.* **62**, 159 (1997).
11. T. C. Badea, Y. Wang, J. Nathans, *J. Neurosci.* **23**, 2314 (2003).
12. Additional material is available at www.ucihs.uci.edu/som/pathology/faculty/emonuki/index.html.
13. S. Hayashi, A. P. McMahon, *Dev. Biol.* **244**, 305 (2002).
14. X. L. Jin et al., *Biochem. Biophys. Res. Commun.* **270**, 978 (2000).
15. M. Gotz, W. B. Huttner, *Nat. Rev. Mol. Cell Biol.* **6**, 777 (2005).
16. T. Takahashi, R. S. Nowakowski, V. S. Caviness Jr., *J. Neurosci.* **15**, 6046 (1995).
17. V. Bryja et al., *Stem Cells* **23**, 965 (2005).
18. A. Nagy, M. Gertsenstein, K. Vintersten et al., in *Manipulating the Mouse Embryo: A Laboratory Manual*, A. Nagy, K. Vintersten, R. Behringer, Eds. (Cold Spring Harbor Press, Cold Spring Harbor, NY, 2003) pp. 453–506.
19. S. Assimakopoulos, E. A. Grove, C. W. Ragsdale, *J. Neurosci.* **23**, 6399 (2003).
20. L. Puelles et al., *J. Comp. Neurol.* **424**, 409 (2000).
21. M. Gotz, A. Wizenmann, S. Reinhardt, A. Lumsden, J. Price, *Neuron* **16**, 551 (1996).
22. A. Stoykova, M. Gotz, P. Gruss, J. Price, *Development* **124**, 3765 (1997).
23. G. Li, S. J. Pleasure, *Dev. Neurosci.* **27**, 93 (2005).
24. A. Bagri et al., *Development* **129**, 4249 (2002).
25. S. Tole, C. Christian, E. A. Grove, *Development* **124**, 4959 (1997).
26. M. Rickmann, D. G. Amaral, W. M. Cowan, *J. Comp. Neurol.* **264**, 449 (1987).
27. C. J. Zhou, C. Zhao, S. J. Pleasure, *J. Neurosci.* **24**, 121 (2004).
28. L. Muzio, A. Mallamaci, *J. Neurosci.* **25**, 4435 (2005).
29. K. Shinozaki, M. Yoshida, M. Nakamura, S. Aizawa, Y. Suda, *Mech. Dev.* **121**, 475 (2004).
30. A. Stoykova, D. Treichel, M. Hallonet, P. Gruss, *J. Neurosci.* **20**, 8042 (2000).
31. H. Ando et al., *Dev. Biol.* **287**, 456 (2005).
32. O. V. Lagutin et al., *Genes Dev.* **17**, 368 (2003).
33. S. S. Blair, D. L. Brower, J. B. Thomas, M. Zavortink, *Development* **120**, 1805 (1994).
34. F. J. Diaz-Benjumea, S. M. Cohen, *Cell* **75**, 741 (1993).
35. D. E. Rincon-Limas et al., *Proc. Natl. Acad. Sci. U.S.A.* **96**, 2165 (1999).
36. D. S. Currel, X. Cheng, C. M. Hsu, E. S. Monuki, *Development* **132**, 3549 (2005).
37. C. Zhao, W. Guan, S. J. Pleasure, *Brain Res.* **1077**, 48 (2006).
38. O. Machon, C. J. van den Bout, M. Backman, R. Kemler, S. Krauss, *Neuroscience* **122**, 129 (2003).
39. C. Kiecker, A. Lumsden, *Nat. Rev. Neurosci.* **6**, 553 (2005).
40. T. T. Kroll, D. D. O'Leary, *Proc. Natl. Acad. Sci. U.S.A.* **102**, 7374 (2005).
41. S. Tole, E. A. Grove, *J. Neurosci.* **21**, 1580 (2001).
42. J. Galceran, E. M. Miyashita-Lin, E. Devaney, J. L. Rubenstein, R. Grosschedl, *Development* **127**, 469 (2000).
43. O. Machon et al., *Dev. Biol.* **311**, 223 (2007).
44. J. M. Hebert, Y. Mishina, S. K. McConnell, *Neuron* **35**, 1029 (2002).
45. X. Cheng et al., *J. Neurosci.* **26**, 7640 (2006).
46. T. Shimogori, V. Banuchi, H. Y. Ng, J. B. Strauss, E. A. Grove, *Development* **131**, 5639 (2004).
47. K.E.H. is the first author for the cKO component and V.S.M., P.R.V.S., and N.G. are the first authors for the ESC chimera component of this study. We thank T. Boehm, V. Chizhikov, E. Grove, E. Lai, Q. Ma, R. Maurer, K. Millen, and J. Rubenstein for gifts of plasmid DNA; F. D. Porter for *Lhx2* mutant breeding pairs; the University of California Irvine (UCI) Transgenic Mouse Facility for ESC targeting and generation of the *Lhx2* cKO mouse; the Tata Institute of Fundamental Research Animal House and UCI University Laboratory Animal Resources staff for excellent support; C. Hsu, R. Vu, B. Cyrus, and G. Asulime for technical support in cKO analyses; S. Kumar (Centre for Cellular and Molecular Biology, India), S. Mani (National Brain

Research Centre, India), and M. Panicker (National Centre for Biological Sciences, India) for training in ESC and chimera techniques; and N. Tole-Trivedi for timely assistance in manuscript preparation. This work was supported by a Swarnajayanti Fellowship (Department of Science and Technology, Government of India) and Wellcome Trust Senior Fellowship 056684/Z/99/Z (S.T.), NIH

MH02029, NIH NS053511, the Whitehall and March of Dimes Birth Defects Foundations (E.S.M.), NIH AG23583 (L.A.F.), a traveling fellowship from the journal *Development* and from the British Council (B.M.), postdoctoral fellowships from the Department of Biotechnology (Government of India) (V.S.M. and N.G.), a Kanwal Rekhi Career Development award (L.S.), and NIH training grant NS07444 (K.E.H.).

Supporting Online Material
www.sciencemag.org/cgi/content/full/319/5861/304/DC1
Materials and Methods
Figs. S1 to S9

12 October 2007; accepted 29 November 2007
10.1126/science.1151695

REPORTS

Million-Degree Plasma Pervading the Extended Orion Nebula

Manuel Güdel,^{1,2,3,4,*} Kevin R. Briggs,^{1,5} Thierry Montmerle,⁴ Marc Audard,^{6,7} Luisa Rebull,⁸ Stephen L. Skinner⁹

Most stars form as members of large associations within dense, very cold (10 to 100 kelvin) molecular clouds. The nearby giant molecular cloud in Orion hosts several thousand stars of ages less than a few million years, many of which are located in or around the famous Orion Nebula, a prominent gas structure illuminated and ionized by a small group of massive stars (the Trapezium). We present x-ray observations obtained with the X-ray Multi-Mirror satellite XMM-Newton, revealing that a hot plasma with a temperature of 1.7 to 2.1 million kelvin pervades the southwest extension of the nebula. The plasma flows into the adjacent interstellar medium. This x-ray outflow phenomenon must be widespread throughout our Galaxy.

The Orion Nebula (M42, Fig. 1), together with its parent Orion Molecular Cloud, is the prototypical massive star-formation region (1), in which thousands of stars are forming from collapsing cloud cores (2, 3). Many forming stars are surrounded by molecular envelopes or show circumstellar disks and bipolar jets (4).

The Huygens region of the nebula is the bright region surrounding the massive, ionizing stars of the Trapezium group, the most important member being θ^1 Ori C (5). This region is a thin layer of ionized (HII) gas lying on the surface of the background molecular cloud, with the ionizing stars offset toward the observer. There is a foreground veil of neutral material that confines the central cavity. To the southwest of the Huygens region, the brightness drops rapidly as one views the much larger Extended Orion Nebula [EON henceforth (6)]. Ionized gas flows through the thin layer at about 10 km s^{-1} and then into the southwest cavity (5, 7, 8), where its density of 30 cm^{-3} or somewhat higher (9) is

much lower than the 10^4 cm^{-3} in the Huygens region (5). The geometry of the EON is not well understood, but it must be confined on the far side by the molecular cloud and seems to be laterally bounded by neutral gas and dust.

The Orion Nebula has been a favorite target of x-ray satellites for 30 years (10–12), the Chandra X-ray Observatory having detected almost every single Orion member star as a vigorous x-ray source in a 17 arc min-by-17 arc min field centered on the Trapezium (12). In this paper, we describe deep x-ray observations with the X-ray Multi-Mirror satellite XMM-Newton (13) that afford much wider spatial coverage of the region. The half-degree diameter field we discuss here is centered to the southwest of the Trapezium, almost fully covering the EON cavity.

XMM-Newton's charge-coupled device (CCD) cameras (14, 15) observed several fields covering this region (Fig. 2A). The combined image shows the anticipated large assembly of x-ray bright stars but also exhibits a faint, extended structure in the EON, roughly consisting of a brighter patch in the north and a more extended area in the south. Overlaying the x-ray extended structure on an infrared image taken by the Spitzer Space Telescope (at 4.5 and 5.8 μm ,

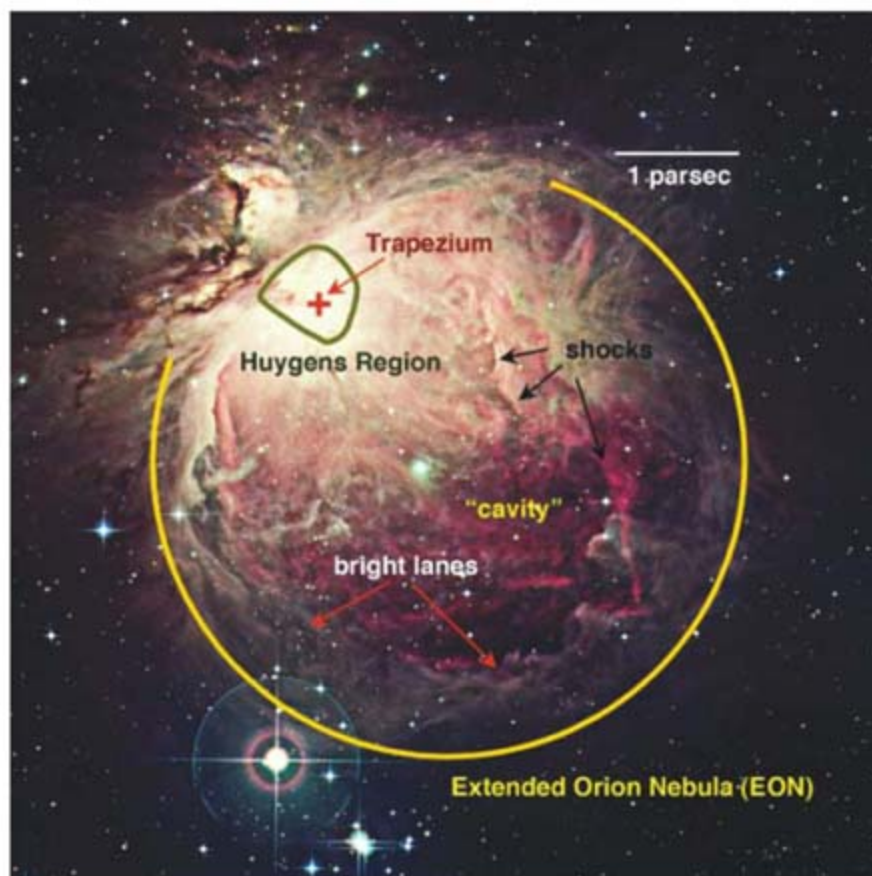


Fig. 1. The Orion Nebula in the optical light (UK Schmidt telescope). [Copyright Anglo-Australian Observatory/David Malin Images] Features described in the text are labeled. The bar in the upper right corner gives the length of 1 pc (3.1×10^{18} cm). North is up, and west is to the right.

¹Paul Scherrer Institut, Würenlingen and Villigen, CH-5232 Villigen PSI, Switzerland. ²Max Planck Institute for Astronomy, Königstuhl 17, D-69117 Heidelberg, Germany. ³Leiden Observatory, Leiden University, Post Office Box 9513, 2300 RA Leiden, Netherlands. ⁴Laboratoire d'Astrophysique de Grenoble, Université Joseph Fourier-CNRS, BP 53, 38041 Grenoble Cedex, France. ⁵Institute of Astronomy, Eidgenössische Technische Hochschule ETH-Zentrum, CH-8092 Zürich, Switzerland. ⁶ISDC, Chemin d'Ecogia 16, 1290 Versoix, Switzerland. ⁷Geneva Observatory, University of Geneva, Ch. des Maillettes 51, 1290 Sauverny, Switzerland. ⁸Spitzer Science Center, California Institute of Technology, Mail Code 220-6, Pasadena, CA 91125, USA. ⁹Center for Astrophysics and Space Astronomy, UCB 389, University of Colorado, Boulder, CO 80309-0389, USA.

*To whom correspondence should be addressed. E-mail: guedel@astro.phys.ethz.ch

Fig. 2. The Orion Nebula with its hot gas bubble. The x-ray image (A) is color-coded for photon energies in the 0.3 to 7.3 keV range (red to blue). The diameter of each of the near-circular fields is 30 arc min (3.5 pc), and the angular resolution is about 5 arc sec. (B) On the same scale, the excess diffuse emission in the 0.3- to 1-keV band with respect to the hard band extracted from the longest observation (16) in blue, overlaid on a composite 4.5- μm (green channel) and 5.8- μm (red channel) mid-infrared image from the Spitzer Space Telescope. X-ray point sources have been removed, and the residual image has been adaptively smoothed (16). The intensity scale is logarithmically compressed. The white contour shows the detector field of view for this x-ray observation. IRAC, Infrared Array Camera. North is up, and west is to the right.

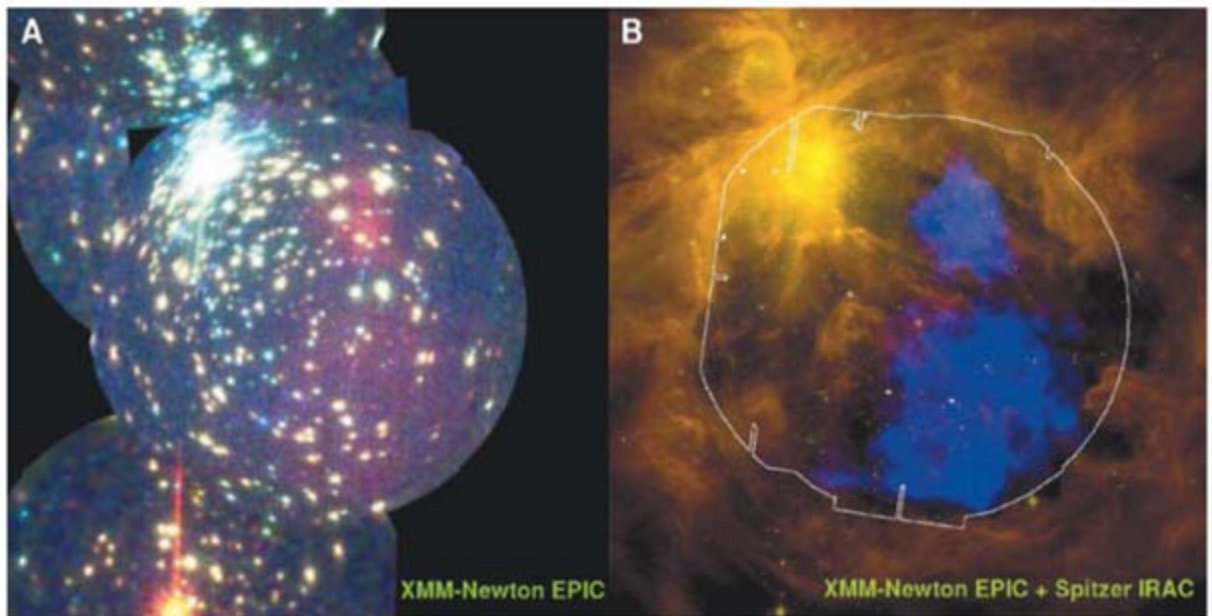


Fig. 2B), we see that the x-ray feature fills in the areas between the infrared structures formed by dense warm dust, such as the shocks (6) in the west and bright lanes in the south of the cavity.

The spectrum of the extended emission (Fig. 3) shows a strong (unresolved) O VII line triplet at 0.55 keV, indicative of 1 to 2 MK plasma. Fitting the derived x-ray spectra with a hot plasma model reveals a dominant temperature of 1.7 to 2.1 MK (16). The observed x-ray luminosity is proportional to the product of the square of the electron density, n_e , and the volume, V , the so-called volume emission measure ($EM = n_e^2 V$), for which the spectral fit found $1.5 \times 10^{54} \pm 0.3 \times 10^{54} \text{ cm}^{-3}$ (SD) and $1.9 \times 10^{54} \pm 0.3 \times 10^{54} \text{ cm}^{-3}$ for the northern and southern area, respectively. Emission from hotter plasma is also present in the spectrum but has been successfully modeled as residual counts from the (incompletely) excised point sources that show much harder emission than our extended structure (16). The much harder stellar emission and the absence of a dense group of young stars in this region in the Spitzer images show that the soft x-rays cannot be unresolved stellar emission but are genuinely diffuse.

Chandra has not detected any diffuse x-ray emission in the central Huygens region (17), most likely because the dense veil of neutral gas located in front of this region, but not of the EON, absorbs soft x-rays. The very low neutral gas column densities we measured in the spectra of the two regions of observed diffuse x-ray emission [$N_{\text{H}} = 4.1 \times 10^{20} \pm 0.7 \times 10^{20} \text{ cm}^{-2}$ for the northern region and $\leq 10^{20} \text{ cm}^{-2}$ at the 1σ level for the southern region] support this view and conclusively demonstrate that the hot plasma is located in front of the dense molecular gas and therefore also the rather thin, optically visible ionization front on the surface of the molecular cloud.

The energy requirement to heat the large-scale x-ray emitting plasma is severe. The absorption-corrected intrinsic x-ray luminosity of the ob-

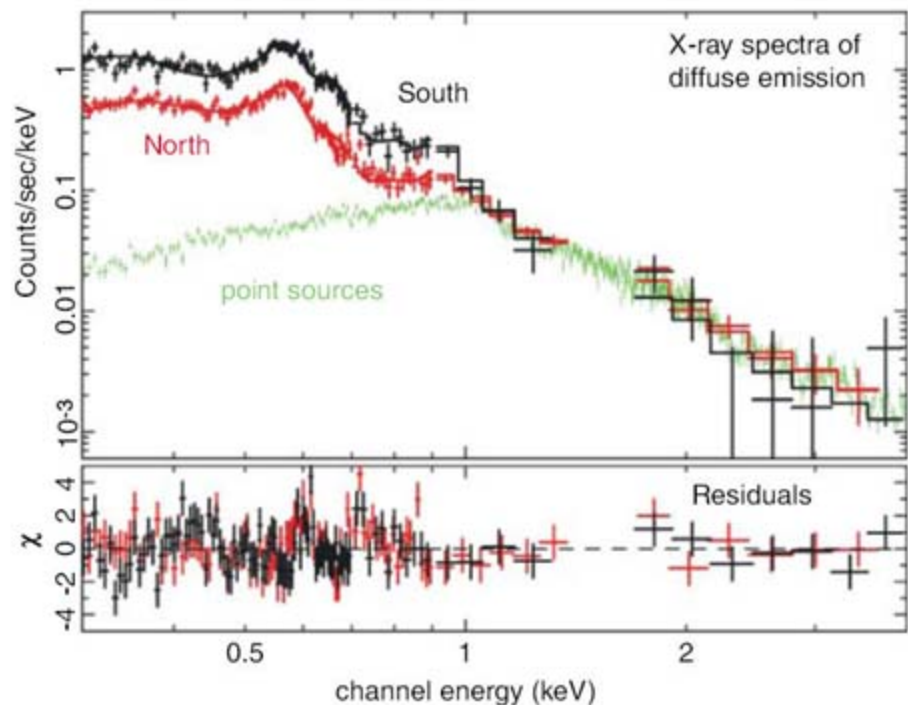


Fig. 3. X-ray spectra of the diffuse emission. The red and black spectrum refer to, respectively, the northern bright patch and the southern more-extended structure in Fig. 2. The error bars attached to each data point reflect 1σ errors from counting statistics. The solid histogram represents a model fit to the spectra on the basis of emission from a thermal plasma (16). The bottom graph gives the fit residuals. The green spectrum shows the contribution from stellar x-rays to the spectrum of the northern diffuse emission.

served diffuse source is $L_X = 5.5 \times 10^{31} \text{ erg s}^{-1}$ in the 0.1- to 10-keV range (or $\approx 3.4 \times 10^{31} \text{ erg s}^{-1} \text{ pc}^{-2}$; additional absorbed radiation may be present). Although massive molecular flows emanate from within the embedded cloud region, their velocities are typically $< 100 \text{ km s}^{-1}$ (18), too slow to shock-heat the gas to the observed temperatures. The total power in fast microjets ejected by the numerous young stars falls short of the observed x-ray power by about two orders of magnitude (4). The structure of the Orion Nebula, its young age [$\approx 3 \text{ My}$ (19)], and the absence of radio shell structures (9) argue against a hot

supernova bubble such as those observed in star-forming regions in the Large Magellanic Cloud (20). The only efficient energy source is provided by the fast winds from the hot Trapezium stars. The wind from $\theta^1 \text{ Ori C}$ alone has a kinetic energy rate $L_w = \dot{M} V_w^2 / 2 \approx 7 \times 10^{35} \text{ erg s}^{-1}$ [$\dot{M} \approx 8 \times 10^{-7} M_\odot \text{ year}^{-1}$ is the mass-loss rate (21), and $V_w \approx 1650 \text{ km s}^{-1}$ is the wind terminal velocity (21)], i.e., four orders of magnitude larger than the observed L_X ; the high velocity wind can easily heat the observed plasma.

The ionization structure and dynamics of the Orion Nebula is very complex and not easily

accessible to comprehensive modeling (5). We can, however, gain insight by applying a simplified, classic interstellar bubble model (22). This model of a massive star wind interacting with a surrounding uniform neutral gas yields four quantities: the radius of the shocked wind bubble, R_b ; its temperature and atomic density, T_b and n_b ; and its luminosity, L_b ; using as input parameters the density n_0 of the gas surrounding the expanding wind bubble, the stellar age t , and the wind parameters \dot{M} and V_w . Because of the weak power-law dependence on the input parameters, T_b is robustly of the order of 1 MK and n_b is of the order of 1 cm^{-3} [with $n_0 = 10^4 \text{ cm}^{-3}$ (8) and $t = 10^6 \text{ year}$ for $\theta^1 \text{ Ori C}$, one finds $T_b = 2.4 \text{ MK}$ and $n_b = 1.3 \text{ cm}^{-3}$]. Given the simplistic model, the computed bubble radius, $R_b \approx 3.9 \text{ pc}$, is acceptably close to the observed EON cavity radius of $\approx 2 \text{ pc}$ (Figs. 1 and 4), especially because the plasma is not entirely confined (in contrast to the model) by the surrounding molecular material.

The cavity depth is likely to be at least 0.9 pc [the distance between the absorbing veil and the ionization front in the Trapezium region (5)] and no more than 4 pc (for a spherical volume filling the EON cavity). With the estimated projected areas of 0.24 pc^2 and 1.4 pc^2 for the northern and the southern diffuse x-ray regions, respectively, the observed x-ray emission measures suggest electron densities of $n_e \approx 0.2$ to 0.5 cm^{-3} and 0.1 to 0.2 cm^{-3} , respectively. Because the density of the radio-emitting material is ≈ 100 to 1000 times higher and its temperature of 0.5×10^4 to $1 \times 10^4 \text{ K}$ is ≈ 200 to 400 times lower (5, 9), the two pressures, $p \approx 2n_e kT$, are comparable; that is, pressure equilibrium approximately holds between the HII gas and the hot plasma if they are in contact. This suggests a leaking cavity in which plasma is continuously replenished. Therefore, the hot x-ray gas is likely to be channeled by the cooler, denser structures rather than disrupting them by expansion.

Extrapolating to the entire cavity (Fig. 4; cavity radius $\approx 2 \text{ pc}$), the above densities suggest

a total mass in the hot gas of $0.07 M_\odot$ (for both geometric models). The mass loss rate of $\theta^1 \text{ Ori C}$, $8 \times 10^{-7} M_\odot \text{ year}^{-1}$ (21), implies replenishment of this gas in only $\approx 10^5$ years, much shorter than the radiative cooling time of 1.8 to 3.9 My derived from the density of the southern source. Because near-pressure equilibrium has been established, the hot gas must flow out of the cavity in the form of an x-ray champagne flow (7); in the case of our observed plasma, mass conservation for the wind of $\theta^1 \text{ Ori C}$ implies a plasma bulk velocity of a few 10 km s^{-1} , depending on the adopted geometry for the channel confined by the cavity. This outflow phenomenon may be common to all massive star-forming regions. The existence of wind-powered extended x-ray emission, theoretically predicted over 30 years ago (22), was demonstrated only recently by Chandra observations of very massive star-forming regions like M17 and Rosette (spectral types O5 and earlier, or $M_* > 60 M_\odot$), the hot gas however showing harder emission (17). Here, in contrast, we suggest that diffuse x-ray emission is commonly present in classic, Orion-like HII regions that host fewer, less massive O stars with powerful winds.

The most likely outlet for the x-ray flow is the nearby Eridanus superbubble discovered by the Röntgen satellite (ROSAT) (23). This huge, hot bubble, 20° in diameter ($\approx 140 \text{ pc}$), is thought to be the result of several supernova explosions having taken place in previous generations of Orion OB stars (24). The wind-shocked gas leaking from the Orion Nebula would thus continuously replenish the Eridanus superbubble. Also, the Orion/Eridanus region has been known to emit 1.809-MeV gamma rays, corresponding to the decay of ^{26}Al in less than a million years. Although the exact site remains uncertain, ^{26}Al production by the Orion massive stars, past or present, followed by funneling into the Eridanus superbubble, has been suggested (25). Our x-ray observations provide a natural explanation for the existence of such a funnel.

Our Galaxy (and other star-forming galaxies) could thus maintain a network of x-ray bubbles and plasma flows, cooling over a few million years but continuously being replenished by shocked winds from a multitude of modest Orion-like star-forming regions, gently leaking out from the parent molecular clouds, in addition to being fed by discrete, but rare, supernova explosions.

References and Notes

1. S. W. Stahler, F. Palla, *The Formation of Stars* (Wiley-VCH, Weinheim, Germany, 2005).
2. M. J. McCaughrean, J. R. Stauffer, *Astron. J.* **108**, 1382 (1994).
3. L. A. Hillenbrand, L. W. Hartmann, *Astrophys. J.* **492**, 540 (1998).
4. J. Bally, C. R. O'Dell, M. J. McCaughrean, *Astron. J.* **119**, 2919 (2000).
5. C. R. O'Dell, *Annu. Rev. Astron. Astrophys.* **39**, 99 (2001).
6. W. J. Henney *et al.*, *Astron. J.* **133**, 2192 (2007).

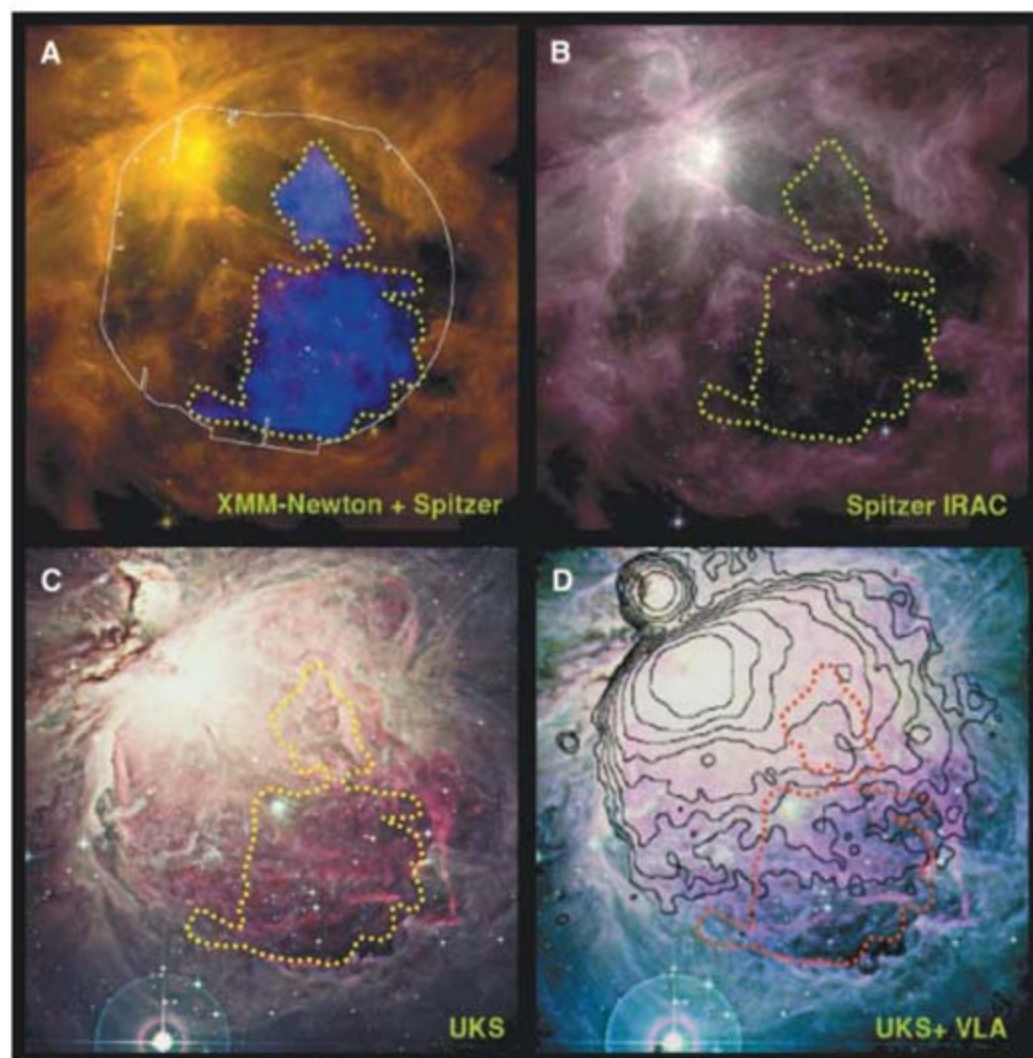


Fig. 4. A multiwavelength view of the Orion Nebula region. The four panels show identical regions; the width of each panel is about 42 arc min, corresponding to 4.9 pc at a distance of 400 pc. (A) Diffuse x-rays (in blue) superimposed on a Spitzer infrared image (Fig. 2B); (B) an infrared image ($3.6 \mu\text{m}$ plus $4.5 \mu\text{m}$ plus $5.8 \mu\text{m}$ composite from the Spitzer Space Telescope); (C) an optical image (from the UK Schmidt telescope) [copyright Anglo-Australian Observatory/David Malin Images]; (D) same with radio contour overlays [from the Very Large Array, observed at 330 MHz (9), reproduced by permission of the American Astronomical Society]. The dotted contour outlines the area where most of the detected diffuse soft x-ray emission is located.

7. G. Tenorio-Tagle, *Astron. Astrophys.* **71**, 59 (1979).
8. W. J. Henney, S. J. Arthur, M. T. García-Díaz, *Astrophys. J.* **627**, 813 (2005).
9. R. Subrahmanyan, W. M. Goss, D. F. Malin, *Astron. J.* **121**, 399 (2001).
10. W. H.-M. Ku, G. Chanan, *Astrophys. J.* **234**, L59 (1979).
11. M. R. Gagné, J.-P. Caillault, J. R. Stauffer, *Astrophys. J.* **445**, 280 (1995).
12. E. D. Feigelson et al., *Astrophys. J. Suppl. Ser.* **160**, 379 (2005).
13. F. Jansen et al., *Astron. Astrophys.* **365**, L1 (2001).
14. L. Strüder et al., *Astron. Astrophys.* **365**, L18 (2001).
15. M. J. L. Turner et al., *Astron. Astrophys.* **365**, L27 (2001).
16. Materials and methods are available as supporting material on Science Online.
17. L. K. Townsley et al., *Astrophys. J.* **593**, 874 (2003).
18. C. R. O'Dell, T. Dai, *Astron. J.* **125**, 277 (2003).
19. F. Palla, S. W. Stahler, *Astrophys. J.* **525**, 772 (1999).
20. L. K. Townsley et al., *Astron. J.* **131**, 2140 (2006).
21. C. Leitherer, *Astrophys. J.* **326**, 356 (1988).
22. J. Castor, R. McCray, R. Weaver, *Astrophys. J.* **200**, L107 (1975).
23. D. N. Burrows, K. P. Singh, J. A. Nousek, G. P. Garmire, J. A. Good, *Astrophys. J.* **406**, 97 (1993).
24. A. Blaauw, in *The Physics of Star Formation and Early Evolution*, C. J. Lada, N. Kylafis, Eds. (Kluwer, Dordrecht, Netherlands, 1991), vol. C342, pp. 125–154.
25. R. Diehl, *N. Astron. Rev.* **46**, 547 (2002).
26. We thank D. Malin for providing the optical image of the Orion Nebula taken with the UK Schmidt telescope and granting permission to use it and R. Subrahmanyan and the American Astronomical Society for granting permission to reproduce the radio panel in Fig. 4D. This

research is based on observations obtained with XMM-Newton, a European Space Agency (ESA) science mission with instruments and contributions directly funded by ESA member states and the United States (NASA). M.A. acknowledges support from a Swiss National Science Foundation Professorship (PP002-110504), and S.S. from NASA grant NNG05GE69G.

Supporting Online Material

www.sciencemag.org/cgi/content/full/1149926/DC1
Materials and Methods
Figs. S1 to S3
Table S1

30 August 2007; accepted 15 November 2007
Published online 29 November 2007;
10.1126/science.1149926
Include this information when citing this paper.

Elementary Structural Motifs in a Random Network of Cytosine Adsorbed on a Gold(111) Surface

Roberto Otero,^{1*} Maya Lukas,^{1†} Ross E. A. Kelly,^{2‡} Wei Xu,¹ Erik Lægsgaard,¹ Ivan Stensgaard,¹ Lev N. Kantorovich,² Flemming Besenbacher^{1§}

Nonsymmetrical organic molecules adsorbed on solid surfaces may assemble into random networks, thereby providing model systems for organic glasses that can be directly observed by scanning tunneling microscopy (STM). We investigated the structure of a disordered cytosine network on a gold(111) surface created by thermal quenching, to temperatures below 150 K, of the two-dimensional fluid present on the surface at room temperature. Comparison of STM images to density functional theory calculations allowed us to identify three elementary structural motifs (zigzag filaments and five- and six-membered rings) that underlie the whole supramolecular random network. The identification of elementary structural motifs may provide a new framework for understanding medium-range order in amorphous and glassy systems.

The microscopic description of glasses and amorphous solids is in general very challenging because of the lack of long-range order in their structure (1). The structure of amorphous solids has traditionally been studied by space-averaging diffraction techniques, which have provided a detailed description of such materials on the macroscopic scale (1, 2). However, much less is known about the local structure of such disordered solids. Important breakthroughs in this respect came from optical microscopy studies of colloidal glasses (3, 4). However, because of the nonscalable behavior of the

energy-relaxation processes with particle size, many details of how the molecular glasses persist and the dynamics of the glass transition cannot be answered with these model systems (4).

Some organic molecules can form hydrogen bonds via peripheral functional groups that may be distributed in a highly anisotropic way. Such molecules have the potential to organize in random arrangements when deposited on atomically flat solid surfaces. The structure and dynamics of these systems can be addressed by scanning probe techniques at the molecular level (5–7), provided the adsorption geometry is planar; they thereby have the potential to become a model system for studies on the structure of amorphous solids. In principle, the realization of such disordered systems also requires molecule-surface interactions to be much weaker than molecule-molecule interactions: If the molecules had an ability to arrange themselves in the gas phase in planar disordered structures, a strong interaction of the molecules with the surface would force them to form well-ordered structures controlled by the surface periodicity.

The formation of a planar network is exemplified by the case of guanine (G) on Au(111) (8). In this case, G self-assembles into a network of G quartets, as determined almost entirely by

hydrogen bonding between the adsorbates; the role of the surface is only that of promoting planarity, as the corrugation of the potential energy surface is rather flat. However, the symmetry of the functional groups around the G molecules enables ordered networks to be formed.

We have studied the molecular-scale self-assembly of a cytosine (C) network on the Au(111) surface in real space by means of scanning tunneling microscopy (STM). In this case, a supramolecular network also forms, but unlike the previously reported case of a G structure, the C network lacks long-range order. DNA base molecules adsorb weakly on noble metal surfaces, with an adsorption potential energy surface displaying a small corrugation and a weak charge transfer between molecule and substrate (8–11). Experimentally we find that the C molecules are sufficiently mobile on the Au(111) surface, so that the molecular layer can be considered as a two-dimensional (2D) fluid at room temperature. Previous theoretical studies indicate that because of the large number of hydrogen-bond donor and acceptor groups with which C is provided, a relatively large number of stable C-C dimer configurations could form, involving double hydrogen bonds between groups of neighboring peripheral functionalities (or “binding sites”; see inset in Fig. 1A) (12). The multiplicity of the strongest C-C dimer states with similar binding energies and the nonsymmetrical distribution of the corresponding binding sites over the periphery of the molecules suggest that intermolecular interactions alone might direct the growth of disordered structures. Indeed, our STM results reveal that the 2D fluid of mobile C molecules found at room temperature, when quenched to low temperatures at a cooling rate of about 20 K/min on average, assembles into disordered structures, thus behaving like a 2D glass.

When C molecules at a coverage of less than one monolayer (ML) are deposited on Au(111) at room temperature and the sample is imaged by STM at temperatures of ≥ 180 K, no individual C molecules are observed because of their high mobility. Instead, noise is observed in the STM signal, the origin of which is associated with mobile C molecules diffusing under the STM tip much faster than the average STM scanning

¹Interdisciplinary Nanoscience Center, Centre for DNA Nanotechnology, and Department of Physics and Astronomy, University of Aarhus, 8000 Aarhus C, Denmark. ²Department of Physics, School of Physical Sciences and Engineering, King's College London, Strand, London WC2R 2LS, UK.

*Present address: Departamento de Física de la Materia Condensada, Facultad de Ciencias, Universidad Autónoma de Madrid, and Instituto Madrileño de Estudios Avanzados en Nanociencia, 28049 Madrid, Spain.

†Present address: Institute for Nanotechnology, Forschungszentrum Karlsruhe, Postfach 3640, D-76021 Karlsruhe, Germany.

‡Present address: Department of Physics and Astronomy, University College London, Gower Street, London WC1E 6BT, UK.

§To whom correspondence should be addressed. E-mail: fbe@inano.dk

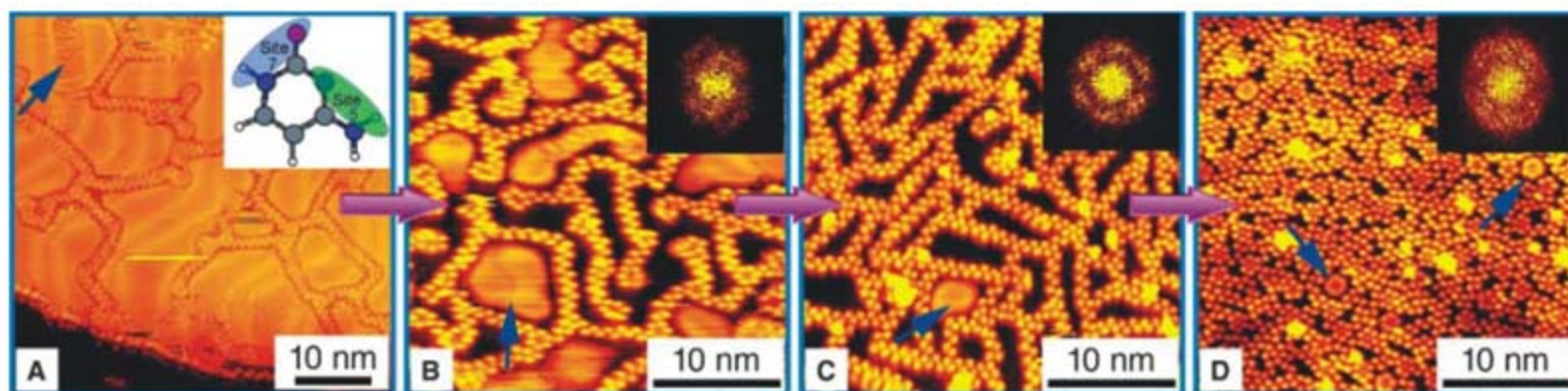


Fig. 1. STM images of cytosine structures with increasing surface coverage (as denoted by the pink arrows). (A to C) Blue arrows indicate mobile C zigzag branches (A) and C molecules or clusters trapped in nanocages that appear as blurs [(B) and (C)]. The inset of (A) shows the most important binding sites used to form

double hydrogen bonds between cytosine molecules. (D) At higher coverages, the blurs show internal structures as 5- or 6-fold rings. Scanning conditions: (A), tunneling current $I_t = -0.5$ nA, tunneling voltage $V_t = -1767$ mV; (B), $I_t = -0.3$ nA, $V_t = -1767$ mV; (C), $I_t = -0.7$ nA, $V_t = -1250$ mV; (D), $I_t = -0.2$ nA, $V_t = -1250$ mV.

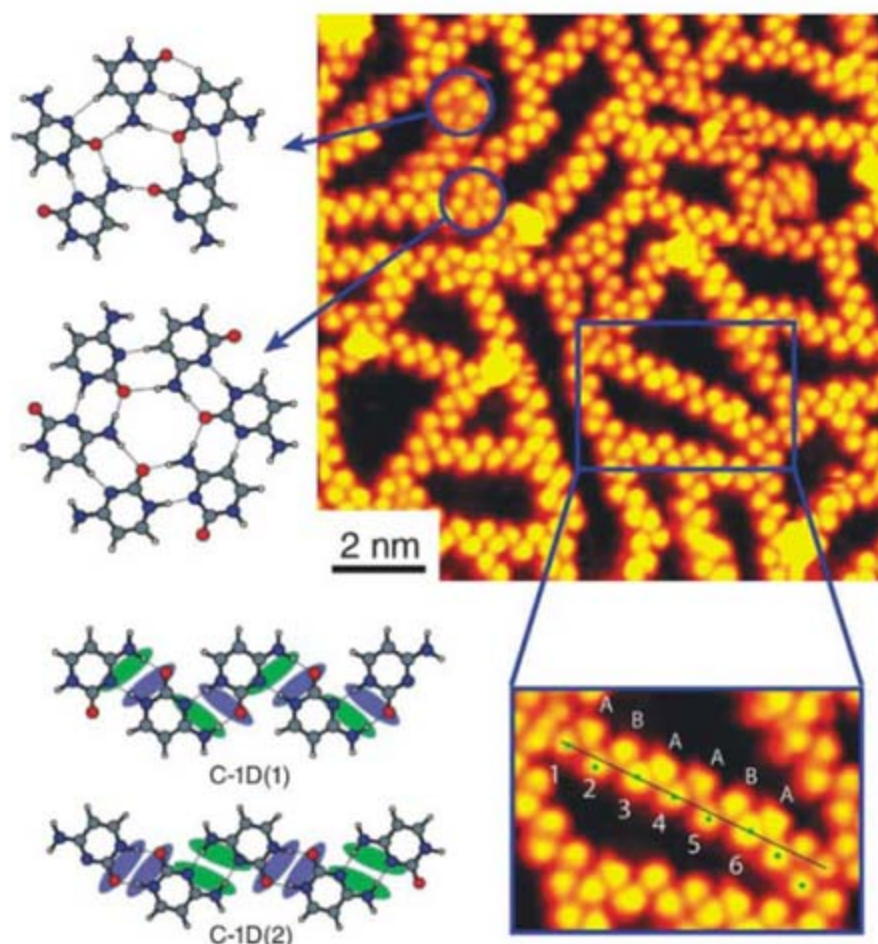


Fig. 2. Three elementary structural motifs (filaments, 5- and 6-fold rings) are compared with the theoretical models. The color coding in the filament models (see inset of Fig. 1A) indicates the binding sites 5 and 7 involved in the two filaments, which makes the chirality of the molecules easier to recognize. The enlarged image shows that the seemingly straight filaments have no translational periodicity. The noncircular shapes of the molecules, which are clearly not tip artifacts (molecules A are mirror images of B), can be recognized in the high-resolution STM images. A line connecting the centers (indicated by green dots) of molecules 1 and 6 is used as a reference. Molecules 1, 3, 4, and 6 binding to molecules A are centered along the reference line, whereas molecules 2 and 5 binding to molecules B are off the reference line. Thus, the above evidence strongly suggests that the dimers 1-A, 3-A, 4-A, and 6-A should be different from dimers 2-B and 5-B, indicating that the filament changes its structure after two or three dimers. Scanning conditions: $I_t = -0.7$ nA, $V_t = -1250$ mV.

time (13, 14). We refer to this state as a 2D fluid. A series of STM images recorded at low temperatures (120 to 150 K) for increasing coverages on the surface is shown in Fig. 1. Near 1 ML, the observed C structure is clearly disordered (Fig. 1D) with no long-range periodicity,

and the C structure thus represents an amorphous 2D system. This long-range disorder is reflected in its fast Fourier transform (FFT), shown in the inset of Fig. 1D, which reveals only a bright rim corresponding roughly to a constant first-neighbors distance. This short-range order is

characteristic of most covalent and metallic glasses, thus indicating that the amorphous structure depicted in Fig. 1D can be described as a 2D glass.

The lack of long-range order is also apparent at lower C coverages (Fig. 1, A to C), although a slight anisotropy in the intensity distribution of the FFT of the STM images along the high-symmetry directions of the gold substrate seems to indicate a small but measurable templating effect of the substrate on the molecular arrangement. For low C coverages (below 0.5 ML), the diffusion dynamics of the C molecules and supra-molecular clusters is revealed even at 100 K. Time-lapse STM movies recorded with the fast-scanning Aarhus STM reveal rearrangements of the different structural elements with respect to each other (see movie S1). Some of the C structures appear as blurred protrusions in the STM images and cannot be resolved into their molecular constituents. In Fig. 1, B to D, these blurred protrusions can be found in the “nanocages” between randomly oriented C filaments. Movie S2 shows that the C-related protrusions may move in and out of a “nanocage” if manipulation with the STM tip breaks one of its “walls.” Upon subsequent increase of the C coverage, the number of blurred protrusions decreases, and these initially featureless blurred protrusions (see Fig. 1B, where one example is indicated by blue arrow) begin to display some internal structure, first appearing like a “doughnut” (Fig. 1C, blue arrow) and subsequently like blurred 5- and 6-fold rings (Fig. 1D, blue arrows). These findings suggest that the blurred structures correspond to mobile C molecules or clusters enclosed in the “nanocages” of the random C network, unable to attach to it.

A detailed analysis of the STM images obtained for coverages below 1 ML revealed that every C molecule belongs to at least one of the following three structural units: (i) zigzag filaments, (ii) 5-fold rings, and (iii) 6-fold rings (Fig. 2). More than 200 images were analyzed for more than five different coverages, and for each coverage at least 20 images were examined. Thus, for our model system, the problem of describing this disordered structure can be reduced to the

much simpler problem of understanding how these three elementary structural motifs link together.

To further characterize the structure of the random C network, we performed *ab initio* density functional theory (DFT) calculations. The minimum-energy configurations for C molecules with geometries similar to the zigzag chains and the 5- and 6-fold rings revealed in the STM images are shown in Fig. 2. By systematically attaching molecules to each other in all possible ways (12), several configurations with very similar binding energies were found for all three structures. The two most stable models for the periodic zigzag filaments, obtained by assuming that the unit cell is composed of two C molecules (that is, a C-C dimer), are denoted C-1D(1) and C-1D(2), respectively. The calculated binding energies of about 0.9 eV/molecule for these two structures are very similar and are much larger than those obtained for 5- and 6-fold C rings (0.6 eV/molecule), in good agreement with the experimental finding that the filaments are the most common structure observed in the STM images. Because the stabilization energies of the two filamentary structures C-1D(1) and C-1D(2) corresponding to the same motif are very similar, we assume that all of them coexist in the random cytosine network, and their very similar geometry makes them indistinguishable by STM. From the calculations we find that the interaction with the gold surface is much weaker (adsorption energy found to be 0.1 eV) than the identified intermolecular hydrogen bonding strength between the C molecules. Although there is a weak indication in the FFT images of a preferential alignment of the filaments along the symmetry directions of the gold surface (Fig. 1C), this effect is much smaller than that of the hydrogen bonding that drives the assembly of C molecules.

We next addressed how these different elementary structural motifs interconnect with each other to form the specific disordered cytosine networks. The ends of the two stable finite filament segments (Fig. 2) exhibit a number of exposed hydrogen-bonding groups—that is, they are “sticky”—whereas the peripheral functional groups exposed on the sides of the filaments are mostly nonpolar and thus are less prone to form stable bonds to neighboring C molecules. Correspondingly, we never observed a “bare” filament termination. As shown in Fig. 3, A and C, the filaments are always linked to some other filament through a 6-fold ring or in a T-junction fashion (possible models for which are displayed in Fig. 3, B, D, and E). Similarly, the “sticky ends” of any two filaments can join head-to-tail, resulting in either bent or apparently linear filament structures (Fig. 3, F and G). Our STM images show that indeed most of the observed filaments that are longer than four to six dimers quite often are bent (Fig. 3C). Furthermore, our high-resolution STM images reveal a change in the shape of molecules (marked as A and B in the enlarged STM image in Fig. 2) along straight filaments in positions that would be equivalent if

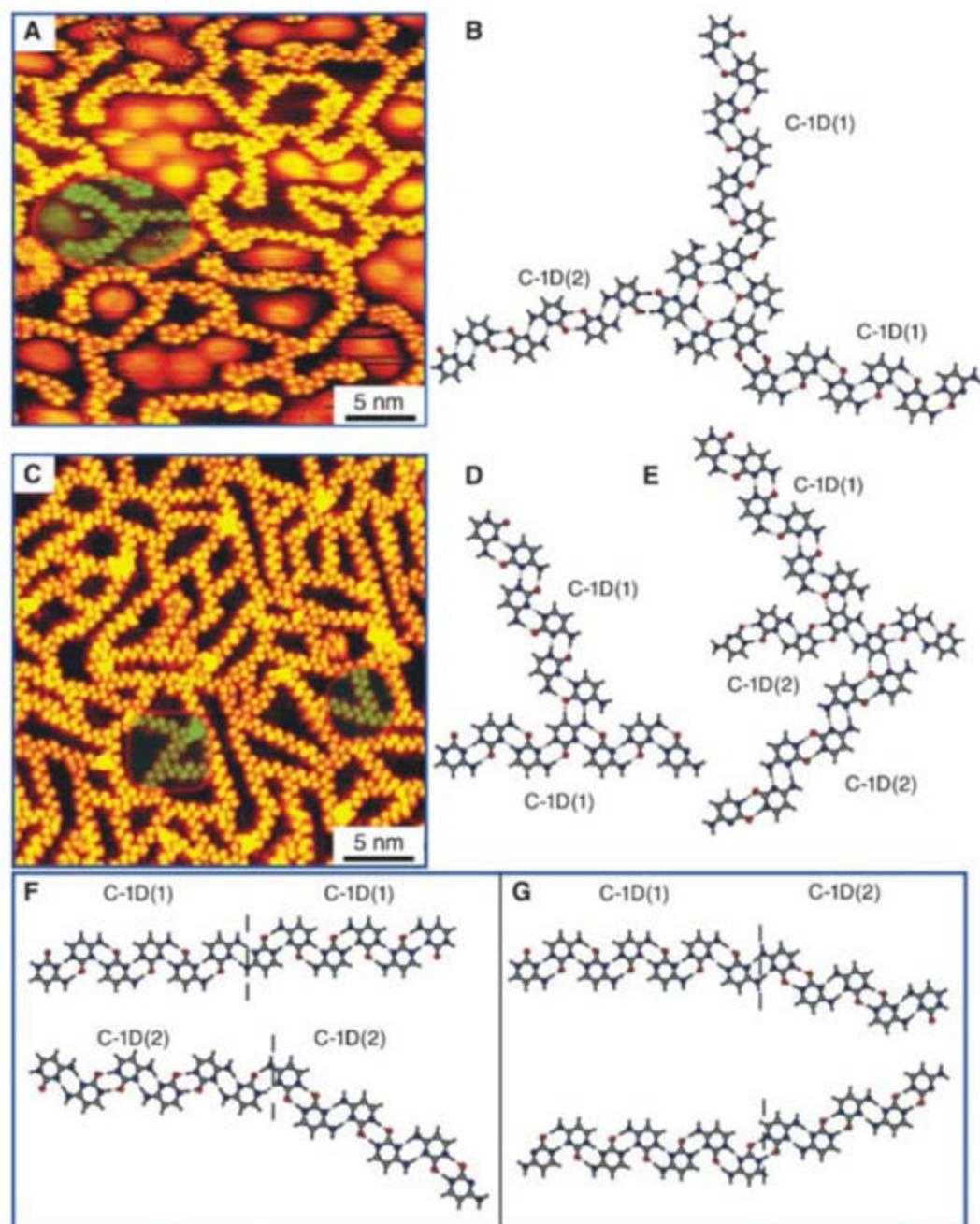


Fig. 3. (A and B) An STM image (A) and a theoretically predicted structure (B) show the connections between C filaments and 6-fold rings in a “roundabout” fashion. (C) An STM image shows the C filaments linked together mainly via T- and bending junctions. (D to G) The corresponding theoretically predicted structures. Examples of “roundabout” and T-junction motifs are highlighted by a red oval in (A) and a red square in (C). Scanning conditions: (A), $I_t = -0.4$ nA, $V_t = -1051$ mV; (C), $I_t = -0.7$ nA, $V_t = -1250$ mV.

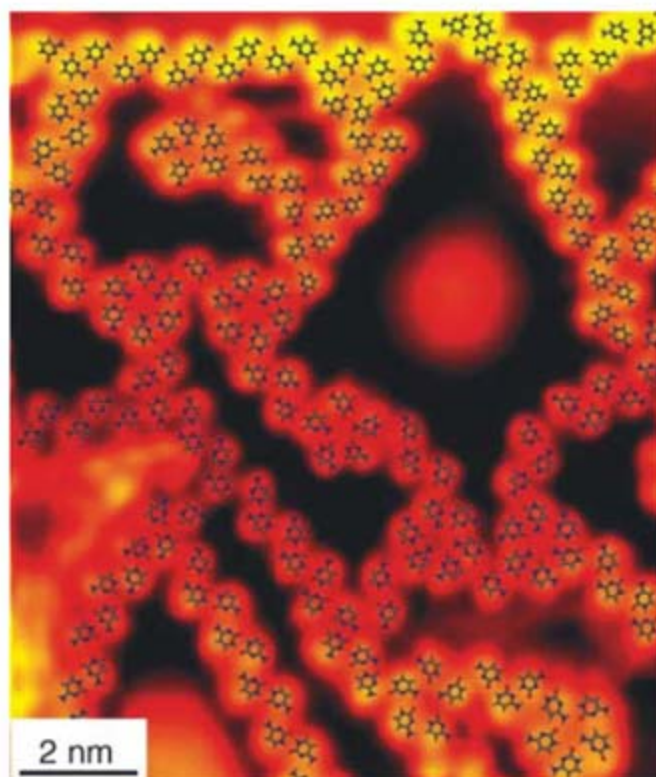
there were translational periodicity. This indicates that these A and B molecules do not have the same orientation; thus, translational periodicity appears only over two to three dimer distances along the filaments.

Figures 3A and 3B depict experimentally and theoretically, respectively, how the “sticky ends” of cytosine filaments can link together through the 6-fold ring in a “roundabout” fashion. As in the case of 5- and 6-fold ring formations, the bonds involved in the interconnections among the different elementary structural motifs will be weaker than those involved in the stabilization of the C-1D structures. On the other hand, the “nonsticky” nature of the filament’s side borders makes it difficult for molecules or molecular clusters trapped inside “nanocages” to attach to

their “walls,” and thus they diffuse fast in the enclosed regions (they appear as blurred protrusions in the STM images discussed above). Thus, by connecting and combining the three elementary structural motifs in the fairly small number of ways just described, the C structures observed in the STM images can be explicitly characterized; an example of this is shown in Fig. 4.

Previous STM experiments performed in an electrochemical environment (15) reveal that another structure for the C-Au(111) system exists in which ordered arrays of zigzag filaments of C molecules lie parallel to each other, bound by weak van der Waals (vdW) forces acting between nonpolar (nonsticky) areas of the filaments. Note that in this arrangement, each molecule is also hydrogen-bonded to two other molecules along

Fig. 4. STM image of a “glassy state” of cytosine on Au(111), with an overlay illustrating that a few elementary hydrogen-bonded structural motifs and their possible connections explain the image. Scanning conditions: $I_t = -0.15$ nA, $V_t = -1767$ mV.



the filament, but it also interacts with two molecules of the neighboring filaments through vdW interactions. In the random network we observed, only hydrogen bonding is involved and the majority of the C molecules are bound to only two neighbors through hydrogen bonding. Hence, because of an additional vdW interaction, the binding energy per molecule in relatively large islands of parallel C filaments will be greater than in a random network containing the same number of molecules. This ensures that the ordered arrangement has the lowest energy, and thus it serves as the 2D cytosine ground state.

Because crystalline islands can only survive if they are larger than some critical size, kinetically their formation is highly unlikely. Indeed, upon fast cooling, the formation rate of a large stable crystalline nucleus cannot compete with the formation rate of much smaller structures such as 5- and 6-fold rings, roundabouts, and T junctions—which are energetically the most stable clusters containing small numbers of C molecules—and the system gets trapped in a random network during the first stage of the kinetic process of assembly formation. Thus, this kinetic process leads to a dynamical capture of the 2D fluid upon fast cooling when the available thermal energy in the system becomes insufficient to facilitate escape from the local order of the liquid state into the ground crystalline state.

We thus conclude that, despite the lack of periodicity in the random cytosine network, we have revealed that only a few elementary structural motifs exist through which C molecules bind to each other, and yet very complex structures can be formed from these structural building blocks. The present cytosine model system is kinetically trapped in a disordered state, much like glass is trapped in the amorphous state, because it would need to

overcome prohibitively large energy barriers to move away from it. Examples of glass-forming systems where the constituents are molecules that can form hydrogen bonds in one of their ends but interact only weakly through their other parts (e.g., ethanol) are known in the literature (16). Our results may reveal an interesting route for studying the structure of organic glasses: performing a systematic search of particularly stable motifs and their possible interconnections.

The structure we describe here is similar to a continuous random network, where the constituents of the network are not individual atoms or molecules but instead consist of a small number of supramolecular elementary motifs, some of

which present medium-range order. The identification of such structural motifs would not have been possible without the proper choice of a model system and the use of STM to reveal the nanoscale order.

References and Notes

1. R. Zallen, *The Physics of Amorphous Solids* (Wiley-VCH, Weinheim, Germany, ed. 1, 2004).
2. S. C. Moss, J. F. Graczyk, *Phys. Rev. Lett.* **23**, 1167 (1969).
3. A. van Blaaderen, P. Wiltzius, *Science* **270**, 1177 (1995).
4. E. R. Weeks, J. C. Crocker, A. C. Levitt, A. Schofield, D. A. Weitz, *Science* **287**, 627 (2000).
5. J. V. Barth, *Annu. Rev. Phys. Chem.* **58**, 375 (2007).
6. F. Rosei et al., *Prog. Surf. Sci.* **71**, 95 (2003).
7. R. Otero, F. Rosei, F. Besenbacher, *Annu. Rev. Phys. Chem.* **57**, 497 (2006).
8. R. Otero et al., *Angew. Chem. Int. Ed.* **44**, 2270 (2005).
9. M. Furukawa, H. Tanaka, T. Kawai, *J. Chem. Phys.* **115**, 3419 (2001).
10. Q. Chen, N. V. Richardson, *Nat. Mater.* **2**, 324 (2003).
11. L. M. A. Perdigo et al., *Phys. Rev. B* **73**, 195423 (2006).
12. R. E. A. Kelly, Y. J. Lee, L. N. Kantorovich, *J. Phys. Chem. B* **109**, 22045 (2005).
13. M. Schunack et al., *Phys. Rev. Lett.* **86**, 456 (2001).
14. M. Schunack et al., *Phys. Rev. Lett.* **88**, 156102 (2002).
15. N. J. Tao, J. A. DeRose, S. M. Lindsay, *J. Phys. Chem.* **97**, 910 (1993).
16. M. A. Ramos et al., *Phys. Rev. Lett.* **78**, 82 (1997).
17. Supported by an EU individual Marie Curie Fellowship, EU-RTN project Atomic and Molecular Manipulation as a New Tool for Science and Technology, and EU project Picolinside (R.O. and M.L.), and by the Danish Ministry for Science, Technology and Innovation through the iNANO Center, the Danish Research Councils, the Danish National Research Foundation, the Carlsberg Foundation, and UK Engineering and Physical Sciences Research Council grant GR/P01427/01. We thank the Materials Chemistry Consortium for computer time on the HPCx supercomputer.

Supporting Online Material

www.sciencemag.org/cgi/content/full/1150532/DC1

Materials and Methods

References

Movies S1 and S2

14 September 2007; accepted 4 December 2007

Published online 13 December 2007;

10.1126/science.1150532

Include this information when citing this paper.

The Subduction Zone Flow Field from Seismic Anisotropy: A Global View

Maureen D. Long* and Paul G. Silver

Although the morphologies of subducting slabs have been relatively well characterized, the character of the mantle flow field that accompanies subduction remains poorly understood. To analyze this pattern of flow, we compiled observations of seismic anisotropy, as manifested by shear wave splitting. Data from 13 subduction zones reveal systematic variations in both mantle-wedge and slab anisotropy with the magnitude of trench migration velocity $|V_t|$. These variations can be explained by flow along the strike of the trench induced by trench motion. This flow dominates beneath the slab, where its magnitude scales with $|V_t|$. In the mantle wedge, this flow interacts with classical corner flow produced by the convergence velocity V_c ; their relative influence is governed by the relative magnitude of $|V_t|$ and V_c .

Upon propagation through an anisotropic medium, a shear wave is split into two orthogonally polarized components and accumulates a delay time, δt , between the fast and slow waves; the fast direction, ϕ , and δt are

measured (1, 2). In the upper mantle, anisotropy results from the strain-induced lattice preferred orientation (LPO) of olivine (3–6), so that if the relationship between deformation and LPO is known or inferred, shear wave splitting measure-

ments can provide a direct constraint on the geometry of upper mantle deformation and, if the fabric is not a fossil one, the upper mantle flow field.

Although anisotropy has been found in most subduction zones (e.g., 7–10), a wide variety of splitting behavior is observed, including both trench-parallel and trench-perpendicular ϕ , substantial lateral heterogeneity, and a large range of δt from 0 s to greater than 2 s. Anisotropic structure likely varies throughout the four-layered structure of subduction zones: the slab, the mantle wedge, and the overlying plate. This complexity makes it difficult to resolve where the anisotropy is originating, and it also limits the ability to construct numerical models of mantle flow with which to compare to observations.

The classical flow model for subduction systems is two dimensional (2D), characterized by corner flow above the slab and entrained flow beneath the slab (e.g., 11). (We use the term “subduction system” to refer to the subduction zone and the surrounding mantle flow.) Assuming A-type (or similar) LPO and the local alignment of the fast direction and the flow direction, this model makes the simple prediction of trench-normal orientations for ϕ for anisotropy originating both in the wedge and below the slab. As is well known, this model fails to account for the dramatic variability in ϕ noted above. Alternative models include trench-parallel flow in the mantle wedge (12), flow induced by crustal foundering (13), trench-parallel flow beneath the subducting slab (14), and transpression due to oblique subduction (15). It has also been proposed that olivine changes from A-type LPO to B-type LPO (thus changing the relationship between anisotropy and strain) as a way to explain trench-parallel fast directions in the mantle wedge while retaining 2D corner flow (16–18). Conditions needed for B-type LPO may be present in portions of the mantle wedge, although A-type [or other fabric types that give the same strain-anisotropy relationship, such as C or E (6)] likely prevails elsewhere in the upper mantle. Each of these explanations has been successful in accounting for local observations in specific subduction zones but none explains the full range of splitting behavior observed globally. We have compiled a global data set of average splitting parameters to reveal broad global trends in splitting behavior in terms of tectonic and kinematic subduction parameters, with the aim of determining the dominant properties of the subduction zone flow field.

Our compilation comes from 26 published studies and new measurements from six permanent stations in the Aleutians, Tonga, and Indonesia, covering 13 subduction zones [see supporting

online material (SOM)]. In regions where both local and teleseismic measurements are available, we characterize the wedge and the subwedge region separately. The data are sufficient to constrain the orientation and magnitude of subwedge anisotropy for 11 subduction zones, and wedge anisotropy for 10 (Fig. 1). We compared average splitting parameters to overriding plate velocity, trench migration rate, the stress state of the overriding plate, subducting plate age, convergence rate, slab depth beneath volcanoes, and slab dip, from previous compilations (19, 20).

The splitting results are relatively simple for the subwedge anisotropic signal (see SOM). Nearly all regions where we identified substantial subwedge splitting exhibit trench-parallel ϕ , although many also show variable orientations (e.g., Japan and South America) (fig. S2). Cascadia is a notable exception, with consistently trench-perpendicular ϕ . We found little or no splitting beneath the Ryukyu or Aleutian wedges, but a large δt (~1 to 2 s) for Tonga and Calabria. One question is whether the anisotropic signature comes primarily from the slab mantle or from the slab itself. Two lines of evidence argue against a primary contribution from the slab:

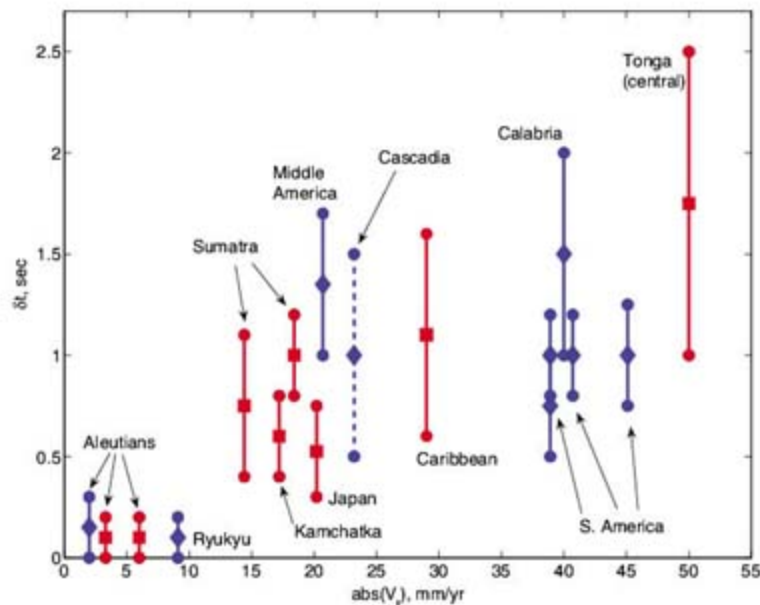
First, the preponderance of trench-parallel ϕ argues for a mechanism related to subduction geometry and not to fossilized anisotropy in the downgoing lithosphere (there is no obvious relationship between fossil spreading direction and ϕ). Second, a slab origin would predict an increase in δt with increasing age (and therefore thickness) of the downgoing lithosphere; we observe no such correlation. Therefore, we interpret the subwedge splitting signal as flow in the slab mantle. Given the physical conditions of the slab mantle, namely low stress, low water content, and relatively high temperature, the LPO is likely to be A-type [or similar (6)], which argues for trench-parallel flow there.

For subduction systems with nearly stationary trenches, there is little or no slab splitting, whereas for systems with migrating trenches, δt tends to increase with the magnitude of trench migration velocity $|V_t|$ (Fig. 2). We propose that slab anisotropy is primarily controlled by 3D return flow, generally parallel to the trench, induced by trench migration, combined with a barrier to entrained flow beneath the slab, likely at either the top or base of the transition zone. As the trench-slab system migrates relative to the



Fig. 1. Summary of available constraints on shear wave splitting in subduction zones. Regions for which robust constraints have been obtained are marked.

Fig. 2. Average slab δt versus $|V_t|$. Retreating trenches are shown with blue diamonds, advancing trenches with red squares. Error bars roughly represent the 95% confidence region on average splitting times (see SOM for further details on error calculations). Cascadia is marked with a dashed line; although it is consistent with the trend with $|V_t|$, its fast directions are not consistent with our preferred model. A linear fit to the data (weighted by errors) produces a relationship of $\delta t = 0.026(|V_t|) + 0.17$; this best-fitting slope is significantly different from zero (the 95% confidence interval on the slope is 0.026 ± 0.07).



Department of Terrestrial Magnetism, Carnegie Institution of Washington, 5241 Broad Branch Road, NW, Washington, DC 20015, USA.

*To whom correspondence should be addressed. E-mail: long@dtm.ciw.edu

upper mantle, subslab mantle is forced around the slab edges and flows parallel to the trench, as has been proposed (14) for South America. The correlation of δt with $|V_t|$ holds regardless of whether the trench is advancing or retreating. We suggest that $|V_t|$ serves as a proxy for the coherence of flow beneath the slab. Subduction systems with fast-moving trenches are more likely to set up a more coherent, larger-scale return flow beneath the slab that results in a larger region of coherent LPO. Similarly, δt , being proportional to the product of intrinsic anisotropy and effective path length, should also be a measure of the length scale of coherent flow, assuming that the intrinsic anisotropy is saturated in the subslab region.

In contrast to the relatively simple trends in subslab anisotropy, anisotropy in the mantle wedge is more difficult to interpret for two reasons. First, the observed splitting patterns in the wedge are much more variable (fig. S3): Many subduction zones exhibit a transition from trench-parallel ϕ close to the trench to trench-perpendicular farther away [e.g., Ryukyu (21), Marianas (10), and Tonga (12)], but a few exhibit the opposite pattern [e.g., Kamchatka (22)]. δt also varies

dramatically between regions: Some wedges are nearly isotropic (e.g., Indonesia and South America), whereas others exhibit large $\delta t > 1$ s (e.g., Ryukyu and Tonga). Second, wedge conditions increase the probability of a change to B-type LPO, which rotates by 90° the expected geometrical relation between strain and ϕ (5).

If 2D corner flow dominated the wedge flow field, one would expect δt to increase with either convergence velocity V_c or with slab dip, which controls path length through the wedge. Yet, there is no such correlation (figs. S4 and S5). After an examination of other plate parameters (e.g., age of subducting lithosphere and stress state of the overriding plate), we find, as with the subslab region, a strong dependence on $|V_t|$. There is a striking relation between δt and $|V_t|$ normalized by V_c , which we define as $V_{\text{norm}} = |V_t|/V_c$ (Fig. 3). Because V_c and $|V_t|$ should govern the strength of 2D corner flow and 3D trench-parallel flow, respectively, this ratio is a measure of the relative importance of these two components in a subduction zone. For subduction systems that are dominated by downdip motion of the slab ($V_{\text{norm}} < -0.2$), δt decreases with increasing V_{norm} . For systems

that are dominated by trench migration ($V_{\text{norm}} > -0.6$), δt tends to increase with increasing V_{norm} , although this pattern is less clear-cut. For systems in between these two regimes, delay times are small.

We hypothesize (Fig. 4) that anisotropy in the wedge is controlled by the competing influences of two flow fields: the 2D corner flow field, which is controlled by viscous coupling between the downgoing slab and the overlying wedge, and the 3D flow field, which is induced by migration of the trench (as in the subslab case). The relative importance of these two flow fields is controlled by the relative magnitudes of $|V_t|$ and V_c . The greater the extent to which the wedge flow field is dominated by coherent corner flow, the stronger the anisotropy and the larger δt . Conversely, for systems where the trench migrates rapidly compared with downdip motion, the wedge flow field is dominated by trench-parallel flow, and for rapidly moving trenches, δt is large as well. For subduction systems in the intermediate regime, the two flows compete, and the resulting flow field is less coherent. In such a situation, where the flow is weak or changes rapidly over short length scales, coherent and strong LPO does not develop (23) and δt is small.

Our model for wedge anisotropy may resolve the apparent conflict between studies that explain trench-parallel ϕ with trench-parallel flow (12, 10) versus with B-type olivine LPO (16, 21, 18). For subduction systems predicted to be dominated by corner flow, such as Ryukyu, the low-temperature conditions in the forearc are expected to favor the development of B-type LPO (17). For systems predicted to be dominated by trench-parallel flow, such as Tonga, we hypothesize that this flow regime increases overall velocities in the mantle wedge. This results in the removal of wedge material that has been conductively cooled by the slab, as found in laboratory models of subduction systems with rollback (24). The resulting higher forearc temperatures would favor A-type (or similar) rather than B-type LPO (6), so that ϕ close to the trench would reflect trench-parallel flow. For either type of subduction zone, farther away from the trench, ϕ should be trench-perpendicular, away from the influence of either the trench-parallel flow or B-type olivine fabric. This pattern is, indeed, observed in many subduction zones (25), including both Tonga and Ryukyu (12, 21). When this change in fast direction is controlled by a fabric transition, the change in orientation should coincide roughly with the arc (17); this would not necessarily be the case for systems with substantial trench-parallel flow. Again, this prediction is consistent with observations from end-member regions (12, 21).

Our model does not include possible effects on anisotropy due to aligned melt, lithospheric anisotropy in the overriding plate, crustal foundering, or trench-parallel flow due to oblique subduction. We have investigated whether splitting parameters correlate with the deformation regime of the overriding plate, subduction obliquity, volcanic production, and other parameters and find

Fig. 3. Average wedge δt versus $V_{\text{norm}} = (|V_t|/V_c)$ (trench velocity normalized by total convergence velocity). The x axis is plotted on a log scale. Retreating trenches are shown with blue diamonds, advancing trenches with red squares. Error bars roughly represent the 95% confidence region on average splitting times.

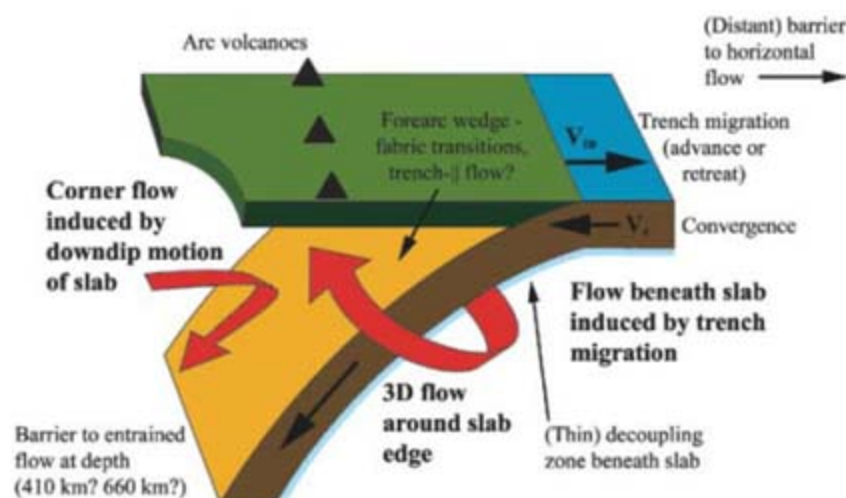
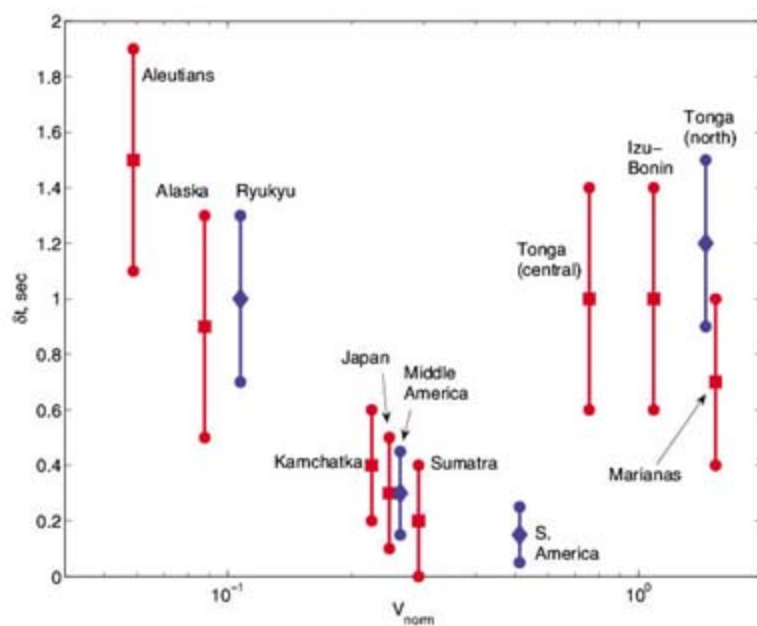


Fig. 4. Schematic diagram of model, showing the dominance of 3D flow beneath the slab and the competing influence of 2D and 3D flow fields in the mantle wedge.

no other notable global correlations. These effects may be important locally, but they do not represent a dominant global pattern. Additionally, we have not evaluated the possible effects of 3D slab morphology on trench-parallel flow in the wedge (e.g., 26) or beneath the slab (14, 27). Such flow is likely important locally and may serve to strengthen or otherwise modulate the trench-parallel flow induced by trench migration.

Our model essentially requires a thin decoupling zone between the downgoing slab and the subslab mantle, because we observe no detectable anisotropic signal from slab-entrained flow. [Cascadia represents an exception (8) to this rule; this may be a consequence of the very young age of the subducting lithosphere or the region's complicated subduction history and slab morphology.] This decoupling zone appears to be universal, in that slab-entrained flow is not generally detected even for subduction zones with a nearly stationary trench, and may be a consequence of the entrainment of a thin layer of buoyant asthenosphere (28). The inferred subslab flow field also requires a partial barrier to mantle flow beneath the slab, as proposed by (14), as well as an effective barrier to horizontal flow in the trench-normal direction (29), so that mantle material is forced to escape laterally in response to the motion of the trench. The barrier to entrained flow beneath the slab provides a constraint on mass transfer between the upper and lower mantle, which in turn has major implications for mantle evolution and dynamics. Finally, the existence of trench-parallel flow in the

mantle wedge as a common (although not ubiquitous) phenomenon implies that along-strike transport of mantle material is important for many arcs, with consequences for magma genesis, volatile transport, and thermal structure.

References and Notes

- P. G. Silver, *Annu. Rev. Earth Planet. Sci.* **24**, 385 (1996).
- M. K. Savage, *Rev. Geophys.* **37**, 65 (1999).
- N. I. Christensen, *Geophys. J. R. Astron. Soc.* **76**, 89 (1984).
- S. Zhang, S.-i. Karato, *Nature* **375**, 774 (1995).
- H. Jung, S.-i. Karato, *Science* **293**, 1460 (2001).
- H. Jung, I. Katayama, Z. Jiang, T. Hiraga, S. Karato, *Tectonophysics* **421**, 1 (2006).
- M. J. Fouch, K. M. Fischer, *J. Geophys. Res.* **101**, 15987 (1996).
- C. A. Currie, J. F. Cassidy, R. D. Hyndman, M. G. Bostock, *Geophys. J. Int.* **157**, 341 (2004).
- M. D. Long, R. D. van der Hilst, *Phys. Earth Planet. Inter.* **151**, 206 (2005).
- S. H. Pozgay, D. A. Wiens, J. A. Conder, H. Shiohara, H. Sugioka, *Geophys. J. Int.* **170**, 371 (2007).
- C. Hall, K. M. Fischer, E. M. Parmentier, D. K. Blackman, *J. Geophys. Res.* **105**, 28009 (2000).
- G. P. Smith *et al.*, *Science* **292**, 713 (2001).
- M. D. Behn, G. Hirth, P. B. Keleman, *Science* **317**, 108 (2007).
- R. M. Russo, P. G. Silver, *Science* **263**, 1105 (1994).
- L. Mehl, B. R. Hacker, G. Hirth, P. G. Kelemen, *J. Geophys. Res.* **108**, 10.1029/2002JB002233 (2003).
- J. Nakajima, A. Hasegawa, *Earth Planet. Sci. Lett.* **225**, 365 (2004).
- E. A. Kneller, P. E. van Keken, S.-i. Karato, J. Park, *Earth Planet. Sci. Lett.* **237**, 781 (2005).
- M. D. Long, B. H. Hager, M. V. de Hoop, R. D. van der Hilst, *Geophys. J. Int.* **170**, 839 (2007).
- A. Heuret, S. Lallemand, *Phys. Earth Planet. Inter.* **149**, 31 (2005).
- E. M. Syracuse, G. A. Abers, *Geochem. Geophys. Geosyst.* **7**, 10.1029/2005GC001045 (2006).
- M. D. Long, R. D. van der Hilst, *Phys. Earth Planet. Inter.* **155**, 300 (2006).
- V. Levin, D. Droznin, J. Park, E. Gordeev, *Geophys. J. Int.* **158**, 1009 (2004).
- É. Kaminski, N. M. Ribe, *Geochem. Geophys. Geosyst.* **3**, 10.1029/2001GC000222 (2002).
- C. Kincaid, R. W. Griffiths, *Nature* **425**, 58 (2003).
- Although the transition described here is more common, trench-perpendicular to trench-parallel transitions in ϕ have also been observed, for example, in Kamchatka and Alaska. These backward transitions are not easily explained by our model; however, because both Kamchatka and Alaska are located near slab edges, local processes may affect these regions.
- E. A. Kneller, P. E. van Keken, *Nature* **450**, 1222 (2007).
- J. Polet *et al.*, *J. Geophys. Res.* **105**, 6287 (2000).
- J. Phipps Morgan, J. Hasendever, M. Hort, L. Rüpke, E. M. Parmentier, *Terra Nova* **19**, 167 (2007).
- L. Husson, C. Faccenna, C. P. Conrad, *Mem. Geosci. Montpellier* **41**, 169 (2007).
- We thank the Alaska Regional Network, Alaska Tsunami Warning Seismic System, the Pacific Orient Seismic Digital Observation Network (POSEIDON), and the Incorporated Research Institutions for Seismology/United States Geological Survey for providing data used in this study. We thank M. Behn and S. Pozgay for useful discussions and L. Wagner for assistance with figures.

Supporting Online Material

www.sciencemag.org/cgi/content/full/319/5861/315/DC1
SOM Text
Figs. S1 to S5
References

21 September 2007; accepted 4 December 2007
10.1126/science.1150809

A Localized Negative Genetic Correlation Constrains Microevolution of Coat Color in Wild Sheep

J. Gratten,¹ A. J. Wilson,² A. F. McRae,³ D. Beraldi,² P. M. Visscher,³ J. M. Pemberton,² J. Slate¹

The evolutionary changes that occur over a small number of generations in natural populations often run counter to what is expected on the basis of the heritability of traits and the selective forces acting upon them. In Soay sheep, dark coat color is associated with large size, which is heritable and positively correlated with fitness, yet the frequency of dark sheep has decreased. This unexpected microevolutionary trend is explained by genetic linkage between the causal mutation underlying the color polymorphism and quantitative trait loci with antagonistic effects on size and fitness. As a consequence, homozygous dark sheep are large, but have reduced fitness relative to phenotypically indistinguishable dark heterozygotes and light sheep. This result demonstrates the importance of understanding the genetic basis of fitness variation when making predictions about the microevolutionary consequences of selection.

Evolutionary theory states that directional selection on a heritable trait should result in evolutionary change (1). Analyses of long-term data sets from wild vertebrate popula-

tions reveal directional selection on heritable traits, yet many studies report no microevolutionary change (stasis) or, in some cases, responses in the opposite direction to that predicted (2). Explaining such discrepancies is a major challenge in evolutionary biology (2). The absence of a predicted microevolutionary response may be due to constraints imposed by genetic correlations between the phenotype of interest

and other fitness-related traits (3). If this is true, then the loci affecting the focal trait should be colocalized in the genome with genes for other fitness-related traits, either because the same genes affect both traits (pleiotropy) or because genetic correlations arise between tightly linked genes (linkage disequilibrium). However, empirical evidence for colocalized antagonistically acting quantitative trait loci (QTLs) that constrain microevolutionary change is currently lacking.

In the free-living Soay sheep of St Kilda, Scotland, coat color is either dark brown or light tawny (Fig. 1) (4); the two phenotypes have been documented for at least 90 years (5, 6). Variation in coat color is controlled by a single autosomal locus at which the dark allele is dominant to the light allele (6). The light phenotype is determined by homozygosity of a single recessive amino acid-changing G→T transversion at coding position 869 in the *tyrosinase-related protein 1* (*TYRP1*) gene (7).

Coat color in Soay sheep is related to fitness because of an association with body size: Dark sheep are larger than light sheep (8). Body size is heritable throughout life (9, 10) and is positively correlated with survival (11) and reproductive success (12). Moreover, a genetic response to selection for increased size has been detected (9). If the association between coat color and body

¹Department of Animal and Plant Sciences, University of Sheffield, Sheffield S10 2TN, UK. ²Institute of Evolutionary Biology, School of Biological Sciences, University of Edinburgh, Edinburgh EH9 3JT, UK. ³Genetic Epidemiology, Queensland Institute of Medical Research, Brisbane 4029, Australia.

size has a genetic basis, then dark sheep should be favored by selection because of their size advantage relative to light sheep. However, a 20-year time series of phenotypic data shows a significant decrease in the frequency of dark sheep (linear regression, slope of $-0.38\%/year$, $R^2 = 0.326$, $P = 0.009$; Fig. 2A).

We considered two competing hypotheses to explain this disparity: first, that the correlation between coat color and body size is a consequence of environmentally induced, rather than genetic, covariance between traits. In this case, selection on body size would not result in a parallel response for coat color. Alternatively, if there is a genetic association between coat color and size, the failure of dark sheep to increase in frequency may indicate a negative genetic correlation between body size and other fitness-related loci in the vicinity of *TYRPI*. Under this scenario, dark sheep are larger but less fit than light sheep. Other explanations for the discrepancy can be dismissed. For example, selection cannot favor light sheep on the basis of cryptic coloration (13), because predators have never existed on St Kilda (4). Similarly, light sheep are not favored by sexual selection because there is no evidence for assortative mating with respect to either coat color [$\chi^2_{(1)} = 0.32$, $P = 0.570$] or *TYRPI* genotype [$\chi^2_{(4)} = 1.53$, $P = 0.822$] on the

basis of 559 phenotyped and genotyped parent/offspring trios.

To test our hypotheses, we genotyped the *TYRPI* mutation in 2509 sheep living between 1985 and 2005 and integrated these data with estimates of body size and individual lifetime fitness. We used a linear mixed model (LMM) (the so-called animal model) (14) that accounts for shared additive genetic effects on phenotype among relatives, in addition to the effects of non-genetic factors and environmental variation on the covariance between traits (15). In all analyses, we present estimates of the mean and standard error (SE) of the differences in trait value between *TYRPI* genotypes and between dark and light sheep, rather than the population means for each genotype and phenotype, because we are primarily interested in these contrasts.

We identified a strong genetic association between *TYRPI* and birth weight [LMM, $F_{(2,1623,1)} = 8.96$, $P = 0.0001$, $n = 1757$ sheep; Fig. 3A and table S1]; sheep with genotypes GG and GT (dark coats) were heavier at birth than sheep with genotype TT (light coats) by an average of 132.3 (± 37.4) g and 111.3 (± 28.5) g, respectively. Dark homozygotes (GG) were largest but not significantly larger than dark heterozygotes (GT) (mean difference 21.0 ± 32.0 g). Overall, dark sheep were an average of 122.4 (± 24.0) g heavier at

birth than light sheep [LMM, $F_{(1,2201,5)} = 26.03$, $P < 0.0001$, $n = 2370$]; this difference is similar to that between males and females (129.9 ± 23.8 g). The general pattern of larger size in sheep carrying the *TYRPI* G allele was also present in lambs [LMM, $F_{(2,800,8)} = 4.39$, $P = 0.014$, $n = 1087$; Fig. 3B] and adults [LMM, $F_{(2,369,8)} = 3.86$, $P = 0.023$, $n = 1367$; Fig. 3D] but was non-significant in yearlings [LMM, $F_{(2,316)} = 0.40$, $P = 0.672$, $n = 556$; Fig. 3C], presumably due to a lack of power associated with the relatively small sample size in that intermediate age class (table S1).

Our results suggest that the *TYRPI* G allele (dominant for dark color) is associated with partial dominance for body size. We determined whether this was due to genetic linkage by applying a transmission disequilibrium test (TDT) (16) to a set of birth weight records from 492 fully phenotyped and genotyped parent/offspring trios (15). This revealed linkage between *TYRPI* and birth weight [LMM, within-families coefficient (b_{TD}), $F_{(1,421)} = 4.60$, $P = 0.034$] and discounted a spurious association arising from recent admixture or the nonrandom spatial distribution of sheep in the study area (17, 18) [LMM, between-families coefficient (b_{PD}), $F_{(1,377,6)} = 1.48$, $P =$

Fig. 1. Dark (left) and light (right) coat color morphs in Soay sheep. [Photograph: J. M. Pemberton]

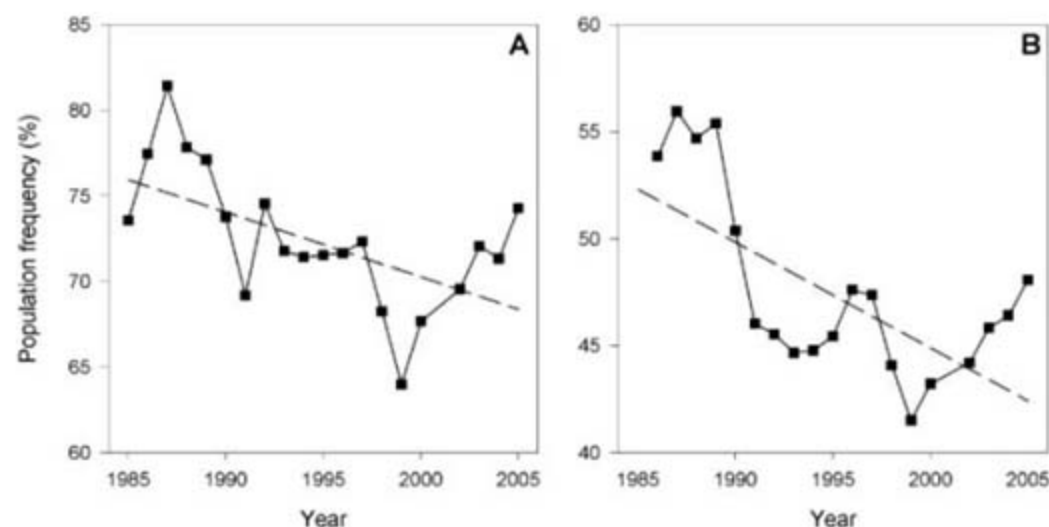


Fig. 2. Estimated frequency of (A) dark sheep and (B) the *TYRPI* G allele (dominant for dark color) in the Village Bay study population from 1985 to 2005. Frequency estimates are from August of each year. Linear regression lines are fitted and show a significant decline in the frequency of both dark sheep (slope of $-0.38\%/year$, $R^2 = 0.326$, $P = 0.009$) and the *TYRPI* G allele (slope of $-0.49\%/year$, $R^2 = 0.390$, $P = 0.004$).

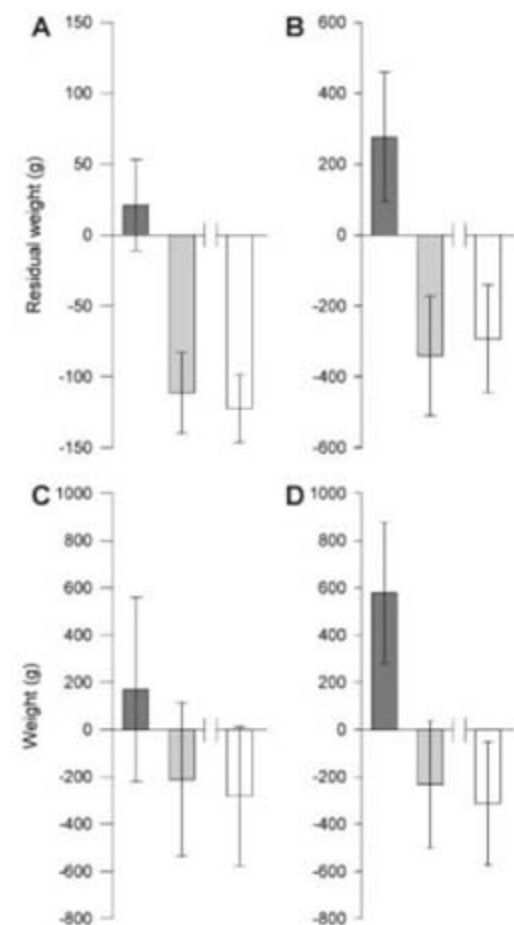


Fig. 3. Bar plots showing the mean (\pm SE) weight differential of homozygous (GG) dark sheep (dark gray bars) and homozygous (TT) light sheep (light gray bars), in each case relative to heterozygous (GT) dark sheep, and of light sheep (white bars) relative to dark sheep at (A) birth, and in (B) lambs, (C) yearlings, and (D) adults.

0.225]. We can therefore reject the hypothesis that the correlation between coat color and body size arises purely from environmental effects. Consequently, because body size is positively correlated with fitness (11, 12) and the *TYRPI* G allele is associated with large size, the failure of dark sheep to increase in frequency may be due to microevolutionary constraints imposed by other genetic factors in the vicinity of *TYRPI*.

We characterized the genetic relationship between coat color and lifetime fitness with the de-lifing approach, which estimates an individual's contribution to annual population growth, $p_{(t)}$, through survival and reproduction (19). De-lifed fitness is standardized by the population mean in each year, correcting for annual environmental variation, which can affect fitness (4). Our analyses were based on the lifetime sum of $p_{(t)}$ from all sheep for which complete life histories were available (15). We identified a significant genetic association between *TYRPI* and lifetime $p_{(t)}$ [LMM, $F_{(2,1336)} = 4.03$, $P = 0.020$, $n = 1355$] and showed, using a TDT, that this is due to genetic linkage [LMM, $F_{(1,427)} = 6.87$, $P = 0.010$, $n = 492$]. Intriguingly, the relationship between coat color and fitness is inconsistent with that between dark coat color and large body size (Fig. 4 and table S2). Homozygous dark sheep (GG) exhibited a fitness disadvantage relative to phenotypically identical heterozygous dark sheep (GT) (i.e., a cryptic difference), but there was no evidence for differential fitness between heterozygous dark sheep and light sheep (TT). At a phenotypic level, the average fitness of dark sheep (genotypes GG and GT combined) was indistinguishable from that of light sheep, and thus there was no evidence for selection on coat color itself [LMM, $F_{(1,2117.8)} = 1.70$, $P = 0.192$, $n = 2334$].

Genetic linkage between *TYRPI* and both birth weight and lifetime $p_{(t)}$ can be explained by either pleiotropy or linkage disequilibrium with neighboring QTLs. We consider pleiotropy unlikely for two reasons. First, *TYRPI* has a limited range of expression, in melanocytes and

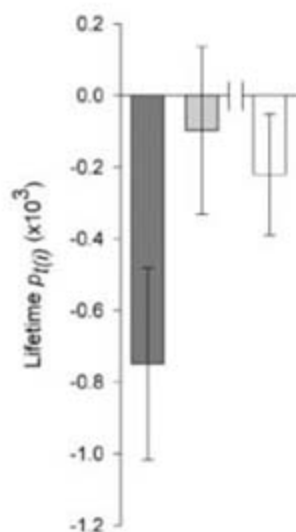


Fig. 4. Bar plots showing the mean (\pm SE) relative lifetime de-lifed fitness $p_{(t)}$ of *TYRPI* genotypes and coat color phenotypes, as in Fig. 3.

retinal pigment epithelium (20). Because there is no evidence of color-associated diseases of the skin or eyes in Soay sheep, it is difficult to envisage how *TYRPI* could directly influence size or fitness. Second, there is no evidence that *TYRPI* has pleiotropic effects on size, survival, or fecundity in mice and humans, despite the characterization of mutations that share a similar molecular basis with the Soay sheep mutation (the loss of a conserved cysteine residue) (7) and that have identical effects on pigmentation (21). Linkage disequilibrium to body size and fitness QTLs is plausible. Strong linkage disequilibrium extends for a considerable distance in the *TYRPI* region in our study population (supporting online text). The *VLDLR* gene, which in mice is associated with variation in neonatal size (22) and is believed to be tightly linked to *TYRPI* on the basis of conserved synteny with cattle (23), is a promising candidate gene for the body-size QTL. Similarly, a fitness-associated phenotype named "brown-associated fitness," determined by the *PTPRD* gene in the vicinity of *TYRPI*, has been described in mice (24).

Our results therefore imply that the relative fitness of *TYRPI* genotypes is determined by linkage to QTLs for both body size and fitness. These QTLs appear to have antagonistic effects because the *TYRPI* G allele (dominant for dark coat color) is associated with large body size (and hence with increased fitness) but also with decreased lifetime $p_{(t)}$. Thus, despite an overall positive correlation between body size and fitness (11, 12), these traits are negatively correlated in the chromosomal vicinity of *TYRPI*. This is because of linkage disequilibrium between the G allele and both a large body size QTL and a recessive QTL allele with deleterious effects on fitness. Notably, the direct fitness cost associated with G outweighs the expected benefits of being larger, and this will constrain the frequency of dark sheep. Our results actually imply that the light mutation (T) should be increasing in frequency, although genetic drift will also play a role in determining the allelic frequencies.

Our findings are therefore consistent with the observed decrease in the frequency of dark sheep (Fig. 2A). They are also consistent with a 20-year time series of *TYRPI* genotype data (linear regression, slope of -0.49% /year for frequency of the G allele, $R^2 = 0.390$, $P = 0.004$; Fig. 2B). Although sensitive to incomplete sampling in the early years of the study (supporting online material), this genotypic trend is supported by a significant increase in light sheep (and hence the TT genotype) (7) that is based on almost perfect sampling (15). Thus, the microevolutionary dynamics of coat color are consistent with expectations arising from the presence of a negative genetic correlation between size and fitness in the vicinity of *TYRPI*. This result holds whether the correlation is caused by pleiotropy or by linkage disequilibrium with nearby loci.

This study shows that selection acting on simple Mendelian traits in natural populations

can have a complex genetic basis. This has implications for the study of microevolutionary change in natural populations, because fitness variation at the level of the genotype may not be evident in an analysis of selection on phenotype. Consequently, phenotypic studies may wrongly conclude that selection is not acting on genomic regions containing the loci underlying focal traits and may be unable to explain the microevolutionary dynamics of trait variation.

References and Notes

- D. A. Roff, *Evolutionary Quantitative Genetics* (Chapman and Hall, New York, 1997).
- J. Merila, B. C. Sheldon, L. E. B. Kruuk, *Genetica* **112**, 199 (2001).
- R. Lande, S. J. Arnold, *Evol. Int. J. Org. Evol.* **37**, 1210 (1983).
- T. H. Clutton-Brock, J. M. Pemberton, *Soay Sheep: Dynamics and Selection in an Island Population* (Cambridge Univ. Press, Cambridge, 2004).
- H. J. Elwes, *Scott. Naturalist* **1**, 25 (1912).
- J. M. Doney, M. L. Ryder, R. G. Gunn, P. Grubb, in *Island Survivors: The Ecology of the Soay Sheep of St. Kilda*, P. A. Jewell, C. Milner, J. M. Boyd, Eds. (Athlone Press, London, 1974), pp. 88–125.
- J. Gratten et al., *Proc. R. Soc. Biol. Sci. Ser. B* **274**, 619 (2007).
- T. H. Clutton-Brock, K. Wilson, I. R. Stevenson, *Philos. Trans. R. Soc. London Ser. B* **352**, 839 (1997).
- A. J. Wilson et al., *Evol. Ecol.* **21**, 337 (2007).
- A. J. Wilson et al., *J. Evol. Biol.* **18**, 405 (2005).
- A. J. Wilson et al., *Evol. Int. J. Org. Evol.* **59**, 451 (2005).
- D. W. Coltman et al., *Am. Nat.* **154**, 730 (1999).
- M. W. Nachman, H. E. Hoekstra, S. L. D'Agostino, *Proc. Natl. Acad. Sci. U.S.A.* **100**, 5268 (2003).
- L. E. B. Kruuk, *Philos. Trans. R. Soc. London Ser. B* **359**, 873 (2004).
- Materials and methods are available as supporting material on Science Online.
- J. Hernandez-Sanchez, P. Visscher, G. Plastow, C. Haley, *Genetics* **164**, 637 (2003).
- D. W. Coltman, J. G. Pilkington, J. M. Pemberton, *Mol. Ecol.* **12**, 733 (2003).
- R. S. Spielman, R. E. McGinnis, W. J. Ewens, *Am. J. Hum. Genet.* **52**, 506 (1993).
- T. Coulson et al., *Proc. R. Soc. Biol. Sci. Ser. B* **273**, 547 (2006).
- F. Murisier, S. Guichard, F. Beermann, *Dev. Biol.* **298**, 644 (2006).
- E. Zdarsky, J. Favar, I. J. Jackson, *Genetics* **126**, 443 (1990).
- H. Yagyu et al., *J. Biol. Chem.* **277**, 10037 (2002).
- J. Slate et al., *Genetics* **160**, 1587 (2002).
- I. M. Smyth et al., *Proc. Natl. Acad. Sci. U.S.A.* **103**, 3704 (2006).
- We thank J. Pilkington, project members, and many volunteers for collecting data and genetic samples; J. Hadfield and S. Nakagawa for statistical advice; F. Pelletier for estimates of de-lifed fitness; T. Coulson and L. Kruuk for helpful discussion; the National Trust for Scotland and Scottish Natural Heritage for permission to access St. Kilda; and QinetiQ for logistical support. Comments from anonymous referees improved this manuscript. Funded by the Natural Environment Research Council. The Australian National Health and Medical Research Council provided support to P.M.V. and A.F.M.

Supporting Online Material

www.sciencemag.org/cgi/content/full/319/5861/318/DC1

Materials and Methods

SOM Text

Tables S1 and S2

References

1 October 2007; accepted 7 December 2007

10.1126/science.1151182

Coastal Ecosystem–Based Management with Nonlinear Ecological Functions and Values

Edward B. Barbier,^{1*} Evamaria W. Koch,² Brian R. Silliman,³ Sally D. Hacker,⁴ Eric Wolanski,⁵ Jurgenne Primavera,⁶ Elise F. Granek,⁷ Stephen Polasky,⁸ Shankar Aswani,⁹ Lori A. Cramer,¹⁰ David M. Stoms,¹¹ Chris J. Kennedy,¹ David Bael,⁸ Carrie V. Kappel,¹² Gerardo M. E. Perillo,¹³ Denise J. Reed¹⁴

A common assumption is that ecosystem services respond linearly to changes in habitat size. This assumption leads frequently to an “all or none” choice of either preserving coastal habitats or converting them to human use. However, our survey of wave attenuation data from field studies of mangroves, salt marshes, seagrass beds, nearshore coral reefs, and sand dunes reveals that these relationships are rarely linear. By incorporating nonlinear wave attenuation in estimating coastal protection values of mangroves in Thailand, we show that the optimal land use option may instead be the integration of development and conservation consistent with ecosystem-based management goals. This result suggests that reconciling competing demands on coastal habitats should not always result in stark preservation-versus-conversion choices.

More than one-third of the world’s human population lives in coastal areas and small islands (1), which together make up just 4% of Earth’s total land area. Coastal population densities are nearly three times that of inland areas (2) and they are increasing exponentially. The long-term sustainability of these populations is dependent on coastal ecosystems and the services they provide, such as storm buffering, fisheries production, and enhanced water quality. Despite the importance of these services, degradation and loss of coastal ecosystems over the past two to three decades—including marshes (50% either lost or degraded), mangroves (35%), and reefs (30%)—is intense and increasing worldwide (2–4).

To aid in conservation of these coastal communities, ecosystem-based management (EBM) has recently been proposed as a benefit op-

timization and decision-making strategy that incorporates often conflicting development and conservation uses (5–7). EBM strives to reconcile these pressures by valuing ecosystem ser-

vices and thus justifying the maintenance of many natural systems “in healthy, productive and resilient conditions so that they can provide the services humans want and need” (5). Yet the implementation of EBM cannot take place without addressing a fundamental challenge: assessing the true value of these ecosystems and the services they generate, so that practical compromises can be made (8–11).

The interrelationship of ecosystem structure, function, and economic value is critical to coastal management decisions, which are often concerned with how much natural habitat to “preserve” and how much to allocate to human development activities (2, 3). In assessing such trade-offs, it is frequently assumed that ecosystem services change linearly with critical habitat variables such as size (e.g., area). This assumption can lead to the misrepresentation of economic values inherent in services, particularly at their endpoints. The endpoint values often either overestimate or underestimate the service value, resulting in an “all or none” habitat scenario as the only decision choice (9–11). A common reason for invoking such an assumption is that few data exist for examining the marginal losses associated with changes in nonlinear ecological functions, making

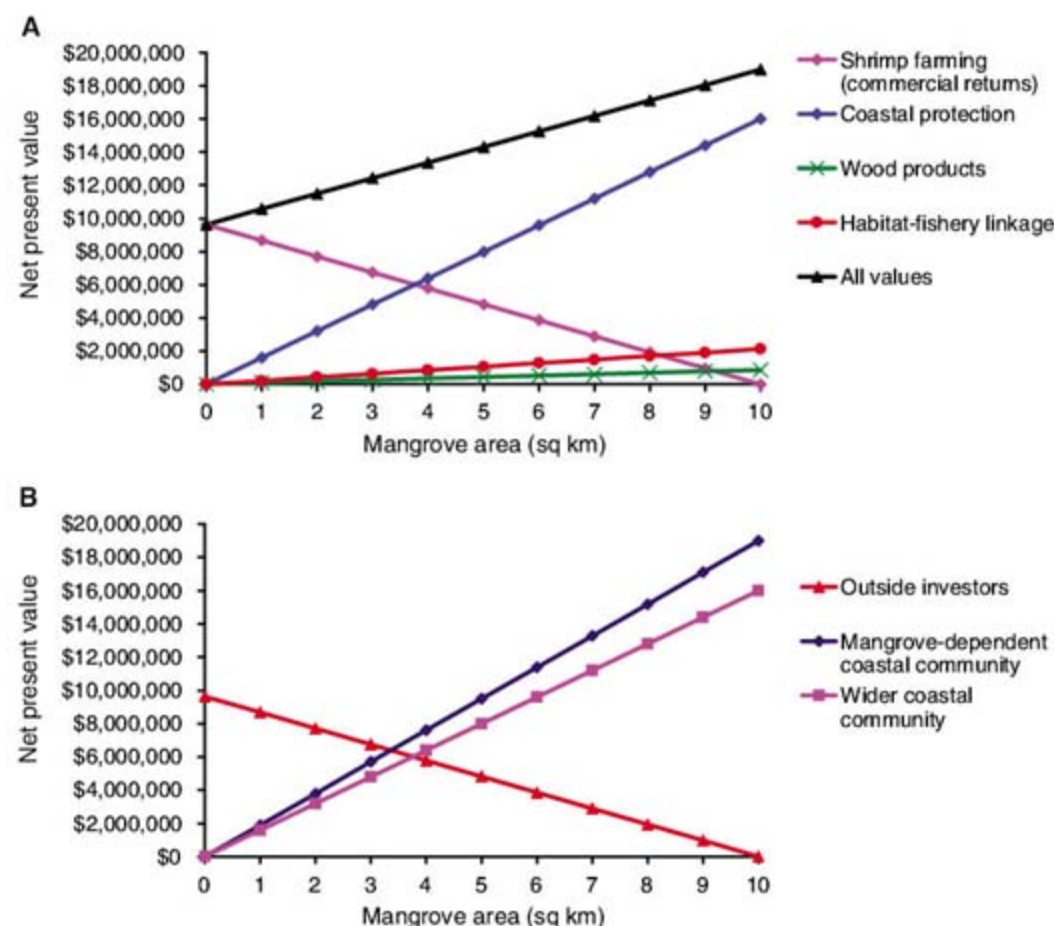


Fig. 1. Conventional comparison of shrimp farming to various mangrove services at coastal landscape level (10 km²), Thailand (net present value, 10% discount rate, 1996 dollars) on the basis of (A) total economic returns as a function of mangrove area (km²) for the commercial returns from shrimp farming plus three mangrove ecosystem service values: coastal protection, wood product collection, and habitat support for offshore fisheries; and (B) the distribution of benefits as a function of mangrove area (km²) among three stakeholders: outside investors in shrimp farms, the mangrove-dependent coastal community, and the wider coastal community (up to 5 km away). [Based on data from (11, 16, 17)]

¹Department of Economics and Finance, University of Wyoming, Laramie, WY 82071, USA. ²Horn Point Laboratory, University of Maryland Center for Environmental Science, Cambridge, MD 21613, USA. ³Department of Zoology, University of Florida, Gainesville, FL 32611, USA. ⁴Department of Zoology, Oregon State University, Corvallis, OR 97331, USA. ⁵Australian Centre for Tropical Freshwater Research, James Cook University and Australian Institute of Marine Science, Townsville, Queensland 4810, Australia. ⁶Aquaculture Department, Southeast Asian Fisheries Development Center, Tigbauan, Iloilo 5021, Philippines. ⁷Environmental Sciences and Resources, Portland State University, Portland, OR 97207, USA. ⁸Department of Applied Economics, University of Minnesota, St. Paul, MN 55108, USA. ⁹Department of Anthropology, University of California, Santa Barbara, CA 93106, USA. ¹⁰Department of Sociology, Oregon State University, Corvallis, OR 97331, USA. ¹¹Bren School of Environmental Science and Management, University of California, Santa Barbara, CA 93106, USA. ¹²National Center for Ecological Analysis and Synthesis, University of California, Santa Barbara, CA 93101, USA. ¹³Instituto Argentino de Oceanografía, B8000FWB Bahía Blanca, Argentina. ¹⁴Department of Earth and Environmental Sciences, University of New Orleans, New Orleans, LA 70148, USA.

*To whom correspondence should be addressed. E-mail: ebarbier@uwyo.edu

it difficult to value accurately the changes in ecosystem services in response to incremental changes in habitat characteristics (e.g., area). If, however, relationships between the structure and function of coastal habitats are nonlinear, as ecological theory suggests (12–14), then assuming that the value of the resulting service is linear (with respect to changes in habitat characteristics) will mislead management decisions.

To test the key assumption that ecosystem services and their economic value are linearly related to habitat area, we used data collected in the field from key coastal interface systems around the globe, including mangroves, salt marshes, seagrass beds, nearshore coral reefs, and sand dunes (15). We focused on arguably the most undervalued ecosystem service until recently: protection against wave damage caused by storms, hurricanes, and tsunamis. These field data reveal that for all these coastal habitats, nonlinear relationships exist between habitat area and measurements of the ecosystem function of wave attenuation (fig. S1). For mangroves and salt marshes, there are quadratic and exponential decreases, respectively, in wave height with increasing habitat distance inland from the shoreline (fig. S1, A and B). In the case of seagrasses and near-

shore coral reefs, wave attenuation is a function of the water depth above the grass bed or reef, and these relationships are also nonlinear (fig. S1, C and D). Additionally, there is an exponential relationship between the percent cover of dune grasses and the size of oceanic waves blocked by sand dunes produced by the grass (fig. S1E). These data suggest that the assumption of linearity is likely to be inaccurate for many ecosystem services that depend on habitat size—a result that could have important implications for conservation, especially as it relates to EBM.

To explore this possibility, we applied these nonlinear wave attenuation relationships for coastal systems to a case study from Thailand (11, 16, 17) where choices have been made between conversion of mangroves to shrimp aquaculture versus their preservation for key ecosystem services (such as coastal protection and fish habitat). Our case study assumes a mangrove habitat that extends 1000 m inland from the seaward edge along 10 km of coast. Nearby communities depend on the mangrove for forest and fishery products in coastal waters that are populated by mangrove-dependent fish. Coastal communities up to 5 km inland are protected from tropical storms by mangroves. The alternative to preserving mangroves is converting

them to intensive shrimp ponds, which overwhelmingly benefits outside investors (11, 16, 17).

Figure 1A depicts the economic returns from converting the 10-km² mangrove habitat to commercial shrimp farms as well as the values generated by three ecosystem services: coastal protection, wood collection, and habitat-fishery linkage. The figure also aggregates all four values to test whether an “integrated” land use option involving some conversion and some preservation yields the highest total value. When all values are linear, the outcome is a typical “all or none” scenario; either the aggregate values will favor complete conversion, or they will favor preserving the entire habitat (Fig. 1A). Because the ecosystem service values are large and increase linearly with mangrove area, the preservation option is preferred (Fig. 1A). The aggregate value of the mangrove system is at its highest (\$18.98 million) when it is completely preserved, and any conversion to shrimp farming would lead to less aggregate value compared to full preservation. Thus, an EBM strategy that considers all the values of the ecosystem would favor mangrove preservation and no shrimp farm conversion.

Figure 1B shows that mangrove-dependent communities and the wider coastal community would benefit from the EBM decision, whereas outside investors would prefer conversion of the mangrove to shrimp ponds. Overall, our analysis shows that the EBM strategy of full preservation of the mangroves would face opposition from outside investors, who would obtain no commercial gains from this scenario but would make profits of more than \$9.6 million from complete conversion (Fig. 1B). It is also clear that the “all or none” decision to preserve mangroves hinges on the coastal protection value service of the mangroves, which is assumed to increase linearly with mangrove area.

However, if we consider that coastal protection afforded by mangroves depends on their functional ability to attenuate storm waves (18–21) and that this relationship is nonlinear (fig. S1A), a different EBM strategy is supported (Fig. 2). In fig. S1A, we show that a wave height of 1.1 m at the offshore edge of the mangrove forest would be reduced to 0.91 m if the forest extended 100 m inland; if the forest extended 200 m inland, the wave would drop to roughly 0.75 m. The wave would continue to fall, albeit at a declining rate, for every additional 100 m of mangroves inland from the sea. For a forest extending 1000 m inland, the wave would be reduced to a negligible 0.12 m.

Using the nonlinear wave attenuation function for mangroves (fig. S1A), it is possible to revise the estimate of storm protection service value for the Thailand case study (22) (Fig. 2). The storm protection service of mangroves still dominates all values, but small losses in mangroves will not cause the economic benefits of storm buffering by mangroves to fall precipitously (Fig. 2A). The consequence is that the aggregate value across all uses of the mangroves (i.e., shrimp farming and ecosystem values) is at

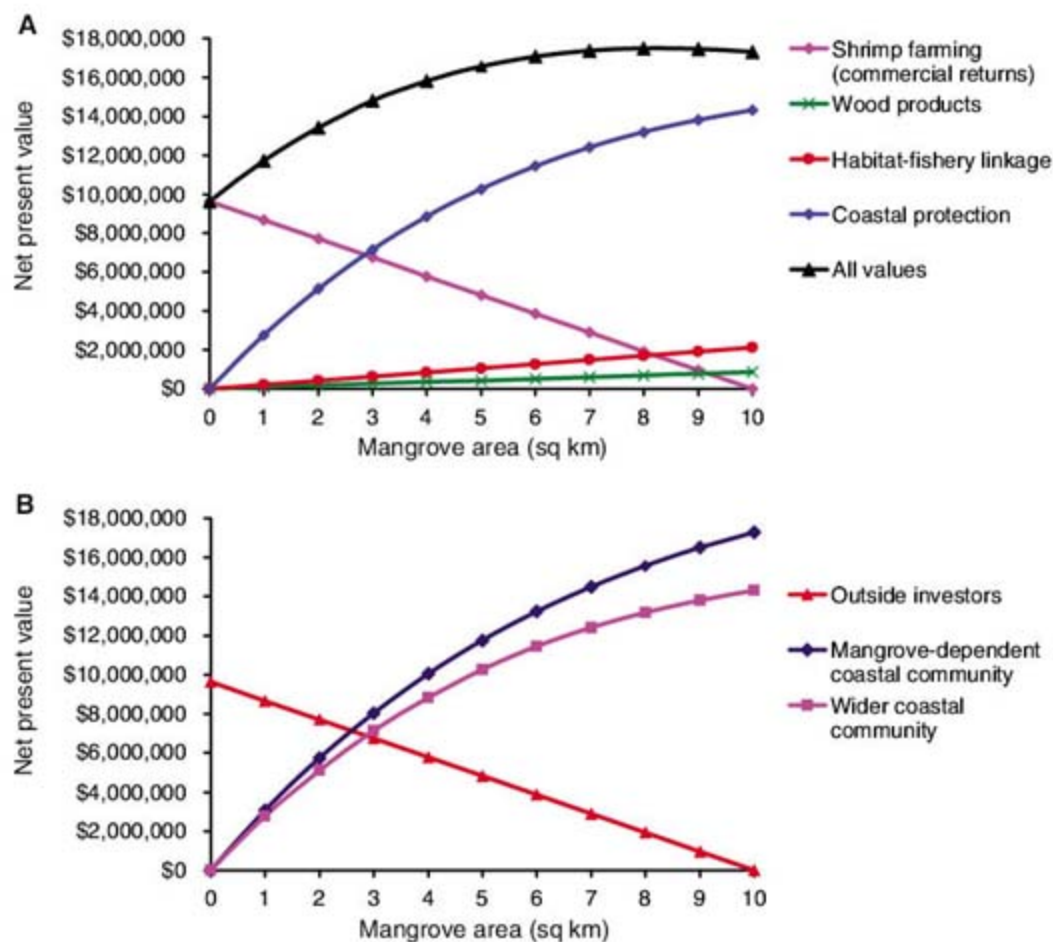


Fig. 2. Alternative comparison of shrimp farming to various mangrove services at coastal landscape level (10 km²), Thailand (calculated as in Fig. 1), incorporating the nonlinear wave attenuation function from fig. S1A, on the basis of (A) total economic returns as a function of mangrove area (km²) for the commercial returns from shrimp farming plus three mangrove ecosystem service values: coastal protection, wood product collection, and habitat support for offshore fisheries; and (B) the distribution of benefits as a function of mangrove area (km²) among three stakeholders: outside investors in shrimp farms, the mangrove-dependent coastal community, and the wider coastal community (up to 5 km away).

its highest (\$17.5 million) when up to 2 km² of mangroves are allowed to be converted to shrimp aquaculture and the remainder of the ecosystem is preserved. This outcome also yields a more equitable distribution across stakeholders (Fig. 2B), which may be an important objective in any EBM strategy for coastal management. Local mangrove-dependent coastal communities and other coastal communities living within 5 km inland would obtain approximately the same share of economic benefits from the mangrove system (\$15.6 and \$13.2 million, respectively), but now outside investors would earn some commercial profits from shrimp farming (\$1.9 million). Finally, we note that the outcome from our Thailand mangrove valuation example corresponds to “best practice” guidelines for mangrove management in Asia, which recommend that ideal mangrove/pond ratios should not exceed 20% of the habitat area converted to ponds (23, 24).

By including nonlinear relationships in an economic valuation of ecosystem services, our results challenge the assumption that the competing demands of coastal interface systems must always result in either conservation or habitat destruction. As the case study of Thailand mangroves illustrates, the way in which ecological and economic analysis is combined to estimate the values of various ecosystem services can have a large impact on coastal EBM outcome. If point estimates of these values are used to project linear relationships between the benefits of ecosystem services with respect to changes in key ecosystem physical attributes, such as area or distance from shore, then the result might be to force EBM decision-making into a simple “all or none” choice. This result is at odds with EBM

strategies, which emphasize reconciliation between economic development pressures and conservation of critical ecosystem resources and services (5–8). However, if the nonlinear ecological function underlying a service, such as coastal protection afforded by mangroves, is incorporated into economic valuation, then we more realistically represent how ecosystem services change with habitat conversion and how EBM may best be used.

References and Notes

- Coastal areas are defined in (2, 3) as habitat from the low water mark (<50 m depth) to the coastline and inland from the coastline to a maximum of 100 km or 50-m elevation (whichever is closer to the sea).
- Marine and Coastal Ecosystems and Human Well-Being: A Synthesis Report Based on the Findings of the Millennium Ecosystem Assessment* (UN Environment Programme, Nairobi, 2006).
- Millennium Ecosystem Assessment, *Ecosystems and Human Well-Being: Current State and Trends* (Island, Washington, DC, 2005), chap. 19.
- I. Valiela, J. Bowen, J. York, *Bioscience* **51**, 807 (2001).
- K. McLeod, J. Lubchenko, S. Palumbi, A. Rosenberg, Scientific Consensus Statement on Marine Ecosystem-Based Management (Communication Partnership for Science and the Sea, 2005; http://compassonline.org/marinescience/solutions_ecosystem.asp).
- T.-E. Chua, D. Bonga, N. Bermas-Atrigenio, *Coast. Manage.* **34**, 303 (2006).
- Ecosystem-Based Management: Markers for Assessing Progress* (UN Environment Programme/GPA, The Hague, 2006).
- P. Kareiva, S. Watts, R. McDonald, T. Boucher, *Science* **316**, 1866 (2007).
- A. Balmford et al., *Science* **297**, 950 (2002).
- L. Brander, R. Florax, J. Vermaat, *Environ. Resour. Econ.* **33**, 223 (2006).
- E. Barbier, *Econ. Policy* **22**, 177 (2007).
- K. Gaston, T. Blackburn, *Pattern and Process in Macroecology* (Blackwell Science, Oxford, ed. 2, 2000).
- J. Petersen et al., *Bioscience* **53**, 1181 (2003).

- E. Farnsworth, *Global Ecol. Biogeogr. Lett.* **7**, 15 (1998).
- See supporting material on Science Online.
- E. Barbier, *Contemp. Econ. Policy* **21**, 59 (2003).
- S. Sathirathai, E. Barbier, *Contemp. Econ. Policy* **19**, 109 (2001).
- S. Massel, K. Furukawa, R. Brinkman, *Fluid Dyn. Res.* **24**, 219 (1999).
- Y. Mazda, M. Magi, M. Kogo, P. N. Hong, *Mangroves Salt Marshes* **1**, 127 (1997).
- Y. Mazda, M. Magi, Y. Ikeda, T. Kurokawa, T. Asano, *Wetlands Ecol. Manage.* **14**, 365 (2006).
- E. Wolanski, in *Coastal Protection in the Aftermath of the Indian Ocean Tsunami: What Role for Forests and Trees?*, S. Braatz, S. Fortuna, J. Broadhead, R. Leslie, Eds. (FAO, Bangkok, 2007), pp. 157–179.
- The wave attenuation relationship of fig. 51A was transformed into percent wave reduction as a function of 100-m inland mangrove distance, and this relationship was used to adjust the net present value per km² estimate for storm protection used in Fig. 1A, assuming that each km² of mangroves deforested involved the equivalent loss of 100 m of mangroves inland along the 10-km coastline. See (15) for details.
- P. Saenger, E. Hegerl, J. Davie, *Global Status of Mangrove Ecosystems* (IUCN, Gland, Switzerland, 1983).
- J. Primavera et al., *Bull. Mar. Sci.* **80**, 795 (2007).
- This work was conducted as part of the “Measuring ecological, economic, and social values of coastal habitats to inform ecosystem-based management of land-sea interfaces” Working Group supported by the National Center for Ecological Analysis and Synthesis, funded by NSF grant DEB-0553768; the University of California, Santa Barbara; the State of California; and the David and Lucile Packard Foundation. We thank B. Halpern for his assistance with this project and work, and three anonymous reviewers for their constructive comments.

Supporting Online Material

www.sciencemag.org/cgi/content/full/319/5861/321/DC1
Materials and Methods
Figs. S1 and S2
Tables S1 to S3
References

11 September 2007; accepted 22 November 2007
10.1126/science.1150349

β-Catenin Defines Head Versus Tail Identity During Planarian Regeneration and Homeostasis

Kyle A. Gurley, Jochen C. Rink, Alejandro Sánchez Alvarado*

After amputation, freshwater planarians properly regenerate a head or tail from the resulting anterior or posterior wound. The mechanisms that differentiate anterior from posterior and direct the replacement of the appropriate missing body parts are unknown. We found that in the planarian *Schmidtea mediterranea*, RNA interference (RNAi) of β-catenin or dishevelled causes the inappropriate regeneration of a head instead of a tail at posterior amputations. Conversely, RNAi of the β-catenin antagonist *adenomatous polyposis coli* results in the regeneration of a tail at anterior wounds. In addition, the silencing of β-catenin is sufficient to transform the tail of uncut adult animals into a head. We suggest that β-catenin functions as a molecular switch to specify and maintain anteroposterior identity during regeneration and homeostasis in planarians.

β-Catenin is a multifunctional protein that controls transcriptional output as well as cell adhesion. During embryonic development of both vertebrates and invertebrates, β-catenin regulates a variety of cellular processes, including organizer formation, cell fate specifi-

cation, proliferation, and differentiation (1–9). In adult animals, the Wnt/β-catenin pathway participates in regeneration and tissue homeostasis; misregulation of this pathway can lead to degenerative diseases and cancer in humans (9–12). In response to upstream cues, such as Wnt ligands

binding to Frizzled receptors, β-catenin accumulates in nuclei (Fig. 1A) and invokes transcriptional responses that direct the specification and patterning of tissues (13, 14). Adenomatous polyposis coli (APC) is an essential member of a destruction complex that phosphorylates β-catenin, resulting in its constitutive degradation. Hence, loss of APC leads to a rise in β-catenin levels that is sufficient to drive transcriptional responses (15). The intracellular protein Dishevelled has multiple functions but plays an essential role as a positive regulator of β-catenin by inhibiting the destruction complex (16).

As part of a systematic effort to define the roles of signaling pathways in planaria, we analyzed the canonical Wnt signaling system in *Schmidtea mediterranea*. We cloned and determined the expression patterns of all identifiable homologs of core pathway components (Fig. 1A) and silenced them, individually or in combina-

Department of Neurobiology and Anatomy, Howard Hughes Medical Institute, University of Utah School of Medicine, 401 MREB, 20N 1900E, Salt Lake City, UT 84132, USA.

*To whom correspondence should be addressed. E-mail: sanchez@neuro.utah.edu

tions, on the basis of likelihood of redundancy as gleaned from the expression data (figs. S1 to S6 and table S1). RNAi-treated animals were then amputated to assess the role of the silenced genes during regeneration (Fig. 1B). After head and tail amputations of control worms, the remaining

trunk formed one anterior and one posterior blastema, which then differentiated to replace the missing structures (Fig. 1C; $n = 28$). However, RNAi of a single β -catenin (*Smed- β -catenin-1*), both *dishevelled* homologs (*Smed-dvl-1*; *Smed-dvl-2*), or APC (*Smed-APC-1*) caused striking

alterations in the anteroposterior (A/P) identity of regenerating tissues (Fig. 1, D to F). Both blastemas of *Smed- β -catenin-1(RNAi)* worms adopted an anterior fate, resulting in animals with two heads of opposite orientation (penetrance = 100%, $n = 39$). *Smed-dvl-1(RNAi)*; *Smed-dvl-2(RNAi)* worms also regenerated heads from both blastemas but displayed additional phenotypes, including ectopic and supernumerary photoreceptors in the anterior region. This is consistent with the multiple roles of Dishevelled in different pathways (Fig. 1E; penetrance = 75%, $n = 20$). On the other hand, *Smed-APC-1(RNAi)* animals regenerated tails from both amputation planes (Fig. 1F; penetrance = 60%, $n = 43$).

To address whether these changes were superficial or reflected a fate transformation of internal cell types and organ systems, we used anatomical and molecular markers of A/P identity. Anatomically, two organ systems with characteristic asymmetries along the A/P axis were examined: (i) the central nervous system (CNS), composed of two anterior cephalic ganglia (brain) and two ventral cords projecting posteriorly (Fig. 1G), and (ii) the digestive system, consisting of a single anterior and two posterior gut branches (Fig. 1K). The "posterior" head of *Smed- β -catenin-1(RNAi)* and *Smed-dvl-1(RNAi)*; *Smed-dvl-2(RNAi)* animals contained a characteristically anterior nervous system and gut, as did the "anterior" tail of *Smed-APC-1(RNAi)* animals was devoid of discernible brain tissue and exhibited posterior structures, as did the "posterior" tail (Fig. 1, J and N).

To define the molecular extent of A/P misspecification, we used two markers identified during our in situ analyses that are specifically expressed at the anterior and posterior ends of intact and regenerating animals (Fig. 1, A, O, and S). *Smed-sFRP-1*, a homolog of secreted Frizzled-related proteins (sFRP), was expressed in an arch of cells capping the anterior edge of the animal. In contrast, *Smed-fz-4*, a homolog of Frizzled receptors, was expressed at the posterior edge in a posterior-to-anterior gradient. We refer to *Smed-sFRP-1* and *Smed-fz-4* as the "anterior marker" and the "posterior marker," respectively, in all subsequent analyses.

In *Smed- β -catenin-1(RNAi)* and *Smed-dvl-1(RNAi)*; *Smed-dvl-2(RNAi)* worms, the "posterior" head expressed the anterior marker, whereas the posterior marker was severely reduced or absent (Fig. 1, P, Q, T, and U). Conversely, the "anterior" tail of *Smed-APC-1(RNAi)* animals expressed the posterior marker, whereas the anterior marker was severely reduced or absent (Fig. 1, R and V). We noted that misspecified heads and tails in RNAi-treated worms moved independently from the rest of the animal, hence this tissue was functioning autonomously (movies S1 to S3). We conclude that silencing *Smed- β -catenin-1*, *Smed-dvl-1(RNAi)*; *Smed-dvl-2(RNAi)*, or *Smed-APC-1* is sufficient to misspecify blastema identity.

The inappropriate regeneration of complete heads and tails in RNAi-treated animals sug-

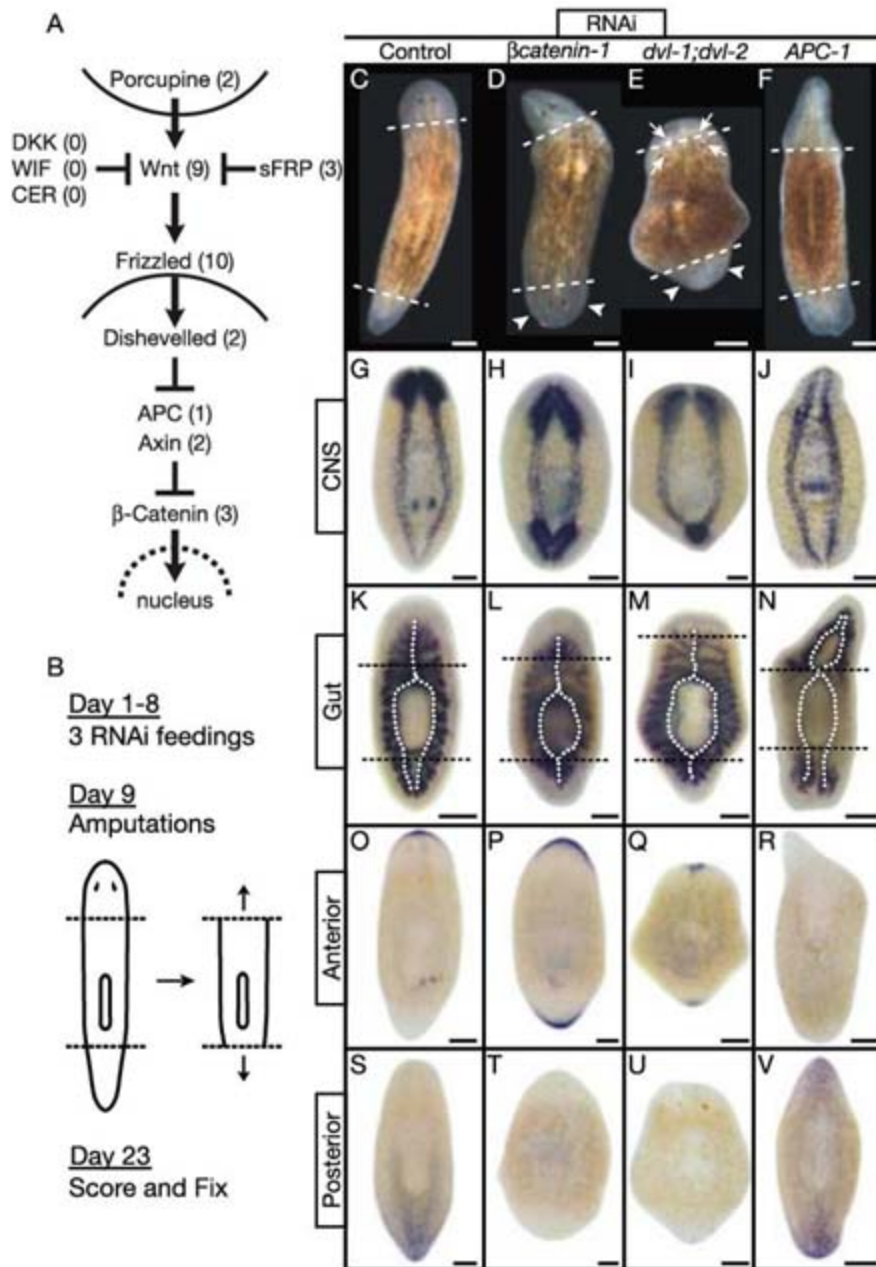
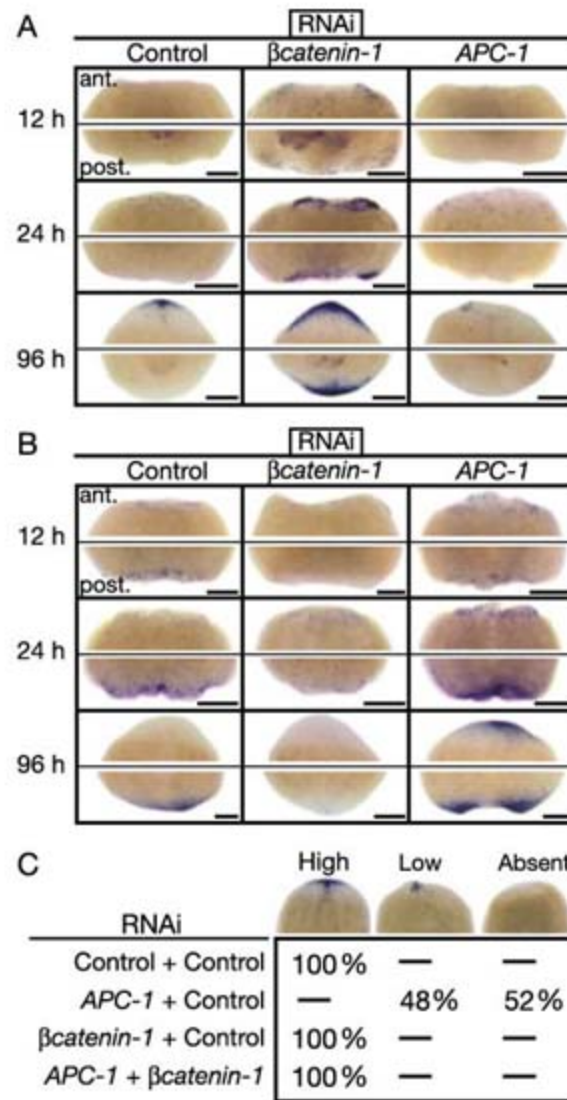


Fig. 1. Signaling through β -catenin defines head versus tail during regeneration. (A) Canonical Wnt pathway. Numbers denote *S. mediterranea* homologs identified and silenced. (B) Experimental strategy. (C to V) Trunk fragments 14 days after amputation. Dashed lines, amputation planes; control, *unc-22(RNAi)*. (C) to (F): Live animals. (D) and (E): *Smed- β -catenin-1(RNAi)* and *Smed-dvl-1(RNAi)*; *Smed-dvl-2(RNAi)* posterior blastemas formed heads with photoreceptors (arrowheads). *Smed-dvl-1(RNAi)*; *Smed-dvl-2(RNAi)* fragments also developed ectopic photoreceptors, often within old tissues (arrows). (F): *Smed-APC-1(RNAi)* anterior blastemas formed tails. (G) to (V): In situ hybridizations ($n \geq 5$ per marker). Markers: CNS, prohormone convertase 2 (PC2); gut, *porcupine* (*Smed-porc-1*); anterior, *secreted frizzled-related protein* (*Smed-sFRP-1*); posterior, *frizzled* (*Smed-fz-4*). (G) and (K): Normal brain and ventral nerve cords; single anterior and dual posterior gut branches (dotted lines). (H), (I), (L), and (M): *Smed- β -catenin-1(RNAi)* and *Smed-dvl-1(RNAi)*; *Smed-dvl-2(RNAi)* posterior blastemas developed brain tissue and head-like gut branches. (J) and (N): *Smed-APC-1(RNAi)* anterior blastemas developed tail-like nerve cords and gut branches. (O) and (S): Normal anterior and posterior marker expression. (P), (Q), (T), and (U): *Smed- β -catenin-1(RNAi)* and *Smed-dvl-1(RNAi)*; *Smed-dvl-2(RNAi)* induced anterior marker expression at both ends, whereas the posterior marker was virtually undetectable. (R) and (V): *Smed-APC-1(RNAi)* induced posterior marker expression at both ends, whereas the anterior marker was virtually undetectable. Scale bars, 200 μ m.

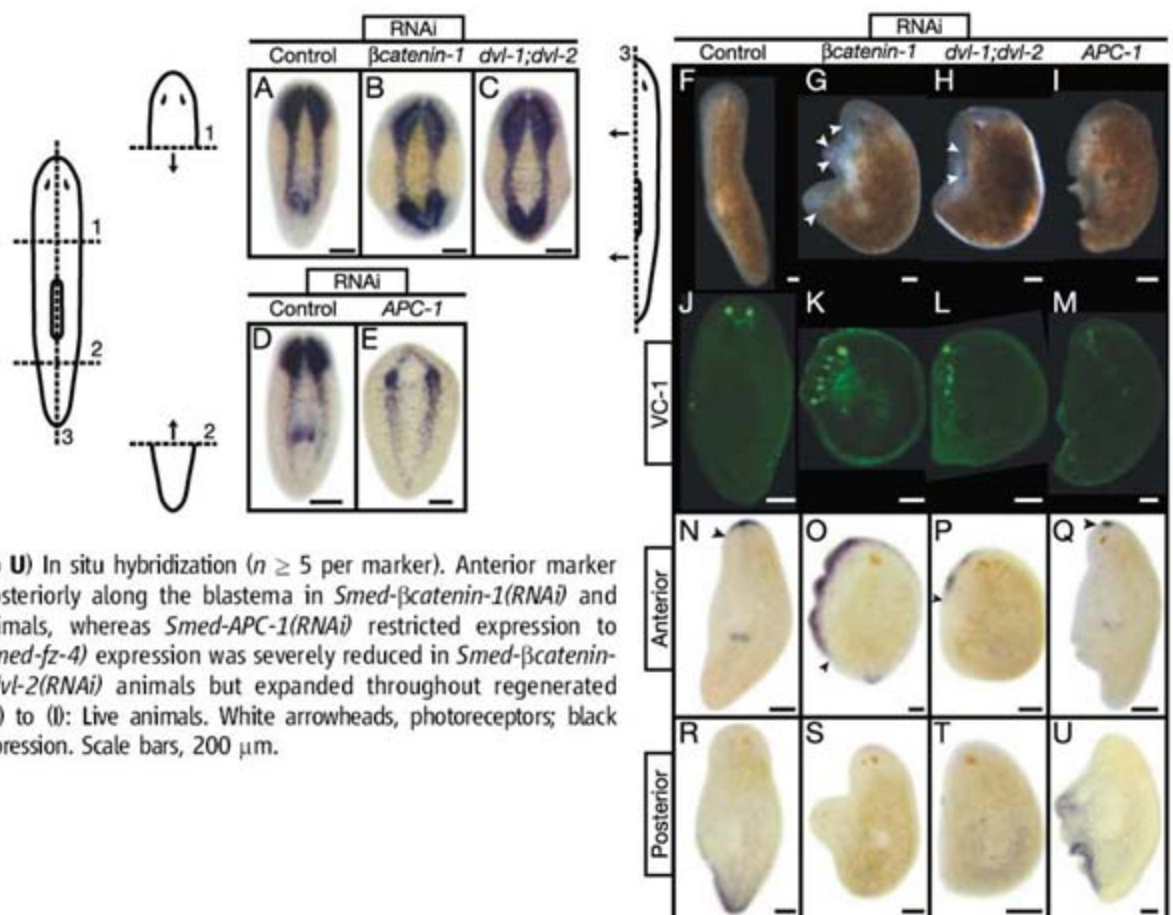
Fig. 2. *Smed-βcatenin-1(RNAi)* and *Smed-APC-1(RNAi)* phenotypes manifest early, and the *Smed-APC-1(RNAi)* phenotype depends on *Smed-βcatenin-1*. (A) Anterior (*Smed-sFRP-1*) and (B) posterior (*Smed-fz-4*) marker expression time course in regenerating trunk fragments. Anterior (ant.) and posterior (post.) blastemas from the same representative fragments are shown ($n \geq 15$ per condition). Scale bars, 200 μ m. (C) Double-silencing experiments assaying *Smed-sFRP-1* expression in anterior trunk blastemas 4 days after amputation; animals were scored as high, low, or absent (see examples, top row). Proportions of scored animals are listed for each category ($n \geq 24$ per condition). Control, *unc-22(RNAi)*.



gested that regulators of β -catenin act early during regeneration. We therefore used the anterior and posterior markers to investigate the onset of blastema differentiation in control and RNAi-treated trunk fragments (Fig. 2, A and B). In control animals at 12 hours after amputation, the anterior marker was virtually undetectable, whereas the posterior marker was clearly evident in the posterior blastema; 24 hours after amputation, the two markers recapitulated the A/P specificity seen later during regeneration and in adult animals (Fig. 1, O and S; Fig. 2, A and B). However, in *Smed-βcatenin-1(RNAi)* trunks, the anterior marker was expressed at both ends by 12 hours and maintained throughout the experiment, whereas the posterior marker remained markedly reduced (Fig. 2, A and B). The reverse was observed in *Smed-APC-1(RNAi)* trunks (Fig. 2, A and B). Consistent with the inferred time window for β -catenin signaling, *Smed-βcatenin-1* and *Smed-APC-1* were expressed at both ends in wild-type animals by 12 hours (fig. S7). These results indicate that β -catenin and APC act very early to determine blastema identity.

We next used animals silenced for both *Smed-βcatenin-1* and *Smed-APC-1* to test whether the *Smed-APC-1(RNAi)* phenotype results from increased β -catenin activity. Under these conditions, anterior blastemas were properly fated, indicating that the misspecification phenotype of *Smed-APC-1(RNAi)* depends on *Smed-βcatenin-1* (Fig. 2C). Additionally, posterior blastemas adopted an anterior fate, indicating that the *Smed-βcatenin-1(RNAi)* phenotype does not depend on APC activity. The

Fig. 3. *Smed-βcatenin-1*, *Smed-dvl-1*; *Smed-dvl-2*, and *Smed-APC(RNAi)* phenotypes do not depend on position or orientation of amputation. Fragments 14 days after amputation are shown; control, *unc-22(RNAi)*. (A to E) PC2 in situ hybridization (CNS) ($n \geq 5$). *Smed-βcatenin-1(RNAi)* and *Smed-dvl-1(RNAi);Smed-dvl-2(RNAi)* fragments regenerated posterior brain tissue; *Smed-APC-1(RNAi)* fragments failed to regenerate anterior brain tissue. (F to M) During lateral regeneration, *Smed-βcatenin-1(RNAi)* and *Smed-dvl-1(RNAi);Smed-dvl-2(RNAi)* animals developed supernumerary heads and photoreceptors; *Smed-APC-1(RNAi)* prevented proper regeneration of these structures ($n \geq 15$). Photoreceptors were visualized with VC-1 antibody (25). (N to U) In situ hybridization ($n \geq 5$ per marker). Anterior marker (*Smed-sFRP-1*) expression expanded posteriorly along the blastema in *Smed-βcatenin-1(RNAi)* and *Smed-dvl-1(RNAi);Smed-dvl-2(RNAi)* animals, whereas *Smed-APC-1(RNAi)* restricted expression to preexisting tissues. Posterior marker (*Smed-fz-4*) expression was severely reduced in *Smed-βcatenin-1(RNAi)* and *Smed-dvl-1(RNAi);Smed-dvl-2(RNAi)* animals but expanded throughout regenerated tissues in *Smed-APC-1(RNAi)* animals. (F) to (I): Live animals. White arrowheads, photoreceptors; black arrowheads, extent of anterior marker expression. Scale bars, 200 μ m.



combined data show that signaling through β -catenin occurs at posterior amputations and is necessary and sufficient to specify tail fate. In contrast, signaling through β -catenin is blocked or never occurs at anterior amputations, and this is necessary and sufficient to specify head fate. The premature expression of the anterior marker in *Smed- β -catenin-1(RNAi)* worms may indicate that in wild-type planarians, β -catenin inhibition does not immediately follow amputation (Fig. 2A). We suggest that β -catenin activity acts as a molecular switch to specify head versus tail fate in planarians.

We then explored whether the β -catenin switch plays a role in blastema identity regardless of the A/P location or angle of amputation. Indeed, the head fragments of *Smed- β -catenin-1(RNAi)* and *Smed-dvl-1(RNAi);Smed-dvl-2(RNAi)* worms regenerated a head from the posterior wound (penetrance = 79%, $n = 24$; penetrance = 82%, $n = 33$, respectively), and the tail fragments of *Smed-APC-1(RNAi)* worms regenerated a tail from the anterior wound (penetrance = 67%, $n = 27$; Fig. 3, A to E, and movie S4). After longitudinal amputation along the midline, control animals formed a blastema along the A/P axis and regenerated mediolaterally (Fig. 3, F, J, N, and R). In contrast, *Smed- β -catenin-1(RNAi)* and *Smed-dvl-1(RNAi);Smed-dvl-2(RNAi)* worms regenerated

anterior tissue and developed multiple ectopic heads along the lateral edge (Fig. 3, G, H, K, L, O, P, S, and T). The most severely affected *Smed-APC-1(RNAi)* worms regenerated posterior tissue and failed to replace the lost head structures (Fig. 3, I, M, Q, and U). Thus, the laterally regenerating tissue in RNAi-treated animals was misspecified. Our data indicate that β -catenin activity is regulated during lateral regeneration and that the β -catenin switch can dominantly misspecify regenerating tissues regardless of A/P position or amputation angle.

Smed- β -catenin-1(RNAi) animals also displayed striking changes in the nonregenerating portions of regenerating fragments. *Smed- β -catenin-1(RNAi)* tail fragments at 24 and 48 hours after amputation expressed the anterior marker in cell clusters around the circumference of the fragment (Fig. 4, A, B, D, and E). By day 14, in addition to a new head, moving head-like protrusions developed from the periphery (Fig. 4, C and F, and movie S5). Similar protrusions also developed in trunk fragments (movie S2).

Such fate changes may have been initiated by amputation. We therefore observed unamputated (intact) worms 14 days after the final RNAi feeding. Ectopic photoreceptors were visible in the tail of all

($n = 20$) *Smed- β -catenin-1(RNAi)* animals and none of the control animals (Fig. 4, G, H, M, and N). Intact RNAi-treated animals also exhibited ectopic lateral protrusions, formed a brain in the tail region, and expressed the anterior marker posteriorly (Fig. 4, I to L and O to R, and movie S6). The molecular basis for such a change of A/P polarity in an adult organism was previously unknown.

Together, our data demonstrate the fundamental importance of β -catenin in the maintenance of polarity and cell fate during tissue regeneration and homeostasis in planarians (fig. S8). Our findings reveal a dynamic control of β -catenin in adult animals that is not readily apparent during the progression of embryogenesis: The precise quantity and location of regenerating tissue is different for each individual and for each regeneration event, newly regenerated tissues must integrate with the old, and ongoing homeostatic cell turnover may require sustained instructive cues. It is interesting that we did not observe any head or tail misspecification phenotypes for any of the upstream components of canonical Wnt signaling (Wnts, Frizzleds, or Porcupines; see table S1). Although we cannot rule out protein perdurance, incomplete gene silencing, or redundancy with known or unidentified components, the intracellular components of β -catenin signaling may be regulated by an unconventional upstream mechanism to specify polarity during regeneration and/or homeostasis. Indeed, β -catenin regulation can be Wnt-independent in vertebrate cells, and Dishevelled remains the most upstream known β -catenin regulator during early sea urchin development (14, 17, 18). With respect to putative downstream effectors, planarians can regenerate double heads after pharmacological gap junction inhibition, and β -catenin is implicated in gap junction formation and function (19–21). Finally, whether specification and maintenance of the planarian A/P axis via β -catenin is or is not independent of Hox proteins remains to be determined.

More than 100 years ago, T. H. Morgan reported that fragments with closely spaced anterior and posterior amputation planes occasionally regenerate two-headed animals (22, 23). He termed these animals “Janus heads” and suggested that “something in the piece itself determines that a head shall develop at the anterior cut surface and a tail at the posterior cut surface” (24). Our results indicate that β -catenin activity is a key target of polarity specification in planarians, providing mechanistic insight into the old, unanswered question of how blastema fate is controlled. We propose that the evolutionarily ancient β -catenin protein, in a manner reminiscent of its role during metazoan embryogenesis (6, 8), acts as a molecular switch in adult planarians and that it may play a similar role in the adult tissues of other animals.

References and Notes

1. S. Schneider, H. Steinbeisser, R. M. Warga, P. Hausen, *Mech. Dev.* **57**, 191 (1996).
2. C. A. Larabell et al., *J. Cell Biol.* **136**, 1123 (1997).

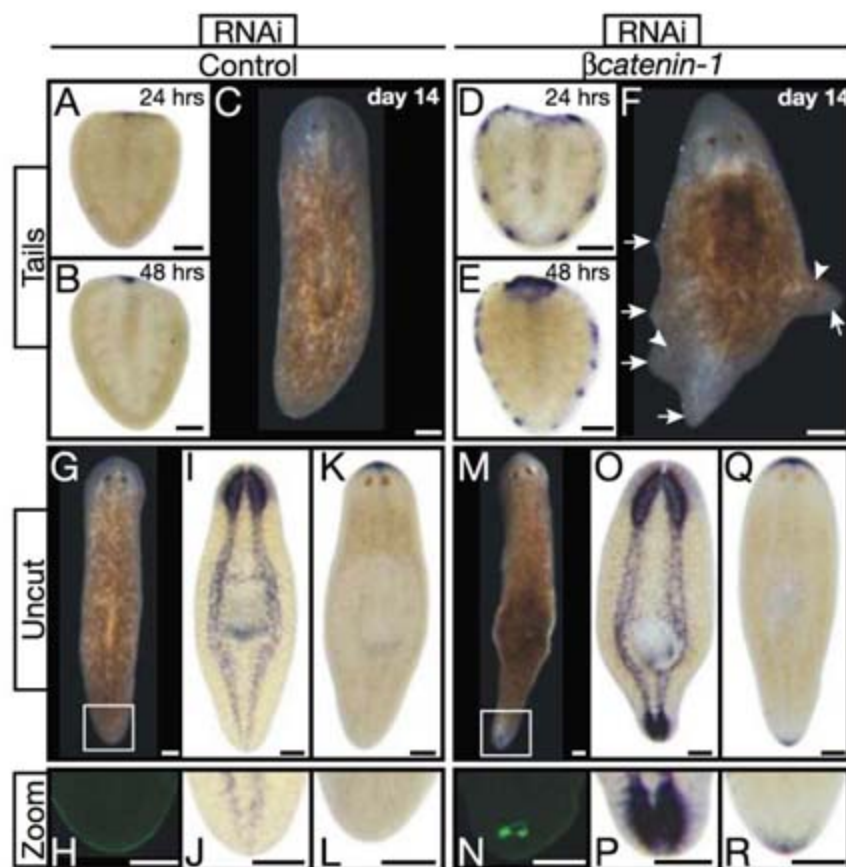


Fig. 4. *Smed- β -catenin-1(RNAi)* transforms nonregenerating tissues. (A to F) Tail fragments. (A), (B), (D), and (E): Anterior marker (*Smed-sFRP-1*) analyses 24 and 48 hours after amputation revealed early ectopic expression in *Smed- β -catenin-1(RNAi)* ($n \geq 5$ per condition). (C) and (F): Live tail fragments 14 days after amputation. *Smed- β -catenin-1(RNAi)* caused lateral ectopic protrusions (arrowheads, ectopic photoreceptors; arrows, abnormal protrusions). (G to R) Transformation of tail into head tissue in uncut *Smed- β -catenin-1(RNAi)* animals 14 days after final RNAi-feeding. (G) and (M): Live animals. (I) and (O): PC2 in situ hybridization (CNS) ($n \geq 4$). (K) and (Q): Anterior marker expression ($n \geq 4$). (H), (J), (L), (N), (P), and (R): Magnification of tail tips [boxes in (G) and (M)]. (H) and (N): VC-1 antibody staining (photoreceptors). Control, *unc-22(RNAi)*. Scale bars, 200 μ m.

3. C. Y. Logan, J. R. Miller, M. J. Ferkowicz, D. R. McClay, *Development* **126**, 345 (1999).
4. A. H. Wikramanayake *et al.*, *Nature* **426**, 446 (2003).
5. S. Orsulic, M. Peifer, *J. Cell Biol.* **134**, 1283 (1996).
6. C. E. Rocheleau *et al.*, *Cell* **90**, 707 (1997).
7. C. E. Rocheleau *et al.*, *Cell* **97**, 717 (1999).
8. S. Q. Schneider, B. Bowerman, *Dev. Cell* **13**, 73 (2007).
9. C. Y. Logan, R. Nusse, *Annu. Rev. Cell Dev. Biol.* **20**, 781 (2004).
10. C. L. Stoick-Cooper *et al.*, *Development* **134**, 479 (2007).
11. H. Yokoyama, H. Ogino, C. L. Stoick-Cooper, R. M. Grainger, R. T. Moon, *Dev. Biol.* **306**, 170 (2007).
12. C. Kobayashi, Y. Saito, K. Ogawa, K. Agata, *Dev. Biol.* **306**, 714 (2007).
13. R. Stadeli, R. Hoffmans, K. Basler, *Curr. Biol.* **16**, R378 (2006).
14. K. Willert, K. A. Jones, *Genes Dev.* **20**, 1394 (2006).
15. M. D. Gordon, R. Nusse, *J. Biol. Chem.* **281**, 22429 (2006).
16. J. B. Wallingford, R. Habas, *Development* **132**, 4421 (2005).
17. F. H. Brembeck *et al.*, *Genes Dev.* **18**, 2225 (2004).
18. C. A. Ettensohn, *Sci. STKE* **2006**, pe48 (2006).
19. T. Nogi, M. Levin, *Dev. Biol.* **287**, 314 (2005).
20. R. M. Shaw *et al.*, *Cell* **128**, 547 (2007).
21. K. A. Guger, B. M. Gumbiner, *Dev. Biol.* **172**, 115 (1995).
22. T. H. Morgan, *Arch. Entw. Mech. Org.* **7**, 364 (1898).
23. P. W. Reddien, A. Sánchez Alvarado, *Annu. Rev. Cell Dev. Biol.* **20**, 725 (2004).
24. T. H. Morgan, *Am. Nat.* **38**, 502 (1904).
25. F. Sakai, K. Agata, H. Orii, K. Watanabe, *Zool. Sci.* **17**, 375 (2000).
26. We thank K. Agata for VC-1 antibody; B. Pearson and G. Eisenhoffer for optimization of in situ protocols; and R. Dorsky, T. Piotrowski, and all Sánchez lab members for comments. Supported by National Institute of General Medical Sciences grants F32GM082016 (K.A.G.),

T32CA093247 (K.A.G.), and RO-1 GM57260 (A.S.A.) and by the European Molecular Biology Organization (J.C.R.). A.S.A. is a Howard Hughes Medical Institute Investigator. For *S. mediterranea* genes, GenBank accession numbers are EU130785, EU130786, EU130787, EU130788, EU130789, EU130790, and EU130791.

Supporting Online Material

www.sciencemag.org/cgi/content/full/1150029/DC1
Materials and Methods
Figs. S1 to S8
Tables S1
Movies S1 to S6

4 September 2007; accepted 28 November 2007

Published online 6 December 2007;

10.1126/science.1150029

Include this information when citing this paper.

Smed-βcatenin-1 Is Required for Anteroposterior Blastema Polarity in Planarian Regeneration

Christian P. Petersen¹ and Peter W. Reddien^{1,2*}

Planarian flatworms can regenerate heads at anterior-facing wounds and tails at posterior-facing wounds throughout the body. How this regeneration polarity is specified has been a classic problem for more than a century. We identified a planarian gene, *Smed-βcatenin-1*, that controls regeneration polarity. Posterior-facing blastemas regenerate a head instead of a tail in *Smed-βcatenin-1(RNAi)* animals. *Smed-βcatenin-1* is required after wounding and at any posterior-facing wound for polarity. Additionally, intact *Smed-βcatenin-1(RNAi)* animals display anteriorization during tissue turnover. Five Wnt genes and a secreted Frizzled-related Wnt antagonist-like gene are expressed in domains along the anteroposterior axis that reset to new positions during regeneration, which suggests that Wnts control polarity through *Smed-βcatenin-1*. Our data suggest that β-catenin specifies the posterior character of the anteroposterior axis throughout the Bilateria and specifies regeneration polarity in planarians.

The ability to regenerate is widespread and varies in degree within the animal kingdom. Planarian flatworms are dramatic examples, capable of regenerating a complete animal from nearly any fragment of the organism. Amputation induces the formation of a regeneration blastema, which differentiates to produce missing structures. Blastema formation requires adult stem cells called neoblasts (1). More than a century ago, Randolph (2) and Morgan (3) noted that transverse planarian pieces can regenerate a head and a tail at the anterior and posterior wound sites, respectively. Furthermore, any body region can become involved in either head or tail regeneration depending upon the identity of the missing tissue (Fig. 1A). Therefore, planarians possess a robust system throughout the anteroposterior (A-P) axis for specifying the identity of missing tissue at wounds. This system has been

named "polarity." Morgan observed that very thin transverse pieces occasionally regenerate animals with two heads and hypothesized that a gradient of material establishes regeneration polarity. Although these features of planarian regeneration are frequently described in textbook examples of polarity, no previous explanation exists for the underlying genetic mechanisms that specify regeneration polarity.

The planarian *Schmidtea mediterranea* has emerged as a powerful molecular genetic system for studying regeneration because of genome sequence availability, the ability to use RNA interference (RNAi) (4, 5), and the evolutionary position of the organism within an understudied protostome superphylum, the Lophotrochozoa (6). To study polarity in planarians, we performed an RNAi screen involving surgically removed heads and tails (Fig. 1B). We identified a single gene required for polarity and named the gene *Smed-βcatenin-1*. The trunks of *Smed-βcatenin-1(RNAi)* animals regenerated apparent heads at both posterior-facing and anterior-facing wounds (Fig. 1C). This dramatic phenotype is reminiscent of the polarity transformations observed in Morgan's classic surgical manipulation experi-

ments. Double-stranded RNA (dsRNA) from *Caenorhabditis elegans unc-22*, a gene not present in planarians, served as the RNAi control (Fig. 1C). The predicted SMED-βCATENIN-1 protein is homologous to β-catenin proteins found in other animals (fig. S1A). β-catenin proteins mediate canonical Wnt signal transduction to regulate many developmental events (7). SMED-βCATENIN-1 possesses at least nine predicted armadillo repeats and a candidate N-terminal GSK-3β phosphorylation site (GSK-3β-mediated phosphorylation can regulate β-catenin stability) (fig. S1B) (8). Because armadillo repeats can be very degenerate (9), more armadillo repeats may exist and not be recognized in this protein. *Smed-βcatenin-1* mRNA was broadly expressed in in situ hybridizations and reduced in *Smed-βcatenin-1(RNAi)* animals (fig. S2).

Smed-βcatenin-1(RNAi) posterior blastemas contained two apparent photoreceptors (Fig. 1C) and possessed headlike stretching behavior ($n = 105/107$). These posterior blastemas also contained cell types normally associated with the head, including photoreceptor neurons and cephalic ganglia (Fig. 1D). Posterior blastemas displayed local headlike polarity, with photoreceptors being more distal to the wound site than cephalic ganglia. Anterior-specific transcripts can be observed in the posterior *Smed-βcatenin-1(RNAi)* blastemas by 72 hours after amputation (fig. S3). Additionally, *Smed-βcatenin-1(RNAi)* posterior blastemas lacked the tail pattern of H.1.3b-zonadhesin expression (Fig. 1E). Together, these data indicate that posterior *Smed-βcatenin-1(RNAi)* blastemas are heads.

Smed-βcatenin-1(RNAi) animals regenerated posterior-facing heads at multiple A-P locations, indicating a requirement for *Smed-βcatenin-1* throughout the A-P axis (Fig. 2A, fig. S4). We injected *Smed-βcatenin-1* dsRNA into freshly amputated wild-type transverse fragments to inhibit *Smed-βcatenin-1* only during regeneration. Because these animals displayed a 100% penetrant polarity reversal, *Smed-βcatenin-1* is required during regeneration for the polarity decision (Fig. 2B). In addition, because these pieces only contained a small region of preexisting tissue, *Smed-βcatenin-1* can be required locally.

¹Whitehead Institute for Biomedical Research, 9 Cambridge Center, Cambridge, MA 02142, USA. ²Department of Biology, Massachusetts Institute of Technology, Cambridge, MA 02139, USA.

*To whom correspondence should be addressed. E-mail: reddien@wi.mit.edu

Multiple incisions made in *Smed-βcatenin-1(RNAi)* animals resulted in the production of side-facing heads, dramatically illustrated by the six-headed *Smed-βcatenin-1(RNAi)* animal in Fig. 2C. Heads grew from side incisions at locations far from either pole of the animal (Fig. 2C) and in animals that retained their original posterior pole (Fig. S4). Thus, *Smed-βcatenin-1* is not required only to specify the posterior-most pole during regeneration. Given this observation, we asked whether *Smed-βcatenin-1* is simply required to suppress a complete head-production program at any wound. *Smed-βcatenin-1(RNAi)* animals could regenerate their head tips, rather than producing an additional head following such injury. This indicates that these animals retained the ability to repair only the extent of tissue missing (Fig. 2D). Therefore, *Smed-βcatenin-1* likely does not simply suppress a complete head formation program.

After transverse amputations, animals are challenged to form a new anterior or posterior pole. Planarians can also regenerate other tissues, such as tissue along the entire A-P axis during lateral regeneration of missing sides. After sagittal amputations to remove the lateral half of animals, *Smed-βcatenin-1(RNAi)* fragments regenerated multiple anterior photoreceptors and side-facing head-like protrusions (Fig. 3A). These animals possessed expanded cephalic ganglia and anterior marker expression in blastemas, as well as ectopic cephalic ganglia in side-facing protrusions (Fig. 3A). Thus, *Smed-βcatenin-1(RNAi)* animals displayed anteriorization of blastemas in which an entire A-P axis must be patterned. Together, our amputation experiments suggest *Smed-βcatenin-1* normally promotes posterior aspects of A-P axis regeneration: tail rather than head formation at posterior poles and A-P regionalization in blastemas that produce tissue along the entire A-P axis.

Uninjured planarians constantly replace aged differentiated cells. To determine whether *Smed-βcatenin-1* is required for instructing the posterior fates of new cells, uninjured *Smed-βcatenin-1(RNAi)* animals were observed during homeostasis. A slow transformation of the body was observed, in which head-like tissue appeared at the posterior pole (Fig. 3B) and, ultimately, around the periphery of the animals and at the pharynx (Fig. 3C, D). Therefore, *Smed-βcatenin-1* is required for the homeostatic maintenance of the A-P axis.

Because β-catenin proteins are well-established effectors of Wnt signaling, we hypothesized that Wnts could provide the A-P positional information necessary for blastema polarity decisions. We characterized five Wnt-family genes in *S. mediterranea* and named them *Smed-wntP-1* through -3, *Smed-wnt2-1*, and *Smed-wnt11-1* (10). As assayed by whole-mount in situ hybridization, these Wnt genes were expressed in distinct domains along the A-P axis and may therefore encode signaling molecules that specify planarian A-P axis polarity (Fig. 4). Expression was detected for *Smed-wntP-1* in one to four cells near the tail tip

(Fig. 4A) and for *Smed-wnt11-1* in a graded fashion from the posterior (Fig. 4B). Expression was detected for *Smed-wntP-2* in the posterior half of the animal and internally around the pharynx (Fig. 4C), for *Smed-wntP-3* at the anterior pharynx end (Fig. 4D), and for *Smed-wnt2-1* laterally in the anterior half of the animal (Fig. 4E). RNAi of Wnt genes did not result in posterior head

regeneration ($n > 25$ animals each), possibly because of redundancy among the many posteriorly expressed Wnt genes. Wnt signaling is known to be inhibited by secreted frizzled-related proteins (sFRP) (11). We cloned an *S. mediterranea* sFRP gene (*Smed-sFRP-1*) (10) and found it to be expressed at the anterior pole (Fig. 4F). The *Smed-wnt* genes *Smed-wntP-1* through -3, as

Fig. 1. Inhibition of *Smed-βcatenin-1* results in posterior blastema polarity reversal. Day 10 of regeneration. (A) Regeneration polarity: cells between planes "I" and "II" can become involved in head or tail regeneration (27). (B) Cartoon, amputations (red); arrow, indicates trunk fragments shown. (C) Anterior, top. PR, photoreceptors. Red dots, approximate blastema/old tissue boundary. A control *unc-22(RNAi)* trunk produced a posterior tail ($n = 114/114$), and a *Smed-βcatenin-1(RNAi)* trunk fragment produced a head at the posterior wound ($n = 105/107$). (D and E) Anterior, left. (D) The photoreceptors (PR), cephalic ganglia (cg), and ventral nerve cords (vnc) of regenerating trunks were labeled with antibodies (VC-1, anti-arrestin; cg, anti-synaptotagmin, SYT). A *Smed-βcatenin-1(RNAi)* posterior blastema showed VC-1 and SYT staining ($n = 6/6$). (E) A *Smed-βcatenin-1(RNAi)* posterior head lacked the normal posterior expression of H.1.3b ($n = 6/6$). Arrow, posterior blastema. Scale bars, 500 μm (C) and 200 μm [(D) and (E)].

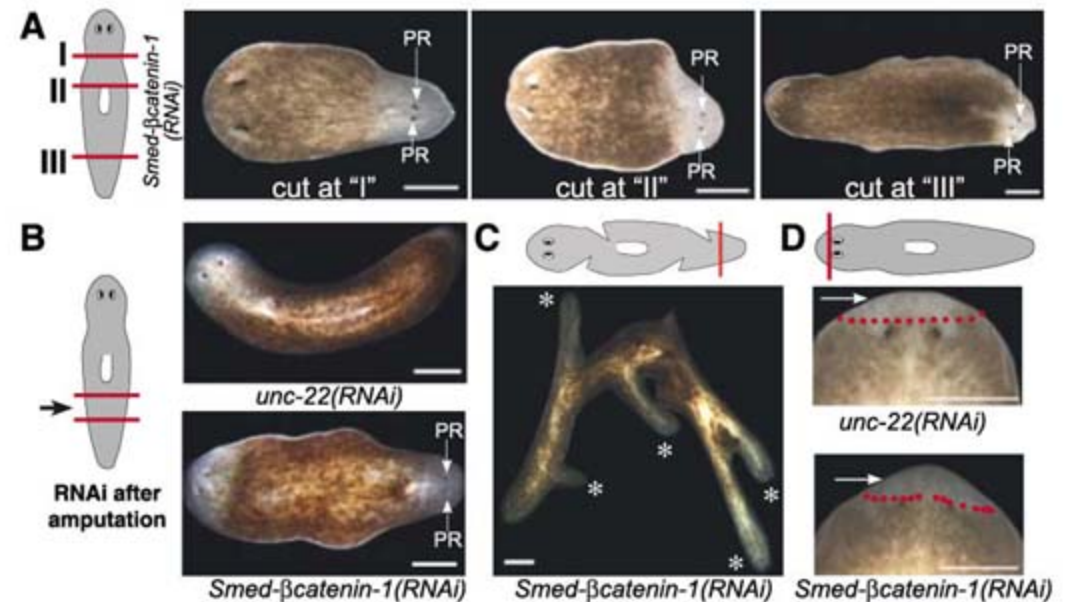
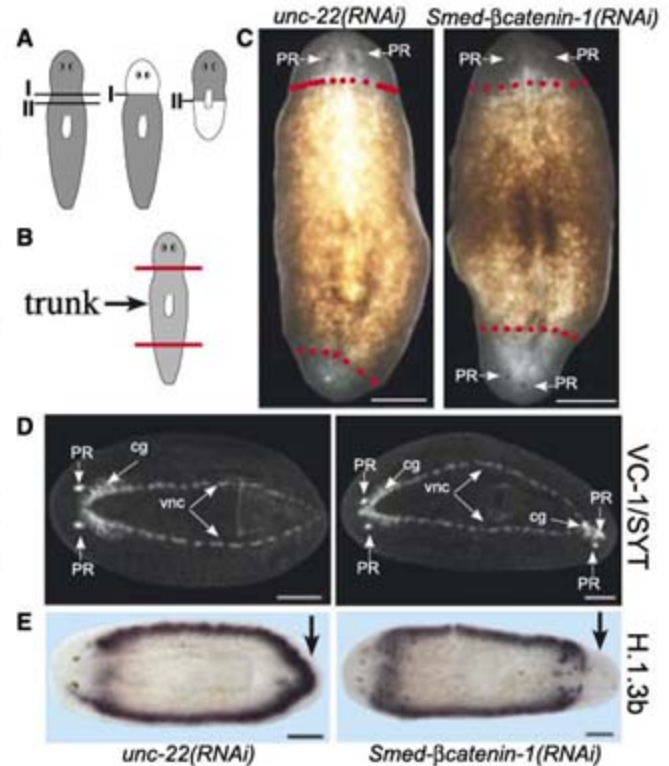


Fig. 2. *Smed-βcatenin-1* inhibition affects polarity throughout the A-P axis, locally after wounding, and can result in supernumerary head regeneration. Amputations (red). Anterior, left. Scale bars, 500 microns. (A) *Smed-βcatenin-1(RNAi)* fragments produced posterior-facing heads at three anteroposterior locations (amputation planes I, II, and III). (B) Transverse fragments were generated 1 hour before dsRNA injection. A *Smed-βcatenin-1(RNAi)* animal formed a posterior head ($n = 10/10$). (C) Multiple side incisions and tail removal were made to generate a six-headed *Smed-βcatenin-1(RNAi)* animal (asterisks, supernumerary heads). (D) *Smed-βcatenin-1(RNAi)* did not impair head tip regeneration (arrows, blastema; red dots, approximate blastema/old tissue boundary; $n = 10/10$). Day of regeneration: (A) and (B), day 11; (C), day 20; (D) day 5.

well as *Smed-wnt11-1*, became expressed near posterior-facing wounds (Fig. 4G-J); *Smed-wnt11-1* and *Smed-wntP-2* expression also were more posteriorly restricted in tail fragments (Fig. 4H, I). By contrast, *Smed-wnt2-1* was expressed near anterior-facing wounds and restricted anteriorly in heads (Fig. 4K). Following amputation, *Smed-sFRP-1* was expressed at new anterior poles (Fig.

4L). These homeostatic and regeneration expression patterns suggest that the A-P planarian axis is regulated by anterior Wnt inhibition and posterior Wnt activation.

Our data suggest that a genetic program—canonical Wnt signaling mediated by *Smed-βcatenin-1*—controls planarian A-P tissue identity in homeostasis and blastema polarity in regener-

ation. We suggest that *Smed-βcatenin-1* acts at posterior-facing wounds to effect the posterior rather than anterior polarity regeneration decision and that polarity is controlled by the A-P location of expression of Wnt genes and Wnt signaling antagonists. Wnt signaling has come to be used for a myriad of patterning and cell proliferation roles in the course of the evolutionary diversification of the three superphyla comprising bilaterally symmetric animals: the deuterostomes and two groupings from the protostomes, the Ecdysozoa and the Lophotrochozoa (6, 7, 12–15). Among these roles, our data provide evidence that an ancestral role of Wnt signaling is to promote posterior aspects of A-P axis specification and regulation. This hypothesis is well supported by data from other organisms (16). For example, in multiple deuterostomes, Wnt and secreted Wnt inhibitor genes are expressed in a manner that resembles the A-P polarity of expression seen in planarians. Specifically, Wnt genes are expressed in the posterior of *Xenopus* embryos after the midblastula transition (17, 18), as well as in the posterior of cephalochordate embryos (19). Furthermore, Wnt genes and a secreted Wnt antagonist are expressed at opposite (oral and aboral) poles of radially symmetric cnidarian larvae (12, 20), and pharmacologic inhibition of the β-catenin-inhibitory GSK-3β protein in hydra leads to expanded oral fates (21). The conservation of Wnt axial expression features in these diverse animals, combined with the requirement for *Smed-βcatenin-1* in A-P regeneration polarity, suggest a functionally critical and deeply conserved role for β-catenin in A-P axis polarity. In ecdysozoans, β-catenin controls anteroposterior axon polarity and cell division polarity in *C. elegans* (22, 23), anteroposterior segment polarity in *Drosophila* (24), posterior segment patterning in the intermediate germ insect *Gryllus bimaculata* (25), and animal-vegetal cell polarity during embryogenesis of the lophotrochozoan annelid *Platynereis dumerilii* (26). We propose that WNT signaling controls A-P axial polarity features of most if not all bilaterally symmetric animals and determines the polarity of regeneration.

References and Notes

1. P. W. Reddien, A. Sánchez Alvarado, *Annu. Rev. Cell Dev. Biol.* **20**, 725 (2004).
2. H. Randolph, *Arch. Entw. Mech. Org.* **5**, 352 (1897).
3. T. H. Morgan, *Arch. Entw. Mech. Org.* **7**, 364 (1898).
4. A. Sánchez Alvarado, P. A. Newmark, *Proc. Natl. Acad. Sci. U.S.A.* **96**, 5049 (1999).
5. P. W. Reddien, A. L. Bermange, K. J. Murfitt, J. R. Jennings, A. Sánchez Alvarado, *Dev. Cell* **8**, 635 (2005).
6. A. Adoutte et al., *Proc. Natl. Acad. Sci. U.S.A.* **97**, 4453 (2000).
7. C. Y. Logan, R. Nusse, *Annu. Rev. Cell Dev. Biol.* **20**, 781 (2004).
8. C. Yost et al., *Genes Dev.* **10**, 1443 (1996).
9. A. R. Kidd 3rd, J. A. Miskowski, K. R. Siegfried, H. Sawa, J. Kimble, *Cell* **121**, 761 (2005).
10. Materials and methods are available as supporting material on Science Online.
11. L. Leyns, T. Bouwmeester, S. H. Kim, S. Piccolo, E. M. De Robertis, *Cell* **88**, 747 (1997).
12. P. N. Lee, K. Pang, D. Q. Matus, M. Q. Martindale, *Semin. Cell Dev. Biol.* **17**, 157 (2006).

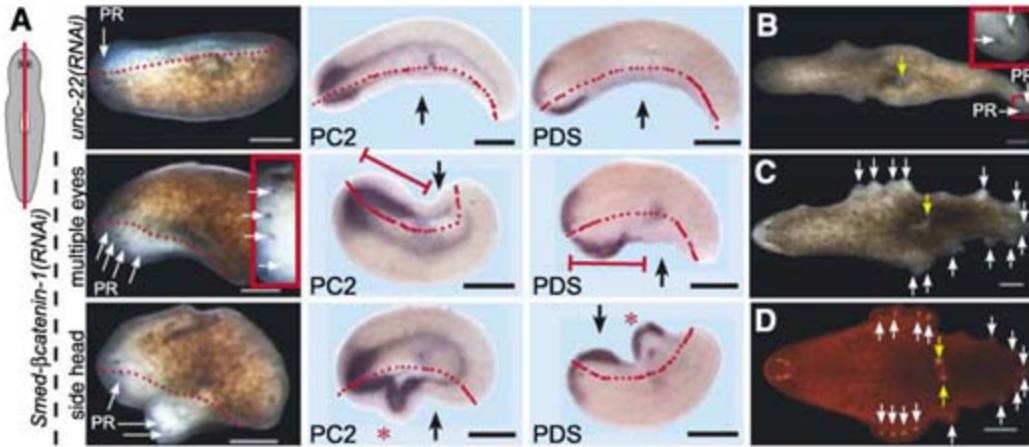


Fig. 3. *Smed-βcatenin-1* inhibition causes anteriorization during lateral regeneration and homeostatic tissue maintenance. PR and white arrows, photoreceptors. Anterior, left. Scale bars, 500 μm. (A) *Smed-βcatenin-1(RNAi)* longitudinal fragments regenerated multiple eyes or a side-facing head (e.g., 32/37 and 8/37, respectively, after dsRNA injection and amputation within hours). (Red box inset) Enlargement of photoreceptors. In situ hybridizations with PC2 or PDS riboprobes showed anteriorization (red brackets) and side-facing heads (red asterisks) in *Smed-βcatenin-1(RNAi)* lateral blastemas. Animals are at day 12 of regeneration. Black arrows, side with blastema. (B to D) Animals between 29 and 35 days of RNAi are shown. Unamputated *Smed-βcatenin-1(RNAi)* animals displayed (B) posterior heads (see red inset) (*n* = 47/48), (C) multiple head-like peripheral protrusions (*n* = 12/25), (D) ectopic photoreceptors in headlike protrusions (VC-1-labeled, white arrows), and [(B) to (D)] protrusions at the pharynx (*n* = 24/25, yellow arrows) containing photoreceptors (*n* = 11/25).

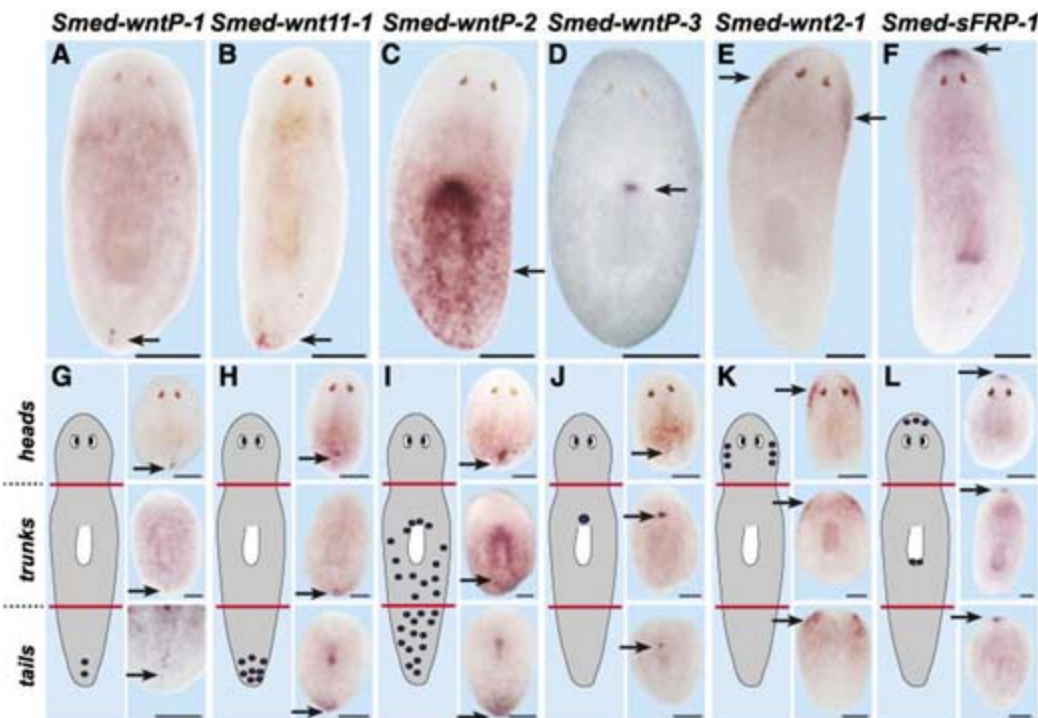


Fig. 4. Planarian Wnt genes and *Smed-sFRP-1* are regionally expressed along the A-P axis during homeostasis and regeneration. Anterior, top. Scale bars, 200 μm. Arrow, *Smed-wnt* or *Smed-sFRP* signal. (A to F) Dorsal views of in situ hybridizations of planarian Wnt genes in intact and (G to L) in day 4 to 5 regenerating head, trunk, and tail fragments. (G to L) Cartoons depict expression patterns (purple dots), as well as surgical strategy (red lines). *Smed-wnt* genes were expressed in overlapping anteroposterior domains, with the majority in the posterior; *Smed-sFRP-1* was expressed at the anterior pole. New expression was observed near wounds in regeneration. Images were taken with gamma = 0.67.

13. E. M. De Robertis, J. Larrain, M. Oelgeschlager, O. Wessely, *Nat. Rev. Genet.* **1**, 171 (2000).
14. H. C. Korswagen, *Bioessays* **24**, 801 (2002).
15. M. T. Veeman, J. D. Axelrod, R. T. Moon, *Dev. Cell* **5**, 367 (2003).
16. C. Niehrs, *Nat. Rev. Genet.* **5**, 425 (2004).
17. C. Kiecker, C. Niehrs, *Development* **128**, 4189 (2001).
18. R. Harland, J. Gerhart, *Annu. Rev. Cell Dev. Biol.* **13**, 611 (1997).
19. J. K. Yu *et al.*, *Nature* **445**, 613 (2007).
20. A. Kusserow *et al.*, *Nature* **433**, 156 (2005).
21. M. Broun, L. Gee, B. Reinhardt, H. R. Bode, *Development* **132**, 2907 (2005).
22. M. A. Hilliard, C. I. Bargmann, *Dev. Cell* **10**, 379 (2006).
23. H. Takeshita, H. Sawa, *Genes Dev.* **19**, 1743 (2005).
24. C. Nusslein-Volhard, E. Wieschaus, *Nature* **287**, 795 (1980).
25. K. Miyawaki *et al.*, *Mech. Dev.* **121**, 119 (2004).
26. S. Q. Schneider, B. Bowerman, *Dev. Cell* **13**, 73 (2007).
27. H. V. Brøndsted, *Planarian Regeneration* (Pergamon Press, London, ed. 1, 1969), pp. 276.
28. We thank the Reddien lab, H. Sive, and A. Hochwagen for discussions and K. Agata for antibodies. This work was supported by American Cancer Society RSG-07-180-01-DDC and awards to P.W.R. from the Rita Allen Foundation, the Searle Foundation, and the Smith

Family Foundation, and by American Cancer Society postdoctoral fellowship PF-07-046-01-DDC to C.P.P. The authors declare no competing financial interests.

Supporting Online Material

www.sciencemag.org/cgi/content/full/1149943/DC1

Materials and Methods

Figs. S1 to S4

References

30 August 2007; accepted 27 November 2007

Published online 6 December 2007;

10.1126/science.1149943

Include this information when citing this paper.

Natural Genetic Variation in *Lycopene Epsilon Cyclase* Tapped for Maize Biofortification

Carlos E. Harjes,^{1*} Torbert R. Rocheford,^{2†} Ling Bai,³ Thomas P. Brutnell,³ Catherine Bermudez Kandianis,² Stephen G. Sowinski,⁴ Ann E. Stapleton,⁵ Ratnakar Vallabhaneni,^{6,7} Mark Williams,⁴ Eleanore T. Wurtzel,^{6,7} Jianbing Yan,⁸ Edward S. Buckler^{1,9,10†}

Dietary vitamin A deficiency causes eye disease in 40 million children each year and places 140 to 250 million at risk for health disorders. Many children in sub-Saharan Africa subsist on maize-based diets. Maize displays considerable natural variation for carotenoid composition, including vitamin A precursors α -carotene, β -carotene, and β -cryptoxanthin. Through association analysis, linkage mapping, expression analysis, and mutagenesis, we show that variation at the *lycopene epsilon cyclase* (*lcyE*) locus alters flux down α -carotene versus β -carotene branches of the carotenoid pathway. Four natural *lcyE* polymorphisms explained 58% of the variation in these two branches and a threefold difference in provitamin A compounds. Selection of favorable *lcyE* alleles with inexpensive molecular markers will now enable developing-country breeders to more effectively produce maize grain with higher provitamin A levels.

Maize is the dominant subsistence crop in much of sub-Saharan Africa and the Americas, where between 17 and 30% of children under age of 5 are vitamin A-deficient. This results in xerophthalmia (progressive blindness), increased infant morbidity and mortality, and depressed immunological responses (1). Vitamin A deficiency starts with inadequate provitamin A or vitamin A content or bioavailability

in foods and is exacerbated by disease-induced malabsorption.

Diet diversification, food fortification, and supplementation (2–4) have all been used to combat dietary micronutrient deficiencies. Ideally, all children would have access to a varied diet rich in fruits and vegetables, but diet diversification is often limited by crop seasonality, expense, and low bioavailability of green leafy plant carotenoids (5, 6). Poor infrastructure in developing countries has limited widespread use of direct vitamin supplementation. Perhaps the most feasible approach to eradicating death and disease caused by dietary deficiencies is biofortification, a process by which staple crops are purposefully bred for higher nutritional density (7, 8). Although biofortified foods can potentially be an inexpensive, locally adaptable, and long-term solution to diet deficiencies, cultural preferences may limit their acceptance. This may be particularly true for those crops where transgenics are the only alternative to boost provitamin A content, given limited acceptance of genetically modified organisms in developing countries.

Carotenoids are derived from the isoprenoid biosynthetic pathway and are precursors of the plant hormone abscisic acid and of other apo-

carotenoids (9). The first committed step of this pathway [as recently revised (10)] is formation of phytoene from geranylgeranyl diphosphate by phytoene synthase (*psy1/psy1*) (Fig. 1) (11). Recent studies in maize suggest that the *psy1* locus has been the target of a selective sweep following selection for endosperm-accumulating carotenoids and shift from white to yellow kernels (12). The first branch point of this pathway (Fig. 1) occurs at cyclization of lycopene where action of lycopene beta cyclase (LCYB) at both ends of linear lycopene produces a molecule with two β rings. Alternatively, the coaction of LCYB and lycopene epsilon cyclase (LCYE) generates a β,ϵ -carotene that is a precursor to lutein (13). Relative activities of LCYB and LCYE are hypothesized to regulate the proportion of carotenes directed to each branch of this pathway (13–15). Indeed, transgenic manipulations of LCYE expression in *Arabidopsis*, potato, and *Brassica* increase the pool of β ring-containing carotenes and xanthophylls (13, 16–18).

Maize exhibits considerable natural variation for kernel carotenoids, with some lines accumulating as much as 66 $\mu\text{g/g}$. The pre-

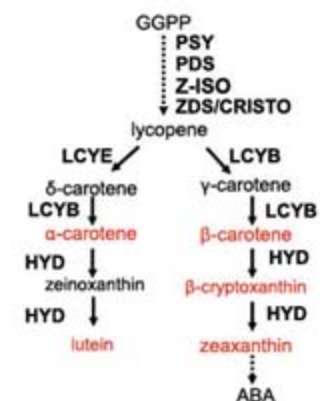


Fig. 1. Simplified carotenoid biosynthetic pathway in plants (29). Enzymatic reactions are represented by arrows, dashed lines represent multiple enzymatic steps. Substrates in red were evaluated in this study. Compounds: GGPP, geranylgeranyl diphosphate; ABA, abscisic acid. Enzymes: PSY, phytoene synthase; PDS, phytoene desaturase; Z-ISO, 15-*cis* zeta-carotene isomerase; ZDS, zeta-carotene desaturase; CRISTO, carotene isomerase; HYD, carotene hydroxylase enzymes, which include ϵ - and β -ring hydroxylases.

¹Institute for Genomic Diversity, Cornell University, Ithaca, NY 14853, USA. ²Department of Crop Sciences, University of Illinois, Urbana, IL 61801, USA. ³Boyce Thompson Institute, Ithaca, NY 14853, USA. ⁴DuPont Crop Genetics Research, Wilmington, DE 19880, USA. ⁵Department of Biology and Marine Biology, University of North Carolina, Wilmington, NC 28403, USA. ⁶Department of Biological Sciences, Lehman College, City University of New York (CUNY), Bronx, NY 10468, USA. ⁷The Graduate School and University Center, City University of New York (CUNY), New York, NY 10016, USA. ⁸International Maize and Wheat Improvement Center (CIMMYT), Apartado Postal 6-64, 06600 Mexico, DF, Mexico. ⁹U.S. Department of Agriculture, Agricultural Research Service, Plant, Soil and Nutrition Research Unit, Ithaca, NY 14853, USA. ¹⁰Department of Plant Breeding and Genetics, Cornell University, Ithaca, NY 14853, USA.

*Present address: Monsanto Company, Leesburg, GA 30903, USA.

†To whom correspondence should be addressed. E-mail: esb33@cornell.edu (E.S.B.); trochefo@uiuc.edu (T.R.R.)

dominant carotenoids in maize kernels, in decreasing order of concentration, are lutein, zeaxanthin, β -carotene, β -cryptoxanthin, and α -carotene. β -Carotene contains two provitamin A structures (two nonhydroxylated β -ionone rings) and β -cryptoxanthin and α -carotene one each (single nonhydroxylated β -ionone ring). Among lines included in our diverse maize panel, β -carotene levels reached 13.6 $\mu\text{g/g}$. However, most yellow maize grown and consumed throughout the world has only 0.5 to 1.5 $\mu\text{g/g}$ β -carotene. Comparisons between β -carotene and total carotenoids with grain color (scaled according to shade of yellow) revealed poor correlations with low R^2 values (Fig. 2), which

indicated that marker-assisted selection (MAS) may prove much more efficient than selection based on color alone.

To dissect the phenotypic diversity, we used an association-mapping approach that exploits the genetic diversity of maize to provide resolution within 2000 base pairs (bp) (19–21). In the context of plant breeding, this has the added advantage of identifying the most favorable allele within a diverse genetic background, which provides the necessary genotypic information to facilitate the design of efficient maize introgression and selection schemes throughout the world. We complemented the association mapping with linkage mapping to evaluate the

effects in a genetically less complex background and with a mutagenesis program to isolate novel allelic variation within an elite near-isogenic background.

To evaluate functional diversity (Fig. 1), eight candidate genes representing select members of gene families encoding biosynthetic enzymes of the carotenoid pathway were sampled across a diverse panel of 288 maize lines, of which 204 were yellow. Subsets of yellow lines were grown in four different years and surveyed for whole-kernel carotenoids by high-performance liquid chromatography (HPLC). The yellow lines averaged 23 $\mu\text{g/g}$ for total carotenoids (range 5.5 to 66.0 $\mu\text{g/g}$) and 1.7 $\mu\text{g/g}$ for β -carotene (range 0.06 to 13.6 $\mu\text{g/g}$).

For association analysis, we used a mixed-model approach that controlled for complex population and pedigree relationships (22). Among our current sampling of candidate genes, *lycopen epsilon cyclase* (*lycE*) (14) had the largest effect on partitioning the two branches of carotenoids and, consequently, on β -carotene and β -cryptoxanthin content. In maize, the single-copy *lycE* gene consists of 10 exons spanning 3640 bp (Fig. 3). After initial association and screening for polymorphisms in key haplotypes, four regions were selected and scored across the entire panel. On the basis of the position of *LYC*E in the biochemical pathway, we predicted that the ratio of the sum of kernel carotenoids from each pathway branch would form the strongest association. Indeed, this was confirmed (Table 1), with the strength of the association confirming that *lycE* plays a key role in controlling this ratio. Correspondingly, levels of predominant provitamin A compounds β -carotene and β -cryptoxanthin were also highly associated with *lycE*.

Subsequent haplotype analysis revealed several probable causative polymorphisms for the ratio of α - and β -carotene branches for the 2003 field season (table S1). A large promoter indel and an amino acid substitution in exon 1 explain most of the variation ($R^2 = 36\%$; $n = 135$; $P = 1.27 \times 10^{-12}$) with a 5.2-fold effect. A second indel in the 3' UTR also has a significant 3.3-fold effect and contributes to variation not explained by the promoter polymorphism (type III SS; $P = 1.9 \times 10^{-4}$). The fourth significant polymorphism at position 2238 in intron 4 was associated with a 2.5-fold effect (type III SS; $P = 0.0003$). The overall, four-term model explains 58% of the variation ($P = 9.2 \times 10^{-17}$). These significant polymorphisms exhibit some linkage disequilibrium (LD), and only nine haplotypic classes exist in our sample, which limits full differentiation of the effects of each polymorphism. Overall, there is a ninefold difference between two of the more differentiated haplotype classes, and sixfold between two more common haplotypes (table S2). There was a threefold increase in the proportion of β -carotene and β -cryptoxanthin between the common haplotypes. Verification of these results was provided by

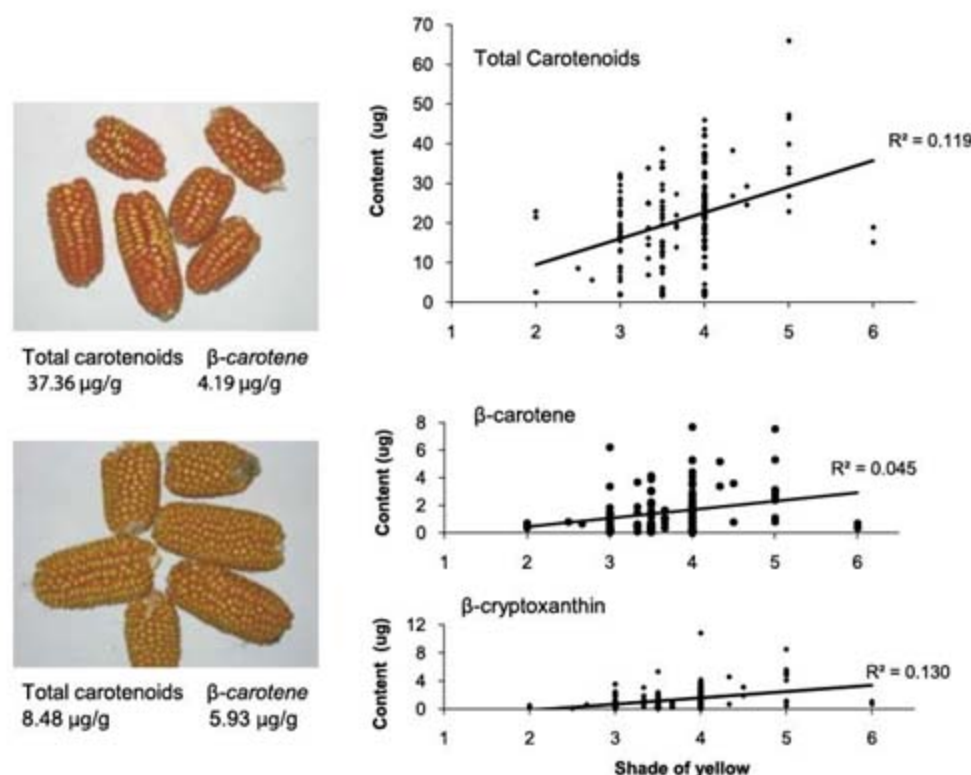


Fig. 2. Grain color and carotenoid content. The graphs depict the low correlation between visual grain color and total carotenoids, β -carotene, and β -cryptoxanthin in diverse inbreds. In these kernels, the shade of yellow ranges from white (score of 1) to dark orange (score of 6). White kernels were excluded from the analysis. The difficulty in visual selection for β -carotene content is further exemplified by the images on the left, where the yellow maize below has higher β -carotene than the orange variety above. These correlations are across the diverse panel of 228 maize inbreds; correlations for grain color and total carotenoids are higher when scored across segregating populations and narrow ranges of germ plasm, but correlations for β -carotene and β -cryptoxanthin remain low.

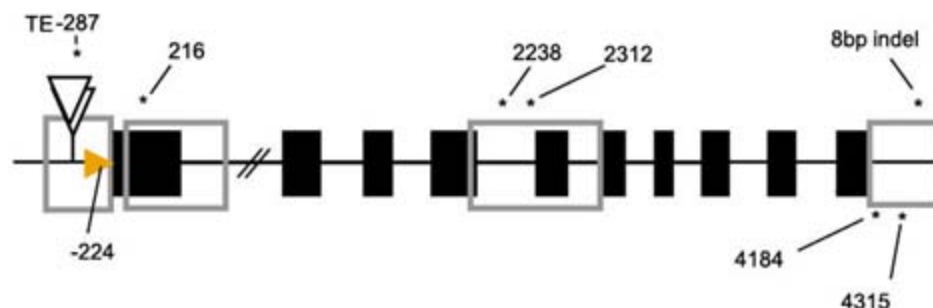


Fig. 3. Schematic diagram of the maize *lycE*. Putative transcription start sites are depicted with orange arrow, translated exons as black squares, and the sampled regions as gray boxes. Polymorphisms that significantly associated with changes in flux between the lutein and zeaxanthin branches of the pathway are labeled with asterisks. The 5' transposable element insertion(s) are represented by the white triangles. Positions relative to the sequence alignment are indicated numerically above the polymorphisms.

significant associations in subsequent field seasons (Table 1).

Expression analysis indicated that *lcyE* is preferentially expressed in the endosperm relative to the embryo (fig. S1). Expression profiling of kernels at 15 and 20 days after pollination (DAP) indicated expression levels correlated well with the ratio of carotenoids from each pathway branch, explaining 70 to 76% of the variance. Lines with transposon insertions near the start site had much lower expression levels [in 15 DAP and 20 DAP lower by a factor of 3.7 and 13, respectively (fig. S2)]. The 3' indel may also have expression effects, but our statistical tests lacked the power to confirm this hypothesis. A quantitative trait locus (QTL) experiment that examined segregation of B73-Mo17 alleles in leaves found significant variation in the cis-regulation of *lcyE* expression, along with several other regions that also contribute to expression level control of *lcyE* (fig. S3).

In a previous study, three major QTL were identified for accumulation of carotenoids in maize (23). Two of these QTL colocalized with *yl* and *zeta carotene desaturase (zds)*; the third QTL mapped to a region without a candidate gene. We mapped *lcyE* to chromosome 8 bin 5, near marker bnlg1599, and it colocalized with this previously undetermined QTL. This QTL showed significant effects for modification of the ratio of α to β branch carotenoids [logarithm of the odds ratio for linkage (or lod) score of 34.05; R^2 54.4%] and explained 31.7% of the variation for lutein (lod 16.5). The magnitude of effects was not as large as in association or mutagenesis analysis. However, this biparental QTL population only segregated for the amino substitution (at codon 216) and a modest promoter polymorphism and does not segregate for the 3' polymorphism. Notably, this QTL was not significant for total carotenoids, which further supports the conclusion that variation within *lcyE* gene underlies this QTL for carotenoid composition.

To confirm association and QTL results, mutagenesis induced by ethane methyl sulfonate (EMS) was conducted to isolate additional alleles of *lcyE*. Two M₂ ears of inbred Qx47 segregated for a distinct change in endosperm color from yellow to orange, with orange recessive to yellow (these color changes were apparent in the inbred isogenic background, but not in diverse breeding materials). HPLC analysis of orange and yellow kernels confirmed a shift in the zeaxanthin:lutein ratio in the direction of zeaxanthin. This orange endosperm mutation was backcrossed into the standard genetic inbred line B73, and *lcyE* was tested as a candidate gene, which revealed that the Qx47 *lcyE* haplotype cosegregates with orange endosperm and ratio of α -carotene versus β -carotene branch carotenoids (fig. S4).

The most favorable haplotype for higher β -carotene branch carotenoids included both the large promoter insertion and 3' 8-bp insertion. In the diverse panel we tested, this haplotype occurs in 5% of temperate inbreds and 16% of tropical inbreds. MAS at this locus should be effective for several reasons: (i) The most favorable haplotype is found with at least modest frequency in different germ plasm sources and thus breeders can select donors from their relatively more adapted sources. (ii) The favorable haplotype has a large effect. (iii) Visual selection is ineffective for differentiating carotenoid composition and selecting provitamin A compounds. (iv) In comparison with HPLC analysis of carotenoids, polymerase chain reaction (PCR) scoring of the *lcyE* locus is much less expensive (costing perhaps 1/1000th that of HPLC) and more accessible to developing countries with greatest need for provitamin A.

An approach that empowers local breeder involvement through inexpensive visual selection for darker yellow to orange kernels to enhance flux into carotenoid pathway, and also incorporates MAS for *lcyE*, should result in

increased levels of provitamin A compounds. To expedite creation of improved germ plasm globally, we provide information on PCR-based markers (fig. S5). Donor inbreds and improved breeding lines derived at the International Maize and Wheat Improvement Center (CIMMYT) from synthetics of diverse panel inbreds with higher β -carotene are available by contacting T. R.R. This will facilitate selection worldwide of the most favorable *lcyE* alleles, which we have begun in our program. We are screening tropical breeding germ plasm collections in collaboration with CIMMYT.

To date, MAS for natural variation has been limited by resolution and scope (germ plasm diversity). Alleles have generally been characterized in the limited genetic background and resolution of biparental QTL studies, leaving in question their relevance to broader germ plasm (24), particularly for germ plasm outside of the temperate United States. As a result, the primary use for MAS is backcross breeding of transgenic traits. In contrast, the association mapping approach used here allows for rapid generation of selectable markers based on performance of diverse germ plasm. This provides markers more relevant in a broad genetic background, and that enables breeders to search for favorable alleles in their locally adapted germ plasm sources.

In ongoing studies, we are attempting to identify alleles for other genes in the pathway that increase total carotenoids and that slow the conversion of β -carotene to β -cryptoxanthin and zeaxanthin, to exploit more fully the natural genetic variation potential in provitamin A biofortification of maize. These results will then be further incorporated in breeding efforts to create a healthier maize crop for the world's poorest people.

Although the genetic results and strategy presented here are encouraging, they need to be placed in context as part of an overall biofortification effort encompassing breeding infrastructure, seed distribution, societal acceptance,

Table 1. *lcyE* associations across seasons. Association results for significant polymorphisms identified in the four regions sampled along the *lcyE* gene. Each polymorphism is labeled numerically by its position on the alignment relative to the exon 1 start codon. Followed by the favorable allele (bold)/unfavorable allele at the site. An initial scan for association using both β -carotene and the ratio of the two pathway branches was

conducted using the mixed model incorporating population structure and kinship. Subsequently a simpler general linear model (GLM) was used to evaluate data sets from additional years, including population structure (Q), given the oligogenic behavior of the trait the change in flux estimates for 2003 do not include Q. Avg., average; n.c., nonconvergence; n.s., not significant.

Polymorphic site	<i>lcyE</i> association (P), mixed model of			<i>lcyE</i> association as a ratio across environments (GLM) (P)			Fold change in flux
	β -Carotene/all	Ratio of branches		(2002)	(2003)	(2004)	
Environment (year)	(2003)	(2003)	(2002)	(2002)	(2003)	(2004)	(2005)
Avg. observation no.	(157)	(154)	(44)	(156)	(154)	(156)	(156)
5' TE 1+4/2/3	5.42×10^{-4}	3.96×10^{-11}	0.024	8.05×10^{-11}	0.008	8.61×10^{-9}	6.5
216 G / T	n.c.	1.35×10^{-10}	0.059	1.24×10^{-10}	0.003	2.93×10^{-10}	2.8
2238 G / T	1.22×10^{-4}	1.69×10^{-9}	0.008	2.12×10^{-10}	0.023	1.08×10^{-9}	2.7
2312 A / T	1.70×10^{-3}	n.c.	n.s.	6.84×10^{-4}	0.026	0.005	2.9
4184 G / A	3.06×10^{-4}	n.c.	8.87×10^{-4}	2.23×10^{-10}	0.019	1.13×10^{-8}	2.6
4315 C / G	1.84×10^{-4}	7.01×10^{-10}	0.012	3.07×10^{-9}	5.75×10^{-4}	6.79×10^{-7}	2.6
3'Indel 8/0	4.80×10^{-3}	2.75×10^{-9}	n.s.	1.46×10^{-8}	8.97×10^{-4}	4.13×10^{-6}	3.5

dietary habits, and nutritional impact. Information now available on some of these issues is encouraging. Results from an animal model for human vitamin A metabolism indicated vitamin A activity of provitamin A in orange maize was greater than assumed by a factor of about four (25). A successful intervention to introduce β -carotene-rich, orange sweet potato in Mozambique, where only white sweet potato was previously cultivated, suggests that orange-colored staple foods can be acceptable, and their regular consumption results in improved vitamin A status (26). Related follow-up acceptance studies of yellow and orange maize in Mozambique and Zimbabwe are in progress with initial results encouraging (27). The dietary habits of many Africans, in which maize is consumed for all three meals a day, indicates that maize is a good target for biofortification (28). The recent positive nutritional and acceptance results will need to be coordinated with comprehensive breeding and seed distribution efforts to realize the potential of provitamin A-biofortified maize, as, for example, is coordinated by the HarvestPlus Global Challenge Program.

References and Notes

1. B. A. Underwood, *J. Nutr.* **134**, 2315 (2004).
2. J. O. Mora, *J. Nutr.* **133**, 2990S (2003).

3. C. E. West, *Nutr. Rev.* **58**, 341 (2000).
4. O. Dary, J. O. Mora, *J. Nutr.* **132**, 2927S (2002).
5. C. E. West, A. Eilander, M. van Lieshout, *J. Nutr.* **132**, 2920S (2002).
6. M. van Lieshout, S. de Pee, *Am. J. Clin. Nutr.* **81**, 943 (2005).
7. R. D. Graham, R. M. Welch, H. E. Bouis, *Adv. Agron.* **70**, 77 (2001).
8. P. D. Fraser, P. M. Bramley, *Prog. Lipid Res.* **43**, 228 (2004).
9. D. DellaPenna, B. J. Pogson, *Annu. Rev. Plant Biol.* **57**, 711 (2006).
10. F. Li, C. Murillo, E. T. Wurtzel, *Plant Physiol.* **144**, 1181 (2007).
11. B. Buckner, P. S. Miguel, D. Janick-Buckner, J. L. Bennetzen, *Genetics* **143**, 479 (1996).
12. K. Palaisa, M. Morgante, S. Tingey, A. Rafalski, *Proc. Natl. Acad. Sci. U.S.A.* **101**, 9885 (2004).
13. B. Pogson, K. A. McDonald, M. Truong, G. Britton, D. DellaPenna, *Plant Cell* **8**, 1627 (1996).
14. F. X. Cunningham Jr. et al., *Plant Cell* **8**, 1613 (1996).
15. I. Pecker, R. Gabbay, F. X. Cunningham Jr., J. Hirschberg, *Plant Mol. Biol.* **30**, 807 (1996).
16. B. Yu, D. Lydiate, L. Young, U. Schäfer, A. Hannoufa, *Transgenic Res.* **10.1007/s11248** (2007).
17. G. Diretto et al., *BMC Plant Biol.* **6**, 13 (2006).
18. B. J. Pogson, H. M. Rissler, *Philos. Trans. R. Soc. London B Biol. Sci.* **355**, 1395 (2000).
19. S. A. Flint-Garcia et al., *Plant J.* **44**, 1054 (2005).
20. D. L. Remington et al., *Proc. Natl. Acad. Sci. U.S.A.* **98**, 11479 (2001).
21. Materials and methods are available as supporting material on Science Online.
22. J. Yu et al., *Nat. Genet.* **38**, 203 (2006).
23. J. C. Wang, R. J. Lambert, E. T. Wurtzel, T. R. Rocheford, *Theor. Appl. Genet.* **108**, 349 (2004).
24. M. J. Asins, *Plant Breed. Rev.* **121**, 281 (2002).
25. J. A. Howe, S. A. Tanumihardjo, *J. Nutr.* **136**, 2562 (2006).
26. J. W. Low et al., *J. Nutr.* **137**, 1320 (2007).
27. R. A. Stevens, A. Winter-Nelson, *Food Policy*, in press.
28. S. Li, F. A. K. Tayie, M. F. Young, T. Rocheford, W. S. White, *J. Agric. Food Chem.* **55**, 10744 (2007).
29. P. D. Matthews, E. T. Wurtzel, in *Food Colorants: Chemical and Functional Properties*, C. Socaciu, Ed. (CRC Press, Boca Raton, FL, 2007), pp. 347–398.
30. We thank S. Islam, C. Paul, W. Liu, and W. White for running HPLC on samples; H. Yates for support of molecular genetics; and N. Stevens for technical editing of the manuscript. This work was supported by NSF DBI-0321467 (to E.S.B.), U.S. Agency for International Development (to T.R.R.), HarvestPlus (to T.R.R.), NIH (S06-GM08225 to E.T.W.), Professional Staff Congress—CUNY research award (to E.T.W.), New York State (to E.T.W.), NSF DBI-0604923 (to T.R.R.), TRIAD Foundation (L.B. and T.P.B.), U.S. Department of Agriculture (USDA) Cooperative State Research, Education, and Extension Service (CSREES), National Research Initiative grant 2003-00745 (to A.E.S.), and USDA—Agricultural Research Service (to E.S.B.). Mention of trade names or commercial products in this publication is solely for the purpose of providing specific information and does not imply recommendation or endorsement by the USDA.

Supporting Online Material

www.sciencemag.org/cgi/content/full/319/5861/330/DC1
Materials and Methods
Figs. S1 to S9
Tables S1 to S5
References

10 September 2007; accepted 11 December 2007
10.1126/science.1150255

Dual Positive and Negative Regulation of Wingless Signaling by Adenomatous Polyposis Coli

Carter M. Takacs, Jason R. Baird, Edward G. Hughes, Sierra S. Kent, Hassina Benchabane, Raehum Paik, Yashi Ahmed*

The evolutionarily conserved Wnt/Wingless signal transduction pathway directs cell proliferation, cell fate, and cell death during development in metazoans and is inappropriately activated in several types of cancer. The majority of colorectal carcinomas contain truncating mutations in the adenomatous polyposis coli (APC) tumor suppressor, a negative regulator of Wnt/Wingless signaling. Here, we demonstrate that *Drosophila* Apc homologs also have an activating role in both physiological and ectopic Wingless signaling. The Apc amino terminus is important for its activating function, whereas the β -catenin binding sites are dispensable. Apc likely promotes Wingless transduction through down-regulation of Axin, a negative regulator of Wingless signaling. Given the evolutionary conservation of APC in Wnt signal transduction, an activating role may also be present in vertebrates with relevance to development and cancer.

The Wnt/Wingless (Wg) secreted proteins activate a signal transduction cascade that directs growth and differentiation in many tissues during animal development [reviewed in (1)]. Activation of target genes in response to the Wnt/Wg signal is dependent on the transcriptional activator β -catenin/Armadillo (Arm). In the absence of Wnt, four factors—APC, Axin, gly-

cogen synthase kinase-3/Zeste white 3, and casein kinase 1—target β -catenin for phosphorylation and subsequent proteasomal degradation (2–8). Axin acts as a scaffold to facilitate β -catenin phosphorylation by binding β -catenin, APC, and the two kinases. Wnt-dependent down-regulation of Axin is important for β -catenin-mediated transcriptional activation (9–11). Mutational inactivation of negative regulatory components in the pathway and the resultant inappropriate activation of Wnt signaling is associated with the development of several types of cancer. The majority of colorectal adenomas and carcinomas

contain mutations that eliminate the carboxy-terminal half of APC (1).

The Wnt/Wg signaling pathway shows considerable conservation among metazoans. Two APC homologs exist in humans, mice, and fruit flies, and the negative regulatory role of APC in Wnt signaling is conserved from flies to mammals (12–15). *Drosophila* Apc1 and Apc2 are ubiquitously expressed, and in most cells act redundantly to negatively regulate Wg signaling (16, 17). However, in retinal photoreceptors, Apc2 activity is low enough that inactivation of Apc1 singly suffices to constitutively activate Wg signaling (13, 16). In response, all photoreceptors undergo apoptosis (13) (Fig. 1, A and B) and before their deaths some photoreceptors adopt an aberrant cell fate, as indicated by ectopic expression of *homothorax* and *Rhodopsin 3* (18, 19) (fig. S1, A to F).

To identify genes that promote Wg signaling, we performed a genetic screen for suppressors of photoreceptor apoptosis in the *Apc1*^{Q8} null mutant (Methods). We found that apoptosis is suppressed by null and hypomorphic *Apc2* alleles (Fig. 1C; fig. S2, A to C; fig. S3, A to H; and table S1). Ectopic expression of *homothorax* and *Rhodopsin 3* is also suppressed, indicating that suppression of Wg signaling is not restricted to apoptosis (fig. S1, G to L, and fig. S4, A to F). Further, ectopic Wg signaling resulting from Arm overexpression is also partially suppressed by reduction of *Apc2* (fig. S5, A to C). These data indicate that in addition to its well-established negative regulatory role, Apc2 also has an activating role in ectopic Wg signaling.

Department of Genetics and the Norris Cotton Cancer Center, Dartmouth Medical School, Hanover, NH 03755, USA.

*To whom correspondence should be addressed. E-mail: yfa@dartmouth.edu

It is unknown whether this Apc-activating function in Wg signaling is also important during normal development. Previous observation of an activating function may have been obscured by the negative regulatory role of Apc1 and Apc2 and by their functional redundancy. Therefore, we developed strategies to reduce the combined activity of Apc1 and Apc2 to different extents. We eliminated all Apc1 activity using the *Apc1^{Q8}* null allele while simultaneously reducing Apc2 activity to various levels using different *Apc2* alleles. We used *Apc2* alleles such as *Apc2⁵⁻³* and *Apc2^{G5028}*, which include insertions in the 5' untranslated region and reduce Apc2 protein to low levels (Fig. 2A and table S1), and alleles that reduce Apc2 activity even further, such as the molecular null allele *Apc2⁷⁹* and the deletion alleles *Apc2³³* and *Apc2¹⁹⁻³* (fig. S2A and table S1).

Inactivation of Wg, Arm, or Arm's transcriptional co-activators dTCF/Pangolin (Pan) and Legless results in loss of sternites, which are bristle-bearing cuticular plates in the ventral abdomen (20–22) (Fig. 2, B and C), and a “wingless” phenotype in which the wing blade is replaced by a duplication of the dorsal thorax or notum (21–24) (Fig. 2E, and fig. S6, C to F). We observe both of these phenotypes in *Apc1^{Q8}Apc2* double mutants that display low levels of Apc protein (Fig. 2, D and F, and fig. S6F). In contrast, abdomen and wing patterning is normal in

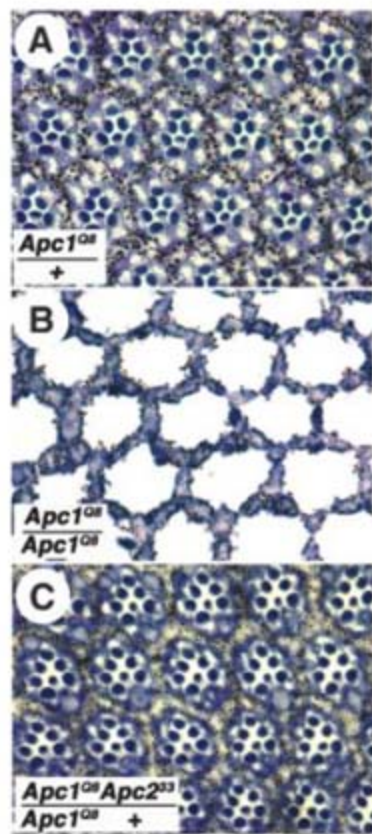


Fig. 1. *Apc2* promotes Arm-induced apoptosis in retinal photoreceptors. (A) A heterozygous *Apc1^{Q8}/+* adult eye; in each ommatidium, seven photoreceptors are observed. (B) All photoreceptors in the homozygous *Apc1^{Q8}* null mutant undergo apoptosis. (C) Apoptosis is suppressed by the heterozygous *Apc2³³* deletion. Each image was obtained at the same magnification.

Apc1 null mutants and in *Apc2* null mutants. Therefore, we conclude that Apc not only promotes ectopic Wg signaling but is also required to promote Wg signaling during normal development. This activity is supplied redundantly by Apc1 and Apc2. Further reduction in the combined activity of Apc1 and Apc2 results in Wg hyperactivation phenotypes in the abdomen and wing, reflecting the negative regulatory role of Apc (figs. S6 and S7). Thus, Apc1 and Apc2 not only prevent signaling when Wg is absent but also promote signaling in cells responding to Wg.

To determine a mechanism by which Apc promotes Wg signaling, we examined Axin levels (Fig. 3, A to C) after simultaneous reduction of Apc1 and Apc2 (Fig. 3, D to I). Upon complete loss of Apc1 and Apc2 (in *Apc1^{Q8}Apc2⁷⁹* null mutant wing clones), not only are Arm levels high (Fig. 3, M to O) but also Axin levels are increased (Fig. 3, D to F). Axin levels also increase in cells with reduced Apc activity, which retain the ability to promote some Arm degrada-

tion (in *Apc1^{Q8}Apc2³³* mutant clones) (table S1 and Fig. 3, G to I and P to R). This Axin increase is present in cells regardless of their location within the wing disc and thus is not restricted to cells exposed to Wg. Furthermore, these increased Axin levels do not result from enhanced Arm-mediated transcription (fig. S8). Our results reveal that Apc1 and Apc2 negatively regulate Axin levels, suggesting a mechanism for the positive effect of Apc on Wg signaling.

To determine whether the Apc domains promoting Wg signaling are distinct from those promoting Arm degradation, we used three *Apc2* truncation alleles that encode only amino-terminal fragments, *Apc2⁴⁴⁰*, *Apc2⁶⁹⁰*, and *Apc2⁸¹⁰* (17, 25, 26) (Fig. 4A and table S1). These alleles eliminate some or all β -catenin/Arm binding sites and thus are severely compromised in promoting Arm degradation (16, 17, 26). However, in contrast with null alleles that eliminate all *Apc2* coding sequences (fig. S2A and table S1), the *Apc2* truncation alleles retain their positive

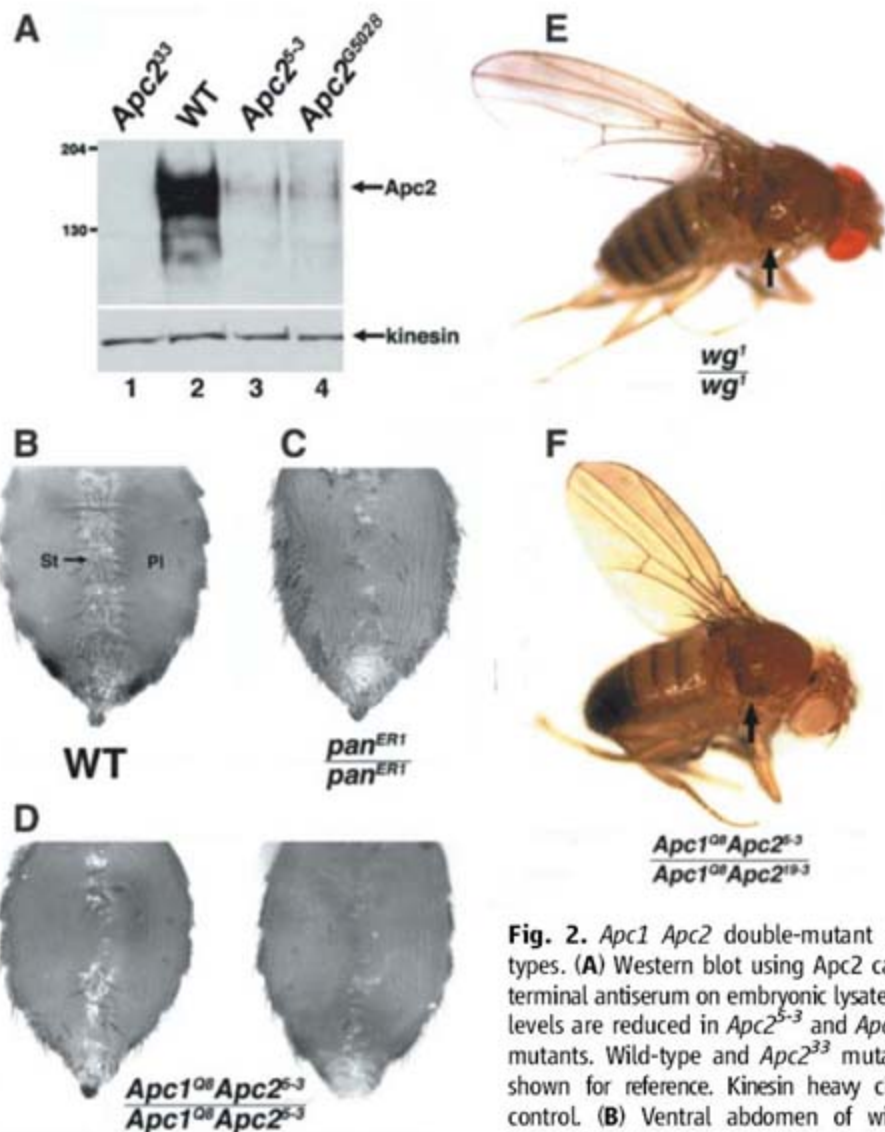
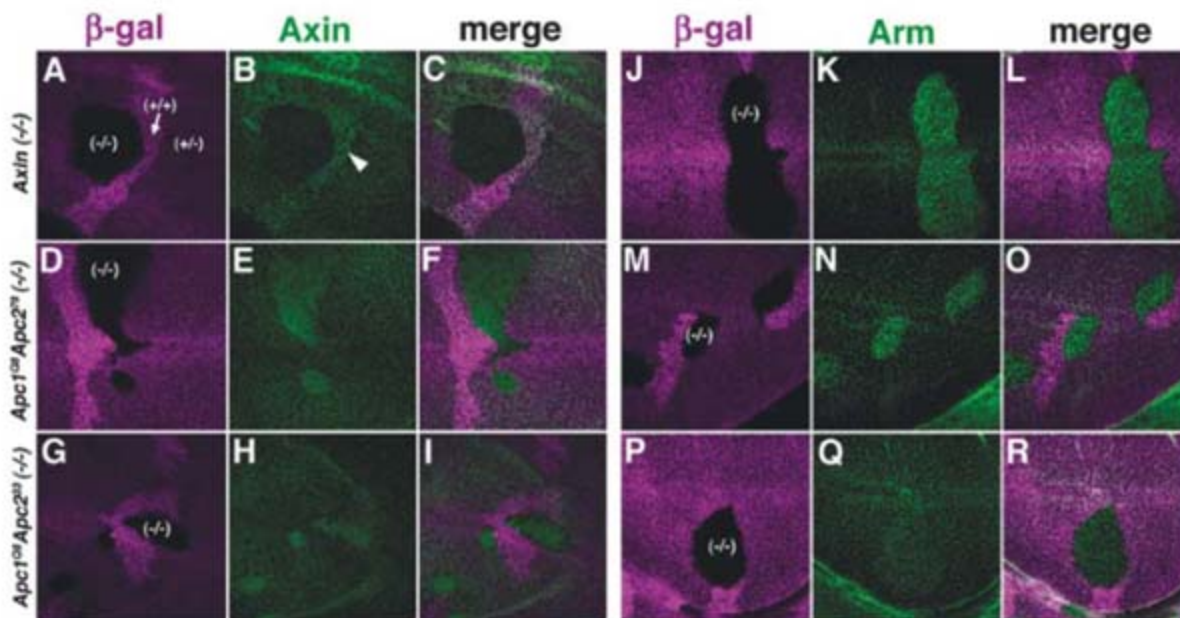


Fig. 2. *Apc1 Apc2* double-mutant phenotypes. (A) Western blot using Apc2 carboxy-terminal antiserum on embryonic lysates. Apc2 levels are reduced in *Apc2⁵⁻³* and *Apc2^{G5028}* mutants. Wild-type and *Apc2³³* mutant are shown for reference. Kinesin heavy chain is control. (B) Ventral abdomen of wild-type female. Sternites and overlying sternal bristles (St, arrow) and pleura (Pl) are indicated. (C and D) Loss of sternites and sternal bristles and expansion of pleura in homozygous *pan^{ER1}* mutants and homozygous *Apc1^{Q8}Apc2⁵⁻³* or *Apc1^{Q8}Apc2⁵⁻³/Apc1^{Q8}Apc2^{G5028}* mutants. This phenotype is present in 65 to 70% of homozygous *Apc1^{Q8}Apc2⁵⁻³* mutant females raised at 25°C with variation in severity between individuals. (E and F) Wing-to-notum transformation (arrow) in homozygous *wg¹* mutants and in *Apc1^{Q8}Apc2⁵⁻³/Apc1^{Q8}Apc2¹⁹⁻³* mutants. *Apc2¹⁹⁻³* is a deletion allele (table S1).

Fig. 3. Axin and Arm levels in *Apc* mutants. Third instar wing discs, stained with antisera on top. Genotypes at left margin. (A to C) *Axin*^{S044230} homozygous mutant clones, indicated by β -gal loss [–/– in (A)], have decreased Axin signal, revealing specificity of Axin antiserum [(B) and (C)]. In some clones of cells with wild-type Axin levels, as indicated by increased β -gal signal [+/+ in (A)], there is increased Axin signal [arrowhead in (B)], as compared with *Axin* heterozygous (+/–) tissue. (D to I) *Apc1*^{Q8} *Apc2*⁷⁹ [–/– in (D)] and *Apc1*^{Q8} *Apc2*³³ [–/– in (G)] mutant clones display increased Axin signal. (J to L) Arm levels are high in *Axin* mutant clones [–/– in (J)]. (M to O) Similarly, high Arm levels are observed in *Apc1*^{Q8} *Apc2*⁷⁹ null mutant clones [–/– in (M)]. (P to R) In contrast, *Apc1*^{Q8} *Apc2*³³ mutant clones [–/– in (P)] display intermediate Arm levels. The *Apc2*³³ allele contains a deletion extending to the fifth Arm repeat (table S1), and its residual ability to down-regulate Arm likely results from production of a carboxy-terminal fragment, at levels below the threshold detectable with our antiserum.



effect on Arm-induced apoptosis and ectopic *lth* expression in *Apc1*^{Q8} mutant photoreceptors (Fig. 4B and fig. S9, A and B). We conclude that *Apc2* amino-terminal fragments retain the ability to promote ectopic Wg signaling, whereas the β -catenin/Arm binding sites are dispensable for this activity. This conclusion is further supported by the observation that an *Apc2* transgene (*P[Apc2- Δ 20rep]*) (Fig. 4A), with an internal deletion of all five 20-amino acid repeats that are important for Arm binding and proteolysis (2), completely rescues compromised Wg transduction in wing discs resulting from reduced *Apc* activity (in *Apc1*^{Q8} *Apc2*⁵⁻³/*Apc1*^{Q8} *Apc2*⁷⁹⁻³ mutants). Furthermore, the presence of the *Apc2- Δ 20rep* fragment also prevents the increase in Axin (Fig. 4, C to E) observed in cells in which *Apc* activity is either completely lost (*Apc1*^{Q8} *Apc2*⁷⁹ mutant clones) (Fig. 3, D to F) or reduced (*Apc1*^{Q8} *Apc2*³³ mutant clones) (Fig. 3, G to I). Finally, in cells with reduced *Apc* activity and intermediate Arm levels (*Apc1*^{Q8} *Apc2*³³ mutant clones) (Fig. 3, P to R), the presence of the *Apc2- Δ 20rep* fragment results in high Arm levels (Fig. 4, G to I) that are similar to those resulting from loss of Axin (fig. S10). Thus, the β -catenin/Arm binding sites are dispensable for the ability of *Apc* to negatively regulate Axin levels, to increase Arm levels, and to promote Wg transduction. These results support the model that *Apc* enhances Wg signaling by negatively regulating Axin-mediated Arm degradation.

Previous experiments in *Xenopus* suggested that the vertebrate APC amino terminus also promotes Wnt signaling (27, 28). Indeed, we find that expression of a human APC amino-terminal fragment (29) (Fig. 4A) in a Wnt-responsive cell line (HEK293T) results in up-regulation of TCF reporter activity (pTOPFlash) (30) that is not observed with a control reporter containing mutated

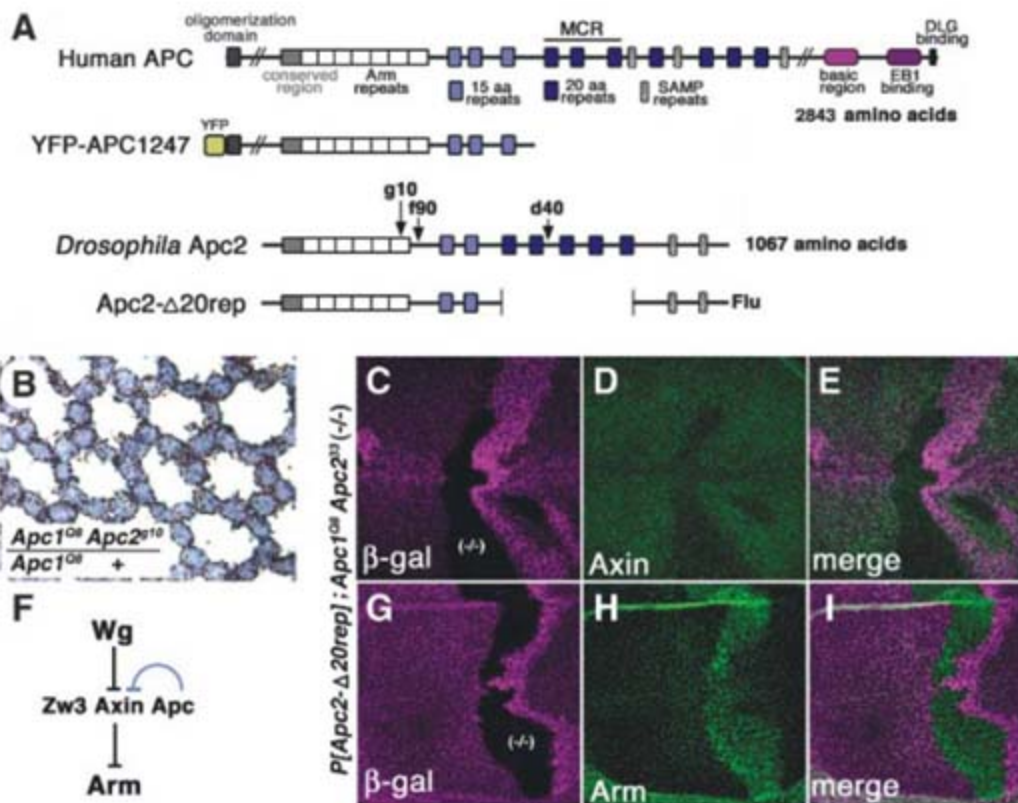


Fig. 4. The *Apc2* amino-terminus affects Axin levels, Arm levels, and Wg signaling. (A) Human APC and *Drosophila* *Apc2* schematic. Conserved region (gray), Arm repeats (white), β -catenin binding sites [15 amino acid repeats (light blue) and 20 amino acid repeats (dark blue)], Axin binding sites (SAMP repeats, hatched boxes), and nonsense mutations in *Apc2*^{g10}, *Apc2*^{f90}, and *Apc2*^{d40} are indicated. Somatic APC mutations in colorectal tumors cluster between codons 1250 and 1450 (mutation cluster region, MCR). Human APC amino-terminal fragment encoding amino acids 2-1247 (YFP-APC1247) and *P[Apc2- Δ 20rep]* transgene are diagrammed. (B) Apoptosis is not suppressed in the *Apc1*^{Q8} *Apc2*^{79/10}/*Apc1*^{Q8} + retina. (C to E and G to I) Third instar wing discs stained with antisera in lower left corner. *Apc1*^{Q8} *Apc2*³³ mutant clones are indicated [–/– in (C) and (G)]. One copy of the *P[Apc2- Δ 20rep]* transgene results in low Axin levels [(D) and (E)] and high Arm levels [(H) and (I)] in *Apc1*^{Q8} *Apc2*³³ clones. Identical results were found with two independent *P[Apc2- Δ 20rep]* lines. (F) Model for dual *Apc* functions in Wg transduction. In addition to facilitating Axin-dependent Arm proteolysis, *Apc* also negatively regulates Axin (blue), thereby promoting Wg signaling. Our results support a proposed regulatory relationship between Axin and *Apc* (36) and also suggest that negative regulation of Axin by *Apc* maintains Arm levels within a range ensuring proper response upon Wg stimulation.

binding sites (pFOPFlash) (fig. S11). Therefore, human APC may also have positive and negative regulatory roles in Wnt transduction, with an amino terminus that promotes Wnt signaling.

Our results demonstrate that Apc1 and Apc2 act redundantly to regulate Wingless transduction both positively and negatively (Fig. 4F). Apc likely promotes Wingless transduction by negatively regulating Axin. For this function, the Apc amino terminus is essential, whereas the β -catenin/Arm binding sites are dispensable. We suggest that opposing activities of Apc keep Axin activity and Arm levels within a range ensuring that downstream signal transduction occurs in the presence of Wg but not in its absence. The *C. elegans* APC-related protein APR-1, which lacks consensus β -catenin binding sites, also promotes Wnt transduction (31, 32), further suggesting that an activating role is evolutionarily conserved. Our data also reveal that retention of an Apc amino-terminal fragment enhances ectopic Wg signaling resulting from reduction in Apc levels. This may explain why APC mutations that eliminate the carboxyl terminus, yet retain the amino terminus, are found in the majority of colonic adenomas and carcinomas (33–35). By analogy to the positive effect of the *Drosophila* Apc amino terminus on ectopic Wg signaling, the conserved human APC amino terminus might similarly enhance ectopic Wnt signaling, accounting for its selective retention in colorectal carcinoma.

References and Notes

- H. Clevers, *Cell* **127**, 469 (2006).
- S. Munemitsu, I. Albert, B. Souza, B. Rubinfeld, P. Polakis, *Proc. Natl. Acad. Sci. U.S.A.* **92**, 3046 (1995).
- H. Aberle, A. Bauer, J. Stappert, A. Kispert, R. Kemler, *EMBO J.* **16**, 3797 (1997).
- J. Behrens et al., *Science* **280**, 596 (1998).
- M. Hart, R. de los Santos, I. Albert, B. Rubinfeld, P. Polakis, *Curr. Biol.* **8**, 573 (1998).
- S. Ikeda et al., *EMBO J.* **17**, 1371 (1998).
- C. Liu et al., *Cell* **108**, 837 (2002).
- A. Salic, E. Lee, L. Mayer, M. Kirschner, *Mol. Cell* **5**, 523 (2000).
- J. Mao et al., *Mol. Cell* **7**, 801 (2001).
- N. Tolwinski et al., *Dev. Cell* **4**, 407 (2003).
- K. Tamai et al., *Mol. Cell* **13**, 149 (2004).
- S. Hayashi et al., *Proc. Natl. Acad. Sci. U.S.A.* **94**, 242 (1997).
- Y. Ahmed, S. Hayashi, A. Levine, E. Wieschaus, *Cell* **93**, 1171 (1998).
- B. McCartney et al., *J. Cell Biol.* **146**, 1303 (1999).
- X. Yu, L. Waltzer, M. Bienz, *Nat. Cell Biol.* **1**, 144 (1999).
- Y. Ahmed, A. Nouri, E. Wieschaus, *Development* **129**, 1751 (2002).
- K. Akong et al., *Dev. Biol.* **250**, 91 (2002).
- A. Tomlinson, *Dev. Cell* **5**, 799 (2003).
- M. Wernet et al., *Cell* **115**, 267 (2003).
- N. Baker, *Development* **102**, 489 (1988).
- E. Brunner, O. Peter, L. Schweizer, K. Basler, *Nature* **385**, 829 (1997).
- T. Kramps et al., *Cell* **109**, 47 (2002).
- R. Sharma, V. Chopra, *Dev. Biol.* **48**, 461 (1976).
- M. Peifer, C. Rauskolb, M. Williams, B. Riggelman, E. Wieschaus, *Development* **111**, 1029 (1991).
- B. McCartney et al., *Nat. Cell Biol.* **3**, 933 (2001).
- B. McCartney et al., *Development* **133**, 2407 (2006).
- K. Vleminckx et al., *J. Cell Biol.* **136**, 411 (1997).
- G. Farr, 3rd et al., *J. Cell Biol.* **148**, 691 (2000).
- J. Schneikert, A. Grohmann, J. Behrens, *Hum. Mol. Genet.* **16**, 199 (2007).
- V. Korinek et al., *Science* **275**, 1784 (1997).
- C. Rocheleau et al., *Cell* **90**, 707 (1997).
- E. Hoier, W. Mohler, S. Kim, A. Hajnal, *Genes Dev.* **14**, 874 (2000).
- H. Lamlum et al., *Nat. Med.* **5**, 1071 (1999).
- A. Rowan et al., *Proc. Natl. Acad. Sci. U.S.A.* **97**, 3352 (2000).
- C. Albuquerque et al., *Hum. Mol. Genet.* **11**, 1549 (2002).
- E. Lee, A. Salic, R. Kruger, R. Heinrich, M. Kirschner, *PLoS Biol.* **1**, E10 (2003).
- We thank C. Pikielny, E. Wieschaus, D. Robbins, S. Ogden, V. Ambros, K. Neufeld, and A. Mehra for their insight; A. Salzberg, S. Cohen, K. Basler, E. Wieschaus, C. Desplan, R. Nusse, K. Willert, J. Jiang, M. Bienz, M. Peifer, B. McCartney, J. Treisman, R. Mann, J. Behrens, M. Cole, J. DiRenzo, Bloomington *Drosophila* Stock Center, Berkeley *Drosophila* Genome Project, and Developmental Studies Hybridoma Bank for reagents; A. Lavanway, A. Tomlinson, and N. Friedenberg for technical advice; and V. Marlar for technical assistance. We acknowledge support from the Norris Cotton Cancer Center, Emerald Foundation, General Motors Cancer Research Foundation, American Cancer Society (IRG-82-003-21), National Institutes of Health (K08CA078532, R01CA105038), and Howard Hughes Medical Institute, through an award to Dartmouth Medical School (76200-560801).

Supporting Online Material

www.sciencemag.org/cgi/content/full/319/5861/333/DC1

Materials and Methods

Table S1

Figs. S1 to S11

References

2 October 2007; accepted 4 December 2007

10.1126/science.1151232

Initiating and Cancer-Propagating Cells in *TEL-AML1*-Associated Childhood Leukemia

Dengli Hong,¹ Rajeev Gupta,¹ Philip Ancliff,² Ann Atzberger,¹ John Brown,¹ Shamit Soneji,¹ Joanne Green,¹ Sue Colman,⁵ Wanda Piacibello,⁴ Veronica Buckle,¹ Shinobu Tsuzuki,³ Mel Greaves,⁵ Tariq Enver^{1*}

Understanding cancer pathogenesis requires knowledge of not only the specific contributory genetic mutations but also the cellular framework in which they arise and function. Here we explore the clonal evolution of a form of childhood precursor-B cell acute lymphoblastic leukemia that is characterized by a chromosomal translocation generating a *TEL-AML1* fusion gene. We identify a cell compartment in leukemic children that can propagate leukemia when transplanted in mice. By studying a monozygotic twin pair, one preleukemic and one with frank leukemia, we establish the lineal relationship between these “cancer-propagating” cells and the preleukemic cell in which the *TEL-AML1* fusion first arises or has functional impact. Analysis of *TEL-AML1*-transduced cord blood cells suggests that *TEL-AML1* functions as a first-hit mutation by endowing this preleukemic cell with altered self-renewal and survival properties.

A popular (1–6), though not unchallenged (7), hypothesis is that fully transformed human cancer clones are arranged, like their normal tissue counterparts, in a hierarchical fashion and maintained by rare “tumor-propagating cells” (also referred to as cancer stem cells). Less is known about the crucial earliest first-hit events in cancer and the “precancerous” cells in which they occur. We have explored these precancerous cell hierarchies in the context of childhood precursor-B cell (pre-B cell) acute lymphoblastic

leukemia (also known as common ALL, cALL) which is frequently associated with a chromosomal translocation creating the *TEL-AML1* (*ETV6-RUNX1*) fusion gene (8). This fusion arises predominantly in utero, producing a persistent but clinically covert preleukemic clone (9–11) that may convert to frank leukemia with acquisition of additional genetic changes (10, 12).

Most of the leukemic cells in cALL coexpress CD19 and CD10 accompanied by clonal rearrangement of the immunoglobulin heavy chain

gene (*IgH*) indicative of a pre-B cell identity (13). However, the identity of the cALL-propagating cell has been contentious (14–17). Interestingly, childhood ALL is associated with a rare population of CD34⁺CD38^{low}CD19⁺ cells that is not detectable in normal bone marrow (17, 18). We prospectively isolated these cells from *TEL-AML1*-positive cALL patients (Fig. 1A, R1) and assessed their capacity to engraft nonobese diabetic, severe combined immunodeficient mice (NOD/SCID mice), an assay of their leukemogenic potential (19). Engraftment was obtained from four patient samples (Fig. 1B and fig. S1) and secondary grafts were obtained from all of these. The CD34⁺CD38^{low}CD19⁺ population was reestablished within both the primary (Fig. 1C) and secondary (Fig. 1D) recipients. Interphase fluorescence in situ hybridization (FISH)

¹Medical Research Council (MRC) Molecular Haematology Unit, Weatherall Institute for Molecular Medicine, John Radcliffe Hospital, University of Oxford, Oxford OX3 9DS, UK. ²Department of Haematology, Great Ormond Street Hospital, and Department of Molecular Haematology and Cancer Biology, Institute of Child Health, University College London, WC1N 3JH, UK. ³Division of Molecular Medicine, Aichi Cancer Research Institute, Nagoya 464-8681, Japan. ⁴Division of Research in Medical Oncology, Institute for Cancer Research and Treatment, Strada Provinciale 142, 10060 Candiolo, Torino, Italy. ⁵Section of Haemato-Oncology, Institute of Cancer Research, Sutton, Surrey SM2 5NG, UK.

*To whom correspondence should be addressed. E-mail: tenver@gwmail.jr2.ox.ac.uk

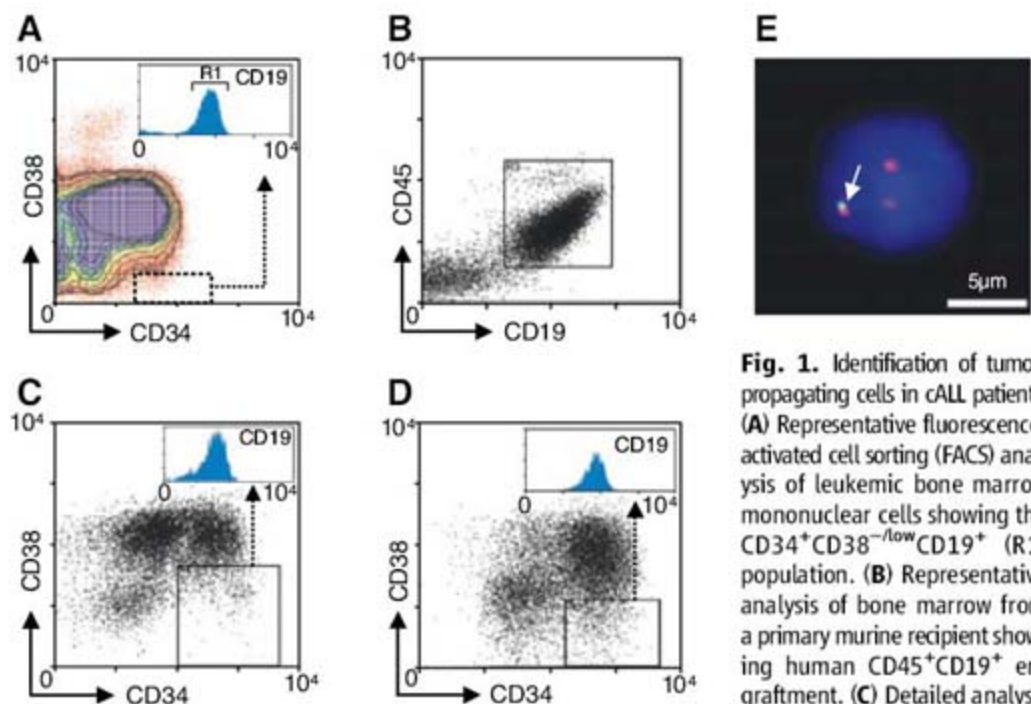


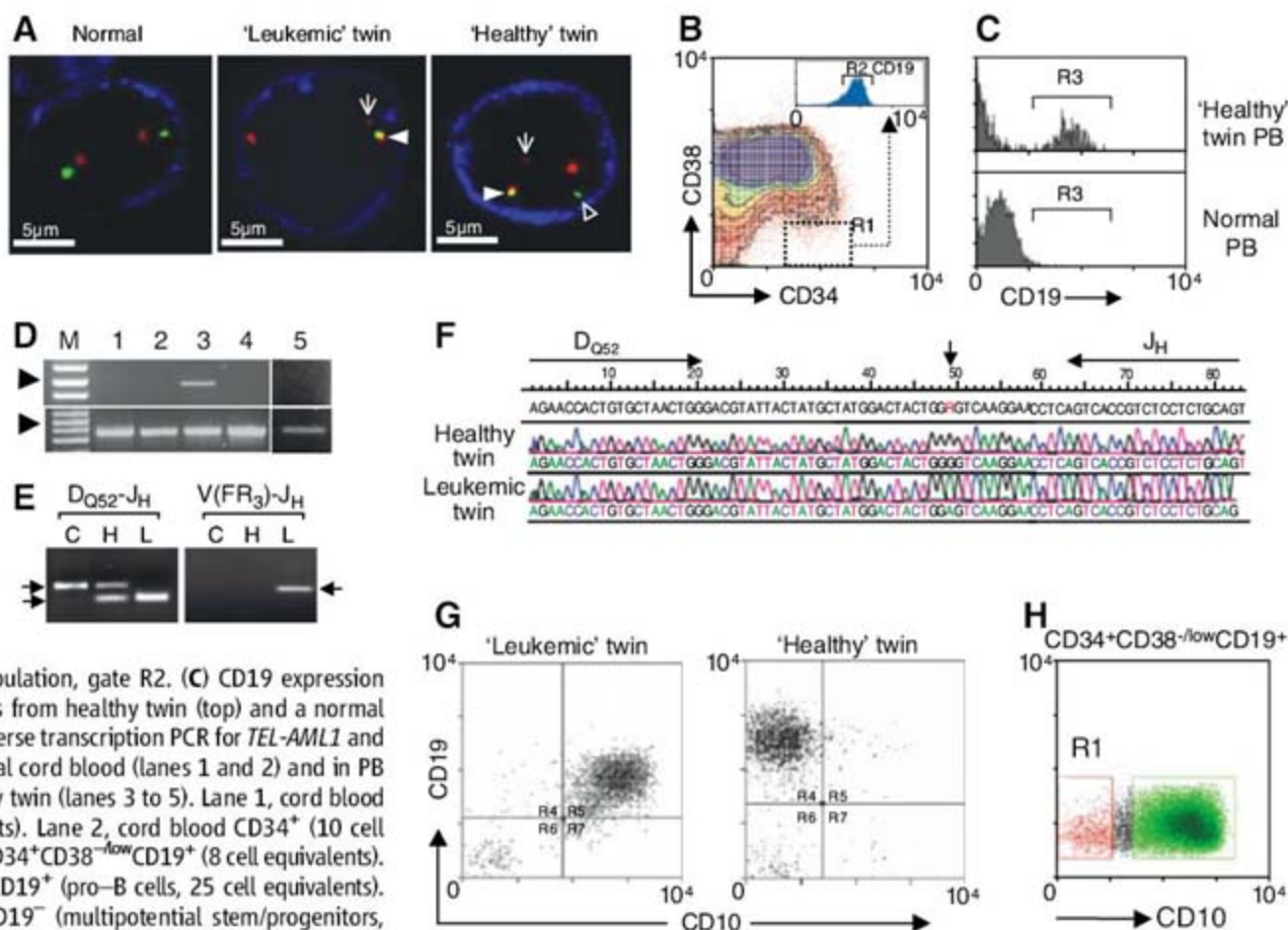
Fig. 1. Identification of tumor-propagating cells in cALL patients. (A) Representative fluorescence-activated cell sorting (FACS) analysis of leukemic bone marrow mononuclear cells showing the CD34⁺CD38^{-low}CD19⁺ (R1) population. (B) Representative analysis of bone marrow from a primary murine recipient showing human CD45⁺CD19⁺ engraftment. (C) Detailed analysis of engrafted cells from a primary recipient showing the CD34⁺CD38^{-low}CD19⁺ population. (D) Similar analysis of engrafted cells from bone marrow of a secondary recipient showing reestablishment of the same population. (E) Interphase FISH showing *TEL-AML1* expression in a human CD19⁺ cell from a secondary recipient. *TEL* signal, green; *AML1*, red; *TEL-AML1* fusion (green-red) indicated by arrowhead. Fusion identified in >97% human cells analyzed from recipients of two separate cALL samples.

primary recipient showing the CD34⁺CD38^{-low}CD19⁺ population. (D) Similar analysis of engrafted cells from bone marrow of a secondary recipient showing reestablishment of the same population. (E) Interphase FISH showing *TEL-AML1* expression in a human CD19⁺ cell from a secondary recipient. *TEL* signal, green; *AML1*, red; *TEL-AML1* fusion (green-red) indicated by arrowhead. Fusion identified in >97% human cells analyzed from recipients of two separate cALL samples.

analysis confirmed the presence of the *TEL-AML1* fusion gene in these grafts (Fig. 1E). These data suggest that the CD34⁺CD38^{-low}CD19⁺ cells can function as self-renewing cancer-propagating cells.

How do these cells relate to those in which the *TEL-AML1* fusion first arises and initiates leukemogenesis? Analysis of monozygotic twins provides a unique opportunity to investigate the initiating events in this disease because a preleukemic clone, established in utero in one twin may spread to the other twin via their shared placenta (9). Because additional mutations are required for progression to leukemia (9, 10), when one twin presents with leukemia, the other may still carry the ancestral preleukemic clone but may remain clinically normal. We investigated a pair of monozygotic female twins. One twin was diagnosed at age 2 with *TEL-AML1*-positive pre-B cell ALL, and her leukemic blasts showed additional loss of the uninvolved *TEL* allele (Fig. 2A). Her bone marrow contained the CD34⁺CD38^{-low}CD19⁺ cancer-propagating population (Fig. 2B). The other twin was healthy. For ethical reasons, our analyses were strictly limited to peripheral blood (PB) [supporting online material (SOM) text]. We detected *TEL-AML1*-positive B lineage-affiliated CD19⁺ cells at low frequency (~0.1%), but these cells all

Fig. 2. Hematopoiesis in monozygotic t(12;21) twins.



(A) Immuno-FISH for *TEL-AML1* translocation and CD19 protein in PB mononuclear cells from the leukemic twin, healthy twin, and a normal individual. CD19 indicated by blue staining, *TEL* by green, *AML1* by red, and *TEL-AML1* by green-red (filled arrowhead). Remnant of the *AML1* locus left by the translocation, small red signal, thin arrow; intact *AML1* allele, large red signal; intact second *TEL* allele, green signal (open arrowhead). (B) Diagnostic bone marrow from the leukemic twin showing a CD34⁺CD38^{-low}CD19⁺ population, gate R2. (C) CD19 expression in PB CD34⁺CD38^{-low} cells from healthy twin (top) and a normal age-matched child. (D) Reverse transcription PCR for *TEL-AML1* and β -actin expression in normal cord blood (lanes 1 and 2) and in PB compartments from healthy twin (lanes 3 to 5). Lane 1, cord blood CD34⁺ (100 cell equivalents). Lane 2, cord blood CD34⁺ (10 cell equivalents). Lane 3, twin CD34⁺CD38^{-low}CD19⁺ (8 cell equivalents). Lane 4, twin CD34⁺CD38⁺CD19⁺ (pro-B cells, 25 cell equivalents). Lane 5, CD34⁺CD38^{-low}CD19⁻ (multipotential stem/progenitors, 10 cell equivalents). (E) Genomic PCR for *IgH* gene rearrangements. D_{Q52} - J_H (heavy-chain joining region) (left) and VJ (right) analyses for control Kasumi cells (C) and CD34⁺CD38^{-low}CD19⁺ populations from healthy (H) and leukemic (L) twin. Arrows indicate 160 bp (germline) and 80 bp (rearranged). (F) Representative sequence analyses of individual cloned D_{Q52} - J_H PCR products from healthy and leukemic twins. Long arrows indicate oligonucleotide primers, short arrow indicates a G-A transversion suggestive of somatic hypermutation.

A minority of (3 out of 11) clones from the CD34⁺CD38^{-low}CD19⁺ cells of the leukemic twin were different from each other and those of her sibling, which may suggest ongoing DJ recombination. (G) CD10 expression in CD34⁺CD38^{-low}CD19⁺ cells from leukemic (bone marrow) and healthy (PB) twins. (H) CD10 expression in bone marrow CD34⁺CD38^{-low}CD19⁺ cells from an unrelated cALL patient (representative of five individuals).

contained a normal *TEL* allele (Fig. 2A), consistent with preleukemia status (11).

We detected a rare population of CD34⁺CD38^{-low}CD19⁺ cells at a frequency of 0.002% of total mononuclear cells in the healthy twin, but not in the PB of hematologically normal age-matched children (Fig. 2C, R3). This cell population has been stable over 18 months of serial observation (fig. S2). *TEL-AML1* transcripts were observed in as few as 10 cell equivalents of this sorted fraction (Fig. 2D, lane 3). In contrast, we did not detect *TEL-AML1* transcripts in similar numbers of progenitor B cells (pro-B cells) from the healthy twin (Fig. 2D, lane 4) consistent with the low proportion of B cells affected in the blood of this hematologically normal child, or in more primitive multipotent stem cell fractions not expressing the B-lineage marker CD19 (Fig. 2D, lane 5).

To investigate the relation between the CD34⁺CD38^{-low}CD19⁺ populations in the healthy and leukemic twins, we examined *IgH* gene rearrangements involving the variable (V), diversity (D), and joining (J) loci. Polymerase chain reaction analysis (PCR) revealed DJ but not VDJ recombination events in the healthy twin sample (Fig. 2E). Sequencing of the cloned DJ recombination PCR products from the healthy twin's CD34⁺CD38^{-low}CD19⁺ cells revealed the presence of only one species, which suggested that these cells represented a clonally expanded population and that the fusion gene arose or had first functional impact in a cell that had already undergone DJ recombination. CD34⁺CD38^{-low}CD19⁺ cells from the leukemic twin harbor DJ, as well as

VDJ, recombination products (Fig. 2E). Sequencing of cloned DJ segments revealed some heterogeneity in recombination products, but crucially, the majority of clones were, with the exception of a single base change, highly related to the DJ segment seen in the CD34⁺CD38^{-low}CD19⁺ population from the healthy twin (Fig. 2F). This suggests that the CD34⁺CD38^{-low}CD19⁺ cancer-propagating population in the leukemic twin is a clonal and more differentiated descendant of the CD34⁺CD38^{-low}CD19⁺ population in the healthy twin. Consistent with this, the majority of CD34⁺CD38^{-low}CD19⁺ cells in the leukemic twin express common ALL antigen, CD10 (20); those in the healthy twin do not (Fig. 2G). It is noteworthy that a minor component of the CD34⁺CD38^{-low}CD19⁺ population in leukemic samples was also found to be CD10⁻ (Fig. 2H, R1). The presence of the *TEL-AML1* fusion gene in these cells was confirmed by FISH (fig. S3).

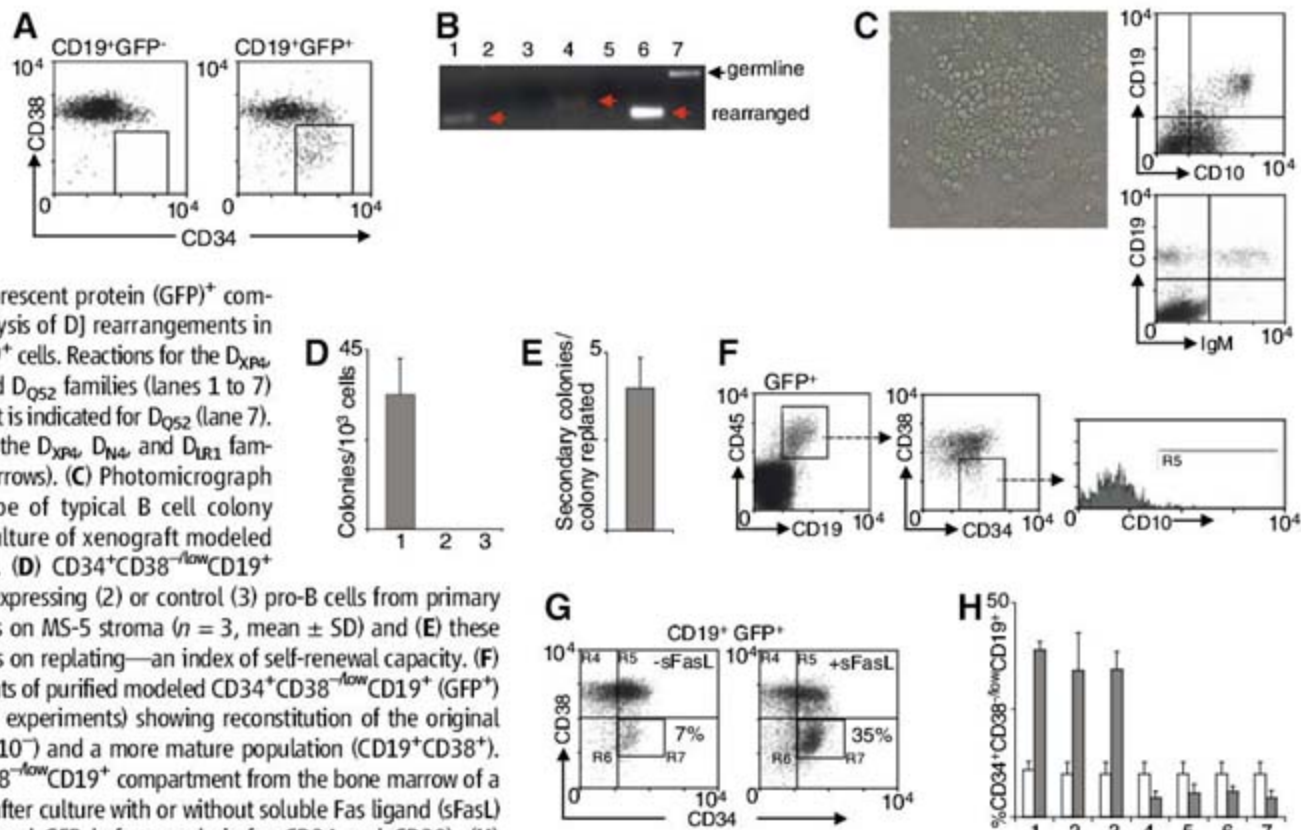
We next established a model of *TEL-AML1*-driven preleukemia by transplanting *TEL-AML1*-transduced human cord blood cells into NOD/SCID mice (fig. S4). At the level of expansion of B cell progenitors and B-lineage differentiation impedance or arrest, this xenograft model exhibits salient features of the preleukemic phase of pre-B cell ALL (fig. S5) (9, 10). CD34⁺CD38^{-low}CD19⁺ cells were observed in the *TEL-AML1*-expressing, but not control, marrow fractions (Fig. 3A and figs. S5 and S6) or in normal cord blood (fig. S7). Xenograft-modeled CD34⁺CD38^{-low}CD19⁺ cells displayed DJ rearrangements (Fig. 3B) and, like their counterparts in the healthy twin

(Fig. 2G), did not express CD10 (fig. S8). Collectively, our data support the notion that *TEL-AML1* can, as a single mutation, generate abnormal cells that resemble the *TEL-AML1*-expressing CD34⁺CD38^{-low}CD19⁺ cells observed in the healthy twin.

The xenograft-modeled, *TEL-AML1*-generated CD34⁺CD38^{-low}CD19⁺ cells displayed B cell differentiation and self-renewal potential in vitro (Fig. 3, C, D, and E, and fig. S9). To investigate whether the *TEL-AML1*-generated CD34⁺CD38^{-low}CD19⁺ population can initiate and maintain a "preleukemic" state in vivo, we prospectively isolated these cells from engrafted primary mice and injected them into the tibiae of secondary NOD/SCID recipients. To our surprise, these cells engrafted and gave rise to more mature B cells (CD38⁺CD19⁺), as well as reconstituting a CD34⁺CD38^{-low}CD19⁺ population (Fig. 3F). In contrast, *TEL-AML1*-expressing CD34⁺CD38⁺CD19⁺ (pro-B) cells did not engraft. These experiments indicate that the *TEL-AML1*-generated CD34⁺CD38^{-low}CD19⁺ population has significant self-renewal potential. Analysis of cell survival characteristics of *TEL-AML1*-generated CD34⁺CD38^{-low}CD19⁺ cells indicates that *TEL-AML1* markedly enhances resistance to some, but not all, apoptotic stimuli (Fig. 3, G and H). Finally, preliminary microarray analysis indicates that CD34⁺CD38^{-low}CD19⁺ cells contain a mixture of both pro-B cell and human stem cell-associated gene expression profiles (fig. S10).

What then are the salient features of the CD34⁺CD38^{-low}CD19⁺ cell observed in the healthy twin and the role of *TEL-AML1* in its

Fig. 3. First-hit functions of *TEL-AML1* in transduced cord blood stem cells. (A) Representative immunophenotype of bone marrow graft from a primary recipient transplanted with *TEL-AML1*-transduced cells showing a CD34⁺CD38^{-low}CD19⁺



population in the green fluorescent protein (GFP)⁺ compartment only. (B) PCR analysis of DJ rearrangements in purified CD34⁺CD38^{-low}CD19⁺ cells. Reactions for the D_{XP4}, D_{A4}, D_{K4}, D_{N4}, D_{M1}, D_{LR1}, and D_{O52} families (lanes 1 to 7) are shown. A germline product is indicated for D_{O52} (lane 7). Rearrangements are seen for the D_{XP4}, D_{N4}, and D_{LR1} families (lanes 1, 4, and 6, red arrows). (C) Photomicrograph (left) and immunophenotype of typical B cell colony after MS-5 stromal cell coculture of xenograft modeled CD34⁺CD38^{-low}CD19⁺ cells. (D) CD34⁺CD38^{-low}CD19⁺ cells (1) but not *TEL-AML1*-expressing (2) or control (3) pro-B cells from primary recipients generated colonies on MS-5 stroma ($\eta = 3$, mean \pm SD) and (E) these generated secondary colonies on replating—an index of self-renewal capacity. (F) Analysis of secondary recipients of purified modeled CD34⁺CD38^{-low}CD19⁺ (GFP⁺) cells (representative of three experiments) showing reconstitution of the original population (which is also CD10⁻) and a more mature population (CD19⁺CD38⁺). (G) Enrichment of CD34⁺CD38^{-low}CD19⁺ compartment from the bone marrow of a *TEL-AML1* primary recipient after culture with or without soluble Fas ligand (sFasL) (cells were gated on CD19 and GFP before analysis for CD34 and CD38). (H) Means (\pm SD) change in size of CD34⁺CD38^{-low}CD19⁺ compartments in the bone marrow of *TEL-AML1* primary recipients after culture with (shaded) or without (open) camptothecin (1), Fas-L (2), melphalan (3), paclitaxel (4), tumor necrosis factor- α (5), methylprednisolone (6), and etoposide (7) (in each case, $n = 5$, $P < 0.05$ by t test).

generation? Its clonal expansion, coupled with its persistence since birth, is highly suggestive of self-renewal. Its clonal relation to more differentiated cell types both in the healthy and in the leukemic twins implies differentiation potential. The balance of evidence thus favors the notion that this cell may itself function as a preleukemic stem cell. This proposal is supported by our xenograft modeling studies, which further suggest that *TEL-AML1* may be sufficient to generate this population of preleukemic stem cells.

Our results suggest that a hierarchical structure, which has been demonstrated in frank leukemia (2, 4), is also a feature of "early" or preleukemic populations. Understanding the nature of the preleukemic hierarchy is fundamental to understanding the function of the first-hit mutation and how it predisposes to leukemic transformation. Our studies therefore have implications for disease etiology, and the xenograft model presented may provide a tool for examining the biological role of genetic alterations that cooperate with the *TEL-AML1* fusion gene. Our

studies may also be relevant to cancer therapy where specific targeting of tumor propagating cells may be desirable. The observation that children in lengthy remission can relapse late with a novel leukemic clone (21), but which nonetheless appears to derive from the identical preleukemic clone that initiated the disease at presentation, suggests that the preleukemic stem cell compartment may persist even when the cells propagating the overt leukemia have been effectively eradicated.

References and Notes

1. J. C. Wang, J. E. Dick, *Trends Cell Biol.* **15**, 494 (2005).
2. M. Al-Hajj, M. S. Wicha, A. Benito-Hernandez, S. J. Morrison, M. F. Clarke, *Proc. Natl. Acad. Sci. U.S.A.* **100**, 3983 (2003).
3. D. Bonnet, J. E. Dick, *Nat. Med.* **3**, 730 (1997).
4. C. F. Kim *et al.*, *Cell* **121**, 823 (2005).
5. S. K. Singh *et al.*, *Nature* **432**, 396 (2004).
6. C. A. O'Brien, A. Pollett, S. Gallinger, J. E. Dick, *Nature* **445**, 106 (2007).
7. P. N. Kelly, A. Dakic, J. M. Adams, S. L. Nutt, A. Strasser, *Science* **317**, 337 (2007).
8. S. A. Shurtleff *et al.*, *Leukemia* **9**, 1985 (1995).
9. M. F. Greaves *et al.*, *Blood* **102**, 2321 (2003).
10. M. F. Greaves, J. Wiemels, *Nat. Rev. Cancer* **3**, 639 (2003).
11. H. Mori *et al.*, *Proc. Natl. Acad. Sci. U.S.A.* **99**, 8242 (2002).
12. C. G. Mullighan *et al.*, *Nature* **446**, 758 (2007).
13. T. R. Golub *et al.*, *Proc. Natl. Acad. Sci. U.S.A.* **92**, 4917 (1995).
14. C. V. Cox *et al.*, *Blood* **104**, 2919 (2004).
15. A. A. George *et al.*, *Blood* **97**, 3925 (2001).
16. M. Hotfilder *et al.*, *Blood* **100**, 640 (2002).
17. A. Castor *et al.*, *Nat. Med.* **11**, 630 (2005).
18. Although the CD34⁺CD38⁻CD19⁺ population seen in cALL was originally described as CD38⁺, we have referred to it as CD38^{-low} to reflect the observation that CD38 expression in human cells is seen as a continuum rather than existing in discrete populations.
19. Materials and methods are available as supporting material on Science Online.
20. M. F. Greaves *et al.*, *Blood* **61**, 628 (1983).
21. J. Zuna *et al.*, *Clin. Cancer Res.* **10**, 5355 (2004).
22. We thank I. Tittle, C. Waugh, and C. Hetherington for technical assistance. This work was supported by a Specialist Programme Grant from the Leukemia Research Fund, the Medical Research Council, and EuroCSC: Targeting Cancer Stem Cells (CSCs) for Therapy.

18 September 2007; accepted 12 December 2007
10.1126/science.1150648

Effects of Molecular Memory and Bursting on Fluctuations in Gene Expression

Juan M. Pedraza¹ and Johan Paulsson^{1,2*}

Many cellular components are present in such low numbers per cell that random births and deaths of individual molecules can cause substantial "noise" in concentrations. But biochemical events do not necessarily occur in single steps of individual molecules. Some processes are greatly randomized when synthesis or degradation occurs in large bursts of many molecules during a short time interval. Conversely, each birth or death of a macromolecule could involve several small steps, creating a memory between individual events. We present a generalized theory for stochastic gene expression, formulating the variance in protein abundance in terms of the randomness of the individual gene expression events. We show that common types of molecular mechanisms can produce gestation and senescence periods that reduce noise without requiring higher abundances, shorter lifetimes, or any concentration-dependent control loops. We also show that most single-cell experimental methods cannot distinguish between qualitatively different stochastic principles, although this in turn makes such methods better suited for identifying which components introduce fluctuations. Characterizing the random events that give rise to noise in concentrations instead requires dynamic measurements with single-molecule resolution.

Gene expression is a complex stochastic process, involving numerous components and reaction steps and spanning several time and concentration scales (1–8). This complexity has motivated two very different views on fluctuations in protein levels. A widespread notion in biology suggests that random variation is restrained because each individual chemical step

only contributes marginally to the total, just as rolling more dice reduces relative fluctuations in the sum of the outcomes. Physics-inspired theory has instead emphasized that all the underlying processes could propagate rather than average out fluctuations, as when one die roll is used to determine how many dice to roll next. Both scenarios are plausible: The mapping from details on finer scales into effective events on coarser scales—coarse graining—depends on molecular mechanisms that support a wide range of features, including precise "gestation" periods between birth events, gradual aging of individual molecules, or sudden random bursts of synthesis.

This raises two central questions: How do single-cell fluctuations in abundances depend on the coarse graining of the biochemical hardware, and how can the effective coarse graining be inferred from measurements of fluctuations in single cells?

Most experimental noise studies have measured how the variation in single-cell protein levels depends on transcription and translation rates and typically compare the results with stochastic models based on specific assumptions about the underlying molecular mechanisms. Gene activation and transcription require numerous chemical events: from repressors falling off DNA to RNA polymerase elongating nascent transcripts. For synthetically engineered gene circuits in *Escherichia coli*, these processes can produce exponential waiting times between transcription events (9–11) despite the many microscopic substeps involved. Similar Poisson statistics have been observed in a wide range of physical systems, starting with Bortkewitsch's classic study on the number of Prussian cavalry officers kicked to death by horses (12). However, most genes have a more complex control, involving several repressors, transcription factors, and mediators, as well as chromatin remodeling or changes in supercoiling. Such systems generate nonexponential time intervals between transcription windows, unless a single elementary reaction step is rate limiting. In particular, promoters that gradually mature through a series of inactive states (with several hidden Poisson steps) before activating can create narrowly distributed gestation periods between transcription windows (Fig. 1). The statistical uncertainty in the waiting times can also be reduced by programmed cell cycle activation, replication-activated transcription, or circadian clocks (13). On the other hand, fluctuations can

¹Department of Systems Biology, Harvard University, Boston, MA 02115, USA. ²School of Engineering and Applied Sciences, Harvard University, Cambridge, MA 02138, USA.

*To whom correspondence should be addressed. E-mail: johan_paulsson@hms.harvard.edu

be increased when many copies of a transcript are made in short-lived transcription windows (Fig. 1), creating random bursts of synthesis. A great variety of scenarios is possible, but the stochastic properties of individual gene expression events have only been measured in a few simple systems (10, 11), and the molecular mechanisms are not sufficiently characterized to predict specific burst or waiting-time statistics. Because gestation and bursting can decrease and increase fluctuations in gene expression, respectively, their combined effect is also hard to intuit. However, it is possible to collectively understand such complex mechanisms by mathematically analyzing families of processes. Here, we consider a cell with m molecules of an mRNA and p molecules of the protein and make two generalizations with respect to previous analyses: We allow transcripts to effectively be made both in arbitrary independent bursts of b molecules ($m \rightarrow m + b$) and at arbitrary independent time intervals T (Fig. 1), where T and b vary randomly. To understand how different types of transcription statistics affect single-cell protein fluctuations, we evaluate these assumptions in the context of a standard model (14, 15), where translation ($p \rightarrow p + 1$) occurs with a constant probability per second per transcript, and where both molecules decay ($m \rightarrow m - 1$, $p \rightarrow p - 1$) exponentially with average lifetimes τ_m and τ_p . Similar models have been suggested for gene activation (6, 16, 17) and many other processes, but as with the earlier gene expression model, these have not considered generalized burst or waiting-time distributions. Basic tools from probability theory (18) can then be used to show that the stationary variance in protein abundance—the most commonly reported noise measure in the experimental literature—is insensitive to the shapes of the distributions for b and T (Fig. 2) and approximately follows

$$\frac{\sigma_p^2}{\langle p \rangle^2} \approx \underbrace{\frac{1}{\langle p \rangle}}_{\text{low-copy noise}} + \underbrace{\frac{\langle b \rangle (\sigma_T^2 / \langle T \rangle^2 + \sigma_b^2 / \langle b \rangle^2) + 1}{2}}_{\text{mRNA noise}} \times \underbrace{\frac{1}{\langle m \rangle}}_{\text{coarse graining}} \times \underbrace{\frac{\tau_m}{\tau_m + \tau_p}}_{\text{protein decay}} \quad (1)$$

where $\langle \dots \rangle$ and σ denote averages and SDs, respectively. The equation is exact for exponential time intervals and is an excellent approximation for many types of strongly nonexponential times but breaks down when large and narrowly distributed bursts occur at precise time intervals (19) and (Fig. 2). At low average protein abundances $\langle p \rangle$, relative protein levels spontaneously fluctuate because each random birth and death of a protein then has a larger relative effect on the total. The simplicity of this low-copy noise term reflects the

assumption of individual protein molecules being produced and degraded at exponential time intervals. Because mRNAs determine the rate of protein synthesis, proteins also inherit noise from mRNAs. The mRNA noise, in turn, depends on the average mRNA abundance $\langle m \rangle$ and the burst and waiting-time statistics. Because the protein level cannot immediately adjust to changes in the protein synthesis rate, proteins effectively take a time average of a series of mRNA fluctuations and $0 < \tau_m / (\tau_m + \tau_p) < 1$.

Equation 1 is related to a previous analysis in which we similarly considered a model for stochastic gene expression and used it to reinterpret experiments (19). That model used fluctuation-dissipation relations to generalize the concentration-dependent tendencies to return to an average, while assuming simple exponential waiting times be-

tween events. Here, we took the opposite approach and generalized the randomness of the individual events, while assuming simple average dynamics.

The different parts of Eq. 1 represent qualitatively different aspects of random processes. The overall topology of the reaction network determines which components produce fluctuations, which are captured by $\langle p \rangle$ or $\langle m \rangle$. The connections between the chemical species in the network, in turn, determine the average amplification or suppression of fluctuations: effects that can be understood from deterministic analyses in which one component adjusts to another (17), which is captured by the time-averaging factor. Finally, the dynamics of how fluctuations are generated—the most central aspect of stochasticity—are captured by the bursts and waiting times in the coarse-graining factor. Most studies overlook

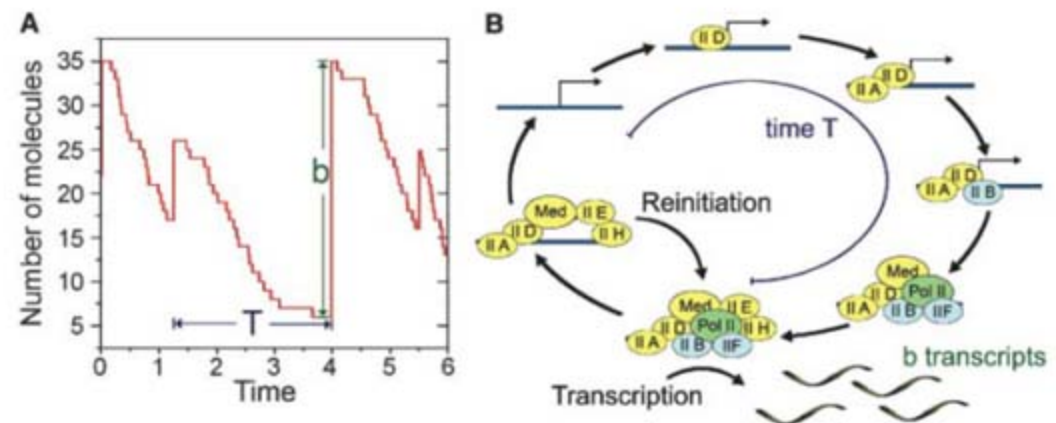
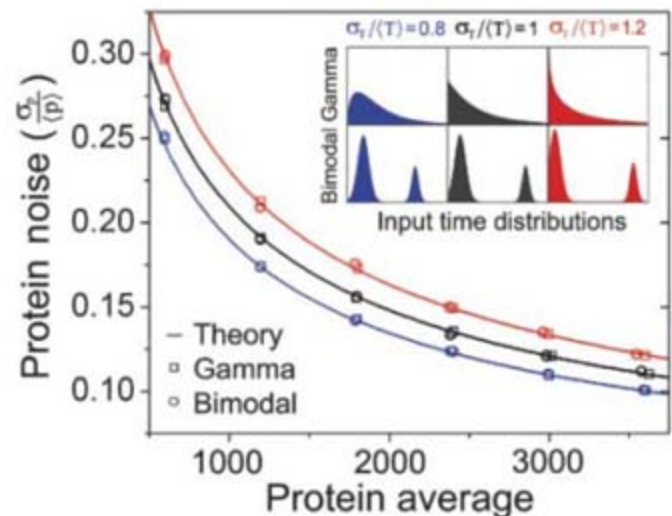


Fig. 1. (A) Generalized birth process where molecules are made in random bursts of b molecules at random time intervals T , where each b and T is independent, as for the mRNAs in Eq. 1. (B) Simplified sketch of polymerase II (Pol II)-mediated transcription in *S. cerevisiae*. Transcription factor TFIID binds DNA and is stabilized by TFIIA, which is followed by TFIIB. This complex then recruits Pol II, a Mediator, and TFIIF, after which TFIIE and TFIIH bind. Upon transcription initiation, Pol II, TFIIB, and TFIIF are released, but the rest of the complex remains, facilitating rapid reinitiation. Depending on parameters, this process can repeat and produce an effective burst of b transcripts, until the entire complex falls off the DNA and has to be reassembled, requiring a time T . The cartoon illustrates a roughly irreversible progression, which requires energy consumption, but the mathematical analysis allows for any distribution of waiting times T between transcription events.

Fig. 2. Random intervals T between transcription events and their effect on protein fluctuations. Noise versus average in protein abundance for varying rates of transcription is shown. Curves are from Eq. 1 and symbols are from exact simulations that sample T from $f(T)$ in the inset. For a given $\sigma_T / \langle T \rangle$, the choice of $f(T)$ has no effect on $\sigma_p / \langle p \rangle$ despite the exotic distributions used. The parameters $\langle p \rangle / \langle m \rangle = 300$ and $\tau_p / \tau_m = 6$ (19) are representative for many genes, and near-perfect matches are also observed over many orders of magnitude in all parameters. (Inset) Hypothetical probability densities $f(T)$, with gamma distributions (exponential for $\sigma_T / \langle T \rangle = 1$) in the top row and examples of bimodal distributions (truncated sum of two Gaussians) in the bottom row, and with the same averages and variances in each column.



nontrivial coarse graining for simplicity (20), though some consider geometrically distributed bursts of mRNA or protein synthesis (14, 15) at exponential time intervals, as observed in certain simple systems (9–11). In this case, the coarse-graining factor (for the mRNA or protein) can be expressed as $1 + \langle b \rangle$, which does not explain the effect of variation in the bursts and waiting times. By contrast, Eq. 1 shows how cells could exploit narrowly distributed gestation periods to greatly reduce variation in protein abundance from cell to cell, with the largest relative effect when synthesis, on average, occurs in large bursts. However, because the effect is determined by the sum of the normalized variances in bursts and

waiting times, it also shows that narrowly distributed gestation periods only marginally reduce noise when burst sizes are widely distributed.

Many macromolecules approach their deaths gradually, passing through a series of states before finally degrading. For example, eukaryotic transcripts have their polyadenylate [poly(A)] tails sequentially chewed up (21) before degrading the protein-coding part of the message (Fig. 3). Measurements in *Saccharomyces cerevisiae* (by researchers using, for example, *PGK1* or *GAL10*) indeed demonstrate (22) strongly nonexponential mRNA decay curves, with long refractory periods where the poly(A) tail is shortened before the mRNA is degraded. Such “senescence” before

death is in some sense similar to gestation before birth, reducing the uncertainty in the lifetimes of individual molecules. Here, we consider how senescence affects fluctuations in abundances across cells in the population. To keep the mathematical analysis as simple as possible, we assume that transcripts are made one by one at exponential time intervals and use the same assumptions regarding translation and proteolysis as previously indicated. The stationary mRNA distribution is then Poissonian, with $\sigma_m^2 = \langle m \rangle$, regardless of the distribution of mRNA lifetimes as long as the deaths of individual transcripts are independent of each other. However, even though the mRNA distribution is unaffected, mRNA fluctu-

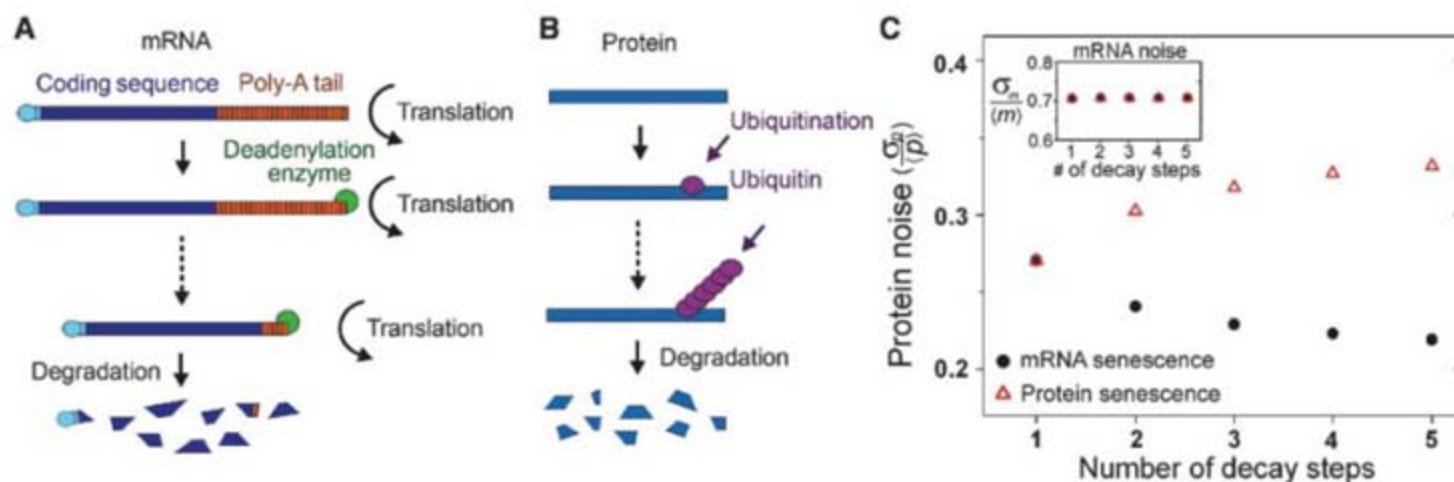
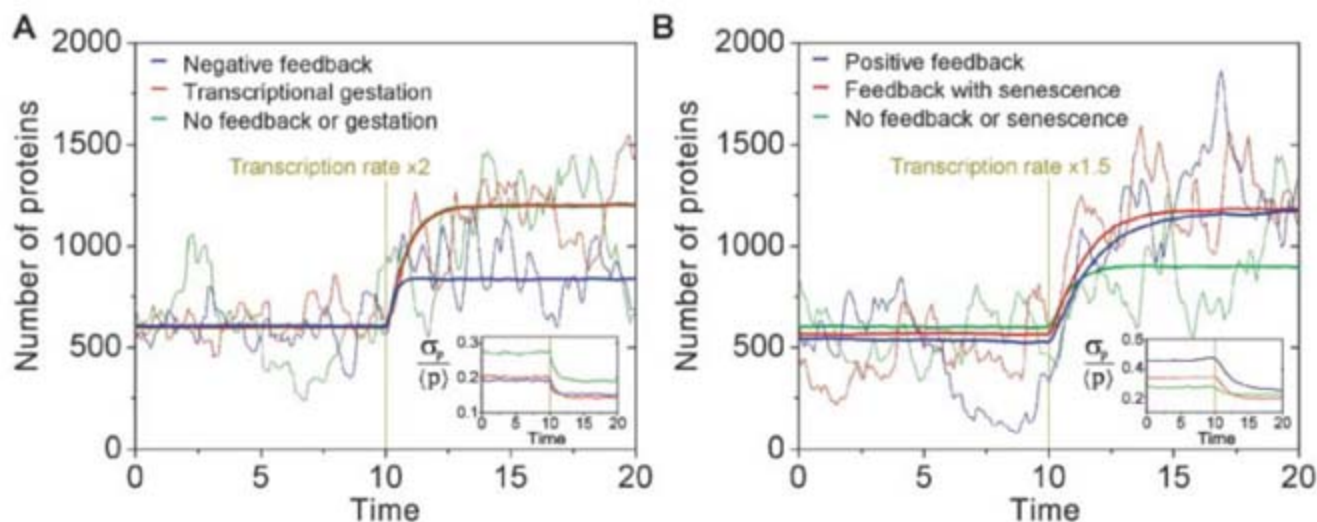


Fig. 3. Molecular senescence and its effects on noise in mRNA and protein abundance. (A) Cartoon of mRNA senescence when the poly(A) tail is progressively shortened before degradation. (B) Cartoon of protein senescence when the protein is ubiquitinated several times before degrading. (C) Noise in the abundance of proteins (main graph) and mRNA (inset) as a function of the number of Poisson steps N in the degradation pathway, as compared for the same average lifetimes. The graphs come from exact analytical calculations (19). For the mRNA

senescence curve, proteins are assumed to decay exponentially, and for the protein senescence curve, mRNAs are assumed to decay exponentially. Parameters are the same as in Fig. 2 for the exponential $f(T)$. The mRNA senescence (black circles) has no effect on the mRNA variance but reduces protein noise because time averaging of the mRNA fluctuations becomes more efficient. Conversely, protein noise increases with more pronounced protein senescence (red triangles) because time averaging of mRNA fluctuations is impaired.

Fig. 4. Simulated time courses for averages (smooth curves) and sample paths (jagged curves) illustrating the difference between feedback and different coarse-graining mechanisms. At time $t = 10$, the rate of transcription is increased by a factor of 2 (A) and 1.5 (B), respectively. (A) Comparison of an idealized negative feedback loop (blue curve), nonexponential gestation between transcription events (red curve), and a reference gene without feedback or gestation (green curve). For the idealized negative feedback, the transcription intensity follows $k_m/2/(1 + (p/600)^2)$, where k_m is the transcription rate of the reference gene. For gestation, the time intervals between creation events follow a gamma distribution of order $N = 8$ and average $1/k_m$. Both negative feedback and gestation produce less noise than the reference gene (inset), but the average response is greatly reduced for negative feedback. (B) Comparison of an idealized positive feedback loop



(blue curve), with the combination of positive feedback and mRNA senescence (five exponential time steps; red curve), and the same reference gene as in (A) (green curve). For the idealized positive feedback, the transcription intensity follows $k_m(0.01 + 0.99 p/(600 + p))$. In both cases, the output level is roughly doubled, but when positive feedback is combined with mRNA senescence, the noise increase is smaller relative to that of the reference gene (inset).

tuations still contribute less to the width of the protein distribution than they would without senescence. If transcripts are degraded after N Poisson steps, producing gamma-distributed lifetimes, the stationary protein variance exactly follows

$$\frac{\sigma_p^2}{\langle p \rangle^2} = \frac{1}{\langle p \rangle} + \frac{1}{\langle m \rangle} \times \underbrace{\left[1 + \frac{\tau_p}{\tau_m} \left(\left(\frac{\tau_p N}{\tau_m + \tau_p N} \right)^N - 1 \right) \right]}_{\text{Course-grained time-averaging factor}} \quad (2)$$

The time-averaging factor now depends on the coarse graining and decreases with increasing number of decay steps N [(19) and (Fig. 3)]. The intuitive explanation for these somewhat unexpected effects lies in the distinction between the dynamics of the noise and the overall distribution: For any given average mRNA lifetime, senescence accelerates changes in the mRNA levels in individual cells without affecting the probability of occurrence in the population. If each molecule lived for exactly τ_m time units, mRNA levels at time t would be completely uncorrelated with the levels before time $t - \tau_m$. This in turn makes it easier for the protein to “time-average out” mRNA fluctuations, because the efficiency of time averaging depends on the rate of change in the protein relative to the rate of change in the mRNA [see (19) for autocorrelation analyses]. Simple and well-documented molecular mechanisms of degradation (22) thus allow cells to exploit the internal transitions of independent molecules to reduce fluctuations in total concentrations. Protein senescence [for example, when multiple ubiquitination events are required before degradation (Fig. 3)] would instead speed up the protein response at any given

average lifetime and thus prevent time averaging. Reducing the variability in the lifetimes then causes increased variability in protein concentrations (Fig. 3).

The bursting, gestation, and senescence mechanisms above modify the spontaneous noise in a system without affecting the average susceptibility to changes in parameters: A change in the rates of synthesis or degradation, which in turn may depend on upstream signaling, still has a proportional effect on average abundances (Fig. 4) in all cases. Positive or negative feedback control, by contrast, amplifies (23) or dampens (24) noise, respectively, while at the same time amplifying or dampening external signals (Fig. 4). Furthermore, negative feedback control only substantially suppresses noise when operating at high gain, but high-gain mechanisms are instead more susceptible to time lags or noisy intermediates, which destabilize feedback control and increase noise levels. Gestation and senescence, by contrast, operate without closing a potentially unstable loop and may therefore reduce spontaneous noise more efficiently. The noise reduction can indeed be extremely efficient when gestation and senescence are combined, because they prevent fluctuations from arising rather than correcting existing fluctuations.

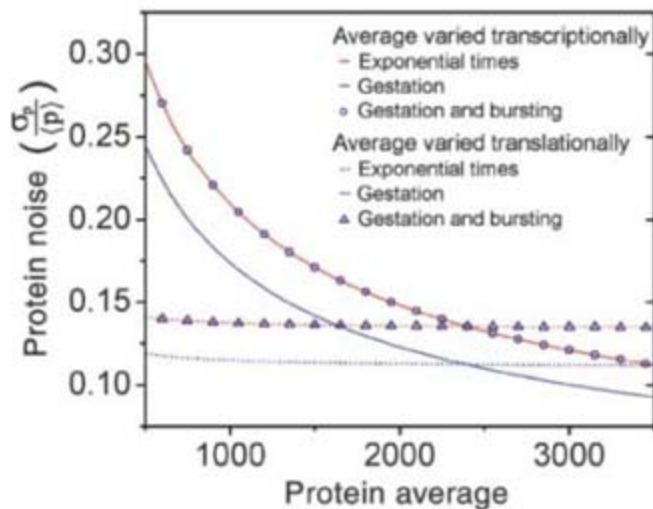
The convenience of fluorescent reporters is creating a shift of focus in quantitative cell biology from bulk averages to individual cells, producing a wealth of data on nongenetic heterogeneity from microbes (25, 26) to humans (27). The extent of heterogeneity is interesting in itself, but single-cell data can also be used to extract more information about the underlying processes: Individual responses to individual signaling events say much more than average responses to average signals. In particular, many quantitative studies have used the properties of the noise to infer microscopic kinetic mecha-

nisms, testing stochastic models by analyzing how the variance in protein abundance responds to changes in the rates of transcription and translation (3–5, 7, 25). Analyses in *Bacillus subtilis* (3), *E. coli* (4, 28), and *S. cerevisiae* (5, 6, 25) studied a range of genes and measured the distributions of protein abundance for different parameter values by changing the expression rates genetically, by changing growth conditions, or by adding inducers or inhibitors: in some cases with the use of dual fluorescent reporters to first separate the “intrinsic” randomness of the chemical events in gene expression from the “extrinsic” intracellular variation in the expression rates (4, 6, 28). Some studies also measured noise correlations between different proteins in genetic activation cascades (7) or between different time points in the same cell (13, 28, 29). The conclusions varied in the specific details but have formed a broad consensus that the intrinsic noise in protein abundance reflects low numbers of transcripts per cell, possibly with burstlike transcription resulting from brief random periods of gene activation.

The qualitative agreement between different studies and the excellent quantitative fits to the accompanying stochastic models seem to support the underlying models, which typically assume memory-less single-step transitions between births and deaths of genes, mRNAs, and proteins. However, Eqs. 1 and 2 show that very different stochastic processes can produce exactly the same response in such experiments. Changing the translation efficiency or the frequency of transcription bursts only affects $\langle p \rangle$ and $\langle m \rangle$, and the response to changes then follows $\sigma_p^2 / \langle p \rangle^2 = 1 / \langle p \rangle + C / \langle m \rangle$ in all cases, where C is a proportionality constant. Such experiments indicate which components in a network produce fluctuations but unexpectedly say nothing about how those fluctuations arise (30). For example, if protein noise was reduced by increasing the transcription rate but not by increasing the translation rate, as shown for some genes in *B. subtilis* (3), all versions of the mRNA-protein models in Eqs. 1 and 2 suggest that the noise comes from mRNA fluctuations (3, 19). However, exactly the same fit is obtained (i) whether transcription is burstlike or perfectly regular or (ii) whether individual transcripts decay exponentially or gradually senesce (Fig. 4). Even in the ideal case where simple models without tunable parameters provide predictions that are later tested experimentally (3, 15), perfect fits are equally consistent with mechanisms that are very random, very regular, or anything in between. Occam’s razor can still eliminate obscuring details, but when several simple yet very different explanations work equally well, choosing one specific model can also brush interesting phenomena under Occam’s “rug.”

What additional tests could be used to discriminate between different types of underlying stochastic processes? One approach is to directly measure the relevant kinetic parameters. If fluc-

Fig. 5. Noise versus average in protein abundance from Eq. 1 for varying rates of transcription (solid lines) and translation (dotted lines). Red and blue lines correspond to exponential ($\sigma_T / \langle T \rangle = 1$) or nonexponential ($\sigma_T / \langle T \rangle = 0.6$) waiting times between transcription events, respectively, without mRNA bursting. Symbols correspond to nonexponential ($\sigma_T / \langle T \rangle = 0.6$) waiting times, with the use of mRNA bursting with $\langle b \rangle = 1$ and $\sigma_b / \langle b \rangle = 0.8$. The noise responds more sharply to changes in the transcription rate than to changes in the translation rate, reflecting the fact that, for the parameters used (19), most of the protein noise comes from random births and deaths of the mRNAs. However, if proteins are measured in arbitrary fluorescence units, the horizontal axis can be scaled and the transcriptional curves are indistinguishable. Similarly, if mRNA numbers are not measured directly, it is impossible to distinguish the effect of low mRNA numbers from that of high coarse-graining factors, because either effect shifts the curves vertically. Finally, the coarse-graining factor itself depends on factors not usually measured. Each line can then correspond to many combinations of timing and bursting.



tuations arise as a result of low abundances, the average levels should be measured in absolute numbers, not in arbitrary units of fluorescence (as is typically the case). This is particularly important for mRNAs: The low-copy components that introduce fluctuations must be counted (instead of the high-copy components that merely respond to underlying randomness). Measuring $\langle p \rangle$ and $\langle m \rangle$ would provide an estimate of C but would still not separate coarse graining from time averaging or other deterministic features (Eqs. 1 and 2). Time averaging could be estimated by measuring the average lifetimes of the components, but the type of time averaging should also be confirmed by manipulation experiments where the degradation rates of mRNAs and proteins are varied. If all these parameters are determined with high accuracy, the coarse-graining factor in Eq. 1 could be estimated. However, even in this ideal case, the relative contributions of gestation and bursting would still be unknown (Eqs. 1 and 2 and Fig. 5). The effects of precise gestation and random bursting could even cancel out and make it appear in these experiments as if molecules were born at exponential time intervals without bursts. More information can also be gained by considering the full distributions rather than just variances, but the exact shapes of distributions are more sensitive to experimental artifacts and have similar problems with experimental discrimination. Conclusive experimental analyses of coarse graining instead require accurate time series where the burst and dwell time statistics can be directly observed. A few pioneering studies have quantitatively monitored transcription (11) and translation (9, 10) in *E. coli* with single-molecule resolution. For simple or synthetically engineered genes, they demonstrated exponential time intervals between geometric bursts of transcripts and proteins, respectively. These methods are now being used to study regulated genes and gene expression in eukaryotes, where gestation, senescence, and complicated bursting patterns are expected (31).

The fact that standard methods cannot discriminate between different types of coarse graining (Fig. 5) may explain why most experimental results have so closely matched the first models that were used. However, it also means that certain aspects of the conclusions are more robust to flaws in some of the most central model assump-

tions: By not distinguishing between how fluctuations arise (i.e., fitting any type of coarse graining), the methods are more suitable for identifying which components produce the fluctuations, which is both nontrivial and important.

Our findings mathematically connect noise in the single-cell protein abundance to bursting, gestation, and senescence in gene expression, describing how 10 molecules in some sense can statistically behave as if they were 5 or 20 molecules without control loops. We also show that standard single-cell measurements cannot detect or exclude these features: They only suggest which components contribute fluctuations, not how they contribute. Similar phenomena have been observed for bunching and antibunching in photon emissions (32), as well as for many molecular-scale cellular processes. Microtubules switch between growth and decay phases (33) where a burst of subunits is added or removed, and opening an ion channel can let a burst of molecules through. Nonexponential gestation periods have, in turn, been demonstrated in the rotational switching of *E. coli* flagellar motors (34) and in the replication control of bacterial plasmids (14), whereas the senescence of active rhodopsin molecules was recently shown to explain the reproducibility of the retinal signaling response to single photons (35). Advances in single-molecule live-cell imaging could now enable similar breakthroughs for mRNAs and proteins and finally reveal the effective coarse graining of gene expression.

References and Notes

- O. G. Berg, *J. Theor. Biol.* **71**, 587 (1978).
- H. H. McAdams, A. Arkin, *Proc. Natl. Acad. Sci. U.S.A.* **94**, 814 (1997).
- E. M. Ozbudak, M. Thattai, I. Kurtser, A. D. Grossman, A. van Oudenaarden, *Nat. Genet.* **31**, 69 (2002).
- M. B. Elowitz, A. J. Levine, E. D. Siggia, P. S. Swain, *Science* **297**, 1183 (2002).
- W. J. Blake, M. Kaern, C. R. Cantor, J. J. Collins, *Nature* **422**, 633 (2003).
- J. M. Raser, E. K. O'Shea, *Science* **304**, 1811 (2004).
- J. M. Pedraza, A. van Oudenaarden, *Science* **307**, 1965 (2005).
- G. M. Suel, R. P. Kulkarni, J. Dworkin, J. Garcia-Ojalvo, M. B. Elowitz, *Science* **315**, 1716 (2007).
- L. Cai, N. Friedman, X. S. Xie, *Nature* **440**, 358 (2006).
- J. Yu, J. Xiao, X. Ren, K. Lao, X. S. Xie, *Science* **311**, 1600 (2006).
- I. Golding, J. Paulsson, S. M. Zawilski, E. C. Cox, *Cell* **123**, 1025 (2005).
- L. v. Bortkewitsch, B. G. Teubner, *Monatsh. Mathematik* **9**, A39 (1898).
- A. Amir, O. Kobiler, A. Rokney, A. B. Oppenheim, J. Stavans, *Mol. Syst. Biol.* **3**, 71 (2007).
- J. Paulsson, M. Ehrenberg, *Q. Rev. Biophys.* **34**, 1 (2001).
- M. Thattai, A. Van Oudenaarden, *Proc. Natl. Acad. Sci. U.S.A.* **98**, 8614 (2001).
- P. S. Swain, M. B. Elowitz, E. D. Siggia, *Proc. Natl. Acad. Sci. U.S.A.* **99**, 12795 (2002).
- J. Paulsson, *Phys. Life Rev.* **2**, 157 (2005).
- Materials and methods are available as supporting material on Science Online.
- J. Paulsson, *Nature* **427**, 415 (2004).
- Nontrivial coarse graining is typically overlooked in the field of biology because the mathematical frameworks come from chemistry, where such effects are less important: The chemical master equation can account for any statistical feature, but this comes at the expense of an extended state space, which greatly complicates derivations and interpretations.
- C. J. Wilusz, M. Wormington, S. W. Peltz, *Nat. Rev. Mol. Cell Biol.* **2**, 237 (2001).
- C. J. Decker, R. Parker, *Genes Dev.* **7**, 1632 (1993).
- A. Becskei, B. Seraphin, L. Serrano, *EMBO J.* **20**, 2528 (2001).
- A. Becskei, L. Serrano, *Nature* **405**, 590 (2000).
- A. Bar-Even et al., *Nat. Genet.* **38**, 636 (2006).
- J. R. Newman et al., *Nature* **441**, 840 (2006).
- A. Sigal et al., *Nature* **444**, 643 (2006).
- N. Rosenfeld, J. W. Young, U. Alon, P. S. Swain, M. B. Elowitz, *Science* **307**, 1962 (2005).
- N. Friedman, S. Vardi, M. Ronen, U. Alon, J. Stavans, *PLoS Biol.* **3**, e238 (2005).
- If the sizes of the bursts are varied, which they have been in some careful analyses (6), it is possible to get closer to estimating the coarse-graining statistics directly from the population variances. Such analyses say more about the underlying process but do not discriminate between different types of coarse graining of the underlying processes that create the bursting.
- J. R. Chubb, T. Trcek, S. M. Shenoy, R. H. Singer, *Curr. Biol.* **16**, 1018 (2006).
- C. G. Hubner et al., *Phys. Rev. Lett.* **91**, 093903 (2003).
- T. Mitchison, M. Kirschner, *Nature* **312**, 237 (1984).
- E. A. Korobkova, T. Emonet, H. Park, P. Cluzel, *Phys. Rev. Lett.* **96**, 058105 (2006).
- T. Doan, A. Mendez, P. B. Detwiler, J. Chen, F. Rieke, *Science* **313**, 530 (2006).
- We thank M. Ehrenberg and O. G. Berg for discussions and A. Hilfinger for comments on the manuscript. This work was supported by Microsoft, the Human Frontier Science Program, and NSF under grant DMS-0720056.

Supporting Online Material

www.sciencemag.org/cgi/content/full/319/5861/339/DC1

SOM Text

Fig. S1

Table S1

References

26 April 2007; accepted 12 December 2007

10.1126/science.1144331

NANO TO NEXT GEN: AUTOMATION GETS PERSONAL

Lab automation – it isn't just for Big Pharma anymore. Providers have developed a range of personal instruments to bring the benefits of automation to the masses. At the same time, new equipment and protocols are enabling the standardization and optimization of such traditionally overlooked areas as cell culture. This article surveys major manufacturers to find out what's new in life science robotics and automation. **By Jeffrey M. Perkel**

One emerging industry trend, according to Douglas Gurevitch, senior development engineer at the **University of California, San Diego**, and executive editor of the *Journal of the Association for Laboratory Automation*, is the move toward reliable nanoliter dispensing.

"Ultras-small-volume liquid transfer has had a resurgence," Gurevitch says. Microfluidic lab-on-a-chip systems work at the nanoscale, but their interfaces—not to mention traditional high throughput screening robotics—have tended to operate at the microliter level, meaning researchers still must make more material than they need, and generate more waste.

"Now there's new technology out there that allows you to work at a smaller scale," he says.

One such system is **TTP LabTech's** mosquito. Commercial director Jas Sanghera says the company had two primary considerations in developing the mosquito: maintaining the accuracy and reliability of microliter-dispensing systems, and avoiding cross-contamination.

The second aim may be accomplished either by washing reusable components or using disposable pipettes. However, since washing becomes less efficient as volumes get smaller and concentrations rise, the company embraced the latter approach, says Sanghera. But TTP LabTech also wanted to avoid traditional disposable tips, as tip boxes eat up instrument deck space, and require robots to handle them.

The mosquito uses a bandolier of 36,000 disposable tips (equivalent to 95 boxes of 384 tips) on a tape reel about the size and thickness of 35-mm film. The tape feeds into the mosquito horizontally and then rotates 90 degrees to bring the tips into contact with the apparatus and samples. Each tip, like the barrel of a syringe, can aspirate, dispense, and mix reagents as needed, in volumes between 25 nl and 1.2 μ l. Once used, the tape rotates back to its original horizontal position and exits the instrument.

Though the mosquito has remained largely unchanged since its release several years ago, new applications have emerged, says Sanghera, such as real-time PCR, crystallography, and MALDI mass spectrometry sample deposition. And the user base is growing, he says; academic institutions now comprise the majority of users.

Labcyte designed its nanoliter dispensing system around a different principle.

"When you get to nanoliter volumes, you need very fine control, and that turns out to be very challenging," says Richard Ellson, the company's chief technology officer. "It's difficult to make holes used in conventional dispensers all the same size and to make sure they do not change in size, as compounds in the screening libraries will often stick to materials."

The Labcyte Echo 555 system overcomes these issues via a completely noncontact approach. Echo systems use sound energy to determine both the level of hydration and volume of DMSO-based samples in each well of a microtiter plate. They then focus a burst of energy customized for the fluid composition directly at the meniscus to eject precise 2.5-nl droplets into an overhanging, [continued >](#)



“When you get to nanoliter volumes, you need very fine control, and that turns out to be very challenging.”

Look for these Upcoming Articles

Mass Spectrometry — February 22

Proteomics 1 — March 7

Biomarker Discovery — March 28

Inclusion of companies in this article does not indicate endorsement by either AAAS or Science, nor is it meant to imply that their products or services are superior to those of other companies.

The Labcyte Echo 555 system focuses a burst of energy directly at the meniscus to eject precise 2.5-nl droplets into an overhanging destination plate.

inverted destination plate, which comprises anywhere from 96 to 3,456 wells.

"As you get smaller and smaller, surface tension forces get very large in relation to gravity," Ellson explains. "The drops stick because there's enough surface tension to hold the drop on the ceiling of the inverted plate." That is true even of larger volumes, he adds, which means the Echo can transfer into prefilled wells.

Multiple droplets can be ejected into a single well to achieve larger volumes, and the system is flexible enough to eject different volumes from different wells, or from a single source well into multiple destination wells.

Though the initial systems were designed specifically to handle samples in DMSO (as is common with pharmaceutical compound libraries), the systems can also be calibrated to work with aqueous samples, says Ellson. The Echo 520, to be released at this month's LabAutomation 2008 meeting in Palm Springs, California, will have this capability out of the box, he adds.

Next Generation Pipettes

Not all liquid handling advances are robotic. Two companies have reinvented the handheld pipette itself, bringing consumer-product aesthetics to the lab bench.

Launched this past October, **Viaflo's** Vision electronic pipettes feature a full-color LCD display and iPod-like touchwheel user interface that was consciously designed to appeal to young, technically savvy lab workers.

According to Viaflo Marketing Director Marc Hamel, the instruments score high on the "wow" scale at product shows. "It's the first product I've been involved with that has real stopping power," he says.

Users easily navigate simple menu options and set aspirate and dispense volumes using the pipette's touch-sensitive touchwheel, just as they select songs on their MP3 player. Favorite volumes can be preset and selected for easy task-switching, and can even be beamed to the pipette from a PC via Bluetooth connectivity. And the system is programmable, with 10 commonly used pipetting modes (such as aspirate, dispense, mix, and purge) that can be used individually or linked together to build custom protocols.

Thermo Fisher Scientific has adopted another approach to simplify manual pipettes: voice-activation. Speak the words "two-three-zero" to the company's new Matrix Hybrid Pipette, for instance, and the instrument display will read "23.0 μ l," says Craig Weiss, director of marketing for Thermo's Matrix Liquid Handling Products. Users can also control the volume by scrolling up and down on a digital display, or by selecting from one of a series of user-defined preset volumes.

All of which serves to increase productivity, Weiss says. "You pay some very highly educated people high dollars to do very manual labor. People are starting to see that the more you can automate that, the more it frees these highly skilled individuals to do the

core research, versus hours turning pipette knobs while pipetting by hand."

The Air Out There

Seahorse Bioscience of North Billerica, Massachusetts, is automating an up-and-coming area of bioscience research: mitochondrial activity.

"The mitochondrion has become the focus for a whole bunch of different diseases," says Steve Chomicz, vice president of sales and marketing. "Whether neurodegeneration, cancer, diabetes, or obesity—all the research leads them to focus on targets that involve the mitochondria."

The best way to study that, he says, is through measurements in living cells of glycolysis and oxygen consumption, two indicators of cellular bioenergetics and mitochondrial function. And that is exactly what Seahorse Bioscience's XF24 Analyzer does.

The XF24 uses a disposable cartridge that can be lowered just above a microlayer of cells in a microplate well to create a transient microenvironment in which changes in pH and oxygen levels can be optically detected in up to 24 wells at once. Up to four drugs can be added during this process, Chomicz says, thereby enabling experiments that are not possible using traditional oxygen-sensing equipment such as Clark electrodes and radiolabels.

"Scientists have said repeatedly that the drug delivery option is one of the most powerful features of the instrument, because you can do live agonist/antagonist measurements and dose-response curves," says Chomicz. "That cannot be done with Clark electrodes, so they like that very much."

Chomicz says the system software is constantly being upgraded based on user feedback, and new sensors (for instance, for glucose and CO₂) are in development.

Personal Automation

A number of companies have shifted focus from large-scale robotics down to smaller, so-called personal automation. According to Wendy Lauber, director of product management for biopharma at **Tecan**, "It is a market need to have all of the power of the high-end market with the pricing requirements of the low-end market."

Tecan, for instance, recently released a low-end addition to its Freedom EVO line of liquid handlers, the Freedom EVO 75, which features a dual-pipetting mode "8 Plus 1 Access 8 arm," says Lauber.

Operating in either an eight- or single-channel mode, "It gives you two functions in one, because at this low entry range, cost is a concern," she says.

Promega is also embracing this automation trend.

"Larger liquid handlers tend to have a high learning curve, where a customer must maintain a certain level of automation expertise," says Christopher Cowan, Promega's integrated solutions and engineering group manager. As a result, labs are forced to keep trained specialists on staff, which is precisely the opposite of what automation is supposed to achieve, he says.

"It's crazy: the lab is buying an open platform to increase throughput and lower the head count, and yet you need that extra head count to maintain it."

Personal automation devices like Promega's Maxwell 16 (released fall 2006), Cowan says, are smaller and simpler than traditional robotics systems. Just plug in the appropriate reagent cartridge—the Maxwell 16 can extract DNA, RNA, or protein from up to 16 samples simultaneously—and come back in about 30 minutes to [continued >](#)

collect your materials.

The company's second-generation instrument, released fall 2007, features a "very different and more robust design," says Cowan. More important, it can elute samples in a smaller volume (and thus, at a higher concentration); while the original Maxwell 16 extracts samples in 300 μ l, the so-called low-elution volume (LEV) protocol elutes in as little as 20 μ l.

Also entering the personal automation arena is **Qiagen**, a company that has for years sold larger-scale automation equipment.

In January 2007 the company automated its spin column-based nucleic acid sample preparation kits with the QIAcube, which can process up to 12 samples at about the same speed as a technician doing the job manually, says Wolfgang Leibinger, business director for automation.

This month, says Leibinger, the company plans to roll out the medium throughput QIASymphony, bringing the simplicity of Qiagen's earlier low throughput BioRobot EZ1 to a higher throughput audience.

The EZ1 is a relatively small, easy-to-use robot for processing nucleic acids from up to six samples at once. Simply insert a magnetic card with the protocol, add prefilled reagents, and go. Now, that simplicity is coming to the microplate level, says Leibinger, which makes such robotics more accessible.

"I see this as a major mind-shift," he says. "What we have seen in the past is if you have these complex instruments, and the guy who used it leaves the lab, the instrument is often not used anymore because no one has the confidence to work with it."

To achieve this simplicity, Qiagen departed from the typical lab robot aesthetic. The QIASymphony has a deck, for instance, but rather than dealing with it directly, users load sample kits and disposables through drawers. A robotic arm then takes the material and places it in its appropriate position. Similarly, the system has no external computer, instead relying on a touch-screen interface.

Automating Cell Culture Work

Another relatively new trend in lab robotics is cell culture automation, says Brad Nelson, director of marketing for instruments and workstations at **Velocity11**, which was recently acquired by Agilent Technologies.

Cell culture places special demands on lab automation, Nelson says. For instance, the devices must be able to fit inside a standard hood footprint and yet not disrupt the flow of air that keeps the hoods sterile.

Velocity11's Bravo liquid handler was "designed specifically to be able to operate inside a standard [laminar] fume hood," says Nelson, who notes, "if you create a device that looks like a giant block, you will disrupt the flow."

The Automation Partnership (TAP) also automates cell culture instrumentation. TAP's new Sonata, for instance, is designed to help biopharma companies evaluate and optimize cell lines and culture conditions before scaling up to larger batch sizes.

Intended as an intermediary between the research and manufacturing stages of biopharmaceutical development, the system uses parallel processing to mimic the conditions inside bioreactors, which are too large and cumbersome to optimize directly. "Sonata enables, say, 200 flasks to be incubated and for all the processing of feeding, maintenance, sampling, measuring metabolites, viability, and so on to be carried out automatically," says Rosemary Drake, director of business development.

"You get much more data, you can be more thorough, and you can reduce the time it takes to identify the best clones and culture conditions to take forward into the next phase of development," she says.

Major Vendors

Major automation vendors have not been idle, either.

PerkinElmer, for instance, continues to develop application-specific workstations based on its JANUS platform, says Nance Hall, vice president and general manager of the automation and detection solutions business. Among its new offerings are workstations specifically designed for forensics and cellular screening, as well as a new AlphaLISA Automated solution, which uses PerkinElmer's novel assay design as an alternative to enzyme-linked immunosorbent assays (ELISAs).

Unlike traditional ELISA assays, which are cumbersome and utilize several separation steps, says Hall, AlphaLISA "is a novel, no-wash technology easily automated and providing less assay variation than ELISA." By eliminating washing, AlphaLISA also removes ELISA's most time-consuming steps, she adds.

For those who need to keep all their disparate automation pieces under control, Thermo Fisher Scientific will shortly be launching a new "mover-independent" software platform, says Hansjoerg Haas, director of marketing for lab automation and cellular imaging. Such software will allow users who have robots from multiple vendors to control all of them using a single software tool, rather than with a collection of incompatible programs.

Beckman Coulter, meanwhile, has begun automating the process of flow cytometry, says Keith Roby, applications product manager for automation. "It's easy to do four or eight tubes by hand," he says. "When you start getting up to 24 tubes, it's very easy to make pipetting mistakes."

Now scale that up to 96 samples, he continues, and mistakes are inevitable. "That's where automation comes in: it will do the same thing every time; human error is taken out."

And that's a lesson that applies no matter what process you might be automating.

Jeffrey M. Perkel is a freelance science writer based in Pocatello, Idaho.

DOI: 10.1126/science.opms.p0800021

Featured Participants

The Automation Partnership
www.automationpartnership.com

Beckman Coulter
www.beckmancoulter.com

Labcyte
www.labcyte.com

PerkinElmer
www.perkinelmer.com

Promega
www.promega.com

Qiagen
www.qiagen.com

Seahorse Bioscience
www.seahorsebio.com

Tecan
www.tecan.com

Thermo Fisher Scientific
www.thermofisher.com

TTP LabTech
www.ttplabtech.com

University of California, San Diego
www.ucsd.edu

Velocity11 (an Agilent Technologies company)
www.velocity11.com

Viaflo
www.viaflo.com

New Products

Thermal Analysis Line

The Thermogravimetric Analysis and Differential Scanning Calorimeter System (TGA/DSC 1) combines the new DSC 1 system and updated STARe Thermal Analysis software. The TGA/DSC 1 cuts analysis time by 50 percent, increases productivity, and provides a wealth of information from a single measurement. The innovative sample temperature sensor is attached directly to the weighing arm and detects temperature deviations of ± 0.25 K from ambient temperature to 1,600 °C. The color touchscreen terminal allows the status of the measurement to be seen even at a distance. The system offers high sensitivity, excellent temperature resolution, flat baseline, and a robust design. The DSC 1 is able to separate closely lying effects at heating rates up to 300°C/min, reducing analysis times. When the touch-free SmartSens infrared sensors are activated, users can open and close the furnace without touching any part of the instrument or disrupting a measurement. The software includes an optional interface for integration with a laboratory management information system.



Mettler Toledo

For information 614-438-4686

www.mt.com/TA

Cell Culture and Image Analysis System

The Cell Growth and Discovery (CGD) WorkCell is a fully enclosed, environmentally controlled, automated solution designed for high capacity cell growth, supply, and in-line image analysis. Combining state-of-the-art software with sophisticated robotics, the CGD WorkCell can simultaneously handle multiple plate and flask formats and perform cell maintenance, colony selection, and RNA interference studies. The system can improve the quantity and quality of characterized cells, eliminating human error and improving data consistency. Designed for the growth and analysis of multiple cell lines and cultures, this high-capacity system offers full level II high efficiency particulate air (HEPA) containment with strategic ports for easy user access while still protecting cells from contamination and users from hazardous aerosols and vapors. It can perform a variety of assays at the optimal point of cell growth and offers extensive process flexibility to meet the culture and experimental demands of varying cell types. The instrument can accommodate multiple container formats to provide cells suitable for a variety of research needs, from cloning and transfection studies to general cell line amplification.

Thermo Fisher Scientific

For information 828-365-1205

www.thermofisher.com

Drug Discovery Robotics

Integrated Industrial Robotics Solutions for high throughput pharmaceutical and biotech applications feature the Motoman HP3JC Robot providing the transportation foundation, SAMI Workstation EX Software providing features tailored to industrial applications, and a safety enclosure to protect operators and samples. The systems are individually tailored to the application by the Beckman Coulter Integrated Solutions Team, which customizes and optimizes the software along with placement of devices, labware, and transport tools. Powerful software facilitates assay design, providing ongoing checks and feedback to the developer and ensuring that the finished method is validated. The software integrates all devices, liquid handlers, actions, and plates for maximum throughput and efficient resource use. The Motoman robot arm has a successful track record in high-workload applications. The custom-tailored systems may incorporate Beckman Coulter liquid handlers, including the Biomek series, and readers such as the DTX Series Multimode Detectors and the new Paradigm Detection Platform.

Beckman Coulter

For information 714-993-8955

www.beckmancoulter.com

Automated Microarray Processing

The QuadChamber is for automated processing of four different microarrays simultaneously on one slide using the HS Pro automated hybridization station. The QuadChamber was developed for use with Agilent's new 4 x 44k 4-Plex Gene Expression as well as CGH Microarrays, which consist of four individual, whole-genome microarrays printed on a single glass slide. It is the first fully automated system that can independently handle four arrays on one slide with no cross-contamination between the arrays. The QuadChamber provides a sealed environment around each of the four arrays on Agilent's 4-Plex slides, with independent channels for wash buffers, independent agitation mechanisms, and independent drying.

Tecan Group

For information +41 44 922 81 11

www.tecan.com

Cell Attachment Studies

The ECIS 800 is an electric cell-substrate impedance sensing (ECIS) system that performs automated studies of cell attachment and spreading. The ECIS 800 provides a novel method for performing real-time cell monitoring, electroporation, and wounding. The system measures changes in impedance of a small electrode to AC current flow to observe changes in cell movement and confluence. The highly specialized eight-well slides make use of an array of gold film electrodes that connect to the ECIS 800 electronics, allowing multiple preparations to be studied in parallel.

BTX

For information 800-272-2775

www.btxonline.com

Electronically submit your new product description or product literature information! Go to www.sciencemag.org/products/newproducts.dtl for more information.

Newly offered instrumentation, apparatus, and laboratory materials of interest to researchers in all disciplines in academic, industrial, and governmental organizations are featured in this space. Emphasis is given to purpose, chief characteristics, and availability of products and materials. Endorsement by *Science* or AAAS of any products or materials mentioned is not implied. Additional information may be obtained from the manufacturer or supplier.

Science Careers Classified Advertising



We've got **Careers** down to a **Science**.

For full advertising details, go to
www.sciencecareers.org and click on
For Advertisers, or call one of our representatives.

United States & Canada

E-mail: advertise@sciencecareers.org
Fax: 202-289-6742

IAN KING

Recruitment Sales Manager/
Industry - US & Canada
Phone: 202-326-6528

ALEXIS FLEMING

Northeast Academic
Phone: 202-326-6578

TINA BURKS

Southeast Academic
Phone: 202-326-6577

DARYL ANDERSON

Midwest/Canada Academic
Phone: 202-326-6543

NICHOLAS HINTIBIDZE

West Academic
Phone: 202-326-6533

Europe & International

E-mail: ads@science-int.co.uk
Fax: +44 (0) 1223 326532

TRACY HOLMES Sales Manager

Phone: +44 (0) 1223 326525

ALEX PALMER

Phone: +44 (0) 1223 326527

ALESSANDRA SORGENTE

Phone: +44 (0) 1223 326529

MARIUM HUDDA

Phone: +44 (0) 1223 326517

LOUISE MOORE

Phone: +44 (0) 1223 326528

To subscribe to Science:

In US/Canada call 202-326-6417 or 1-800-731-4939
In the rest of the world call +44 (0) 1223-326-515

Science makes every effort to screen its ads for offensive and/or discriminatory language in accordance with US and non-US law. Since we are an international journal, you may see ads from non-US countries that request applications from specific demographic groups. Since US law does not apply to other countries we try to accommodate recruiting practices of other countries. However, we encourage our readers to alert us to any ads that they feel are discriminatory or offensive.

Science Careers

From the journal *Science*



POSITIONS OPEN

FACULTY POSITION in TERRESTRIAL BIOGEOCHEMISTRY

The Appalachian Laboratory (AL) of the University of Maryland Center for Environmental Science (UMCES) invites applications for a full-time faculty position in terrestrial biogeochemistry at open rank. We seek to hire an outstanding researcher with interests in the following: carbon sequestration by soils, forest nutrient transformations, and effects of land use change and ecosystem disturbances on elemental cycles in multi-use landscapes. The successful candidate must have a Ph.D. and bring a vigorous, sustainable research program with a strong empirical component in an area of terrestrial biogeochemistry that complements current AL strengths in terrestrial and aquatic ecology, landscape and watershed ecology, and remote sensing. AL has excellent research facilities, including plant/soil laboratories with state-of-the-art analytical instrumentation, growth chambers, and a greenhouse. Collaborative interdisciplinary and synthesis activities with clear management and policy relevance are strongly encouraged within AL and among the three UMCES laboratories. The main responsibility of this position is research. UMCES faculty participate in graduate education, outreach, and application of basic science to regional (e.g., restoration of Chesapeake Bay) and global (e.g., land use and climate change) environmental problems.

Applicants should send curriculum vitae; statement of research interests, including a brief discussion of how the applicant's research could complement ongoing research at AL/UMCES; selected reprints; and list of four references (name, title, mailing address, telephone, fax, and e-mail address) to: **Terrestrial Biogeochemistry Search Committee, Appalachian Laboratory, University of Maryland Center for Environmental Science, 301 Braddock Road, Frostburg, MD 21532**. Review of applications will begin on February 1, 2008. Information about AL and UMCES can be found at websites: <http://www.al.umces.edu/> and <http://www.umces.edu/>. UMCES is an Affirmative Action/Equal Opportunity Employer. Women and minorities are strongly encouraged to apply.

FACULTY POSITIONS Human Gross Anatomy

The Department of Cell Biology and Genetics of the University of North Texas Health Science Center at Fort Worth invites applications for human gross anatomy positions with teaching responsibilities in one or more of the following areas: medical human gross anatomy (cadaver based), neuroanatomy, and/or embryology. Candidates at all ranks are encouraged to apply. The successful applicant(s) must have a Ph.D., M.D., D.O., or equivalent degree and experience in teaching a clinically oriented human anatomy with cadaver dissection. The anatomical sciences at UNTHSC are team taught, and the applicant will be expected to contribute to both lecture and laboratory instruction. Other teaching responsibilities may include lecture and laboratory instruction in the prosection-based Physician Assistant (PA) Human Anatomy Program and a new Physical Therapy Program. Current research funding is not a requirement; however, candidates will be expected to develop a sustainable research program in clinical human anatomy, cell biology, anatomical education, and/or science educational outreach programs. Competitive salary and generous startup packages are provided. Consideration of applications will start immediately and the positions will remain open until suitable candidates are selected. Candidates must apply by submitting their curriculum vitae through the human resources online applicant tracking system at website: <http://www.unthscjobs.com>, along with a letter of interest, summary of past research accomplishments, future research plans, current funding, and teaching philosophy. Three letters of reference should be mailed to: **Dr. Robert Wordinger, Professor and Chairman, Department of Cell Biology and Genetics, University of North Texas Health Science Center, 3500 Camp Bowie Boulevard, Fort Worth, TX 76107**.

The University of North Texas Health Science Center at Fort Worth is an Equal Employment Opportunity/Affirmative Action Institution.

POSITIONS OPEN

THE UNIVERSITY of TENNESSEE HEALTH SCIENCE CENTER

TENURE-TRACK FACULTY POSITIONS The Department of Molecular Sciences College of Medicine, University of Tennessee Health Science Center, Memphis

The University of Tennessee Health Science Center Department of Molecular Sciences seeks two full-time tenure-track faculty at the JUNIOR or SENIOR level with basic or translational research experience investigating aspects of molecular pathogenesis of infections, vaccine development, emerging infections and select agents, genetics of host-pathogen interactions, and antimicrobial resistance. We seek to expand our strong interdisciplinary group of basic and clinical scientists as we integrate additional research programs into our campuswide clinical and translational research programs and new Regional Biocontainment Laboratory. Core campus resources include extensive mouse genomics and informatics, Molecular Resource Center, good manufacturing practice facilities, and BSL-3 suites for high throughput screening, small animal imaging, and microscopy. Adjunct appointment in the appropriate clinical departments and collaboration with the V.A. Hospital and St. Jude Children's Research Hospital are encouraged. Applicants must have a Ph.D., M.D., or D.V.M. with an established reputation in one of the above areas of research.

Successful candidates will be responsible for developing and maintaining an extramurally funded, independent research program, and contribute to graduate and professional student teaching. Interested applicants should send a letter of interest, brief description of research accomplishments, short summary of future research plans, and curriculum vitae, and arrange to have three letters of reference sent to: **Dr. Lorraine Albritton, Chair of the Search Committee, Department of Molecular Sciences, The University of Tennessee Health Science Center, 858 Madison Avenue, Memphis, TN 38163, or e-mail: lalbritt@utmem.edu**. Review of applications will begin immediately and continue until all positions are filled. For additional information, see website: http://www.utmem.edu/molecular_sciences. The University of Tennessee is an Equal Opportunity/Affirmative Action/Title VI/Title IX/Section 504/ADA/ADEA Employer. Women and minorities are encouraged to apply.

RESEARCH ASSISTANT PROFESSOR

The Department of Biological Sciences at the University of Illinois at Chicago (UIC) invites applications for a nontenure-track position as a Research Assistant Professor. Applicants must possess a Ph.D. and at least four years of postdoctoral training in the area of intracellular trafficking. Experience with DNA, protein, genetic, and cell-biological techniques in yeast is essential. Send curriculum vitae, brief summary of research experience, and three reference letters to: **Ms. Stephanie Davis, e-mail: sydavis@uic.edu or University of Illinois at Chicago, Biological Sciences, 845 W. Taylor Street, M/C 066, Chicago, IL 60607** by February 8, 2008. UIC is an Affirmative Action/Equal Opportunity Employer.

POSTDOCTORAL POSITION available at the Chicago Medical School of Rosalind Franklin University to investigate cell and molecular biology of muscle fiber type development, particularly focusing on mechanisms of signal transduction and gene regulation. Must have Ph.D. in cellular biology and/or molecular biology. Experience in protein expression systems, mutagenesis, proteomics, cell culture, immunoprecipitation, and calcium imaging is desired. Send curriculum vitae to **Joseph DiMario, Ph.D. at e-mail: joseph.dimario@rosalindfranklin.edu**. RFU is an Equal Opportunity and Affirmative Action Employer.

The Pennsylvania State University will recruit and hire at least 25 new tenure-track faculty members in energy science, engineering, and policy during the next 3 years. This is part of an initiative to enhance an already vigorous program of environmental and energy research and education at Penn State that includes strategic alliances with major energy companies and the Commonwealth of Pennsylvania. The first 9 positions target coal-derived fuels, bioenergy, and carbon sequestration.

Applications at the Assistant/Associate Professor level are sought, but appointments to senior ranks will be considered for qualified candidates. Most positions will be co-funded by the participating academic departments and by the Penn State Institutes of Energy and the Environment (PSIEE). For more details please see www.psiee.psu.edu/open_positions.asp. Applications are hereby solicited for the first nine positions.

COAL-DERIVED FUELS:

Catalysis for Efficient Hydrocarbon Conversion—Friederich G. Helfferich Professorship in Chemical Engineering

The Department of Chemical Engineering (www.che.psu.edu) is seeking a candidate with research interests in catalysis or reaction engineering as applied to efficient hydrocarbon processing. The applicant will become the first holder of the Friederich G. Helfferich Professorship in Chemical Engineering, an endowed position that provides unrestricted annual support. Applicants will be considered at all ranks. The successful applicant is expected to develop and maintain a research program leading to national and international recognition and to teach at the undergraduate and graduate levels. Candidates must have a Ph.D. in Chemical Engineering or in a closely related field. Contact: Kristen Fichthorn at fichthorn@psu.edu.

Coal Conversion to Liquids and Molecular Modeling of Coal Structure and Reactivity (2 positions)

The Department of Energy and Mineral Engineering (EME) (www.emc.psu.edu) is seeking two candidates with strong research interests in the structure-reactivity relationships that affect the conversion of coal to liquids and gases. These two positions are part of Penn State's new Clean Carbon Energy Initiative. The candidates are expected to establish a vigorous sponsored research program and have the ability to collaborate effectively on research in related areas with faculty members in EME and those associated with the PSIEE. EME is home to Penn State's degree programs in Energy Engineering, Environmental Systems Engineering, Mining Engineering, Petroleum and Natural Gas Engineering, and Energy Business and Finance. Successful candidates are expected to develop a strong record in teaching undergraduate and graduate courses in Energy Engineering and related degree programs. Requirements include a doctoral degree in a related field. Contact: Joan Andrews at jxa1@psu.edu.

Fuel Flexible Combustion of Coal Derived Fuels

The Department of Mechanical and Nuclear Engineering (www.mne.psu.edu) is seeking a candidate with strong research and teaching interests in combustion science and technology specifically related to coal-derived fuels. The candidate is expected to establish a vigorous sponsored research program, collaborate effectively on research in related areas, and develop a strong record in teaching undergraduate and graduate courses in Mechanical Engineering and related degree programs. Penn State's Mechanical Engineering Undergraduate and Graduate Program's are currently 12th and 15th, respectively, in the U.S. News and World Report rankings. Requirements include a doctoral degree in mechanical engineering or a related field. Contact: Domenic Santavicca at das8@psu.edu.

BIOENERGY:

Biomass Energy Economics and Policy

The Department of Agricultural Economics and Rural Sociology (www.aers.psu.edu) is seeking a candidate with research interests in spatially explicit modeling and the interaction between the environment and economy as mediated through land use and landscape. The successful candidate will join a multi-college team of economists and other scientists working on issues of energy and environment, and will be expected to work with interdisciplinary teams to conduct research and seek external

funding in areas such as the economics of biomass energy, modeling of the environmental impacts of biomass energy development, land use change, and land use policy. Contact: Jim Shortle at jshortle@psu.edu.

Enzymology, Transcriptional Control, or Systems Biology of Cellulosic Feedstocks

The Department of Biochemistry and Molecular Biology (www.bmb.psu.edu) is seeking a candidate with research interests in (a) enzymatic mechanisms for the syntheses and transferases involved in formation of plant cell wall polymers; (b) transcription factors regulating cell wall synthesis pathways; or (c) understanding how cell wall formation works as an integrated system. The successful candidate is expected to maintain a vigorous, externally funded research program. Access to graduate students is also available through several interdisciplinary programs under the Huck Institutes of the Life Sciences (www.huck.psu.edu). Review of applications will begin February 15, 2008 and will continue until the position is filled. Contact: Nancy Wilson at njw12@psu.edu.

Synthetic Biology Engineer

The Department of Agricultural and Biological Engineering (www.abe.psu.edu) is seeking a candidate that will apply engineering paradigms of design, fabrication, and system synthesis to biological science with particular emphasis directed toward renewable biomass energy. The successful candidate is expected to collaborate with biological scientists and biological engineers; to develop an internationally recognized research program with substantial external funding; and to develop and teach undergraduate and graduate courses on synthetic biology engineering principles and applications as well as to enhance several existing biological engineering courses. Requirements include a doctoral degree in a related field and at least one engineering degree (B.S., M.S., Ph.D.). Contact: Paul Heinemann at hzh@enr.psu.edu.

CARBON SEQUESTRATION:

Geologic Carbon Sequestration (2 positions)

The Department of Geosciences (www.geosc.psu.edu) and the Department of Energy and Mineral Engineering (www.emc.psu.edu) are seeking two candidates whose research falls into one or more of the challenging areas of engineering and geoscience associated with the introduction and fates of carbon-bearing fluids in the subsurface environment: (1) Basin Analysis and Modeling, where the development of process models for the stratal architecture, sedimentary facies, and stratigraphic stacking patterns is needed to define and characterize sequestration targets; (2) Formation Characterization and Imaging, where advances in 4D formation imaging are needed for monitoring and performance assessment of CO₂ storage; and (3) Fluid-Rock Interactions, where effective sequestration will be promoted by characterization and modeling fluid trap and seal evolution, and process-based understanding of the transmission, transformation, and trapping of fluid and solid components within the subsurface. Outstanding candidates who creatively apply theoretical, observational, and/or experimental approaches are encouraged to apply. Applicants should have a doctoral degree in petroleum engineering or geosciences and demonstrate a distinguished record of scholarship and potential for developing a vigorous externally funded research program. They are expected to contribute to core teaching in geosciences or petroleum engineering. Contact: Teresa Craig at tcraig@geosc.psu.edu.



UNIVERSITY OF FLORIDA

Department Chair Department of Molecular Genetics and Microbiology College of Medicine

The University of Florida's College of Medicine invites applications and nominations for the position of Chair in the Department of Molecular Genetics and Microbiology (www.mgm.ufl.edu). The department is active in both teaching and research missions in the college with 24 full-time faculty members whose research interests encompass all aspects of genetics and microbiology, with high levels of NIH funding, and a commitment to interdisciplinary research. As such, the department is directly involved in a campus-wide initiative to develop genetics and microbiology into major research areas at the University of Florida. The recent construction of a 280,000 sq. ft. Cancer and Genetics Research Building supporting the Genetics Institute (www.ufgi.ufl.edu) and the Cancer Center (www.ufcc.ufl.edu), as well as the planned construction of the UF Emerging Pathogens Institute Building (100,000 sq. ft.) to support the Emerging Pathogens Initiative (www.epi.ufl.edu) are components of these new initiatives. Department faculty currently participate in all three initiatives, which allows for further strengthening of an already strong department.

The successful candidate will have an M.D., Ph.D. or M.D./Ph.D. degree. We seek an accomplished scholar with a distinguished record of research, international recognition, leadership and administrative skills. The major responsibilities of the department chair are to promote the individual scholarship of the faculty and students in the department, provide leadership in articulating the department's vision to enhance the research and teaching programs in the department, and to work closely with institute and center directors to promote academic excellence. This is a full-time, tenure-accruing faculty appointment at the rank of Associate Professor or full Professor.

Applicants should provide a letter of application that incorporates a statement of vision for future departmental growth and direction, curriculum vitae, and the names of three references to: **Stephen P. Sugrue, Ph.D., Chair of the Search Committee, University of Florida, PO Box 100235, Gainesville, FL 32610-0235** or by email to: mgmchairsearch@health.ufl.edu. Applicants also may apply online at <https://jobs.ufl.edu> referencing requisition number 0704504. Nominations should be forwarded to Stephen P. Sugrue, Ph.D. Salary is negotiable and will be commensurate with experience. The review of applicants will begin on **March 3, 2008**, and will continue until the position is filled.

The University of Florida is an Equal Opportunity Institution dedicated to building a broadly diverse and inclusive faculty and staff. Minorities, women and those from other underserved groups are encouraged to apply.

HARVARD UNIVERSITY DEPARTMENT OF MOLECULAR AND CELLULAR BIOLOGY, HARVARD ORIGINS OF LIFE INITIATIVE

The Department of Molecular and Cellular Biology and the Harvard Origins of Life Initiative invite applications for a tenure-track faculty position in molecular biology investigating pathways from simple molecules to life. This newly created position is part of a broad inter-faculty effort at Harvard University to develop interdisciplinary study of the early evolution of life.

The tenure-track Assistant or Associate Professor faculty member will reside in the Department of Molecular and Cellular Biology and become a core faculty member of the Prebiotic Chemistry facility in the Origins of Life Initiative. We seek outstanding candidates with experimental, theoretical or combined research interests and teaching experience in the molecular biology of the emergence of life. We particularly encourage applications from women and minorities.

Applications should include a CV; names, addresses and e-mail of three to five referees; and a statement of research and teaching interests. Review of applications will begin on **February 22, 2008**. Submit applications to <http://www.mcb.harvard.edu/Jobs/Faculty>. For information contact: **J. Blackbourn/ MCB-HOLI Search Committee, juliab@mcb.harvard.edu**, Department of Molecular and Cellular Biology Harvard University.

Harvard University is an Affirmative Action/ Equal Opportunity Employer.



CHAIR

DEPARTMENT OF CELL BIOLOGY AND PHYSIOLOGY UNIVERSITY OF PITTSBURGH SCHOOL OF MEDICINE

The University of Pittsburgh School of Medicine is seeking a chair for the Department of Cell Biology and Physiology. The Department comprises 22 tenure/tenure-stream faculty with a research focus on cell polarity and the trafficking of proteins and lipids, on the function and dysfunction of ion channels, on reproductive biology, and on signal transduction in diabetes and metabolism. The successful candidate must demonstrate an outstanding record of scholarship commensurate with appointment at the rank of Full Professor with tenure. An outstanding startup package has already been committed for this position, and the person who holds this position will occupy the fully endowed Richard King Mellon Chair in Cell Biology and Physiology.

The new chair will lead a significant expansion of the department and will benefit from interactions with the Center for Biological Imaging and the University of Pittsburgh Cancer Institute, and the recently established Clinical and Translational Science Institute and Drug Discovery Institute, as well as with other research units within the School of Medicine. The University of Pittsburgh School of Medicine is enjoying unparalleled growth in its research, clinical, and academic missions. The University is currently ranked 7th among educational and research institutions in NIH funding and has doubled its NIH support in the last 10 years.

Please send curriculum vitae and bibliography to the head of the CBP Chair Search Committee (**Jeffrey L. Brodsky, Ph.D.**) at: jbrodsky@pitt.edu.

The University of Pittsburgh is an Affirmative Action, Equal Opportunity Employer. Women and members of minority groups under-represented in academia are especially encouraged to apply.



PROGRAM OFFICER, PHYSICAL CHEMISTRY

The Office of Naval Research is seeking a qualified individual to manage sponsored basic/applied research, and advanced development programs and projects in the broad area of physical chemistry. The sponsored efforts are conducted principally at U.S. universities and industry or Federal laboratories. This is a Federal Civil Service position at the GS-14/15 level (\$97,093 - \$148,477) depending on individual qualifications.

The position requires knowledge and experience in the fundamental theories, concepts, and current state-of-the-art research and/or technology development in the area of physical chemistry, including, but not limited to, first principle understanding of complex phenomena; characterization, understanding and simulation of the properties and reactions that are unique to surfaces and interfaces; and emerging computational tools and experimental techniques, including in-situ sensing.

For information on qualifications and how to apply, see ONR's Job Announcements at our website <http://www.onr.navy.mil/hr>. Applications must be submitted by the date noted in the job announcement. For technical information contact us at hrdeptjobs@onr.navy.mil.

U.S. CITIZENSHIP REQUIRED • AN EQUAL OPPORTUNITY EMPLOYER



DEPARTMENT OF HEALTH AND HUMAN SERVICES
NATIONAL INSTITUTES OF HEALTH
OFFICE OF THE DIRECTOR
OFFICE OF PORTFOLIO ANALYSIS AND STRATEGIC INITIATIVES
DIVISION OF RESOURCE DEVELOPMENT AND ANALYSIS



The Office of the Director, National Institutes of Health (NIH) in Bethesda, Maryland, is seeking a Director of the Division of Resource Development and Analysis (DRDA) within the Office of Portfolio Analysis and Strategic Initiatives (OPASI). If you are an exceptional candidate with an M.D. and/or Ph.D., we encourage your application.

The OPASI's primary objective is to develop: a transparent process of planning and priority-setting characterized by a defined scope of review with broad input from the scientific community and the public; valid and reliable information resources and tools, including uniform disease coding and accurate, current and comprehensive information on burden of disease; an institutionalized process of regularly scheduled evaluations based on current best practices; the ability to weigh scientific opportunity against public health urgency; a method of assessing outcomes to enhance accountability; and a system for identifying areas of scientific and health improvement opportunities and supporting regular trans-NIH scientific planning and initiatives.

As the DRDA Director, you will be responsible for employing resources (databases, analytic tools, and methodologies) and developing specifications for new resources, when needed, in order to conduct assessments based on NIH-owned and other databases in support of portfolio analyses and priority setting in scientific areas of interest across NIH.

Salary is commensurate with experience and includes a full benefits package. A detailed vacancy announcement with the mandatory qualifications and application procedures can be obtained on **USAJOBS** at www.usajobs.gov (announcement number **OD-08-236976-T42**) and the NIH Web Site at <http://www.jobs.nih.gov>. Questions on the application procedures may be addressed to Brian Harper on 301-594-5332. Applications must be received by midnight eastern standard time on **February 14, 2008**.

This position is subject to a background investigation.

DHHS and NIH are Equal Opportunity Employers

Division Director, Experimental Hematology and Cancer Biology



change the outcome®

The Division of Experimental Hematology and Cancer Biology at Cincinnati Children's Hospital Medical Center is initiating a search for an outstanding scholar and leader. The successful applicant may hold an MD, PhD or combined MD/PhD degrees. S/he may have a translational or basic focus in cancer or hematopoiesis, including but not limited to stem cells. Very significant resources are available to build a joint cancer program with the University of Cincinnati. The successful candidate will be expected to maintain and advance outstanding scientific programs, and lead a collaborative, translationally-oriented division with extensive external funding.

The division currently houses 16 faculty members with strength in hematopoiesis, neuro-oncology, signaling and gene therapy. The division maintains outstanding cores for vector development, flow cytometry, mouse

modeling, and pre-clinical translational laboratories, and is moving to a new research building in January 2008. Cincinnati Children's is currently ranked second in NIH funding for Departments of Pediatrics and in the top five in Pediatric Cancer Care. Ample laboratory space in the new building and a generous multi-year start-up package will be provided.

Applications should be emailed to:
Jeff.Robbins@cchmc.org



Cincinnati Children's Hospital Medical Center is an Affirmative Action/Equal Opportunity Institution. Women and minorities are encouraged to apply.

Visit our website at
www.cincinnatichildrens.org



Institute for Diabetes, Obesity and Metabolism/Department of Radiology

The Institute for Diabetes, Obesity and Metabolism (IDOM) and the Department of Radiology at the University of Pennsylvania School of Medicine seek candidates for an Assistant or Associate Professor position in the tenure track. Rank will be commensurate with experience. Responsibilities include doing basic or translational research using new spectroscopic technologies, particularly nuclear magnetic resonance, to approach scientific problems relevant to normal metabolism and/or disorders such as the metabolic syndrome, diabetes or obesity. The successful candidate will complement and synergize with existing strengths and will receive an excellent start-up package including newly renovated space in a superb scientific environment. Applicants must have an M.D. or Ph.D. or M.D./Ph.D. degree and have demonstrated excellent qualifications in Education and Research. The faculty appointment will be in Radiology or an appropriate department in the School of Medicine.

Development of an independently funded research program must be demonstrated. To learn more about IDOM and Radiology at Penn, visit our websites: <http://www.med.upenn.edu/idom/> and <http://www.uphs.upenn.edu/radiology/>

Please submit a cover letter, curriculum vitae, a statement of research interests and 3 reference letters to: IDOM@mail.med.upenn.edu.

The University of Pennsylvania is an Equal Opportunity, Affirmative Action Employer. Women and minority candidates are strongly encouraged to apply.

THE SAINSBURY LABORATORY

GROUP LEADER POSITION

Plant and Microbial Sciences

The Sainsbury Laboratory (<http://www.tsl.ac.uk>) invites applications for a group leader position in plant and microbial sciences. The successful candidate will develop a research program in any area of biology that is relevant to the laboratory objective of making fundamental discoveries in the science of plant-microbe interactions and is complementary to the activities of the current group leaders. We encourage applications from scientists who seek to "cross over" to plants and plant-associated microbes, bringing with them new expertise and approaches to fundamental biological problems.

Currently, The Sainsbury Laboratory hosts six research groups funded by the Gatsby Charitable Foundation and linked with the University of East Anglia and the John Innes Centre. The Group Leader position is a 100% research position with no formal teaching duties and with minimal administrative responsibilities. Each group receives an allocation of ~£1.6M over six years in addition to an internationally competitive group leader salary and shared resources for large equipment.

Review of applications will start February 1, 2008. Applications will be accepted until a suitable candidate is found. Informal enquiries should be directed to Sophien Kamoun (sophien.kamoun@tsl.ac.uk). Please email formal applications with a CV, names of 3 referees and a 2 page statement of research interests to hr@tsl.ac.uk. Please quote reference number HoL04/2007.



Deputy Director



Lawrence Berkeley National Laboratory's Molecular Foundry Opened March 24, 2006.

Lawrence Berkeley National Laboratory (LBNL) is a world leader in science and engineering research, with 11 Nobel Prize recipients over the past 75 years, and 59 present members of the National Academy of Sciences. LBNL conducts unclassified research across a wide range of scientific disciplines and hosts four national user facilities. www.lbl.gov

LBNL is seeking an internationally recognized scientific leader to serve as Deputy Director. The Deputy Director works to develop the strategic vision of LBNL and assists in all aspects of the specific implementation of this vision. The Deputy will be principal partner and counsel to the Director in making decisions on the balance of programs within the laboratory; attending reviews of existing programs; and approving the seeding of new programs and the scaling back of others. The candidate must possess a broad scientific perspective and may have an active research program; a track record of academic and management success; and the ability to substitute for the Laboratory Director providing leadership to a multidisciplinary group of scientists.

For fastest consideration, apply online at: <http://jobs.lbl.gov>, select "Search Jobs", and enter 21297 in the keyword search field. Enter "Science" as your source.

LBNL is an Affirmative Action/Equal Opportunity Employer committed to the development of a diverse workforce.

TENURE TRACK FACULTY POSITIONS

Texas Tech University Health Sciences Center School of Pharmacy

Applications are invited for several tenure-track faculty positions at the Assistant/Associate/Full Professor rank in the Department of Pharmaceutical Sciences of Texas Tech University Health Sciences Center (TTUHSC). Candidates are sought in the areas of pharmacology, drug discovery, development and delivery, signal transduction, and/or pharmacogenomics. The Department comprises 22 full-time faculty with 40 graduate students. Growth over the next 4 years is expected to take the Department to 30 faculty. A new 48,000 sq ft research facility is under construction to supplement the current >100,000 sq. ft. facility adjacent to the Amarillo campus of the TTUHSC School of Medicine and the Harrington Cancer Center. Collaborations are available within the University through funded research institutes/centers in aging, women's health, cardiovascular disease, stroke and cancer. Amarillo is a town of ~200,000 on the high plains of Texas with excellent opportunities for cultural activities, family life, and outdoor sports. For further information, visit our website: <http://www.ttuhsu.edu/sop/PharmSci/>.

Applicants must have an earned doctoral degree in a biomedical or pharmaceutical science with relevant postdoctoral experience. In addition to maintaining an extramurally funded research program, the successful candidate will teach and mentor students in the professional (Pharm.D) and graduate (Ph.D./M.S.) programs of the University. Competitive start-up packages, incentives and lab space are available. Please submit a curriculum vitae, a summary of research and teaching interests and names and addresses of three references online at <http://jobs.texastech.edu> (Job Requisition # 75707). Applications will be reviewed beginning February 15, 2008. For questions, contact the search committee chair, Dr. Margaret Weis, Texas Tech University School of Pharmacy, 1300 Coulter, Amarillo, TX 79106; Email: margaret.weis@ttuhsc.edu; Fax: 806-356-4034.

TTUHSC is an Equal Opportunity/Affirmative Action Institution. Minorities and Women are encouraged to apply.

nature chemistry

Associate Editors

The Nature Publishing Group is pleased to announce the launch of *Nature Chemistry* in 2009. Following the success of *Nature Materials*, *Nature Chemical Biology* and *Nature Physics*, and given the strength of the parent journal *Nature*, we fully expect *Nature Chemistry* to seize the commanding heights of the chemistry-publishing landscape.

Alongside the highest-quality original research, *Nature Chemistry* will cover news, commentary and analysis from and for the chemistry community, as well as striving to develop a voice that chemists care about.

As part of this exciting new publishing venture, we are now seeking three Associate Editors for *Nature Chemistry*, to be based in our London, Boston and Tokyo offices.


Applicants should have a PhD in a chemistry-related discipline, with demonstrable research achievements. Although postdoctoral experience is preferred (not required), emphasis will be placed on broadly trained applicants with a good knowledge of the chemistry community. Key elements of the position include the selection of manuscripts for publication, and commissioning, editing and writing other content for the journal. Candidates who wish to be considered for the role in our Japan office must demonstrate a good understanding of the East Asian research communities (in particular Japan, China and Korea) as well as being fluent in English and preferably an Asian language (Japanese, Chinese or Korean).

These are demanding and extremely stimulating roles, which call for a keen interest in the practice and communication of science. The successful candidates will, therefore, be dynamic, motivated and outgoing, and must possess excellent interpersonal skills. The salary and benefits, will be competitive, reflecting the critical importance and responsibilities of each position.

Applicants should send a CV (including their class of degree and a brief account of their research and other relevant experience), a News & View style piece (no more than 500 words) on a recent paper from the chemical literature, and a brief cover letter explaining their interest in the post, salary expectations, and indicating whether they wish to be considered for a position in London, Boston or Tokyo.

To apply please send your CV and covering letter, quoting reference number NPG/LON/797 to Denise Pitter at londonrecruitment@macmillan.co.uk

Closing date: 31st January 2008.

nature publishing group 

THE UNIVERSITY OF SOUTHERN CALIFORNIA

The Saban Research Institute



ChildrensHospitalLosAngeles
International Center in Pediatrics

DEVELOPMENTAL
NEUROBIOLOGY



The Saban Research Institute of Childrens Hospital Los Angeles and Keck School of Medicine, University of Southern California invites applications for a tenure-track position of Assistant Professor in the Department of Pediatrics, with the possibility of a joint appointment in the USC College of Letters, Arts and Sciences. The position will be based in the newly constructed Saban Research Institute building and will include membership in the University wide USC Neuroscience Program. Qualifications include a Ph.D., or M.D./Ph.D. degrees, and appropriate postdoctoral experience. We are particularly interested in applicants who are applying molecular genetic approaches to fundamental problems in neural circuit formation, but individuals studying other aspects of nervous system development are also encouraged to apply. The successful candidate is expected to establish and maintain an extramurally funded research program with international visibility, and contribute to graduate level courses in developmental neurobiology. Competitive start up funds and state-of-the-art research space will be provided. Applicants should send a copy of their CV, a statement of research interests, and the names and contact information of three references to: **Richard Simerly, Ph.D. Director, Neuroscience Program, The Saban Research Institute, Childrens Hospital Los Angeles, Keck School of Medicine, University of Southern California, 4650 W. Sunset Blvd., MS #135, Los Angeles, CA 90027.**

The University of Southern California and Childrens Hospital Los Angeles are AA/EOE employers.



From physics
to nutrition

For careers in science, turn to *Science*
www.ScienceCareers.org

- Search Jobs
 - Career Advice
 - Job Alerts
 - Resume/CV Database
 - Career Forum
 - Graduate Programs
- All features FREE to job seekers.*

Science Careers

From the journal *Science* 



Weill Cornell Medical College in Qatar



BIOLOGIST FACULTY POSITION

WCMC-Q seeks candidates for a faculty position with major responsibility for the teaching of an introductory biology sequence of two courses in a premedical program leading to entry to the medical school. Another faculty member conducts a complementary laboratory course sequence. Beyond the principal teaching obligation a successful applicant is expected to participate in advising, committee work, and the academic life of WCMC-Q. Research space is available as well as research funding support. Details regarding the WCMC-Q program and facilities can be accessed at:

www.qatar-med.cornell.edu

Candidates should hold a Ph.D. degree and possess demonstrable teaching skills as well as experience and training in research. Candidates must be willing to relocate to Doha, Qatar for the duration of the appointment. Academic rank and salary are commensurate with training and experience and are accompanied by a competitive foreign-service benefits package. Qualified applicants should submit a curriculum vitae and a letter of interest outlining their teaching and research experience to:

facultyrecruit@qatar-med.cornell.edu

***Please quote Faculty Search #08-sci-B01 on all correspondence**

Cornell University is an equal opportunity, affirmative action educator and employer.

The screening of applications will begin immediately and continue until suitable candidates are identified. Service is expected to begin in August 2008.

Please note, short-listed candidates will be asked to provide names of three references.

Department of Health and Human Services National Institutes of Health National Institute on Aging



Staff Scientist DNA Repair/Signal Transduction

The Intramural Research Program (IRP) of the National Institute on Aging (NIA), Baltimore, Maryland, is recruiting for a Staff Scientist position in the DNA Repair Unit of the Laboratory of Cellular and Molecular Biology (LCMB). This is a renewable position with an initial 5 year appointment for highly motivated individuals with a strong background and extensive experience in cellular and molecular biology. Specialized knowledge and expertise in the biochemistry of DNA damage and repair as well as signal transduction pathways is required. Experience with DNA repair techniques that are employed to examine human DNA repair capacity and to assess levels of oxidative DNA damage in human samples is desirable. The incumbent will have major roles in training staff and postdoctoral fellows and maintaining research continuity within the laboratory. A Ph.D. or equivalent degree is required.

Salary is commensurate with research experience and accomplishments. The salary range for a Staff Scientist is \$80,000 - \$162,371. A full Civil Service package of benefits (including retirement, health, life and long term care insurance, Thrift Savings Plan participation, etc.) is available. Additional information regarding the NIA IRP and the LCMB are available at the following websites: <http://www.grc.nia.nih.gov> and <http://www.grc.nia.nih.gov/branches/osd/2006factbook.pdf>.

To apply: Please send a cover letter, curriculum vitae, bibliography, statement of research interests, and three letters of recommendation to: **Peggy Grothe, Intramural Program Specialist; Office of the Scientific Director (Box 09); Vacancy # IRP-08-03; National Institute on Aging, 5600 Nathan Shock Drive, Baltimore, MD 21224-6825.** Applications must be received before **February 18, 2008**. If additional information is needed, please call **410-558-8012** or email: grothep@grc.nia.nih.gov.

DHHS and NIH are Equal Opportunity Employers.

The NIH is dedicated to building a diverse community in its training and employment programs.

NC STATE UNIVERSITY

North Carolina State University Announces Four Faculty Positions in Horticultural Science Located at the Fruit and Vegetable Science Institute in Kannapolis, NC

North Carolina State University and the College of Agriculture and Life Sciences (CAL S) recently established the NC State University Fruit and Vegetable Science Institute (FVSI) at the new North Carolina Research Campus (NCRC), a private-public venture, being built in Kannapolis, NC (near Charlotte). The goal of the FVSI is to conduct advanced multidisciplinary research to enhance the nutritional content of fruits and vegetables to improve human health; increase agricultural production and good agricultural practices leading to a sustainable food supply; and provide scientific ideas and technologies that will contribute to NC's economic growth. Other university programs based at the NCRC include UNC-Chapel Hill, UNC-Charlotte, UNC-Greensboro, NC A & T State University, and Duke University. The NCRC will provide unparalleled infrastructure for basic and applied research including the 300,000 ft² D.H. Murdock core support laboratory, technical support, and extensive greenhouse and field facilities. A team of world-class scientists will be located at the FVSI, with academic homes in CAL S departments in Raleigh, NC. As a part of this team, the Department of Horticultural Science is seeking to fill four positions (100% Research, 12 month – tenure track) at FVSI:

Two breeding positions: Leafy Vegetable Breeder – Assistant/Associate Professor (Position # 01-10-0715); Strawberry Breeder – Assistant/Associate Professor (Position # 01-10-0714): Develop superior cultivars that are adapted to NC production systems, with enhanced nutritional and nutraceutical properties, resistance to major production constraints, high yields, and extended postharvest shelf-life. Develop research programs to understand the genetic control and inheritance of important traits, and work within a team of a dozen or more principal investigators ranging from breeders to molecular geneticists and other faculty to develop molecular markers for trait selection and to fulfill the overall mission of FVSI.

Applied Molecular Geneticist for Fruit and Vegetable Cultivar Development – Assistant/Associate Professor (Position # 01-10-0712): Develop a molecular genetics and genomics research program in fruits and vegetables on traits that lead to the development of improved cultivars. Traits of interest may include bioactive phytochemical content and nutritional value, stability of health-promoting attributes pre- and postharvest, disease and pest resistance, maturity, adaptation and yield. Research topics will include development of tools and technologies for rapid cultivar development such as molecular markers and other appropriate molecular approaches, as well as functional and/or structural genomic studies of fruits and vegetables.

Postharvest Physiologist – Assistant/Associate/Full Professor (Position # 01-10-0713): Conduct translational research on the biochemical and molecular bases for ripening, senescence and quality changes of horticultural crops in the postharvest environment. The specific research area is flexible, but should focus on understanding the mechanisms that contribute to preserving full bioactive health benefits of fruits and vegetables pre- and postharvest with the ultimate goal of improving produce quality for the consumer.

The incumbents are expected to establish collaborative partnerships with faculty based at the NCRC, NC State University main campus in Raleigh and other research stations, as well as with other universities and the private sector; provide input to NC commodity industries; establish a rigorous, nationally recognized, extramurally funded research program; publish research results in relevant peer reviewed publications; and chair and serve on graduate student committees.

Applicants should apply online at <https://jobs.ncsu.edu> (refer to the appropriate position number). Attach a cover letter and CV to the online applicant profile, and include the names and contact information for at least three references. For more information, contact: **Dr. Julia Kornegay, Professor and Head, Department of Horticultural Science, Box 7609, NC State University, Raleigh, NC 27695-7609; Phone: 919-515-3131; Fax: 919-513-3191; Email: julia_kornegay@ncsu.edu.** Review of applications will begin **February 29, 2008**, and continue until an acceptable candidate is identified.

Minority candidates are encouraged to apply. NCSU is an EEO/AA Employer.

POSITIONS OPEN

AVIAN RESEARCH ECOLOGIST
U.S. Geological Survey's Patuxent
Wildlife Research Center

The U.S. Geological Survey's Patuxent Wildlife Research Center in Laurel, Maryland (website: <http://www.pwrc.usgs.gov/>) seeks a Research Ecologist with experience conducting research in avian biology, ecology, and conservation. The candidates' research interests may be broad but special consideration will be given to those with research interests that bridge population ecology, monitoring, and conservation biology. As lead investigator the Ecologist conducts original research that responds to regional and national conservation goals, primarily in support of Department of Interior agencies missions. Applications must be completed online at website: <http://www.usgs.gov/ohr/oars/>. Announcement ER-2008-0042 is open to all qualified U.S. citizens; announcement ER-2008-0043 is open to current and former Federal employees. Announcements will open on January 7, 2008, and close at midnight eastern standard time on February 19, 2008. Applications must be filled out completely and all supplemental materials, such as proof of education, must be submitted to be considered. Additional details regarding position and application are provided on the website. *The U.S. Geological Survey is an Equal Opportunity Employer.*

ASSISTANT or ASSOCIATE PROFESSOR, Genetics York College of the City University of New York (CUNY) invites applications for an Assistant or Associate Professor of Biology (tenure track) specializing in genetics and bioinformatics with a start date of September 1, 2008. Applicants should have a Ph.D. and postdoctoral experience, and interest and experience in teaching undergraduates. Instructional responsibilities will include genetics lecture and laboratory courses, a bioinformatics course, introductory biology, and nonmajor courses as needed. Faculty are expected to develop and maintain an externally funded research program involving undergraduates; participation in the CUNY Ph.D. program via the CUNY Graduate Center is also expected. This position is dependent on financial availability.

Applicants should submit a cover letter, curriculum vitae, three letters of recommendation, and brief statements of research plans and teaching philosophy to: **Dr. Louis Levinger, Department of Biology, 4E03, York College/CUNY, 94-20 Guy R. Brewer Boulevard, Jamaica, NY 11451.**

Visit the York College website: <http://www.york.cuny.edu> to discover more about our exciting programs and events. For information regarding this position, please see website: <http://york.cuny.edu/hr/jobs>; apply by the positions-specific deadline.

RESEARCH ASSOCIATE (ASSISTANT PROFESSOR)

The Section of Endocrinology, Diabetes, and Metabolism at the University of Chicago is seeking qualified applicants for a full-time Research Associate (Assistant Professor) position to participate in research on the molecular mechanism of pancreatic beta-cell function with a particular regard to the role of ion channels in control of insulin production and secretion, as well as beta-cell calcium regulation. The primary activity of an R.A. (Assistant Professor) is academic research in association with a faculty member or team. Qualified applicants are required to possess a Doctorate degree, have postdoctoral experience, and substantial experience conducting research on protein kinase phosphorylation signaling cascades related to regulation of ionic events in insulin secretion, gene expression, and advanced electrophysiologic and confocal cellular imaging techniques. Please send cover memo, curriculum vitae, and three letters of reference to: **Ann Leu, Section Administrator, Endocrinology, via e-mail: aleu@medicine.bsd.uchicago.edu.** *The University of Chicago is an Affirmative Action/Equal Opportunity Employer.*

POSITIONS OPEN



POSTDOCTORAL RESEARCH POSITIONS: IMMUNOLOGY and HOST-PATHOGEN INTERACTIONS
Department of Microbiology, Boston University
School of Medicine

We invite applications from talented researchers for Postdoctoral opportunities. Research in the Department focuses on the molecular mechanisms underlying microbial infection and the host immune response (see website: <http://www.bumc.bu.edu/microbiology>).

Thomas W. Geisbert (e-mail: geisbert@bu.edu). Pathogenesis of emerging viruses and development of rational countermeasures.

Suryaram Gummuru (e-mail: rgummuru@bu.edu). Role of dendritic cells in HIV pathogenesis.

Andrew J. Henderson (e-mail: hender@bu.edu). Cellular signals regulating HIV transcription.

Ann Marshak-Rothstein (e-mail: amrothst@bu.edu). Innate/adaptive immunity in animal models of systemic autoimmunity.

Barbara S. Nikolajczyk (e-mail: bnikol@bu.edu). Regulation of systemic inflammation in type 2 diabetes and inflammatory bowel disease.

Gregory A. Viglianti (e-mail: gviglian@bu.edu). Nuclear and toll-like receptor cross-regulation of HIV mucosal infection.

BUSM is an Affirmative Action/Equal Opportunity Employer.

The newly established Department of Genetics at the Scripps Research Institute (TRSI) is recruiting outstanding investigators (all levels) with the ability to establish and maintain a research program in the area of host resistance to infection. The Department offers newly renovated laboratory and office space on the La Jolla campus. Preference will be given to applicants with a strong publication record, imaginative approaches to understanding the molecular requirements for innate immunity in any species, and an ability to participate in a strongly interactive program of cutting-edge research. Applicants should send curriculum vitae and three letters of reference to the: **Search Committee, Department of Genetics, The Scripps Research Institute, 10550 N. Torrey Pines Road, La Jolla, CA 92037.** TSRI embraces diversity and recognizes it as being a key to our success. We believe in developing and maintaining a diverse workforce. *Equal Opportunity Employer/Minorities/Females/Persons with Disabilities/Veterans.*

ASSISTANT/ASSOCIATE PROFESSOR
Department of Pharmaceutical Sciences
The Feik School of Pharmacy
University of the Incarnate Word
San Antonio, Texas

Two 12-month, tenure-track faculty positions, one in pharmacology and one in medicinal chemistry, in the Department of Pharmaceutical Sciences; preferred start date is June 2008. Candidate for this position should have a Ph.D. in pharmacology or medicinal chemistry, teaching, and/or postdoctoral experience is preferred. The candidates will be expected to develop and teach the pharmacology/medicinal chemistry section of the integrated pharmacotherapy courses in the Pharm.D. Program.

See our website: <http://jobs.uiw.edu> for further information.

MEDICAL RESEARCHER sought to study the genetic basis of microcephaly. Requirements include M.D. with significant experience in pediatric neurology including ability to perform clinical analysis of research subjects, gene mapping, and cloning. Salary \$80,000 per year. Send resumes to: **Christina Venckus, Human Resources, Beth Israel Deaconess Medical Center, 330 Brookline Avenue, Boston, MA 02215.** *BIDMC is an Equal Opportunity/Affirmative Action Employer.*

POSITIONS OPEN

UNIVERSITY of CALIFORNIA, IRVINE
School of Medicine

POSTDOCTORAL RESEARCHER/SCHOLAR, University of California, Irvine Epilepsy Research Training Program and the Department of Anatomy and Neurobiology. The Multidisciplinary Postdoctoral Training Program in Epilepsy Research has multiple openings for nontenured, academic-term appointments as Postdoctoral Scholar. The Program supports diverse approaches to the understanding of the fundamental neurobiological processes leading to epilepsy and/or holding promise for its cure. Participating Laboratories include: **Tallie Z. Baram, Ph.D., M.D.:** neuroplasticity, mechanisms of epileptogenesis, febrile seizure models, hyperpolarization activated ion channels, and animal imaging; **Devin Binder, M.D.:** water transport and water channels in epilepsy, aquaporins, and optical imaging; **Steven Cramer, M.D.:** functional imaging and robotics for identification and cure of excitotoxic and ischemic insults; **Christine M. Gall, Ph.D.:** neurotrophins, integrins, and activity-dependent plasticity; **Alan L. Goldin, M.D., Ph.D.:** sodium channels, transgenic approaches, and electrophysiology; **Gary Lynch, Ph.D.:** regulation of excitability and synaptic function and plasticity; **Charles E. Ribak, Ph.D.:** granule cell plasticity and neuroanatomy; **Mick Rugg, Ph.D.:** functional imaging of learning and memory circuits in health and disease; **Ivan Soltesz, Ph.D.:** electrophysiology, computational neurobiology, interneurons, and inhibition; **Martin Smith, Ph.D.:** covel signaling-Agrin and neuronal excitability; **Oswald Steward, Ph.D.:** mechanisms of vulnerability to excitotoxicity; **John Weiss, M.D., Ph.D.:** excitotoxicity, calcium, and zinc trafficking. See website: <http://www.ucihs.uci.edu/epilepsyresearch/>.

These positions are funded by an NIH training grant (T-32); *eligible candidates must be U.S. citizens or noncitizen nationals or must be lawfully admitted for permanent residence.* An M.D. or Ph.D. degree is required, and M.D. qualified candidates, as well as minorities and women, are highly encouraged to apply. Salary is commensurate with experience and based on the Kirschstein-National Research Service Awards postdoctoral stipend levels for 2008. Candidates should submit resume and references to **e-mail: sara.johnson@uci.edu; Postdoctoral Search/ Epilepsy, c/o Department of Anatomy and Neurobiology, University of California, Irvine, Irvine, CA 92697-1275.** *The University of California, Irvine is an Equal Opportunity Employer committed to excellence through diversity.*

The Del E. Webb Center for Neuroscience, Aging, and Stem Cell Research (NASCR) of the Burnham Institute for Medical Research (BIMR) seeks independent investigators with strong research programs in stem cell and developmental biology, aging and neurodegenerative disorders, or cardiac and pancreatic/metabolic diseases. Applications using genetic model systems are particularly welcome. Individuals at any career level, including **JUNIOR INVESTIGATORS**, are encouraged to apply. BIMR offers an outstanding interdisciplinary and highly collaborative research environment, supported by a wide range of shared resources, including the La Jolla-Wide Interdisciplinary Neuroscience Center Core Facilities Grant funded by NIH. For more details visit our websites: <http://www.burnham.org/> and <http://www.lajollaneuroscience.org/>. Informal inquiries should be directed to appropriate **NASCR Center Program Directors** (contact information listed on the website). To apply, please submit curriculum vitae and research summary electronically by March 1, 2008 (mail to **e-mail: nascrecruit@burnham.org**). Candidates should arrange to have at least three letters of reference sent to this e-mail address (preferred) or by regular mail to: **Neuroscience, Aging, and Stem Cell Research Recruitment Committee, c/o Stuart A. Lipton, M.D., Ph.D., Scientific Director, NASCR Center, Burnham Institute for Medical Research, 10901 North Torrey Pines Road, La Jolla, CA 92037.** *Equal Opportunity Employer/Affirmative Action.*

POSITIONS OPEN

**INDUSTRIAL MICROBIOLOGIST
FACULTY POSITION
Colorado State University**

The Department of Microbiology, Immunology, and Pathology in conjunction with the Department of Chemical and Biological Engineering seeks applications for a nine-month, tenure-track faculty position at the ASSISTANT PROFESSOR level with research interests in industrial microbiology and bioprocess engineering. Candidates with expertise in these and closely related areas of research or that complement the University Superclusters in Infectious Diseases and Clean Energy are strongly encouraged to apply.

Further information is available at website: <http://www.cvms.colostate.edu/mip>. Candidates must have a Ph.D. (or equivalent degree), postdoctoral and/or industrial experience, the abilities to establish and sustain an independent research program, to participate effectively in undergraduate and graduate teaching, and to enhance the Department's commitment to diversity and multiculturalism through research, teaching, and/or service activities.

Applicants should submit electronically a letter expressing their interest and qualifications for the position including current curriculum vitae, brief (one page) statements of research and teaching experience and interests, and provide names and contact information for three references. Application materials should be sent to: **Industrial Microbiologist Search Committee, c/o Jeanette Fritzier (e-mail: jeanette.fritzler@colostate.edu).**

For full consideration, a complete application must be received by March 18, 2008.

CSU is Equal Employment Opportunity/Affirmative Action Employer.

**MOLECULAR DEVELOPMENTAL
GENETICIST
VISITING ASSISTANT PROFESSOR**

The Department of Biology, Hamilton College, invites applications for a two-year visiting Assistant Professorship, effective July 1, 2008. Ph.D. and teaching experience expected. The successful applicant will supervise senior thesis research, and teach: (1) genetics, (2) biochemistry, and additional lecture/laboratory course of the candidate's choosing, or an upper-level seminar and nonmajors course, as complements the Department's offerings. Support is available for research and conference travel. Send curriculum vitae, a statement about teaching, and names of three references to: **Herman K. Lehman, Chair, Department of Biology, Hamilton College, 198 College Hill Road, Clinton, NY 13323-1292.** Review of application materials will begin February 1, 2008, and continue until the position is filled. *Women and members of minority groups are encouraged to apply. Hamilton College is an Affirmative Action, Equal Opportunity Employer and is committed to diversity in all areas of the campus community.*

NEUROSCIENCE

Oberlin College invites applications for a one-year, noncontinuing position beginning July 1, 2008. Incumbent will teach two sections of introductory neuroscience laboratory and either two upper-level lecture courses with one accompanying laboratory, or one introductory course/seminar and one upper-level course with laboratory. Position open to all applicants, but candidates with expertise in developmental, molecular, or cognitive neuroscience encouraged to apply. Ph.D. required (in hand or expected by July 1, 2008).

Submit applications including curriculum vitae, three letters of recommendation, and transcripts by March 1, 2008, to: **Chair, Neuroscience Department, Oberlin College, Oberlin, OH 44074.** Applications may be reviewed until position filled. *Affirmative Action/Equal Opportunity Employer.*

POSITIONS OPEN

**POSTDOCTORAL POSITION
University of Pennsylvania
Philadelphia, Pennsylvania**

Description: Postdoctoral position is available in the Laboratory of **Dr. Marianthi Kiriakidou** at the Department of Medicine, University of Pennsylvania, Philadelphia, Pennsylvania. The research emphasis in the Laboratory is on understanding the biochemical and molecular mechanisms of microRNA mediated gene expression regulation and the regulatory role of microRNAs in the hematopoietic cells. Applicants should forward their resume and three references to:

**Marianthi Kiriakidou, M.D.
University of Pennsylvania
Department of Medicine
752 BRB II-III
421 Curie Boulevard
Philadelphia, PA 19104
E-mail: kiriakim@uphs.upenn.edu**

**CHAIR, DEPARTMENT of ANIMAL SCIENCE
The University of Vermont**

The University of Vermont seeks a Chair of the Department of Animal Science to lead the Department into the next decade. Candidates must have a doctoral degree in animal science or a related area, a nationally recognized research program consistent with a tenured academic appointment, and demonstrated leadership and administrative skills necessary to guide a large and academically diverse department within the College of Agriculture and Life Sciences.

Candidates must demonstrate a commitment to excellence in undergraduate and graduate education, and be willing to foster relationships within the Vermont dairy industry and with other stakeholders. Full information about the position can be found at website: <http://www.uvmjobs.com>.

Applications, including a letter describing the individual's qualifications for the position as described above, curriculum vitae (with research funding history and scholarly accomplishments), and names of five references (with addresses, telephone numbers and e-mail addresses), should be sent to:

**Dr. Jean Harvey-Berino, Chair
Search Committee for the Animal Science Chair
c/o Dean's Office
College of Agriculture and Life Sciences
The University of Vermont
Morrill Hall
Burlington, VT 05405
Telephone: 802-656-0137
E-mail: ascichairsearch@uvm.edu**

The University of Vermont is an Affirmative Action, Equal Opportunity Employer. Women and minority candidates are especially encouraged to apply.

Two fully funded **POSTDOCTORAL RESEARCH ASSOCIATE POSITIONS** are open to study the role of nucleolar oncogenes and tumor suppressors in cell growth. These studies are being carried out in a newly renovated laboratory within the recently established Molecular Oncology Program. The Laboratory consists of several highly motivated and collaborative postdoctoral fellows and graduate and undergraduate students with daily personal contact with the principal investigator. Qualified applicants should hold a recent Ph.D., M.D., or M.D./Ph.D. and be committed to a career in cancer research. Candidates with experience in mouse models, cancer biology, and molecular and cell biology are encouraged to apply. Please send curriculum vitae and names of three references to: **Dr. Jason D. Weber, Washington University in St. Louis, e-mail: jweber@im.wustl.edu.** *Washington University is an Affirmative Action/Equal Opportunity Employer.*

POSITIONS OPEN

A **POSTDOCTORAL POSITION** is available immediately to study role of interferon-inducible genes in autoimmune diseases using mouse models. Only candidates with Ph.D. in molecular immunology, a strong publication record, and an excellent communication skills (written and verbal) should send their curriculum vitae to **Divaker Choubey, Ph. D. (e-mail: divaker.choubey@uc.edu)** at the University of Cincinnati, Cincinnati, Ohio.

ANNOUNCEMENTS

INDO-U.S. SCIENCE and TECHNOLOGY FORUM

Fulbright House, 12 Hailey Road
New Delhi-110 001, India

Website: <http://www.indoustf.org>
FIRST CALL FOR PROPOSAL 2008

The Indo-U.S. Science and Technology Forum (IUSSTF), established under an agreement between the Governments of India and the United States of America, is an autonomous, not-for-profit society that promotes and catalyzes the Indo-U.S. bilateral collaborations in science, technology, engineering, and biomedical research through substantive interaction among government, academia, and industry.

The IUSSTF seeks to support innovative programs aimed to stimulate interactions that have a strong potential for generating follow-on activities and building long-term Indo-U.S. S&T relationships.

The IUSSTF solicits proposals thrice a year (submission deadline: 15th of February, June, October) jointly submitted by the U.S. and Indian Principal Investigators from academia, government funded institutions/laboratories, and private R&D entities for: (1) Knowledge R&D networked and public-private networked Indo-U.S. centers, (2) Indo-U.S. workshop, conference, and symposium, (3) Training schools, and (4) Travel grants, (i) To avail already awarded fellowship and sabbatical positions in U.S./ India, (ii) For selected U.S. participants to attend international conferences/events in India, and (iii) For specific exploratory/ planning visits aimed at large-scale collaborations.

Detailed format available at website: <http://www.indoustf.org>.

For further details and electronic submission, contact: **Arabinda Mitra, e-mail: amitra@indoustf.org** and **Michael Cheetham, e-mail: mcheetham@si.edu**.

Submission deadline: 15 February 2008. Award announcement: mid May 2008.

Find your future here.



Science Careers

From the journal *Science* AAAS

www.ScienceCareers.org

MARKETPLACE

MCLAB DNA Sequencing from \$3.50

Free shipping for 20+ reactions. High throughput. Direct sequencing from bacteria, phage, genomic DNA, PCR products, hairpin, etc.

1-888-mclab-88, www.mclab.com